The Behaviour of Base Metals in Arc-Type Magmatic-Hydrothermal Systems – Insights from Merapi Volcano, Indonesia

Olivier Nadeau

Department of Earth & Planetary Sciences

McGill University

Montreal, Quebec, Canada

October 2011

A thesis submitted to McGill University in partial fulfillment of the requirements of the degree of Doctor of Philosophy

© Olivier Nadeau, 2011

Abstract

Porphyry and high sulfidation epithermal ore-forming systems are genetically associated with calc-alkaline volcanism in subduction zones, and where erosion has not been too deep, the volcanic rocks are still commonly exposed in close proximity to the deposits. Most models for porphyry copper and high sulfidation epithermal gold systems include a shallow magmatic reservoir (the porphyry stock), an overlying hydrothermal cell, its alteration paragenesis and a stratovolcano. Some investigations also discuss the importance of underlying granitoid batholiths as feeders for porphyry stocks and their hydrothermal systems. Although it is commonly believed that the ores deposit during the waning stages of volcanism, given the time span over which these deposits form (tens of thousands to several million years) and the undeniable existence of hydrothermal systems beneath volcanoes, it is quite probable that their formation is initiated at times when volcanoes are still active. Although currently mined ore deposits are excellent places to focus research, subduction zone stratovolcanoes provide important windows on the magmatic-hydrothermal processes at play.

This thesis describes an investigation of the magmatic-hydrothermal environment that resides beneath Merapi volcano, Indonesia. The research involved sampling and chemical analysis of minuscule aliquots of evolving silicate and sulfide melts trapped as inclusions at different times and in different locations in growing crystals subsequently ejected during eruptions. The research also involved sampling and analysis of fumarolic gases (and their precipitates) emitted at Merapi volcano during times of quiescence and eruptive activity, as well as compilation of published compositional data for fumarolic gases from other arc volcanoes. These gases are the surface equivalents of ore-forming magmatic-hydrothermal fluids. Finally the research involved compilation from the literature of compositional data for fluid inclusions (micron-scale droplets of magmatic volatile phases) trapped in gangue minerals in porphyry copper deposits. The focus of the research was the behaviour of copper, nickel, cobalt, zinc, lead and molybdenum in magmatic hydrothermal systems.

The research reported in Chapter 1 showed that injections of sulfide meltsaturated mafic magma into shallower, more evolved and more oxidized resident magma at Merapi volcano induced exsolution of a magmatic volatile phase from the mafic magma. This hydrothermal fluid dissolved the sulfide melt and became enriched in chalcophile (notably copper) and siderophile metals. An argument is presented that the overpressure generated by the exsolution of a fluid originating in this manner triggered an explosive eruption at Merapi volcano in 2006. This is supported by the observation that the metal content, particularly of copper, was higher in the volcanic gas sampled immediately after this eruption than during periods of quiescence and that metal ratios of the gas are remarkably similar to those of sulfide melt inclusions. In Chapter 2, it is shown that the mafic magma mixed poorly with the more felsic magma, that both magmas evolved via assimilation and fractional crystallization and, most importantly, that the magmatic volatile phase transferred base metals to the more felsic magma. In Chapter 3, the fluid inclusion and volcanic gas data are used to make inferences about the evolution of porphyry ore-forming systems and link mechanisms of oreformation to those operative during the eruptive cycles of volcanoes. Finally, the thesis integrates the findings of this study into a model that provides new insights into the formation of porphyry copper deposits below stratovolcanoes.

Résumé

Les gîtes de types porphyriques et épithermaux acides à or et argent sont génétiquement associés au volcanisme calco-alcalin des zones de subduction et les roches volcaniques cogénétiques à ces gisements sont souvent encore présentes, lorsqu'elles n'ont pas encore été érodées. Tous les modèles actuels de mise en place de ces gîtes définissent un réservoir magmatique peu profond (le porphyre), lequel est coiffé d'une cellule hydrothermale et de sa séquence complexe d'altération, ainsi que d'un stratovolcan. Certains auteurs discutent aussi de l'importance de batholites sous-jacents ayant généré le porphyre et ses fluides hydrothermaux. Quoiqu'il soit généralement accepté que ces gîtes se forment durant le déclin du volcanisme, étant donné la longévité des périodes proposées pour la formation de ceux-ci (de dizaines de milliers à plusieurs millions d'années) et l'existence indéniable de systèmes hydrothermaux associés, il est fort probable que la formation de ces gîtes soit initiée alors que le volcanisme est encore actif. Bien que les gisements actuels soient d'excellents endroits à étudier pour améliorer notre compréhension de la façon dont ils se sont formés, les volcans situés en zones de subduction représentent d'importants points d'observation des processus magmatiques-hydrothermaux actuels.

La présente recherche porte sur l'environnement magmatique-hydrothermal qui existe sous le volcan Mérapi, situé en Indonésie. Des échantillons de liquides silicatés et sulfurés (postérieurement solidifiés) piégés à l'intérieur de cristaux durant leur croissance à différents moments et endroits dans le magma et avant d'être éjectés hors des réservoirs magmatiques lors d'éruptions volcaniques (inclusions magmatiques et sulfurées) ont été prélevés et dosés. Des gaz fumerolliens de haute température et leurs sublimats émis au volcan Mérapi durant des phases de dégazage passif et d'éruption explosive ont été échantillonnés et analysés. Des résultats similaires pour les gaz d'autres volcans, ainsi que des analyses d'inclusions fluides de systèmes hydrothermaux de porphyres cuprifères ont été compilés à partir de la littérature. Les gaz

volcaniques analysés sont les équivalents superficiels des fluides magmatiqueshydrothermaux qui génèrent les gisements métallifères. Cette recherche a ciblé les métaux de base que sont le cuivre, le nickel, le cobalt, le zinc, le plomb et le molybdène.

Dans le premier chapitre, il a été démontré que des magmas mafiques d'origine profonde et saturés en liquide sulfuré ont été injectés dans le réservoir magmatique peu profond de Mérapi, celui-ci contenant un magma plus évolué et plus oxydé. La décompression qu'a subie le magma mafique a provoqué l'exsolution d'une phase magmatique volatile (un fluide hydrothermal) qui a dissous le liquide sulfuré et ses métaux chalcophiles et sidérophiles (notamment le cuivre). La surpression générée par l'exsolution de ce fluide hydrothermal a provoqué l'éruption explosive du volcan Mérapi de mars à août 2006. Ceci est corroboré par l'observation que certains métaux, particulièrement le cuivre, étaient enrichis dans les gaz volcaniques émis après l'explosion par rapport aux niveaux mesurés durant la phase de dégazage passif, et par le fait que les rapports des métaux dans ces gaz post-explosion étaient soudainement semblables à ceux mesurés dans les inclusions sulfurées, alors qu'ils étaient bien différents durant les phases de dégazage passif du volcan. Dans le second chapitre, je démontre que le magma plus mafique et le magma plus felsique ne se sont pas bien mélangés, que les deux magmas ont évolué via l'assimilation de roches encaissantes et la cristallisation fractionnée, et que la phase magmatique volatile qui s'est séparée du magma mafique et qui a dissous le liquide sulfuré a transféré ses métaux au magma plus felsique. Dans le troisième et dernier chapitre, les inclusions fluides et les gaz volcaniques ont été utilisés en conjonction avec les connaissances acquises et décrites dans les deux premiers chapitres afin de proposer un modèle pour l'évolution du système porphyrique et d'établir les liens qui existent entre les mécanismes de formation des gîtes porphyriques et épithermaux acides, et ceux qui opèrent durant les cycles éruptifs des volcans. Un modèle pour la formation des porphyres cuprifères sous les stratovolcans actifs des zones de subduction est finalement proposé.

Contribution of Authors

This thesis is divided into five chapters of which three are scientific papers. One of these has been published in a peer-reviewed journal, a second is in review for publication in a peer-reviewed journal, and the third has been submitted to a peer-reviewed journal for publication. I am the first author of each of the papers and share the authorship with my two co-supervisors. I carried out the field work, prepared and analysed the samples, interpreted the data, and wrote the papers. One of my supervisors participated in the field work and both supervisors contributed to the data interpretation and edited the chapters. I developed the ideas and the models proposed in the papers with input from my supervisors.

Dédicace

À mes parents, Michèle et Robert, pour avoir fait de moi ce que je suis devenu... À ma blonde, Isabelle, pour m'avoir supporté et sans qui je ne serais pas là! Et à mes enfants, Gaspard et Léo, pour m'avoir donné la force de continuer...

Acknowledgements

I hereby acknowledge the fundamental help of my supervisors, without which all of this would not have been possible, Willy Williams-Jones and John Stix. Thanks bosses! I would also like to underline the source of inspiration which Professor Don Francis has represented for me. I am grateful for the advisory and technical help provided by Bill Minarik (advisory committee member; LA-ICP-MS), Lang Shi (electron probe), Brigitte Dionne (computer problems and associated headaches), Artaches Migdisov (discussions about anything, science or not, as long as it is philosophical, with or without wine), Kristy Thornton (all this help by email), Anne Kosowski (all this money) and Professor Tobias Fischer (volcanic gas expert and professor at the University of New Mexico). I would like to acknowledge the fact that the Department of Earth & Planetary Sciences is a very fertile environment for science. Over these years (8 of them!), I enjoyed and benefitted from informal discussions with Denis Zezin and Alexandre Brosseau-Liard, my deskmates, Kirsten Rempel, Artaches Migdisov, Julia King, Michael Patterson, Guillaume Girard, Dirk Schumann, Simon Gagné, Laura Petrella, Vincent van Hinsberg and Stéphane De Souza. Above all, I would like to acknowledge that without Isabelle and our two boys, I would not have survived!

Table of contents

Title page · · · · · · · · · · · · · · · · · · ·	····· i
Abstract ····	···· ii
Résumé····	····iv
Author contribution	····vi
Dédicace ····	··· vii
Acknowledgements	·· viii
Table of contents · · · · · · · · · · · · · · · · · · ·	····ix
List of tables · · · · · · · · · · · · · · · · · · ·	xv
List of figures ····	·· xvi
List of appendices · · · · · · · · · · · · · · · · · · ·	·· ixx
General introduction · · · · · · · · · · · · · · · · · · ·	
1. Introduction ·····	
2. Arc magmatism · · · · · · · · · · · · · · · · · · ·	
2.1 Assimilation and fractional crystallization · · · · · · · · · · · · · · · · · · ·	
2.2 Magma mixing · · · · · · · · · · · · · · · · · · ·	
2.3 Gas sparging·····	
3. Arc hydrothermal processes ·····	4
3.1 Porphyry $Cu \pm Mo \pm Au$ ore deposits · · · · · · · · · · · · · · · · · · ·	5
3.2 Skarn deposits ·····	
3.3 Epithermal ore deposits ·····	6
3.4 Sulfide and magmatic-hydrothermal ore deposits······	7
3.5 Fluid inclusions ·····	8
3.6 Physico-chemical pathways	
in magmatic-hydrothermal systems ·····	9
4. Arc volcanism · · · · · · · · · · · · · · · · · · ·	10
4.1 Merapi volcano·····	10
4.2 Volcanic gas condensates and sublimates	12

(T1	nesis rationale······13
6. 11	nesis organization · · · · 14
7. Th	nesis objectives · · · · · 14
8. O	verview of chapter 1 ······ 15
9. O	verview of chapter 2 ······ 16
10. 0	Overview of chapter 3······ 16
Refe	rences
Preface to cl	napter 1 · · · · · · 28
-	- Sulpide magma as a source of metals in arc-
related mag	matic hydrothermal ore fluids
1. Su	alfide dissolution in scoria and sulfide oxidation in dome lavas ······ 32
2. Su	alfide melt composition
3. Vo	plcanic gases · · · · · 34
4. Si	gnificance of the volcanic gas metal signature
Ackr	nowledgements · · · · · 38
	rences
Refe	or Contributions
Refe Auth	
Refe Auth Table	or Contributions · · · · 41
Refe Auth Table Figur	or Contributions
Refe Auth Table Figur	or Contributions
Refe Auth Table Figur	or Contributions 41 e 42 res 42 endices 47
Refe Auth Table Figur	or Contributions 41 e 42 res 42 endices 47 Appendix 1 : Geological Setting 47
Refe Auth Table Figur	or Contributions 41 e 42 res 42 endices 47 Appendix 1 : Geological Setting 47 Appendix 2 : Supplementary methods 48
Refe Auth Table Figur	or Contributions 41 e 42 res 42 endices 47 Appendix 1 : Geological Setting 47 Appendix 2 : Supplementary methods 48 Appendix 3 : δD versus $\delta^{18}O$ in Merapi gas condensates 49

Chapter 2 – The Behaviour of Copper, Zinc and Lead during Magmatic-Hydrothermal Activity at Merapi Volcano, Indonesia · · · · · 54 3. Geological Setting ······ 57 4. Methodology 59 4.1 Analytical Method · · · · · 59 4.2 Thermodynamic modelling · · · · · 59 5.2 FC and AFC Simulations of Melt Composition 63 5.2.1 Mafic Melt 64 7. Conclusions 70 Acknowledgement · · · · · 71 References · · · · · 71 Appendices101 Appendix 1: MELTS model for fractional crystallization of the most primitive mafic melt inclusion.101 Appendix 2: MELTS model for assimilation and fractional crystallization in the mafic melt104 Appendix 3: MELTS model for fractional crystallization of the most primitive felsic melt inclusion ······110 Appendix 4: MELTS model for assimilation and

Preface to cha	pter 3	121
Chapter 3 – T	The Nature of Ore-forming (Cu, Mo, Pb, Zn)	
-	ydrothermal Systems: Insights from the Composition	s of
Volcanic Gas	es and Fluid Inclusions ······	122
1. Abs	tract	123
	oduction ·····	
	logical setting of Merapi volcano	
	hodology·····	
	4.1 Fluid inclusions ······	
	4.2 Volcanic gas condensates · · · · · · · · · · · · · · · · · · ·	127
	4.3 Volcanic gas sublimates ·····	127
	4.4 Data analysis · · · · · · · · · · · · · · · · · ·	128
5. Res	ults·····	129
	5.1 Fluid inclusions ·····	129
	5.2 Volcanic gas condensates · · · · · · · · · · · · · · · · · · ·	130
	5.3 Conparison of fluid inclusion and volcanic gas data	132
	5.4 Volcanic gas sublimates ·····	133
6. Disc	cussion ·····	134
	6.1 Physico-chemical evolution of	
	magmatic-hydrothermal fluids·····	135
	6.2 Relationship between magmatic-hydrothermal fluid	ls and
	volcanic gases ······	138
	6.3 Cyclic deposition of ores in porphyry systems ······	140
	6.4 Model for the formation of porphyry deposits	141
7. Con	clusions	142
Aknov	vldegement ······	143
Refere	nces ·····	143
Tables	,	150

Figures ····	152
Appendices ·····	171
Appendix 1 : Fluid inclusion data from the literature · · ·	171
Appendix 2: Volcanic gas data from the literature	178
Appendix 3 : Additional Merapi gas data ······	181
Thesis conclusions ·····	183
1. Main findings·····	183
2. Contribution to knowledge·····	184
3. Future work ·····	184
Thesis appendices ·····	186
Appendix 1 – Chemical composition of sulfide melt inclusions	s ······186
Appendix 2 – Chemical composition of volcanic gas condensa	ates · · · · · 189
Appendic 3 – Chemical composition of silicate melt inclusions	s ······191

List of tables

Chapter 1
Table 1. Compositions of phases in sulfide melt inclusions and the reconstructed
composition of the sulfide melt. 42
Chapter 2
Table 1. Major and trace element concentrations in matrix glasses and silicate
melt inclusions from Merapi volcano 79
Table 2. Partition coefficients for sulfide melt-silicate melt,
MVP-silicate melt, crystal-sulfide melt, crystal-mafic silicate melt
and crystal-felsic silicate melt. 84
Table 3. Bulk composition of enclaves found in Merapi rocks · · · · · 85
Table 4. Initial melt compositions used in MELTS
Chapter 3
Table 1. Concentration of selected elements
in volcanic gas condensates at Merapi ······150
Table 2. Chemical formulae and depositional temperatures of minerals
precipitated from Merapi volcanic gases in 2004 and 2006

List of figures

Chapter 1
Figure 1. Reflected light photomicrographs of variably dissolved
sulfide globules hosted by amphibole megacrysts
Figure 2. Reflected light photomicrographs of oxidized sulfide melt inclusions
hosted in amphibole from samples of dome lava
Figure 3. Trace metal concentrations and ratios in volcanic gas
condensates and sulfide melt inclusions
Figure 4. Ternary diagram showing relative concentrations of
SO ₄ , H ₂ O and Cl in volcanic gas condensates
Chapter 2
Figure 1. SiO ₂ versus MgO for melt inclusions and matrix glass 86
Figure 2. Lithophile element concentrations of
silicate melt inclusions and matrix glasses as a function of MgO 87
Figure 3. Ore and volatile element (Cu, Zn, Pb, Cl and S) concentrations in
silicate melt inclusions and matrix glasses as a function of MgO 89
Figure 4. Concentrations of SiO ₂ , Cu, and Pb versus MgO concentration
using the MELTS model for fractional crystallization of the most primitive mafic
melt inclusion. 91
Figure 5. Concentrations of SiO ₂ , Cu and Pb versus MgO concentrations using the
MELTS model for assimilation of calc-silicate rocks and fractional crystallization
of the most primitive mafic melt inclusion.

Figure 6. Concentrations of SiO2, Cu, and Pb versus MgO concentration using the
MELTS model for fractional crystallization of the most primitive of the more
felsic melt inclusions. 93
Figure 7. Concentrations of SiO2, Cu and Pb versus MgO concentrations using
the MELTS model for assimilation of calc-silicate rocks and fractional
crystallization of the most primitive of the more felsic melt inclusions 95
Figure 8. Concentration of Cu, Zn and Pb in Merapi bulk rocks and melt
inclusions compared to other bulk arc rocks 97
Figure 9. Photomicrographs of selected silicate melt inclusions 96
Figure 10. Concentration of Cu, Zn and Pb in fluid inclusions
Figure 11. Plots of Cu and Pb versus MgO comparing AFC modelled
concentrations of these elements versus the measured concentrations in melt
inclusions and the amount of volatile fluxing required100
Chapter 3
Figure 1. Violin plots displaying the concentrations of
Cu, Zn, Pb and Mo in fluid inclusions from selected
porphyry Cu (Mo) magmatic-hydrothermal systems
Figure 2. Violin plots displaying the concentrations of Cu, Zn, Pb and Mo in
volcanic gas condensates from island arc volcanoes
Figure 3. Histogram of concentrations of Cu, Zn, Pb and Mo and their ratios to K
in volcanic gas condensates sampled at Woro fumarole field

Figure 4. Violin plots comparing Cu/Na, Zn/Na, Pb/Na and Mo/Na
ratios in supercritical fluid, brine and vapor inclusions
and in volcanic gas condensates
Figure 5. Volcanic gas sublimate mineralogy and precipitation temperatures in
silica tubes inserted in fumaroles at Merapi volcano164
•
Figure 6. Phase diagram for the H ₂ O-NaCl system in pressure-temperature-
composition space emphasising the liquid-vapor solvus present at magmatic-
hydrothermal conditions. Modified from Geiger et al., 2005
Figure 7. Schematic evolution of a subduction zone magmatic-hydrothermal
system during eruptive cycles168

List of appendices

Chapter 1	
A	ppendix 1 : Geological Setting · · · · · 47
A	ppendix 2 : Supplementary methods · · · · · 48
A	ppendix 3 : Plot of δD versus $\delta^{18}O$ in Merapi gas condensates $\cdots 49$
$\mathbf{A}_{\mathbf{j}}$	ppendix 4 : Chemical compositions of
se	elected silicate melt inclusions
A	ppendix 5 : Appendix references ······ 52
Chapter 2	2
$\mathbf{A}_{\mathbf{j}}$	ppendix 1 : MELTS model for fractional crystallization
of	f the most primitive mafic melt inclusion
$\mathbf{A}_{\mathbf{j}}$	ppendix 2 : MELTS model for assimilation and
fra	actional crystallization in the mafic melt ······104
$\mathbf{A}_{\mathbf{i}}$	ppendix 3: MELTS model for fractional crystallization
of	f the most primitive felsic melt inclusion ·······110
$\mathbf{A}_{\mathbf{j}}$	ppendix 4 : MELTS model for assimilation and
fra	actional crystallization in the felsic melt ······115
Chapter 3	3
A	ppendix 1 : Fluid inclusion data from the literature ·······171

	Appendix 2 : Volcanic gas data from the literature · · · · · · · · 178
	Appendix 3 : Additional Merapi gas data · · · · · · 181
Thesis	Appendices
	Appendix 1 – Chemical composition of sulfide melt inclusions ······186
	Appendix 2 – Chemical composition of volcanic gas condensates ······189
	Appendix 3 – Chemical composition of silicate melt inclusions ······191

General introduction

1. Introduction

Hydrothermal systems are responsible for a large proportion of the Earth's resources of metallic minerals. Many of these systems are fuelled by magmatism, thereby giving rise to a major sub-class termed magmatic-hydrothermal ore deposits. The most important of these types of deposits (porphyry and epithermal Cu, Au, and Mo deposits) are found in subduction zones and are typically associated with magmas of calc-alkaline affinity. Commonly they occur within or beneath the edifices of stratovolcanoes (e.g., Sillitoe, 1973; Sillitoe, 2010).

In this thesis, I use Merapi volcano as a window through which to observe the action of hydrothermal processes which are considered to form porphyry-epithermal deposits. Merapi volcano is located on central Java, part of an island arc originating from the subduction of the Indo-Australian plate under the Asian plate. Using rock and gas samples collected at Merapi volcano, together with data published for other arc volcanoes and magmatic-hydrothermal systems, this thesis helps improve our understanding of how metals are concentrated by arc-type magmatism and hydrothermal processes to potentially exploitable levels.

Magmatic and hydrothermal processes that are active beneath Merapi have important genetic, temporal and spatial links. Hence, in the present chapter the reader is introduced to the fundamentals of arc magmatism, hydrothermalism and volcanism, which are tied together in subduction zones. Concepts such as assimilation and fractional crystallization, magma mixing and gas sparging are briefly reviewed. A brief description of current models for the formation of magmatic-hydrothermal ore deposits is provided, as well as important related notions such as fluid inclusions and physico-chemical evolution of hydrothermal fluids. The reader is then provided with a portrait of Merapi volcano and an overview of the methods by which the metal content of volcanic gases are assessed. The rationale for the thesis, its objectives, and the manner of its

organization are presented. Finally, this introductory chapter ends with a short summary of each of the three main chapters of the thesis.

2. Arc magmatism

Merapi is an island arc volcano that results from subduction of the continental and oceanic Indo-Australian plate beneath the continental Eurasian plate. It is commonly accepted that the subduction of a hydrothermally altered and sedimentcovered oceanic crust results in dehydration of subducted material and the liberation of a free aqueous volatile phase (Grove, 2000). According to this model, the volatile phase lowers the melting point of the depleted lherzolitic mantle wedge and triggers partial melting. The primary melt thus has an 'arc' signature, induced by incorporation of the free volatile phase, which promotes its ascent by buoyancy. These magmatic systems typically form crustal magma chambers where they may pond, fractionate, assimilate country rock and exsolve magmatichydrothermal fluids (Bowen, 1928; Burnham and Davis, 1974; DePaolo, 1981; Hildreth and Moorbath, 1988). By contrast, active continental arcs occur where oceanic plates are subducted under continental plates. The processes identified at island arcs, such as metamorphic dehydration of the hydrothermally altered subducted slab and its sediments and partial melting within the mantle wedge are also active in active continental margins. The main difference is that the overiding continental lithosphere is thicker (~150 km instead of a maximum of 80 km for oceanic lithosphere; Wilson, 1989). Consequently, the resulting partial melts are more evolved while rising through the continental plate and assimilating continental material.

2.1 Assimilation and fractional crystallization

Silicate magmas respond to slow and gradual cooling by equilibrium crystallization of silicates, sulfides, oxides and other less common minerals (e.g., carbonates, sulfates, phosphates, etc). However, the cooling is generally too fast

and/or the crystals do not generally remain available for element exchange with the silicate melt, so crystallization usually proceeds at disequilibrium. This is a very common process called fractional crystallization (Bowen, 1928). Another very common process through which magmatic systems are modified is assimilation; silicate magmas can incorporate variable proportions of their wall rock. Assimilation is often thought to combine to fractional crystallization since the heat released by crystallization can fuel the melting of the contaminant (AFC; De Paolo, 1981).

2.2 Magma mixing

Injections of magma into magma chambers may lead to the mixing of the two magmas; this process is thought to be common in active subvolcanic environments (Eichelberger, 1975; Anderson, 1976). Given the temperature and chemical contrasts between the two magmas, their interaction may result in triggering volcanic eruptions (Eichelberger et al., 1976). However, it is also possible that the two magmas do not mix, provided the input flow is laminar, the contrast in viscosity between the two magmas is high and the magma chamber extends laterally rather than vertically (Huppert et al., 1986). In any case, mixing of magmas is a common petrologic process by which subduction zone magmas are modified. Although it was suggested previously that at Merapi, injections were mixing with the resident magma (Camus et al., 2000; Gertisser and Keller, 2003), in the second main chapter of this thesis, I show that late injections do not appear to mix well with Merapi resident magma, but that they do transfer their magmatic volatile phase (MVP) to the resident magma.

2.3 Gas sparging

The MVP mentioned above may exchange material with the resident magma as hydrothermal bubbles percolate upward through the magma. This is a main highlight of the second main chapter of this thesis and is conceptually very similar

to the 'gas sparging' introduced by Bachmann and Bergantz (2003; 2006) to explain the rejuvenation and eruption of the Fish Canyon magma body. In their paper, they show that the injection of volatile-rich magma into the resident magma chamber resulted in the exsolution of the MVP. As a result, the MVP was heated and pressurized the resident magma, thus rejuvenating the system and triggering its eruption. The idea of percolating bubbles illustrates well that resident magma reservoirs are not necessarily the source of the mineralizing fluids, but instead may simply act as conduits for the flowing fluids (Sillitoe, 2010). This is an important concept for the model of porphyry epithermal mineralization that I propose in the third main chapter of this thesis.

3. Arc Hydrothermal Processes

Since ancient times, it was observed that metals precipitate in fractures of rocks of the Earth's crust. This led René Descarte in 1644 to suggest that these metals precipitated from a fluid that circulated in the crust. There has been longstanding debate regarding the source of this fluid and of the metals it contained, some arguing that it came from magmas and others proposing that they were leached from the crust (Hedenquist and Lowenstern, 1994). However, recent advances in knowledge of magmatism and hydrothermal processes have shown that this volatile phase and the metals it contains may be of purely magmatic origin, with or without subsequent admixture of other fluids (e.g., groundwater) (Hedenquist and Lowenstern, 1994). It has also been demonstrated that the capacity of the magmatic-hydrothermal fluid phase to carry metals varies according to its physical state, i.e., whether it is a supercritical fluid, a liquid or a vapor (e.g., Williams-Jones et al., 2002; Williams-Jones and Heinrich, 2005), as well as its chemical state, i.e., the presence of ligands suitable for the complexing of metals (e.g., Candela and Holland, 1984; Crerar et al., 1985; Seward et al., 1981; Seward and Barnes, 1997). In the present thesis, I show that a porphyry Cu system is being installed beneath Merapi volcano where hydrothermal processes are currently active. I thus briefly review the current models for the types of deposits

that are thought to form in such systems, namely porphyry $Cu \pm Mo \pm Au$ ore deposits, skarns, and high and intermediate sulfidation epithermal ore deposits.

3.1 Porphyry $Cu \pm Mo \pm Au$ ore deposits

Current models for the formation of porphyry $Cu \pm Mo \pm Au$ ore deposits (hereafter simply named porphyry Cu) are related to intrusions of granitoids emplaced in the crust overlying subduction zones (Candela and Piccoli, 2005; Seedorff et al., 2005; Sillitoe, 2010). Porphyry stocks are emplaced at relatively shallow levels, usually within the first four kilometers of the crust, and can even extrude as stratovolcanoes (Deino and Keith, 1997; Longo and Teal, 2005), although the deposits tend to form during the waning stages of the volcanic activity. The shallow porphyry systems are fueled by deeper (5 to 15 km), larger (on the order of 50 km³ but up to an order magnitude greater in cases of giant deposits; Sillitoe, 2010) batholiths which represent the source of the hydrothermal fluids that are focused through the shallower mineralizing systems (Sillitoe, 2010). These magmas are commonly water-rich ($H_2O \approx 4$ wt.%), oxidized and calcalkaline (Candela and Piccoli, 2005; Seedorff et al., 2005; Sillitoe, 2010). The magmatic volatiles exsolve from the melt, circulate in fracture- and in porositybased networks, reacts with and alter their host rocks, cool down, and deposit metal-bearing minerals. This explains why alteration and mineralization are intimately linked. Potassic alteration is found in the cores of the systems, proximally to the porphry stocks, and hosts most of the mineralization. Chloritic and sericitic alteration usually overlies the porphyries and may also host some mineralization. Propylitic alteration is distal, surrounds the porphyry system and is usually barren. Finally, the system may also be topped by an advanced argilic alteration lithocap that may host high and intermediate sulfidation epithermal deposits.

3.2 Skarns

Skarn deposits have an origin similar to that of porphyry Cu deposits but differ in that the intrusions are emplaced within rocks – usually carbonates – that react strongly with the intrusion and its waters and are thus heavily metasomatized. The magmatic volatile phase exchanges components with its surrounding wall rock, usually crystallizing calc-silicate mineral assemblages that host the skarn deposits. Deposits of Au and Fe are usually found in more mafic intrusions, whereas concentrations of Cu, Zn, Pb and W are usually associated to shallow oxidized I-type intrusions, and deposits of Mo and Sn are found in more reduced, S-type intrusions (Meinert et al., 2005). It is thought that Merapi volcano is underlain by carbonate rocks and that these interact with its source magma (Chadwick et al., 2005; 2007). It is quite probable that such metasomatic mechanisms are operating beneath Merapi.

3.3 Epithermal ore deposits

Epithermal ore deposits have demonstrable spatial and genetic links with porphyry ore deposits (e.g., Hedenquist et al., 1998). They have been subdivided into two end-member families, namely high sulfidation ore deposits (HSE) and low sulfidation ore deposits (LSE) (White and Hedenquist, 1990; 1995). Although other classification schemes exist (Simmons et al., 2005), this one is preferred since it summarizes and distinguishes their characteristics as related to their genesis. Similarly to porphyry ore deposits, epithermal deposits form when hydrothermal fluids cross sharp physico-chemical gradients (e.g., boiling and/or mixing) (Simmons et al., 2005). Epithermal fluids are lower temperature (< 300°C) and form at shallower depths (< 1.5 km) than porphyries (< 700°C and < 4 km) (Simmons et al., 2005; Sillitoe, 2010). High-sulfidation epithermal Au-Ag, Ag-Au or Ag-Pb-Zn deposits form immediately above the porphyry stocks within the subvolcanic environment and are associated with magmatic, acidic (pH 1 to 3) and oxidized fluids, consistent with their alteration paragenesis containing quartz

 \pm alunite \pm pyrophyllite \pm dickite \pm kaolinite (Simmons et al., 2005). By contrast, low-sulfidation epithermal Au \pm Ag \pm Cu ore deposits are thought to form further away from the central plumbing system of the volcano, and/or during the waning stages of magmatism, by focused flow of diluted magmatic, neutral-pH and reduced fluid across sharp physico-chemical gradients. The composition of this fluid is consistent with the associated assemblage of alteration minerals, which contains quartz \pm calcite \pm adularia \pm illite (Simmons et al., 2005). It is noteworthy that there is still considerable debate regarding the pH of the ore fluids, which is not necessarily the same as that causing alteration of the rocks. Some workers argue that in high-sulfidation epithermal deposits, the ore fluids occur later than and are different from the fluids responsible for earlier alteration. These researchers argue that the ore fluids are of intermediate pH because of the perceived need to transport the gold as bisulfide complexes.

3.4 Sulfide melts and magmatic-hydrothermal ore deposits

Conventional wisdom derived from the collective knowledge summarized above for porphyry, skarn and epithermal deposits is that metals partition directly from silicate melt into exsolving magmatic-hydrothermal fluid. However, recent studies have suggested alternative metal pathways. Specifically, it has been demonstrated that metals may first partition into an immiscible sulfide melt which may in turn be dissolved by a magmatic volatile phase (Keith et al., 1991; 1997; Larocque et al., 2000; Halter et al., 2002; 2005). This is a central thrust of this thesis and is briefly discussed below.

Saturation of sulfide in silicate melts may lead to the exsolution of an immiscible sulfide melt (Naldrett, 2004). Magmatic PGE-Ni-Cu ore deposits are formed by the partitioning of chalcophile metals in this sulfide melt and by its subsequent cooling and crystallization (Barnes and Lightfoot, 2005). Cooling sulfide melts will first crystallize an Fe-Ni-rich monosulfide solid solution (MSS) and subsequently crystallize a Cu-rich intermediate solid solution (ISS). Upon further cooling, the MSS will exsolve into pyrrhotite and pentlandite, whereas the

ISS will exsolve into chalcopyrite, pyrrhotite and cubanite. These minerals are the most common phases in magmatic sulfide deposits.

Silicate melts may also become saturated with respect to a magmatic fluid as discussed above. The major constituents of this MVP are H₂O, CO₂, SO₂ and H₂S in various proportions, as well as Cl and other ligands. The idea that an immiscible sulfide melt may get dissolved and digested by a magmatic volatile phase and thereby contribute its metals to an ore-forming fluid is central in the first chapter of this thesis.

The first evidence for the dissolution of a sulfide melt by a hydrothermal fluid was presented for the porphyry Cu (Mo) of Bingham and Central East Tintic Mountains of Utah by Keith et al. (1991; 1997). Larocque et al. (2000) subsequently extended this observation to several other economic and barren magmatic-hydrothermal and volcanic systems. They proposed that the metals present in the ore deposits were derived from this fluid. Halter et al. (2002; 2005) then proposed a genetic model in which porphyry Cu (Mo) such as Bajo de la Alumbrera (Argentina) formed by deposition of the metals from a fluid that had previously dissolved a sulfide melt. This model explains the fact that metal ratios are similar in the sulfide melt inclusions and in ore-bearing fluid inclusions.

3.5 Fluid Inclusions

Collective understanding of hydrothermal ore deposits has accelerated since the initiation of fluid-inclusion studies. Edwin Roedder, a pionneer in this domain, has contributed a significant amount of knowledge to this field of study (Roedder, 1984). The more recent advances in micro-analytical techniques such as laser ablation ICP-MS (Halter et al., 2002; 2004) have led to the detection of trace metal concentrations in minuscule fluid inclusions. In turn, this has improved our understanding of the behaviour of trace metals in hydrothermal systems. Since then, numerous studies have been published that report trace metal concentrations in fluid inclusions from subduction zones in both economic and barren magmatic-hydrothermal systems (e.g., Audetat et al., 2000a; 2000b; Audetat and Pettke,

2003; 2008; Baker et al., 2004; Klemm et al., 2007; 2008; Kouzmanov et al., 2010; Landtwing et al., 2005; Pudack et al., 2009; Rusk et al., 2004; Ulrich et al., 1999; 2001 Williams-Jones et al., under review; Zajacz et al., 2008). In the third main chapter of the present thesis, I grouped these data and compared them to volcanic gas condensates in order to study their differences and similarities.

3.6 Physico-chemical pathways in magmatic-hydrothermal systems

Sillitoe (2010) reported that most porphyry Cu deposits form at less than 4 km in the crust. The associated shallow magmatic systems are connected to deeper magma chambers sitting at depths varying between 5 to 15 km. It is these deep magma reservoirs that are the source of the mineralizing fluids, which are focused through the shallower porphyries. Fluids exsolved in such systems can be either single-phase supercritical fluids, which can subsequently exsolve into brine and vapor or may evolve above the liquidus to gradually become a liquid, without any abrupt phase change. This is discussed in greater detail in the third main chapter of this thesis.

It has been established that upon exsolution of brine and vapor, Cl partitions preferentially into the brine (Candela and Picolli, 1995) whereas S prefers to partition into the vapor (Heinrich et al., 1999). These two elements are the most common ligands with which metals are complexed to be transported. Specific metals pair with specific ligands: Pearson's rule (1963) states that hard metals (e.g., Mo) prefer to form and transport complexes with hard ligands (e.g., OH⁻, SO₄²⁻) while soft metals (e.g., Cu⁺, Au⁺) prefer to do the same with soft ligands (e.g., HS⁻, H₂S, S₂O₃²⁻). In between these two end-members lies a gray area where borderline metals (e.g., Zn²⁺ and Pb²⁺) complex with borderline ligands (e.g., Cl⁻). Hence, as Zn and Pb prefer to complex with Cl, they are enriched in brines and by contrast, as Cu prefer to complex to S, it is enriched in vapors (Heinrich et al, 1999; Seo et al., 2009).

Webster and Mandeville (2007) discussed the fact that magmatic liquids are highly saline, alkaline, Cl-rich fluids, which will precipitate their metals upon

crossing steep physico-chemical gradients, e.g., rapid decompression, cooling or mixing with ground water. By contrast, magmatic vapors usually consist of low salinity, acidic, S-rich fluids which are more buoyant, react more agressively with wall rock, and may or may not condense into a liquid of very low pH. In fact, depending on pressure, temperature and chemical composition, a supercritical magmatic fluid may either gradually decompress and expand into a liquid or a vapor or abruptly exsolve into a brine and a vapor, and precipitate metals during ascent in the porphyry-epithermal environment (Williams-Jones and Heinrich, 2005). This topic is explored in the third main chapter of this thesis.

4. Arc volcanism

Island arc volcanoes produce shield-like to conical stratovolcanoes made of basaltic to andesitic lavas and tephras. Their compositions range from tholeiitic basalts to calc-alkaline andesites, with minor high-K andesites, shoshonites, dacites and rhyolites. Most arc magmas are 'wet' and many eruptions are thus generally explosive, and many magmas exsolve their volatiles before eruption. This increases their viscosity and can result in eruptions of lava domes which grow and collapse into Merapi-type, incandescent pyroclastic flows. These free volatile phases also play a role in the formation of hydrothermal ore deposits. By contrast, volcanic products of active continental margins are slightly more evolved than those of island arcs. They consist primarily of calc-alkaline andesites and dacites, with minor proportions of basalts and rhyolites. High-K and shoshonitic lavas are more common than in island arcs, and tholeiitic basalts less common. The magmas are also volatile-rich and eruptions are generally explosive. However, the magmas often degas prior to eruption forming lava domes.

4.1 Merapi volcano

Merapi volcano has been active within the last 40,000 years (Camus et al., 2000). It has experienced plinian- to sub-plinian explosive eruptions (Newhall et al.,

2000; Andreastuti et al., 2000, Camus et al., 2000), but underwent a change in its eruptive behaviour during the 20th century and now erupts viscous lava domes which grow and collapse into incandescent pyroclastic flows. These Merapi-type lava dome collapses have been interspersed with occasional St-Vincent-type explosions, also generating incandescent pyroclastic flows but with added more primitive material, i.e., pumice and scoria, and associated surges. Eruptive periods, which usually last several months, are separated by periods of quiescent degassing typically lasting a few years. Merapi volcano is periodically recharged by injections of fresh magma. I have shown previously that these injections may comprise a mafic magma saturated with respect to an immiscible sulfide melt (Nadeau et al., 2010). Camus et al. (2000) and Gertisser and Keller (2003a) reached the conclusion that injections of magma mix with the resident magma at Merapi. Gertisser and Keller (2003a) suggested that these periods of mixing are interspersed by periods that are dominated by fractional crystallization. The work of Chadwick et al. (2005; 2007) has shown that these magmas also assimilate carbonate rocks (limestones and dolomites) during their evolution and gabbroic, calc-silicates and volcano-sedimentary enclaves were indeed found in Merapi lavas (Camus et al., 2000; Chadwick et al., 2007). Finally, Gertisser and Keller (2003b) concluded a stable isotope study at Merapi by noting that "any assimilation must not have been extensive". All of these observations explain: (1) complexely zoned and resorbed phenocrysts, (2) scorias containing light, rhyolitic glass dispersed amongst darker dacitic glass, and (3) eruptive products including gabbroic, volcanosedimentary and calc-silicate enclaves (Camus et al., 2000; Chadwick et al., 2007). Merapi lavas are of calc-alkaline affinity, range from andesites to basalts, with SiO₂ from 49.5 to 60.5 wt. % and K₂O from about 0.5 to 2.5 wt.% and plot into two distincts families of medium-K and high-K basaltic andesites (Gertisser and Keller, 2007a). The layas contain abundant normally and reversely zoned plagioclase (An₃₄₋₉₃), which coexists with fresh, resorbed and zoned clinopyroxene (augite) and amphibole (pargasite, magnesio-hornblende and magnesio-hastingsite), titanomagnetite, and occasional olivine, orthopyroxene and apatite (Camus et al., 2000). Alkali feldspar occurs as microlites or rims the

plagioclase phenocrysts (Hammer et al., 2000). The melt inclusions I have analyzed constitute the main part of the second main chapter of the thesis and come from one of three major outcrops located at Kaliadem, Ngipik Sari and Windusabrang. Kaliadem was the locus of the 2006 eruption, and this is where I sampled the 2006 lava dome. Ngipik Sari is a major roadside outcrop where I could sample 19 distinct stratigraphic layers, which consisted of lavas and fine ashes. Windusabrang hosted a quarry where I found the scoria. Since at least 1978, three high-temperature fumarole fields have been active at the summit of the volcano, namely the Dome, Gendol and Woro fields (Allard and Tazieff, 1979). The highest temperatures have been recorded at Gendol, reaching 900°C in 1978 (LeGuern and Bernard, 1982). Stable isotopes of oxygen and hydrogen, which I have reported in the first main chapter of the thesis, show that the gases emanating from Gendol fumaroles are very close to pure magmatic, whereas those sampled from Woro, while still considered to be magmatic gases (Symonds et al., 1994), had a significant contribution of meteoric water. The Gendol field was destroyed during the eruption of 2006.

4.2 Volcanic Gas Condensates and Sublimates

Volcanic gases have been collected and analyzed for approximately 50 years. Some of the most important developments in this field of study result from the pioneering work of Werner Giggenbach on the fumaroles of White Island, New Zealand (e.g., 1972). Important work on the metal content of these gases also was conducted by Symonds and others (e.g., Symonds et al., 1987a; 1987b; 1992; 1993a; 1993b). Before my work, only two groups examined metal concentrations in Merapi gases (Symonds et al., 1987; Kavalieris, 1994). In the third main chapter of this thesis, I consider these fluids to be proxies for mineralizing magmatic-hydrothermal fluids.

Another mean by which volcanic gases have been assessed is by channelizing fumarolic gases through silica tubes that have been inserted in fumaroles and then collecting and analyzing the minerals which sublimate along the temperature gradient on the inner wall of the tube. This type of experiment was first conducted by LeGuern and Bernard (1982) at Merapi and was repeated at Merapi by Symonds et al. (1987), and elsewhere by many others (e.g., Quisefit et al., 1989; Wahrenberger et al., 2002). I performed this experiment at Merapi in 2004 and 2006. The samples that I collected are important to the findings reported in the third main chapter of this thesis.

5. Thesis rationale

In this thesis, I focus on pathways used by economically important metals such as Cu, Ni, Co, Zn, Pb and Mo in the Merapi magmatic system, from its roots to the surface. By investigating the nature of sulfide and silicate melt inclusions found in Merapi scorias and lavas, and also evaluating fluid inclusion and volcanic gas data from the literature and from Merapi, I assess magmatic-hydrothermal processes active in subvolcanic environments that are associated with the construction of magmatic-hydrothermal ore deposits. Merapi is an ideal site for this study for the following reasons:

- 1) Volcanoes are windows which allow insight into deep to shallow magmatichydrothermal phenomena;
- 2) Merapi is part of a subduction environment where magmatic-hydrothermal ores may be forming;
- 3) Merapi emits high-temperature volcanic gases which can be thought of as surface equivalents of a magmatic volatile phase, which have been shown to contain high concentrations of economic metals (Symonds et al., 1987; Kavalieris, 1994);
- 4) Merapi commonly experiences alternating periods of quiescence and eruption, some of which are explosive and erupt undegassed primitive material. We were

fortunate to sample rocks (scorias) and gases (in 2006) originating from explosive eruptions as well as rocks (from lava dome growth and collapse) and gases (in 2004) during a period of quiescence;

- 5) Melt inclusions found in Merapi scorias provide rare evidence of the dissolution of an immiscible sulfide melt by a magmatic volatile phase;
- 6) These melt inclusions represent two melts (one more mafic and one more felsic) that had not mixed but had exchanged economic metals via a magmatic volatile phase transferred from the mafic to the more felsic melt.

6. Thesis organization

This thesis is divided into a general introduction, three main chapters, and a concluding chapter. The first part introduces the reader to the issues I have addressed in my research and provides the reader with a brief summary of my current understanding of the formation and evolution of magmatic arcs and the genesis of the magmatic-hydrothermal deposits contained within. Some of the concepts that are addressed in the thesis, such as dissolution of sulfide melts, magma mixing, gas sparging and physico-chemical pathways of magmatic-hydrothermal systems, are briefly reviewed. The three main chapters are in the form of journal articles. The conclusion highlights the main findings, summarizes the contributions to knowledge and suggests directions for future research.

7. Thesis objectives

The main objectives of this thesis are:

1) To investigate the role played by mafic magma and immiscible sulfide melt in the Merapi magmatic-hydrothermal system and apply my findings to other magmatic-hydrothermal systems;

- 2) To investigate the nature of the interaction of the magmas at Merapi;
- 3) To investigate the origin and the behaviour of Cu, Zn and Pb in more evolved, resident magma, and transport pathways in mafic magma and more evolved magma to the surface
- 4) To investigate the behaviour of Cu, Zn, Pb and Mo in the MVP circulating in the porphyry-epithermal system underlying Merapi, and generalize my findings to other arc-related magmatic-hydrothermal systems;
- 5) To use volcanic activity and volcanic gases at Merapi to establish links between magmatic-hydrothermal processes and the chemistry of the magmatic volatile phase, and to integrate these links into a model of magmatic-hydrothermal ore deposits.

8. Overview of chapter 1

Chapter 1 is a paper published in Nature Geoscience in 2010 entitled: "Sulphide Magma as a Source of Metals in Arc-Related Magmatic Hydrothermal Ore Fluids". In this paper, I demonstrate that at Merapi, a sulfide-saturated mafic magma was injected upward into a more felsic, resident magma, which resulted in decompression of the mafic magma and exsolution of a MVP, which in turn dissolved the sulfide melt and was transferred to the atmosphere. This also resulted in an explosive eruption at Merapi in 2006, which emitted gases having the chemical signature of the sulfide melt. Chapter 1 provides the foundation on which the second chapter is built.

9. Overview of chapter 2

Chapter 2 is entitled "The Behaviour of Copper, Zinc and Lead during Magmatic-Hydrothermal Activity at Merapi Volcano, Indonesia" and is under review by Economic Geology and the Bulletin of the Society of Economic Geologists. I show that the sulfide-melt-saturated more mafic magma and the more oxidized, more felsic magma residing beneath Merapi did not mix. I go on to show, however, that the MVP which was exsolved from the mafic magma and dissolved its sulfide melt also transferred Cu, Zn and Pb from the mafic to the more felsic magma. The felsic magma thus evolved through a synchronous combination of fluid-melt partitioning of Cu, Zn and Pb gradually enriching Cu and Pb in the melt, and by assimilation and fractional crystallization. Zn concentration was buffered by the crystallization of titanomagnetite.

10. Overview of chapter 3

Chapter 3 comprises a manuscript entitled "Arc Volcanoes as Proxies for Porphyry Epithermal Ore Deposition". In this manuscript, the chemical compositions of fluid inclusions found in arc-type magmatic-hydrothermal deposits are compared with those of volcanic gases emanating from calc-alkaline stratovolcanoes in arc-type settings. This comparison has enabled us to infer that Cu, Zn, Pb and Mo are being deposited in porphyry-epithermal environment beneath these stratovolcanoes, and that Cu, Zn and Pb are zonally distributed around magmatic centers, with Cu being deposited earlier and proximally, and Zn and Pb being deposited progressively later and more distally. Using volcanic gases as proxies for porphyry-epithermal fluids and taking Merapi as an example, we develop a model according to which: (1) injections of fresh mafic magma, with the associated explosive eruptions, lead to pulses of reducing, Cu, Zn and Pb-rich fluid which deposit a reduced mineral paragenesis in the magmatic-hydrothermal environment, and (2) subsequent periods of assimilation and fractional crystallization, and the associated volcanic quiescence, lead to gradual

oxidation of the magma and its magmatic volatile phase, to depletion of Cu and Pb and preferential enrichment of Mo, and to deposition of a more oxidized mineral paragenesis.

References

- Allard, P., Tazieff H. (1979). "Volcanologie. Phénoménologie et cartographie thermique des principales zones fumeroliennes du volcan Mérapi (Indonésie)." <u>Comptes-Rendus de l'Académie des Sciences de Paris Série D 288</u>: 747-750.
- Anderson, A. T. (1976). "Magma mixing; petrological process and volcanological tool." Journal of Volcanology and Geothermal Research 1(1): 3-33.
- Andreastuti, S. D., B. V. Alloway, Smith, I. E. M. (2000). "A detailed tephrostratigraphic framework at Merapi Volcano, central Java, Indonesia; implications for eruption predictions and hazard assessment." <u>Journal of Volcanology and Geothermal Research</u> **100**(1-4): 51-67.
- Audetat, A., D. Guenther, Heinrich, C. A. (2000a). "Causes for large-scale metal zonation around mineralized plutons; fluid inclusion LA-ICP-MS evidence from the Mole Granite, Australia." <u>Economic Geology and the Bulletin of</u> the Society of Economic Geologists **95**(8): 1563-1581.
- Audetat, A., D. Guenther, Heinrich, C. A. (2000b). "Magmatic-hydrothermal evolution in a fractionating granite; a microchemical study of the Sn-W-F-mineralized Mole Granite (Australia)." Geochimica et Cosmochimica Acta **64**(19): 3373-3393.
- Audetat, A. and T. Pettke (2003). "The magmatic-hydrothermal evolution of two barren granites; a melt and fluid inclusion study of the Rito del Medio and Canada Pinabete plutons in northern New Mexico (USA)." Geochimica et Cosmochimica Acta 67(1): 97-121.
- Audetat, A., T. Pettke, Heinrich, C. A., Bodnar, R. J. (2008). "Special paper; The composition of magmatic-hydrothermal fluids in barren and mineralized intrusions." Economic Geology and the Bulletin of the Society of Economic Geologists 103(5): 877-908.
- Bachmann, O. and G. W. Bergantz (2003). "Rejuvenation of the Fish Canyon magma body; a window into the evolution of large-volume silicic magma systems." Geology **31**(9): 789-792.

- Bachmann, O. and G. W. Bergantz (2006). "Gas percolation in upper-crustal silicic crystal mushes as a mechanism for upward heat advection and rejuvenation of near-solidus magma bodies." <u>Journal of Volcanology and</u> Geothermal research **149**: 85-102.
- Baker, T., E. van Achterberg, E., Ryan, C. G., Lang, J. R. (2004). "Composition and evolution of ore fluids in a magmatic-hydrothermal skarn deposit." <u>Geology</u> **32**(2): 117-120.
- Barnes, S.-J. and P. C. Lightfoot (2005). Formation of magmatic nickel sulfide deposits and processes affecting their copper and platinum group element contents. J. W. T. Hedenquist, John F H; Goldfarb, Richard J; Richards, Jeremy P, Society of Economic Geologists, Littleton, CO, United States (USA): 179-213.
- Bowen, N. L. (1928). "The evolution of igneous rocks." Princeton University Press. 334 p.
- Burnham, C. W. and N. F. Davis (1974). "The role of H₂O in silicate melts; II, Thermodynamic and phase relations in the system NaAlSi₃O₈-H₂O to 10 kilobars, 700 degrees to 1100 degrees C." <u>American Journal of Science</u> **274**(8): 902-940.
- Camus, G., A. Gourgaud, Mossand-Berthommier, P. C., Vincent, P. M. (2000). "Merapi (central Java, Indonesia); an outline of the structural and magmatological evolution, with a special emphasis to the major pyroclastic events." <u>Journal of Volcanology and Geothermal Research</u> **100**(1-4): 139-163.
- Candela, P. A. and H. D. Holland (1984). "The partitioning of copper and molybdenum between silicate melts and aqueous fluids." <u>Geochimica et Cosmochimica Acta</u> **48**(2): 373-380.
- Candela, P. A. and Picolli, P. M. (1995). Model ore-metal partitioning from melts into vapor and vapor/brine mixtures. <u>Magmas, fluids, and ore deposits</u>. J. F. H. Thompson. Victoria, British Columbia. 23: 101-127.

- Candela, P. A. and P. M. Piccoli (2005). <u>Magmatic processes in the development of porphyry-type ore systems</u>. United States, Society of Economic Geologists: Littleton, CO, United States: 25-37.
- Chadwick, J. P., Troll, V. R., Ginibre, C., Morgan, D., Gertisser, R., Waight, T. E., Davidson, J. P. (2007). "Carbonate assimilation at Merapi Volcano, Java, Indonesia; insights from crystal isotope stratigraphy." <u>Journal of Petrology</u> **48**(9): 1793-1812.
- Chadwick, J. P., Troll, C.G., Ginibre, C., Morgan, D., Gertisser, R., Waight, T., Davidson, J.P. (2005). "Magma crust interaction at Merapi volcano, Java, Indonesia: insights from in situ analyses." <u>Irish Journal of Earth Sciences</u> **23**: 128.
- Crerar, D., Wood, S., Brantley, S., Bocarsly, A. (1985). "Chemical controls on solubility of ore-forming minerals in hydrothermal solutions." <u>The Canadian Mineralogist</u> **23**(3): 333-352.
- Deino, A. and J. D. Keith (1997). "Ages of volcanic and intrusive rocks in the Bingham mining district, Utah." <u>Guidebook Series (Society of Economic Geologists (U. S.)</u> **29**: 91-100.
- DePaolo, D. J. (1981). "Trace element and isotopic effects of combined wallrock assimilation and fractional crystallization." <u>Earth and Planetary Science Letters</u> **53**(2): 189-202.
- Eichelberger, J. C. (1975). "Origin of andesite and dacite; evidence of mixing at Glass Mountain in California and at other Circum-Pacific volcanoes."

 <u>Geological Society of America Bulletin 86(10)</u>: 1381-1391.
- Eichelberger, J. C., R. Gooley, Nitsan, U., Rice, A. (1976). "A mixing model for andesitic volcanism." <u>Eos, Transactions, American Geophysical Union</u> **57**(12): 1024.
- Gertisser, R. and Keller J. (2003a) "Temporal variations in magma composition at Merapi Volcano (Central Java, Indonesia): magmatic cycles during the past 2000 years of explosive activity." <u>Journal of Volcanology and Geothermal research</u> **123**: 1-23.

- Gertisser, R. and Keller J. (2003b) "Trace element and Sr, Nd, Pb, O isotope variations in medium-K and high-K volcanic rocks from Merapi volcano, Central Java, Indonesia: Evidence for the involvement of subducted sediments in Sunda Arc magma genesis." <u>Journal of Petrology</u> **44**(3): 457-489.
- Grove, T. L. (2000). Origin of magmas. <u>Encyclopedia of Volcanoes</u>. H. Sigurdsson, Academic Press: 133-147.
- Halter, W. E., C. A. Heinrich, Pettke, T., Bierlein, F. P., Foster, D. A., Gray, D. R.,
 Davidson, G. J. (2005). "Magma evolution and the formation of porphyry
 Cu-Au ore fluids; evidence from silicate and sulfide melt inclusions."
 Mineralium Deposita 39(8): 845-863.
- Halter, W. E., T. Pettke, Heinrich, C. A. (2002). "The origin of Cu/Au ratios in porphyry-type ore deposits." <u>Science</u> **296**(5574): 1844-1846.
- Halter, W. E., T. Pettke, Heinrich, C. A. (2004). "Laser-ablation ICP-MS analysis of silicate and sulfide melt inclusions in an andesitic complex; I, Analytical approach and data evaluation." <u>Contributions to Mineralogy and Petrology</u> **147**(4): 385-396.
- Hammer, J. E., K. V. Cashman, Voight, B. (2000). "Magmatic processes revealed by textural and compositional trends in Merapi dome lavas." <u>Journal of Volcanology and Geothermal Research</u> **100**(1-4): 165-192.
- Hedenquist, J. W. and J. B. Lowenstern (1994). "The role of magmas in the formation of hydrothermal ore deposits." <u>Nature</u> **370**(6490): 519-527.
- Hedenquist, J. W., Arribas, A. Jr., Reynolds, T. J. (1998). "Evolution of an intrusion-centered hydrothermal system; Far Southeast-Lepanto porphyry and epithermal Cu-Au deposits, Philippines." <u>Economic Geology and the Bulletin of the Society of Economic Geologists</u> **93**(4): 373-404.
- Heinrich, C. A., D. Guenther, Audetat, A., Ulrich, T., Frischknecht, R. (1999). "Metal fractionation between magmatic brine and vapor, determined by microanalysis of fluid inclusions." <u>Geology</u> **27**(8): 755-758.

- Hildreth, W. and S. Moorbath (1988). "Crustal contributions to arc magmatism in the Andes of central Chile." <u>Contributions to Mineralogy and Petrology</u> **98**(4): 455-489.
- Huppert, H. E., R. S. J. Sparks, et al. (1986). "Replenishment of magma chambers by light inputs." <u>Journal of Geophysical Research</u> 91(B6): 6113-6122.
- Kavalieris, I. (1994). "High Au, Ag, Mo, Pb, V and W content of fumarolic deposits at Merapi volcano, central Java, Indonesia." <u>Journal of Geochemical Exploration</u> **50**: 479-491.
- Keith, J. D., R. D. Dallmeyer, Kim, C.-S., Kowallis, B. J. (1991). The volcanic history and magmatic sulfide mineralogy of latites of the central East Tintic Mountains, Utah. Geology and ore deposits of the Great Basin; Symposium Proceedings: 461-483.
- Keith, J. D., J. A. Whitney, Hattori, K., Ballantyne, G. H., Christiansen, E. H., Barr, D. L., Cannan, T. M., Hook, C. J. (1997). "The role of magmatic sulfides and mafic alkaline magmas in the Bingham and Tintic mining districts, Utah." <u>Journal of Petrology</u> 38(12): 1679-1690.
- Klemm, L. M., T. Pettke, Heinrich, C. A., Campos, E. (2007). "Hydrothermal evolution of the El Teniente Deposit, Chile; porphyry Cu-Mo ore deposition from low-salinity magmatic fluids." <u>Economic Geology and the Bulletin of the Society of Economic Geologists</u> **102**(6): 1021-1045.
- Klemm, L. M., T. Pettke, et al. (2008). "Fluid and source magma evolution of the Questa porphyry Mo deposit, New Mexico, USA." <u>Mineralium Deposita</u> **43**(5): 533-552.
- Kouzmanov, K., T. Pettke, Heinrich, C. A., Bodnar, R., Cline, J. (2010). "Direct analysis of ore-precipitating fluids; combined IR microscopy and LA-ICP-MS study of fluid inclusions in opaque ore minerals." <u>Economic Geology</u> and the Bulletin of the Society of Economic Geologists **105**(2): 351-373.
- Landtwing, M. R., T. Pettke, Halter, W. E., Heinrich, C. A., Redmond, P. B., Einaudi, M. T., Kunze, K. (2005). "Copper deposition during quartz dissolution by cooling magmatic-hydrothermal fluids; the Bingham porphyry." Earth and Planetary Science Letters **235**(1-2): 229-243.

- Larocque, A. C. L., J. A. Stimac, Keith, J. D., Huminicki, M. A. E. (2000). "Evidence for open-system behavior in immiscible Fe-S-O liquids in silicate magmas; implications for contributions of metals and sulfur to oreforming fields." The Canadian Mineralogist 38(5): 1233-1250.
- Le Guern, F. and Bernard A. (1982). "A new method for sampling and analyzing volcanic sublimates application to Merapi volcano." <u>Journal of Volcanology and Geothermal research</u> **12**: 133-146.
- Longo, A. A., Teal, L. (2005). A summary of the volcanic stratigraphy and the geochronology of magmatism and hydrothermal activity in the Yanacocha gold district, northern Peru. <u>Symposium 2005: Window to the world</u>. H. N. Rhoden, Steininger, R.C., and Vikre, P.G., eds. **V.2:** 797-808.
- Meinert, L. D., G. M. Dipple, et al. (2005). World skarn deposits. <u>Economic Geology</u>; one hundredth anniversary volume, 1905-2005. J. W. T. Hedenquist, John F H; Goldfarb, Richard J; Richards, Jeremy P, Society of Economic Geologists, Littleton, CO, United States (USA): 299-336.
- Nadeau, O., Williams-Jones, A. E., Stix, J. (2010). "Sulphide magma as a source of metals in arc-related magmatic hydrothermal ore fluids." <u>Nature</u> Geoscience **3**(7): 501-505.
- Naldrett, A. J. (2004). <u>Magmatic sulfide deposits; geology, geochemistry and</u> exploration, Springer-Verlag, Berlin, Federal Republic of Germany (DEU).
- Newhall, C. G., S. Bronto, Alloway, B. V., Banks, N. G., Bahar, I., del Marmol, M. A., Hadisantono, R. D., Holcomb, R. T., McGeehin, J. P., Miksic, J. N., Rubin, Meyer, Sayudi, D. S., Sukhyar, R., Andreastuti, S. D., Tilling, R. I., Torley, R., Trimble, D. A., Wirakusumah, A. D. (2000). "10,000 years of explosive eruptions of Merapi Volcano, central Java; archaeological and modern implications." <u>Journal of Volcanology and Geothermal Research</u> 100(1-4): 9-50.
- Pearson, R. G. (1963). "Hard and soft acids and bases." <u>Journal of the American</u> <u>Chemical Society</u> **85**: 3533-3539.
- Pudack, C., Halter, W. E., Heinrich, C. A., and Pettke, T. (2009). "Evolution of magmatic vapor to gold-rich epithermal liquid; the porphyry to epithermal

- transition at Nevados de Famatina, northwest Argentina." <u>Economic Geology and the Bulletin of the Society of Economic Geologists</u> **104**(4): 449-477.
- Quisefit, J. P., Toutain J.P., Bergametti G., Javoy M., Cheynet B., Person A. (1989). "Evolution versus cooling of gaseous volcanic emissions from Momotombo Volcano, Nicaragua: Thermochemical model and observations." Geochimica et Cosmochimica Acta 53: 2591-2608.
- Roedder, E. (1984). <u>Fluid Inclusions</u>, Ribbe, P. H. ed. Mineralogical Society of America. Reviews in Mineralogy, v. 12, 646 p.:
- Rusk, B. G., M. H. Reed, Dilles, J. H., Klemm, L. M., and Heinrich, C. A. (2004).
 "Compositions of magmatic hydrothermal fluids determined by LA-ICP-MS of fluid inclusions from the porphyry copper-molybdenum deposit at Butte, MT." Chemical Geology 210(1-4): 173-199.
- Seedorff, E., Dilles, J. H., Proffett, J. M., Jr., Einaudi, M. T., Zurcher, L., Stavast, W. J. A., Johnson, D. A., and Barton, M. D. (2005). Porphyry deposits; characteristics and origin of hypogene features. <u>Economic Geology; one hundredth anniversary volume</u>, 1905-2005. J. W. T. Hedenquist, John F H; Goldfarb, Richard J; Richards, Jeremy P, Society of Economic Geologists, Littleton, CO, United States (USA).
- Seo, J. H., Guillong, M., and Heinrich, C. A. (2009). "The role of sulfur in the formation of magmatic-hydrothermal copper-gold deposits." <u>Earth and Planetary Science Letters</u> **282**(1-4): 323-328.
- Seward, T. M. and H. L. Barnes (1997). "Metal transport by hydrothermal ore fluids." <u>Geochemistry of hydrothermal ore deposits</u>. H. L. Barnes, John Wiley and Sons Inc.: 465-486.
- Seward, T. M., Rickard, D. T., and Wickman, F. E. (1981). "Metal complex formation in aqueous solutions at elevated temperatures and pressures."

 <u>Physics and Chemistry of the Earth</u> **13-14**: 113-132.
- Sillitoe, R. H. (1973). "The tops and bottoms of porphyry copper deposits."

 <u>Economic Geology and the Bulletin of the Society of Economic Geologists</u> **68**(6): 799-815.

- Sillitoe, R. H. (2010). "Porphyry copper systems." <u>Economic Geology and the</u> Bulletin of the Society of Economic Geologists **105**(1): 3-41.
- Simmons, S. F., White, N. C., and John, D. A. (2005). Geological characteristics of epithermal precious and base metal deposits. <u>Economic Geology; one hundredth anniversary volume, 1905-2005</u>. J. W. T. Hedenquist, John F H; Goldfarb, Richard J; Richards, Jeremy P, Society of Economic Geologists, Littleton, CO, United States (USA) 455-522.
- Symonds, R. B., Reed M.H. (1987a). <u>Thermodynamic calculations of trace species in volcanic gases: new insight on gas geochemistry</u>. International union of geodesy and geophysics (IUGG); XIX general assembly.
- Symonds, R. B., Rose W.I., Reed M.H., Lichte F.E. (1987b). "Volatilization, transport and sublimation of metallic and non-metallic elements in high temperature gases at Merapi Volcano, Indonesia." <u>Geochimica et Cosmochimica Acta</u> 51: 2083-2101.
- Symonds, R. B., Reed M.H., Rose W.I. (1992). "Origin, speciation, and fluxes of trace-element gases at Augustine volcano, Alaska: Insights into magma degassing and fumarolic processes." <u>Geochimica et Cosmochimica Acta</u> **56**: 633-657.
- Symonds, R. B., Reed M.H. (1993a). "Calculation of multicomponent chemical equilibria in gas-solid-liquid systems: calculation methods, thermochemical data, and applications to studies of high-temperature volcanic gases with example from Mount St. Helens." <u>American Journal</u> of Science **293**: 758-864.
- Symonds, R. B. (1993b). "Scanning electron microscope observations of sublimates from Merapi Volcano, Indonesia." <u>Geochemical Journal</u> **26**: 337-350.
- Symonds, R. B., Rose W.I., Bluth G.J.S., Gerlach T.M. (1994). Volcanic-gas studies: Methods, results, and applications. <u>Volatiles in Magma</u>. M. S. o. America. Reviews in Mineralogy, **30:** 1-66.

- Ulrich, T., Guenther, D., and Heinrich, C. A. (1999). "Gold concentrations of magmatic brines and the metal budget of porphyry copper deposits." Nature 399(6737): 676-679.
- Ulrich, T., Guenther, D., and Heinrich, C. A. (2001). "The evolution of a porphyry Cu-Au deposit, based on LA-ICP-MS analysis of fluid inclusions; Bajo de la Alumbrera, Argentina." <u>Economic Geology and the Bulletin of the Society of Economic Geologists</u> **96**(8): 1743-1774.
- Wahrenberger, C., Seward T.M., Dietrich V. (2002). Volatile trace-element transport in high-temperature gases from Kudryavy volcano (Iturup, Kurile Islands, Russia. <u>A tribute to A. Crerar.</u> R. H. a. S. A. Wood, The Geochemical Society. **Special Publication No. 7:** 307-327.
- Webster, J. D. and C. W. Mandeville (2007). "Fluid immiscibility in volcanic environments." Reviews in Mineralogy and Geochemistry **65**(1): 313-362.
- White, N. C. and J. W. Hedenquist (1990). "Epithermal environments and styles of mineralization; variations and their causes, and guidelines for exploration." <u>Journal of Geochemical Exploration</u> **36**(1-3): 445-474.
- White, N. C. and J. W. Hedenquist (1995). "Epithermal gold deposits; styles, characteristics and exploration." <u>SEG Newsletter</u> **23**: 9-13.
- Williams-Jones, A. E. and C. A. Heinrich (2005). "Vapor transport of metals and the formation of magmatic-hydrothermal ore deposits." <u>Economic Geology and the Bulletin of the Society of Economic Geologists</u> **100**(7): 1287-1312.
- Williams-Jones, A. E., Migdisov A.A., Archibald S.M., Xiao Z. (2002). Vaportransport of ore metals. <u>A tribute to A. Crerar</u>. R. H. a. S. A. Wood, The geochemical Society. Special Publication No. 7: 279-305.
- Williams-Jones, A. E., Samson, I.M., Ault, K.M., Gagnon, J.E., Fryer, B.J. (2010).
 "The Genesis of Distal Zinc Skarns; Evidence from the Mochito deposit,
 Honduras." Economic Geology and the Bulletin of the Society of
 Economic Geologists, v. 105, no. 8, p. 1411-1440.
- Wilson, M. (1989). <u>Igneous Petrogenesis</u>. Springer Inc. 466 p.

Zajacz, Z., W. E. Halter, Pettke, T., and Guillong, M. (2008). "Determination of fluid/melt partition coefficients by LA-ICPMS analysis of co-existing fluid and silicate melt inclusions; controls on element partitioning."

<u>Geochimica et Cosmochimica Acta</u> 72(8): 2169-2197.

Preface to chapter 1

In the first main chapter of this thesis, which is a scientific article published in a peer-review journal (Nadeau et al., 2010), we build on previous work by Keith et al. (1991, 1997), Larocque et al. (2000) and Halter et al. (2002, 2005) who have shown that magmatic volatile phases may acquire their metal content by dissolution of an immiscible sulfide melt which must have previously exsolved from the magma. By comparing sulfide melt inclusions from megacrysts found in scorias erupted at Merapi and volcanic gases emitted immediately after an explosive eruption at Merapi, we conclude that injections of reduced, sulfide-saturated mafic magmas into shallower resident magma lead to dissolution of the sulfide melt and degassing of its consituents through the magmatic-hydrothermal system to the atmosphere. We generalize these findings to other arc-related magmatic-hydrothermal systems where magma injections are (a) sufficiently reduced to allow the unmixing of a sulfide melt, and (b) volatile-saturated to allow dissolution of the sulfide melt and subsequent degassing to take place.

Chapter 1

Sulphide Magma as a Source of Metals in Arc-Related Magmatic Hydrothermal Ore Fluids

Olivier Nadeau, Anthony E. Williams-Jones and John Stix

Manuscript published in Nature Geoscience, 2010, vol. 3, iss. 7, p. 501-505

As magma ascends in subduction zones, decreasing pressure and temperature cause it to separate into two or more phases in a process known as exsolution. Hydrothermal ore fluids and metal-rich sulfide melts may be products of this exsolution. Conventionally, the ore fluids are thought to acquire their metal content directly from the parent magma. However, it is probable that the ore fluids and sulfide melts interact after exsolution, and therefore possible that the sulfide melts are a major source of metals for the ore fluids. Here we use petrographic analyses of erupted sulfide melts and compositional analyses of volcanic gases emitted immediately after an eruption at Merapi Volcano, Indonesia, to show that magmatic hydrothermal fluids can derive their metals from dissolution of sulfide melts. The volcanic gases exhibit metal ratios that are comparable to those in the erupted sulfide melts. Furthermore, gases sampled immediately after the eruption have metal concentrations orders of magnitudes higher than those of gases emitted during periods of quiescence. We propose that the metal content of ores forming in volcanic arc environments is established by exsolution accompanying injections of mafic magma immediately prior to explosive eruptions.

Mafic magmas commonly exsolve appreciable quantities of iron sulfide melt containing significant proportions of Cu, Ni and Co. As the sulfide melt cools, it first crystallizes a Fe-Ni monosulfide solid solution (MSS), then a Curich intermediate solid solution (ISS). The MSS subsequently converts to pyrrhotite via exsolution of pentlandite, while the ISS unmixes to form chalcopyrite and cubanite (O'Neil and Mavrogenes, 2002; Naldrett, 1989; 2004; Barnes and Lightfoot, 2005; Mungall, 2007). In subduction zones, these magmas are typically volatile rich (Johnson et al, 1994; Arculus, 2004) and, as the solubility of the most abundant magmatic volatile species (H₂O and CO₂) is directly proportional to pressure (Holloway and Blank, 1994), decompression of such magmas will inevitably result in exsolution of a magmatic hydrothermal fluid. If this fluid interacts with the sulfide melt or its crystallized products, it is likely that the sulfide melt will undergo substantial dissolution, leading to incorporation of major quantities of copper, iron, and possibly some cobalt and nickel in the hydrothermal fluid. Indeed, observations of partly decomposed

sulfide globules in volcanic rocks from the Tintic and Bingham mining districts and comparisons of their compositions to those of the bulk ores have led to precisely this conclusion, namely that a crystallized sulfide melt was dissolved into a magmatic hydrothermal phase to produce the metalliferous fluids responsible for ore formation in the district (Keith et al., 1991; Keith et al., 1997; Larocque et al., 2000). The nature of oxide globules in arc volcanoes and their textural relationships to sulfide globules have led to speculation that the former might represent sulfide melt stripped of sulfur and chalcophile elements (e.g., Cu and Au) by magmatic hydrothermal fluids during injection of reduced, sulfide-bearing mafic magma into oxidized felsic magma (Keith et al., 1991; Keith et al., 1997; Larocque et al., 2000). A similar conclusion was reached for the Bajo de la Alumbrera porphyry Cu-Au deposit, Argentina, based on the observation that sulfide melt inclusions, fluid inclusions and the bulk ore have similar Cu/Au ratios (Halter et al., 2002; 2005).

In this paper, we report results of a study of sulfide and silicate melt inclusions occurring in mafic scoria and more evolved lava dome material collected from the flanks of Merapi volcano, Indonesia, and of volcanic gases sampled near its summit (information on the geological setting of Merapi Volcano is linked to the online version of this paper at www.nature.com/nature and is provided in appendix 1 of this thesis chapter). Using textural relationships among sulfide melt, silicate melt and fluid inclusions, we show that there was widespread and intense dissolution of sulfide melt inclusions in both mafic and more evolved samples; in the latter, sulfide melt inclusions were also oxidized. We then compare the composition of the sulfide melt to those of volcanic gas condensates sampled during quiescent periods (in 1984 (Symonds et al., 1987), 2004, 2005) and immediately after an explosive eruption (2006). These data show that the metal ratios of the volcanic gases sampled in 2006 are remarkably similar to those of the sulfide melt, and that the copper and sulfur contents of the gases are at least an order of magnitude higher than for the other sampling periods. Based on the above observations, we develop a model in which the volcanic gases acquire their metal content immediately prior to explosive volcanic eruptions as a result of interaction of exsolving hydrothermal fluids with sulfide-saturated mafic magma injected into more oxidized felsic magma.

1. Sulfide dissolution in scoria and sulfide oxidation in dome lavas

Scoria samples host mafic melt inclusions (SiO₂ 52.5-61 wt.% anhydrous), numerous sulfide melt inclusions (up to 500 μ m in diameter) and fluid inclusions in megacrysts of amphibole and clinopyroxene (up to 2.5 cm in length). These observations indicate that the scoria samples represent an explosive event originating relatively deep in the magma chamber. By contrast, samples of lava dome material, representing much shallower volcanic activity, host felsic melt inclusions (61-72 wt.% SiO₂ anhydrous) and small numbers of partially to completely oxidized sulfide inclusions (\leq 100 μ m in diameter) in phenocrysts of clinopyroxene, plagioclase, titanomagnetite and partly corroded and resorbed amphibole.

The sulfide melt inclusions in the scoria samples crystallized to pyrrhotite, cubanite and an unidentified Cu-bearing mineral (Table 1). Some of these inclusions also contain silicate glass and bubbles representing former pockets of fluid that were opened during grinding and polishing. Photomicrographs of partly reacted sulfide globules in contact with bubbles formerly occupied by an aqueous phase provide incontrovertible evidence of sulfides at different stages of dissolution by a hydrothermal fluid (Fig. 1). These inclusions are interpreted to represent heterogeneous entrapment of coexisting silicate melt, sulfide melt and aqueous fluid (Fig. 1a). In some cases, there is evidence that the sulfide melt was almost completely dissolved by aqueous fluid after entrapment and after crystallization. Figure 1b shows an inclusion in which remnants of sulfide define the boundary of a former sulfide globule that was largely dissolved. This inclusion also contains vesiculated silicate melt and is surrounded by open channels that extend from the inclusion to the edges of the host crystal. These observations are consistent with decompression of ascending magma, exsolution of an aqueous phase, and overpressure-induced hydrofracturing, which created pathways for

fluid infiltration. We doubt that vesiculation within the inclusion would have produced sufficient fluid to dissolve the comparatively large sulfide globule. Instead, we propose that dissolution of the sulfide globule was effected by a much larger volume of aqueous fluid introduced along these new pathways from a much larger body of vesiculating magma. This interpretation is supported by the absence of sulfide in the groundmass of the scoria and by the observation that in the few cases where the sulfide largely escaped dissolution, e.g., the inclusion in Figure 1a, fractures surrounding the inclusions are conspicuously absent.

Apart from their smaller size, the sulfide inclusions in lava dome material are indistinguishable from those in scoria, except where oxidized. However, they do not show evidence of the extensive dissolution that characterizes scoria-hosted sulfide melt inclusions. These oxidized inclusions contain sulfide (pyrrhotite) surrounded by magnetite and/or hematite (e.g., Fig. 2a). In some cases, they contain pyrrhotite, magnetite and pyrite (Fig. 2b). This indicates an increase in the oxidation state of iron from +2 in pyrrhotite to +3 in magnetite (part of the iron remains in the +2 state), and of sulfur from -2 in pyrrhotite to -1 in pyrite. Observations of textural relations among pyrrhotite, pyrite, and magnetite in these inclusions suggest reactions of the type:

$$3 \text{ FeS}_{(s)} + 3 \text{ H}_2\text{O} + 0.5 \text{ O}_2 \qquad \Rightarrow \qquad \text{Fe}_3\text{O}_{4(s)} + 3 \text{ H}_2\text{S}_{(gas)}$$
 (1)

$$3 \text{ FeS}_{(s)} + 5 \text{ O}_2$$
 \rightarrow $\text{Fe}_3\text{O}_{4(s)} + 3 \text{ SO}_{2(gas)}$ (2)

$$4 \text{ FeS}_{(s)} + 2 \text{ H}_2\text{O} + \text{O}_2$$
 \Rightarrow $\text{FeS}_{2(s)} + \text{Fe}_3\text{O}_{4(s)} + 2 \text{ H}_2\text{S}_{(gas)}$ (3)

$$4 \text{ FeS}_{(s)} + 4 \text{ O}_2$$
 \rightarrow $\text{FeS}_{2(s)} + \text{Fe}_3 \text{O}_{4(s)} + 2 \text{ SO}_{2(gas)}$ (4)

Whether the oxidation produced a mixture of oxide mineral and pyrite or oxide mineral alone would have depended on the ambient fO_2 , the activity of sulfur species and temperature. At high fO_2 and low activity of sulfur species, reactions 1 and 2 would be favored, whereas at lower fO_2 or high activity of sulfur species, reactions 3 and 4 would be favored. In both cases, oxidation is promoted by degassing, which removes H_2S and SO_2 from the system, driving the above reactions to the right. We propose that oxidation was favored wherever sulfide

inclusions were breached and exposed to hydrothermal fluid, and that this effect was most marked in the shallow parts of the system where cooling was strongest (favoring the right hand side of reactions 1 to 4). This explains the observation that oxidized sulfide melt inclusions occur predominantly in dome lavas, implying that there was significant associated transfer of sulfur and metals, particularly chalcophile metals such as Cu, to the hydrothermal fluid.

2. Sulfide melt composition

A total of 76 sulfide melt inclusions were analyzed chemically using an electron microprobe. Five of these inclusions from three different samples showed no evidence of dissolution or oxidation, and were sufficiently large for reliable analysis of their constituent phases. These inclusions ranged from spherical to ellipsoidal in shape and contained pyrrhotite and a Cu-rich phase in mean volumetric proportions of 81 ± 7 and 19 ± 7 , respectively. The proportions were calculated from measurements of phase areas in plan view representing sections through the inclusions at different orientations. The compositions of the pyrrhotite and the Cu-rich phase in these inclusions were weighted by these proportions to obtain the bulk composition of each inclusion. The mean of these compositions was used to represent that of the sulfide melt. (Supplementary information on methods is linked to the online version of this paper at www.nature.com/nature and is provided in the appendix 2 of this thesis chapter). Based on this calculation, the sulfide melt was estimated to contain approximately 54.3 wt. % Fe, 38.2 wt. % S, 5.2 wt. % Cu, 2200 ppm Co and 2307 ppm Ni, and a few hundred ppm of Mo and Ti (Table 1). The calculated bulk compositions of the five sulfide melt inclusions are shown on Figure 3.

3. Volcanic gases

Fumarolic gases were sampled at Merapi in 1984 (Symonds et al., 1987), 2004, 2005 and 2006 (this study). Until 2006, fumaroles were concentrated in three

fields, Gendol, Woro and Dome. However, the Gendol field was destroyed by the eruption of 2006, and the Dome field was too dangerous to sample. From observations made in 2004, temperatures in the Gendol field ranged from about 515°C to a high of 754°C. Temperatures in the Woro field were much lower, with a maximum of 572°C. The values of $\delta^{18}O$ and δD of H_2O in gas condensates collected in 2004 show that gases exiting the Gendol field had a composition close to that of 'andesitic water', whereas those released at Woro contained a larger proportion of meteoric water (Appendix 3).

As the trace element concentrations of volcanic gases will differ from one field to another because of different degrees of dilution by groundwater and/or interaction with wall rock, and even within the same fumarole field will vary due to differences in temperature and cooling-induced sublimation of minerals, individual fumarole analyses are treated separately. The concentrations of Fe, Cu, Ni, and Co in the gases in 1984, 2004, 2005 and 2006 are shown on Figure 3. Three of these sampling periods, namely 1984, 2004 and 2005, were two to three years after an eruption and thus represent periods of volcanic quiescence, whereas sampling in 2006 took place only weeks after a relatively large explosive event. As expected from the preceding discussion, the data vary considerably. However, concentrations of Cu in the 2006 gases from the Woro field are more than an order of magnitude greater than the highest concentration measured at either Woro or Gendol in previous years; the concentrations of Co are also substantially higher. Moreover, the Fe/Cu, Ni/Cu and Co/Cu ratios of the Woro 2006 gases are very similar to those of the sulfide melt, whereas the Fe/Cu (with one exception) and Ni/Cu ratios of gases measured in 1984, 2004 and 2005 (Gendol and Woro) are generally 10 to 100 times higher. Finally, the Woro gases sampled in 2006 were much more enriched in sulfur than in preceding years; only one sample from the Gendol field contained as high a proportion of sulfur (Fig. 4).

4. Significance of the volcanic gas metal signature

The common occurrence of numerous large, partially to nearly dissolved sulfide melt inclusions associated with vesiculated mafic silicate melt and aqueous fluid inclusions provides compelling evidence for 1) widespread immiscibility of sulfide melt and mafic silicate melt and 2) dissolution of sulfide melt by a magmatic hydrothermal fluid. Furthermore, the similarity of the Fe/Cu, Ni/Cu and Co/Cu ratios of the sulfide melt and volcanic gases sampled in 2006 strongly suggests that the signature of this dissolution is preserved in the composition of the volcanic gases, but only if sampled near the time of an explosive volcanic eruption. This signature is expressed most strongly by very large increases in the proportions of sulfur and the chalcophile element, copper, which, after iron and sulfur, is the most important constituent of the sulfide melt. At times of quiescent degassing, i.e., in 1984, 2004 and 2005, the concentration of Fe was, on average, higher than in 2006, which likely reflects its high concentration in the silicate magma and wall rock, as well as its preference to form complexes with chlorine rather than sulfur in the aqueous phase (Crerar et al., 1985). The failure of the Ni concentration to increase during the 2006 eruption is more difficult to explain. However, the high-temperature precipitation from the 2004 gases of an unidentified mineral with the stoichiometry FeNiS, and smythite [(Fe,Ni)₉S₁₁] from the 2006 gases (Nadeau et al., under review, chapter 3 of the present thesis), suggests that the Ni concentration in the gas may have been limited by mineral saturation. The substantial increase in Co concentration in the 2006 gases, on the other hand, indicates that its concentration was not limited by mineral saturation. This is not unexpected, given that its concentration in gases sampled in previous years was an order of magnitude lower than that of Ni, despite the similar chemical behavior of the two metals. Furthermore, no Co-bearing mineral was identified in sublimates of fumarole gases sampled in 2004 and 2006.

We calculate that the amount of sulfide required to produce the concentrations of metals observed in the 2006 volcanic gases is trivial, approximately 8 grams sulfide melt per ton of gas. Although our data point

strongly to sulfide melt as the source of Cu, Co and Ni in the volcanic gas, we have also examined the possibility that these metals were supplied directly by the silicate melt, by evaluating the results of analyses of Cu, Co and Ni in silicate melt inclusions (Nadeau et al., under review, chapter 2 of the present thesis). Mafic melt inclusions contain an average of 25 ppm Cu and 13 ppm Co corresponding to a Co/Cu ratio of 0.52, whereas felsic melt inclusions contain an average of about 60 ppm Cu and 7 ppm Co, corresponding to a Co/Cu ratio of 0.12 (Fig. 3). By comparison, the Co/Cu ratio of the two gas samples analyzed in 2006 was 0.05 and 0.17, and that of the sulfide melt ranged from 0.02 to 0.05. The concentration of Ni in the melt inclusions was below the level of detection. The comparatively high Co/Cu ratio of the mafic melt inclusions rules out the mafic magma as a possible source of the metals. The felsic silicate melt could have acted as a source for the metals, if there was congruent dissolution of the melt by the magmatic hydrothermal fluid, or if the partition coefficients for Cu and Co between melt and magmatic hydrothermal fluid were similar. The former is highly unlikely because silicate melts dissolve incongruently. There are no published partition coefficients for Co between melt and aqueous fluid. However, as a siderophile element, Co is likely to behave similarly to Fe, for which partitioning data are available (Zajacz et al., 2008). These data suggest that Fe has similar preference for melt and aqueous fluid, whereas Cu has a strong preference for the aqueous fluid; experimentally determined partition coefficients for Cu may exceed 100 in moderately saline fluids (Williams et al., 1995). We therefore predict that the Co/Cu ratio of a fluid equilibrating with a silicate melt will be one to two orders of magnitude lower than that of Woro fumarolic gases in 2006. This prediction and our failure to detect Ni in both felsic and mafic silicate melt inclusions allow us to exclude silicate magma as the main source of the metals.

The abundance of large sulfide melt inclusions in scoria and their association with mafic silicate melt inclusions, as well as their much lower abundance and smaller size associated with felsic silicate inclusions in lava dome material, suggest that mafic magma was the principal source of the sulfide melt. This conclusion is supported by the observation that mafic magmas commonly

exsolve quantities of sulfide melt sufficient to form magmatic ore deposits, whereas this is never the case for felsic magmas. However, the magma resident at relatively shallow levels in the volcanic edifice at Merapi and responsible for current dome formation is more evolved in composition. Based on its association with magnetite-hematite-altered sulfide inclusions, this evolved magma is relatively oxidizing. In view of this and our conclusion that the constituents of the sulfide melt are transferred to the volcanic gas mainly during explosive eruptions, we therefore propose that our melt inclusion data reflect the upward injection and decompression of a sulfide-saturated mafic magma that interacted with more evolved and oxidizing resident magma. We further propose that such injections trigger massive hydrothermal fluid exsolution, extensive sulfide dissolution and metal transfer, fluid overpressure, and ultimately explosive eruptions. These processes can occur on a timescale of weeks to months.

The results of this study serve to explain the origin of the metals and sulfur present in magmatic hydrothermal fluids in arc settings. They also explain why magmatic sulfide ore deposits typically do not form in this environment. Unlike continental rift-related mafic magmas that give rise to magmatic sulfide deposits, arc magmas are hydrous and oxidizing. This leads to the dissolution of magmatic sulfides and the transport of metals and sulfur in an aqueous hydrothermal phase. Thus, instead of hosting magmatic sulfide deposits, magmatic arcs are host mainly to magmatic hydrothermal deposits, e.g., porphyry and epithermal deposits, which also ultimately owe their origin to immiscible sulfide melts. Volcanic gases such as those released by Merapi volcano record the signature of the fluids that are currently forming such deposits beneath active arc volcanoes.

Acknowledgements

Reviews by J. Mungall, M. J. Rutherford and B. Scaillet contributed significantly to improving the manuscript. This study was funded by scholarships to ON by the Natural Sciences and Engineering Research Council (NSERC) and

the Fond Québécois de la Recherche sur la Nature et les Technologies (FQRNT), and research grants to AEWJ and JS from NSERC and FQRNT.

References

- Arculus, R. J. Evolution of arc magmas and their volatiles. *Geophys. Monogr.* 150, 95-108 (2004).
- Barnes, S.-J. & Lightfoot, P. C. Formation of magmatic nickel sulfide deposits and processes affecting their copper and platinum group element contents. 179-213 (Society of Economic Geologists, Littleton, 2005).
- Crerar, D., Wood, S., Brantley, S. & Bocarsly, A. Chemical controls on solubility of ore-forming minerals in hydrothermal solutions. *Can. Mineral.* 23, 333-352 (1985).
- Halter, W. E., Pettke, T. & Heinrich, C. A. The origin of Cu/Au ratios in porphyry-type ore deposits. *Science* 296, 1844-1846 (2002).
- Halter, W. E. Halter, W. E., Heinrich, C. A., Pettke, T., Bierlein, F. P., Foster, D. A., Gray, D. R., Davidson, G. J. Magma evolution and the formation of porphyry Cu-Au ore fluids; evidence from silicate and sulfide melt inclusions. *Miner. Deposita.* 39, 845-863 (2005).
- Holloway, J. R. & Blank, J. G. Application of experimental results to C-O-H species in natural melts. *Rev. Mineral.* 30, 187-230 (1994).
- Johnson, M. C., Anderson, A. T., Jr. & Rutherford, M. J. Pre-eruptive volatile contents of magmas. *Rev. Mineral.* 30, 281-330 (1994).
- Keith, J. D., Dallmeyer, R. D., Kim, C.-S. & Kowallis, B. J. The volcanic history and magmatic sulfide mineralogy of latites of the central East Tintic Mountains, Utah. 461-483 (Geological Society of Nevada, Reno, 1991).
- Keith, J. D., Whitney, J. A., Hattori, K., Ballantyne, G. H., Christiansen, E. H., Barr, D. L., Cannan, T. M., Hook, C. J. The role of magmatic sulfides and mafic alkaline magmas in the Bingham and Tintic mining districts, Utah. *J. Petrol.* 38, 1679-1690 (1997).

- Larocque, A. C. L., Stimac, J. A., Keith, J. D. & Huminicki, M. A. E. Evidence for open-system behavior in immiscible Fe-S-O liquids in silicate magmas; implications for contributions of metals and sulfur to ore-forming fields. *Can. Mineral.* 38, 1233-1250 (2000).
- Mungall, J. E. Crystallization of magmatic sulfides; an empirical model and application to Sudbury ores. *Geochim. Cosmochim. Ac.* 71, 2809-2819 (2007).
- Naldrett, A. J. Sulfide melts; crystallization temperatures, solubilities in silicate melts, and Fe, Ni, and Cu partitioning between basaltic magmas and olivine. *Rev. Econ. Geol.* 4, 5-20 (1989).
- Naldrett, A. J. Magmatic Sulfide Deposits; Geology, Geochemistry and Exploration. (Springer-Verlag, Berlin, 2004).
- O'Neill, H. S. C. & Mavrogenes, J. A. The sulfide capacity and the sulfur content at sulfide saturation of silicate melts at 1400 degrees C and 1 bar. *J. Petrol.* 43, 1049-1087 (2002).
- Symonds, R. B., Rose W.I., Reed M.H., Lichte F.E. Volatilization, transport and sublimation of metallic and non-metallic elements in high temperature gases at Merapi Volcano, Indonesia. *Geochim. Cosmochim. Ac.* 51, 2083-2101 (1987).
- Williams, T. J., Candela, P. A. & Piccoli, P. M. The partitioning of copper between silicate melts and two-phase aqueous fluids; an experimental investigation at 1 kbar, 800 degrees C and 0.5 kbar, 850 degrees C. Contrib. Mineral. Petr. 121, 388-399 (1995).
- Zajacz, Z., Halter, W. E., Pettke, T. & Guillong, M. Determination of fluid/melt partition coefficients by LA-ICPMS analysis of co-existing fluid and silicate melt inclusions; controls on element partitioning. *Geochim. Cosmochim. Ac.* 72, 2169-2197 (2008).

Author Contributions

This paper is the product of research conducted by ON during his Ph.D. ON made the petrographic observations and undertook the chemical analyses. AEWJ participated in the field work and all three authors contributed to the interpretation of the data and to the writing of the manuscript.

Table 1. Compositions of phases in sulfide melt inclusions and the reconstructed composition of the sulfide melt. See text for details.

Sample name	Mineral	Fe (wt%)	S (wt%)	Cu (wt%)	Total	Cu (ppm)	Co (ppm)	Ni (ppm)	Mo (ppm)	Ti (ppm)
WD.1.4(1).1A	Fe ₃ Cu ₂ S ₅ (?)	36.36	35.72	27.52	99.60	275210	300	290	360	270
WD.1.4(1).1B	pyrrhotite	58.85	38.33	0.08	97.25	760	1190	890	390	nd
reconstructed		53.64	37.72	6.44	97.80	64350	984	751	383	nd
WD.3.3(1).12A	cubanite	39.98	35.62	23.47	99.06	234650	1570	80	410	nd
WD.3.3(1).12B	pyrrhotite	53.35	40.60	1.04	94.99	10390	6640	7150	370	nd
reconstructed		51.57	39.93	4.03	95.53	40306	5964	6207	375	nd
WD.3.3(1).14A	cubanite	41.62	35.33	20.96	97.90	209550	1250	1230	380	nd
WD.3.3(1).14B	pyrrhotite	60.27	38.11	0.18	98.56	1840	1480	2110	250	nd
reconstructed		57.87	37.75	2.86	98.48	28635	1450	1996	267	nd
WD.3.3(1).15B	cubanite	41.18	35.43	22.22	98.83	222190	900	220	420	nd
WD.3.3(1).15A	pyrrhotite	60.59	37.99	0.25	98.83	2500	1120	810	350	nd
reconstructed		57.50	37.58	3.74	98.83	37387	1085	716	361	nd
WD.3.4(2).5A	$Fe_3Cu_2S_5$ (?)	35.29	35.11	27.65	98.05	276530	800	840	460	440
WD.3.4(2).5B	pyrrhotite	58.57	39.10	0.06	97.73	570	1850	2340	350	340
reconstructed		51.16	37.83	8.85	97.83	88491	1515	1862	385	372
average sulfide melt		54.35	38.16	5.18	97.69	51834	2200	2307	354	372

average sulfide melt 54.35 38.16 5.18 97.69 51834 2200 2307 354 nd: not detected. Fe₃Cu₂S₅ (?) refers to an unidentified mineral.

Figure 1. Reflected light photomicrographs of variably dissolved sulfide globules hosted by amphibole megacrysts. A) Heterogeneously entrapped sulfide melt, mafic silicate melt (53 wt.% SiO₂) and aqueous fluid (released during sample preparation). The original margins of the sulfide melt and outlines of the minerals crystallized from it are identified by dotted lines. B) A vesiculated silicate melt inclusion containing a dissolved sulfide globule. Open fractures are indicated by dashed lines radiating from the inclusion and are interpreted to have resulted from overpressures developed within the inclusion during decompression. These fractures provided pathways for subsequent infiltration of magmatic hydrothermal fluids that dissolved the sulfide globule.

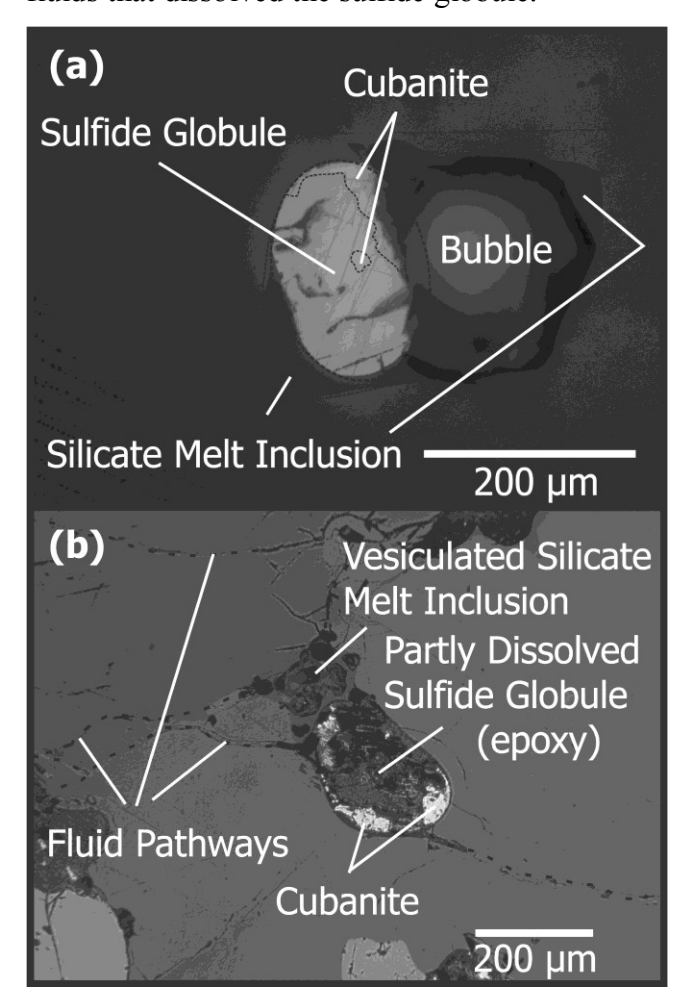


Figure 2. Reflected light photomicrographs of oxidized sulfide melt inclusions hosted in amphibole from samples of dome lava. A) A partly hematized sulfide globule. Open fractures radiating from this inclusion and indicated by dashes provided pathways for infiltration of oxidizing fluids and removal of sulfur. B) A sulfide globule that was partly oxidized to pyrite and magnetite. Po: pyrrhotite; Py: pyrite; Cu: cubanite; Mt: magnetite.

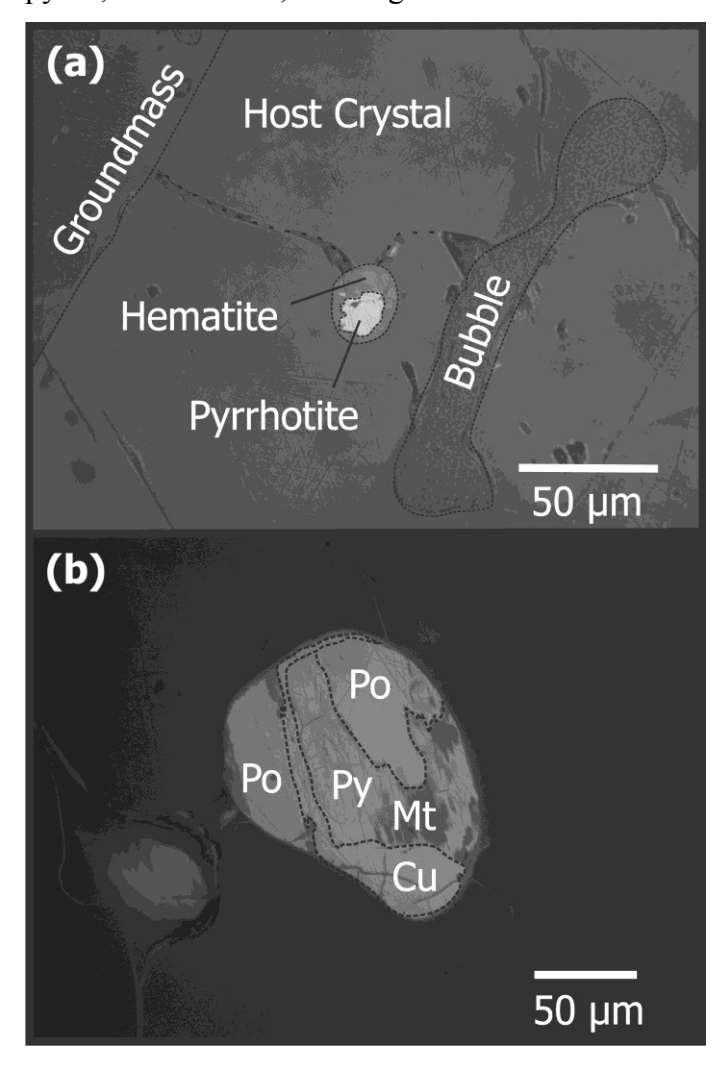


Figure 3. Trace metal concentrations and ratios in volcanic gas condensates and sulfide melt inclusions. Note the similarity of the metal ratios in the gases collected at Woro in 2006 to that of the sulfide melt. The composition of the sulfide melt is given in Table 1. Data from 1984 is from Symonds et al., 1987.

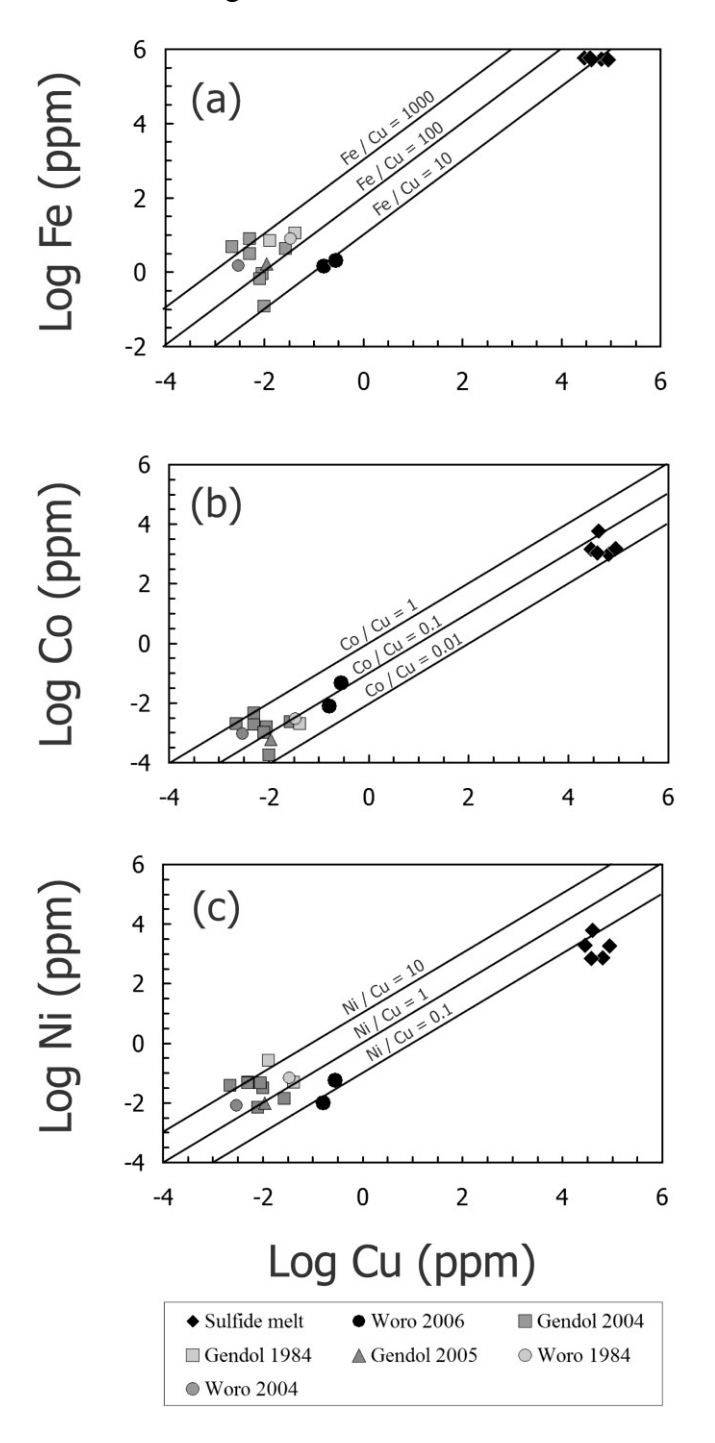
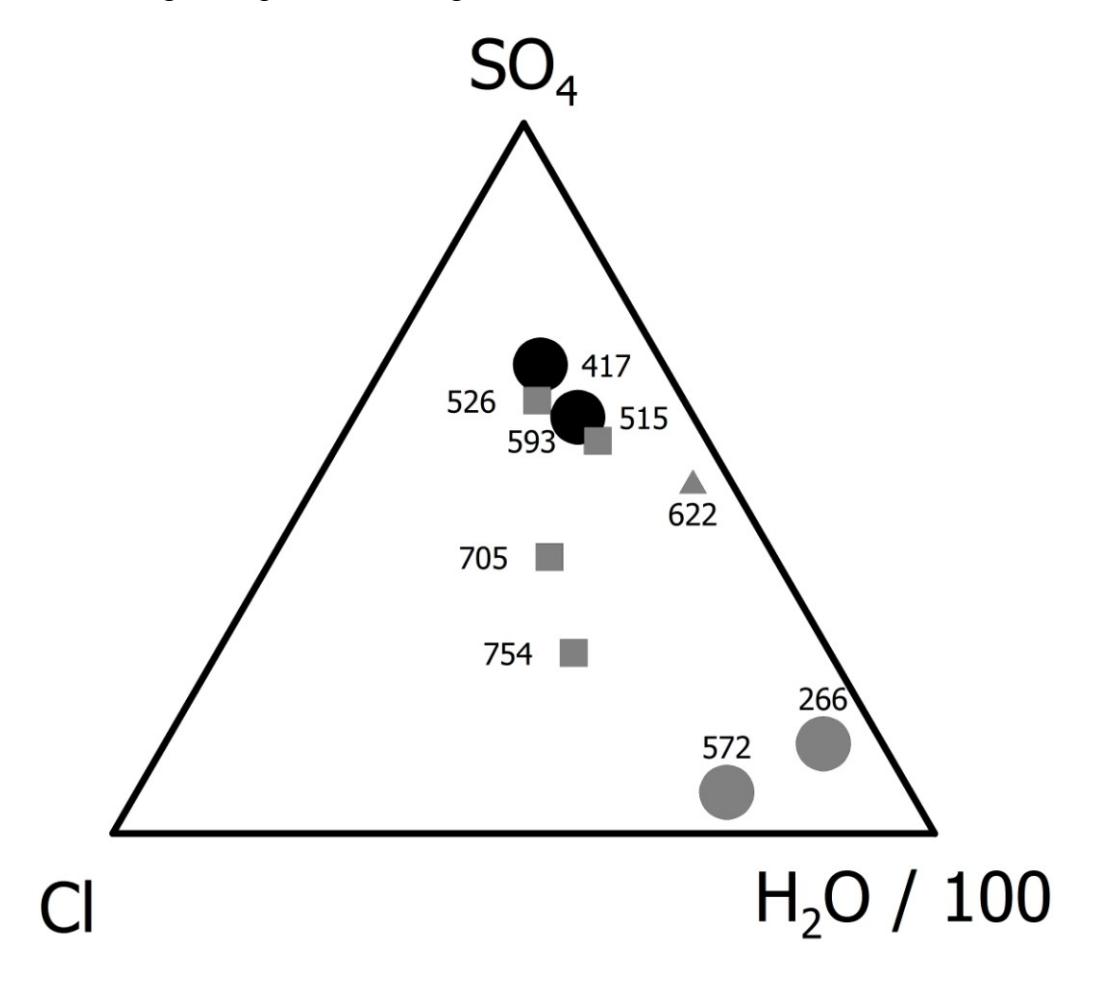


Figure 4. Ternary diagram showing relative concentrations of SO₄, H₂O and Cl in volcanic gas condensates. Symbols are the same as in Figure 3. Labels refer to fumarole gas temperatures in degrees celsius.



Appendices

Appendix 1 – Geological Setting

Merapi is an active calcalkaline stratovolcano located in Central Java, Indonesia and is a product of the ongoing subduction of the Australian oceanic plate under the Eurasian continental plate. The volcano appears to have begun its activity during the Pliocene; the oldest volcanic rocks associated with Merapi volcano have been dated at 3.44 Ma (Newhall et al., 2000) although most of its activity appears to have occurred within the last 40 000 years (Camus et al., 2000). During its lifetime, the volcano has experienced frequent plinian- to sub-plinian explosive eruptions (Newhall et al., 2000; Camus et al., 2000; Andreastuti et al., 2000). At the beginning of the 20th century, Merapi underwent a change in its style of activity that has continued to the present day. During the current phase of activity, Merapi has been erupting viscous lava domes, which grow and collapse. These eruptions have been interspersed with occasional St-Vincent-type explosions, generating incandescent pyroclastic flows and associated surges. The eruptive periods, which are usually of several months duration, are separated by periods of quiescent degassing typically lasting a few years. Merapi lavas are of calcalkaline affinity, range in composition from 49.5 to 60.5 wt. % SiO₂, and contain abundant zoned plagioclase (An₃₄₋₉₃), coexisting with fresh and resorbed clinopyroxene (augite) and amphibole (magnesio-hastingsite), titanomagnetite, as well as rare olivine, orthopyroxene, alkali feldspar and apatite as phenocrystic phases (Andreastuti et al., 2000).

Until 2006, fumaroles at Merapi volcano were concentrated in three fields: Gendol, Woro and the Dome. During the years covered in this study, Gendol was the hottest field ($T \le 754^{\circ}C$) whereas Woro was the coolest field ($T \le 572^{\circ}C$) (the Dome was too dangerous to sample). The Gendol field was destroyed by the eruption of 2006. The values of $\delta^{18}O$ and δD of H_2O in gas condensates collected in 2004 show that gases exiting the Gendol field had a composition close to that of 'andesitic water', whereas those released at Woro contained a larger proportion

of meteoric water (Appendix 3). The volcanic gases of Gendol were also sampled in 2005, and those of Woro in 2006. Temperatures have been highest at the Gendol field, reaching 900°C in 1978 (Le Guern et al, 1980).

Appendix 2 – Supplementary methods

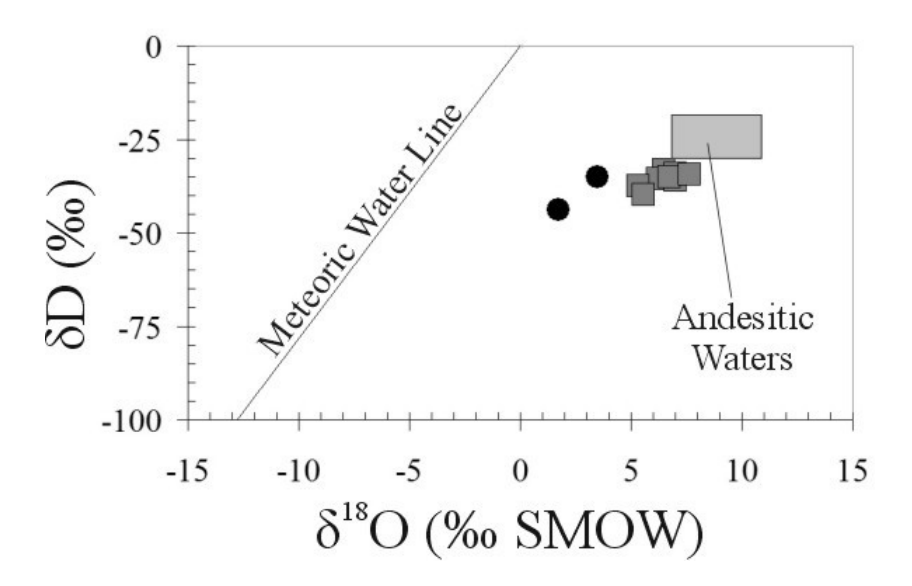
Volcanic gas condensates were collected in 2004, 2005 and 2006 at summit fumaroles by pumping the gas through an ice trap condenser. To avoid condensation within the sampling train, an inner fused silica tube was inserted within a wider silica tube, and both were placed into fumaroles. The silica tubes and the silicone rubber tubing were very short (30 cm) and the rubber tubing kept straight to avoid water accumulation. If the spontaneous flow of gas through the condenser was low or absent (evident by a low rate of bubble formation or absence of bubbles in the condensed liquid), the gases were pumped slowly through the condenser at a constant rate with a hand-held pump. Condensates commonly contained a yellowish precipitate, which was filtered and analyzed separately. Solid and liquid fractions of the condensates were analyzed by Actlabs Inc., Ancaster, Ontario, using inductively coupled plasma mass spectrometry (ICP-MS), inductively coupled plasma optical emission spectrometry (ICP-OES), instrumental neutron activation (INAA), ion chromatography (IC) and conductivity for total dissolved solids. The water content of the condensates was calculated by subtracting the mass of dissolved solids from the total mass.

A total of 76 analyses of sulfide melt inclusions, found in 8 lava and 4 scoria hand samples and hosted in phenocrysts of plagioclase, clinopyroxene and amphibole, and in megacrysts of clinopyroxene and amphibole, were analyzed using a JEOL JXA-8900L electron microprobe with a fully focused beam in the Geochemical Laboratories at McGill University, Montreal, Quebec, for Fe, Cu, Co, Ni, Mo, Ti. Only the best inclusions were kept for restoring the bulk composition of the sulfide melt (Table 1). All others were rejected because they were altered, dissolved, corroded or because they were simply too small to allow analysis of both the Cu-rich and the Fe-rich phases. Five pristine sulfide globules

were used to calculate the bulk composition of the sulfide magma; these globules displayed volumetric ratios of the Cu-rich phase to the Fe-rich phase ranging from 13:87 to 32:68. The composition of the sulfide melt was assumed to correspond to the average composition of the five restored sulfide melt inclusions.

A total of 156 silicate melt inclusions, hosted in the same samples as those containing the sulfides, also were analyzed by electron microprobe for major and minor elements, with a 20 µm defocused beam to avoid volatile element loss. Care was taken to avoid inclusions that were degassed, devitrified and/or oxidized. Trace elements concentrations were quantified by laser ablation ICP-MS, also at McGill University. The laser ablation system consists of a New-Wave UP-213 laser coupled to a PerkinElmer/SCIEX ELAN 6100 DRCplus ICP-MS.

Appendix 3 – A plot of δD versus $\delta^{18}O$ values of gas condensates collected in 2004 at Woro and Gendol. Symbols are the same as those in Figures 3 and 4 of the article. The meteoric water line is from Craig (1961) and the 'Andesitic Water' box is from Giggenbach (1992) (See Appendix 5 for references).



Appendix 4 – Compositions of selected silicate melt inclusions in samples of scoria and lava dome material. Values for the oxides are in wt. % while those of Cl, S, Cu and Co are in ppm. Oxides, Cl and S were analyzed by electron microprobe and Cu, Ni and Co by laser ablation ICP-MS. Nickel always was below the detection limits ranging from 2.8 to 79.1 ppm. The detection limits ranged from 0.2 to 29.9 ppm for Co and from 1.2 to 73.5 ppm for Cu.

Sample Name	SiO ₂	MgO	Al_2O_3	FeO	Na ₂ O	CaO	K ₂ O	P_2O_5	MnO	TiO ₂	CI	S	Cu	Co	Total
Scorias															
M6.WD.3.4(1).4A	51.64	1.40	19.89	8.23	3.05	10.37	2.08	0.44	0.28	0.47	1850	645	38		98.15
M6.WD.3.4(1).4B	51.97	1.35	19.92	7.78	3.11	10.18	2.07	0.45	0.21	0.56	1820	489	38		97.86
M6.WD.3.3(1).1B	52.02	1.10	20.19	7.88	3.12	9.89	2.05	0.48	0.23	0.46	1890	469	19		97.69
M6.WD.3.4(1).2	52.50	1.47	19.93	7.46	3.19	9.80	2.18	0.46	0.26	0.54	1620	605	23		98.07
M6.WD.3.3(1).1A	53.23	1.11	20.15	7.84	2.97	9.84	2.10	0.49	0.26	0.50	2000	485	19		98.75
M6.WD.3.3(1).5A	53.51	1.57	21.34	7.20	3.64	7.71	2.39	0.48	0.20	0.62	1840	433			98.90
M6.WD.3.3(1).5B	54.11	1.60	21.56	7.08	3.61	7.54	2.46	0.44	0.21	0.63	1600	280			99.43
M6.WD.3.3(1).7A	54.99	1.03	20.81	5.86	3.90	6.87	2.29	0.36	0.28	0.67	1840	212			97.25
M6.WD.3.3(1).7B	55.31	1.25	21.51	6.46	3.95	7.18	2.20	0.36	0.18	0.75	1930	429	16	13	99.40
M6.WD.3.4(1).7B	56.97	0.98	19.52	6.40	4.25	6.53	3.69	0.47	0.20	0.40	2280	188			99.63
M6.WD.3.4(1).7A	57.71	1.05	19.02	6.85	4.75	6.34	2.69	0.43	0.26	0.46	2700	228			99.82
Lavas															
M6.NS.11.3(1).13A	61.24	0.99	17.09	4.95	4.97	3.14	4.87	0.25	0.21	0.66	1990		29		98.53
M6.NS.6-10.1.3B	61.39	1.11	17.53	3.60	3.95	3.07	6.05	0.19	0.16	0.48	3020	392	45		97.86
M6.NS.6-10.1.13A3bis	63.29	0.98	16.37	3.98	4.71	2.36	5.11	0.19	0.16	0.60	2455			8	97.97
M6.NSB.1.3(1).4B	63.74	1.12	16.26	3.83	4.57	2.12	5.38	0.19	0.18	0.50	2820	200			98.14
WD-3-3-mt6-cx3-mi7	65.12	1.09	15.32	3.31	5.10	1.81	4.25	0.15	0.13	0.29	2590		26		96.77
M6.KALI06.1.16F	65.27	0.49	16.10	2.24	4.56	1.79	5.21	0.08	0.11	0.57	2610	156			96.67
wd-3-2-mt1-cx18-mi1	65.68	0.54	15.46	3.36	4.86	1.84	4.59	0.19	0.13	0.47	3490		39		97.38
M6.WD.3.4(2).7A2	65.70	0.22	15.84	2.64	5.25	1.46	5.16	0.10	0.16	0.31	3110	212			97.13
WD-3-3-mt5-cx19-mi1	65.88	0.39	15.46	2.79	5.42	1.42	4.94	0.06	0.13	0.23	3760		66		96.99
WD-3-3-mt4-cx5-mi1	66.06	0.57	15.35	3.18	4.57	1.53	4.89	0.15	0.15	0.45	2960		46		97.13

M6.KALI06.1.17D	66.11	0.76	15.84	2.20	3.99	1.99	4.95	0.13	0.11	0.45	2490	244			96.79
M6.KALI06.1.2A	66.33	0.57	16.20	2.09	4.13	1.95	5.03	0.14	0.11	0.67	2640	152			97.46
WD.3.3.MT2.CX17.MI2	66.55	0.29	14.86	2.36	4.88	1.50	4.84	0.12	0.13	0.33	3190		57		96.09
WD.3.2.MT1.CX10.MI1	66.79	0.84	15.67	3.67	4.83	2.34	4.67	0.14	0.13	0.48	2960		44		99.78
WD-3-3-mt4-cx8-mi4	66.95	0.24	15.70	2.23	4.96	1.66	4.56	0.14	0.20	0.37	3470		61		97.28
M6.KALI06.1.1B	66.98	0.51	15.33	2.08	4.08	1.39	4.90	0.11	0.06	0.45	2430	120			96.11
WD.3.3.MT5.CX22.MI1B	67.13	0.14	15.49	1.96	4.82	1.88	4.36	0.14	0.10	0.34	3350		62		96.63
M6.KALI06.1.1C	67.42	0.55	15.42	2.06	4.17	1.32	4.77	0.15	0.03	0.74	2540	216			96.87
WD.3.3.MT3.CX12.MI8	67.72	0.01	16.30	1.07	5.28	2.39	3.84	0.16	0.13	0.33	2920		73	5	97.43
WD-3-3-mt2-cx17-mi1	67.92	0.13	15.82	1.76	4.98	1.59	4.73	0.07	0.09	0.46	3320		29		97.79
WD.3.2.MT1.CX18.MI2	67.96	0.58	15.08	2.78	4.62	1.46	4.99	0.13	0.12	0.40	3470		29		98.40
M6.KALI06.2.10A	67.96	0.16	16.12	1.80	4.52	1.49	4.58	0.13	0.11	0.53	2710	124			97.63
WD.3.3.MT2.CX17.MI3	67.96	0.06	15.88	1.68	5.07	1.63	4.79	0.15	0.13	0.39	3420		54		97.99
WD-3-3-mt6-cx3-mi12-pt1	68.00	0.23	14.84	2.20	4.62	1.32	4.98	0.15	0.06	0.34	3560		38		97.02
M6.KALI06.2.7C	68.45	0.15	15.18	1.71	4.15	1.20	4.82	0.16	0.07	0.41	2710	148			96.54
WD.3.3.MT4.CX8.MI5	68.61	0.34	15.79	2.66	6.04	1.32	5.11	0.12	0.17	0.34	3020		51		100.75
WD-3-3-mt3-cx11-mi6	68.98	0.00	15.68	0.93	5.02	1.71	4.46	0.12	0.10	0.33	2780		41	4	97.54

Appendix 5 – Appendix references

- Andreastuti, S. D., Alloway, B. V. & Smith, I. E. M. A detailed tephrostratigraphic framework at Merapi Volcano, central Java, Indonesia; implications for eruption predictions and hazard assessment. *J. Volcanol. Geotherm. Res.* 100, 51-67 (2000).
- Camus, G., Gourgaud, A., Mossand-Berthommier, P. C. & Vincent, P. M. Merapi (central Java, Indonesia); an outline of the structural and magmatological evolution, with a special emphasis to the major pyroclastic events. *J. Volcanol. Geotherm. Res.* 100, 139-163 (2000).
- Craig, H. Isotopic variations in meteoric waters. *Science* 133, 1702-1703 (1961).
- Giggenbach, W. F. Isotopic shifts in waters from geothermal and volcanic systems along convergent plate boundaries and their origin. *Earth Planet. Sci. Lett.* **113**, 495-510 (1992).
- LeGuern, F., Gerlach, T. M., Riddihough, R. P. & Johnson, S. High temperature gases from Merapi Volcano, Indonesia; application of a new technique for field gas measurements. *Eos.* 61, 67 (1980).
- Newhall, C. G., Bronto, S., Alloway, B. V., Banks, N. G., Bahar, I., del Marmol, M. A., Hadisantono, R. D., Holcomb, R. T., McGeehin, J. P., Miksic, J. N., Rubin, Meyer, Sayudi, D. S., Sukhyar, R., Andreastuti, S. D., Tilling, R. I., Torley, R., Trimble, D. A., Wirakusumah, A. D. 10,000 years of explosive eruptions of Merapi Volcano, central Java; archaeological and modern implications. *J. Volcanol. Geotherm. Res.* 100, 9-50 (2000).

Preface to chapter 2

Now that I have clearly established that the sulfide melt beneath Merapi volcano was dissolved and degassed to the atmosphere, I study the pathways through which this magmatic volatile phase must have circulated, from the deeper mafic magma, through the shallower resident magma and its hydrothermal system, to the surface. I first show that the mafic and the more felsic magma did not mix well. Instead, the free volatile phase was transferred from the mafic to the more felsic melt establishing communication between both magmas. Thermodynamic simulations and petrographic observations are used to confirm that the mafic and the more felsic magmas evolved through a combination of equilibration with the Cu-, Zn- and Pb-rich magmatic volatile phase and assimilation and fractional crystallization. These findings are generalized into a model whereby porphyry Cu and related epithermal deposits may form when sulfide melt-saturated mafic magmas are injected into shallower magmatic systems, during which the chalcophile metals are rapidly transferred to a shallower, volatile-saturated magma chamber

Chapter 2

The Behaviour of Copper, Zinc and Lead during Magmatic-Hydrothermal Activity at Merapi Volcano, Indonesia

Olivier Nadeau, Anthony E. Williams-Jones and John Stix

Manuscript under review in Economic Geology and the Bulletin of the Society of Economic Geologists.

1. Abstract

Understanding the behaviour of copper, zinc, and lead in magmatic-hydrothermal systems is essential in developing models for the genesis of hydrothermal ore deposits in subduction environments. A commonly held view is that the metals originate in magmas of intermediate to felsic composition from which they partition directly into exsolving aqueous fluids. In this paper, we build on the results of an earlier study in which we showed that iron, copper, cobalt and nickel at Merapi volcano, Indonesia, were transferred from a mafic melt to an immiscible sulfide melt, and then to a magmatic volatile phase which carried them to the surface. Here we examine the pathways taken by the volatile phase and the behaviour of copper, zinc and lead in the upper part of the magmatic system beneath Merapi volcano. Based on the composition of a suite of silicate melt inclusions and thermodynamic modelling, we show that the more mafic melt did not mix with the resident, more felsic melt but instead transferred metals to the latter by exsolving a magmatic volatile phase which percolated upwards through the felsic melt, enriching it in copper and lead. It is this fluid which transported the metals to the surface and potentially to subsurface environments of ore formation.

2. Introduction

The behaviour of Cu, Zn and Pb in subduction zones is controlled by their initial abundance in the primitive silicate melt, their solubility in evolving melts, and their partitioning among melt, minerals on the liquidus, and immiscible phases such as a sulfide melt and a magmatic volatile phase (MVP). The content of Cu in igneous rocks of calc-alkaline affinity generally decreases with increasing concentration of SiO₂ and decreasing concentration of MgO, whereas Zn content reaches a maximum in mafic to intermediate magmas and Pb is continuously enriched throughout magmatic evolution (Stanton, 1994). Copper and lead occur mostly in sulfides, although small amounts of these metals can be incorporated in

Fe (Ti) oxides, whereas Zn is compatible in sulfides, oxides, biotite and ferromagnesian minerals such as olivine and orthopyroxene (Stanton, 1994). Consequently, the timing of the formation of these phases relative to the exsolution of the MVP is a major factor in determining the level of enrichment of Cu, Zn and Pb in the MVP.

The properties of sulfide melts are of considerable interest for this study as the distribution of Cu, Zn and Pb in the MVP will be affected by exsolution of a sulfide melt. Nernst partition coefficients between sulfide and silicate melts have been determined experimentally for a number of chalcophile transition metals at a variety of physicochemical conditions; in general, $D_{Cu} = 30$ to 1303, $D_{Pb} = 3$ to >10, and $D_{Zn} = 0.1$ to 130 (Table 1; MacLean and Shimazaki, 1976; Shimazaki and MacLean, 1976; Ripley et al., 2002; Mengason et al., 2006). Although these coefficients vary with the physicochemical conditions, the values presented here are sufficient to demonstrate that an immiscible sulfide melt is capable of sequestering significant quantities of these metals.

Theoretical (e.g., Candela, 1989; Candela and Picolli, 1995), experimental (e.g., Urabe, 1987; Keppler and Wyllie, 1991; Keppler, 1996; Hemley et al., 1992; Bai and Koster Van Groos, 1999; Simon et al., 2005) and field-based studies (e.g., Heinrich et al., 1992; 2003; Heinrich et al., 1999; Halter et al., 2005; Zajacz et al., 2008) have helped determine the partitioning of ore metals between a silicate melt and its exsolving volatile phase. Aqueous fluid/melt partition coefficients are typically in the range 10 to 20 for Cu, but can reach up to 2700 in aqueous vapor (Zajacz et al., 2008). Corresponding coefficients for Zn range from 7.6 to 44 and for Pb from 4.2 to 20 (Table 1; Urabe, 1987; Candela, 1989; Candela and Picolli, 1995; Keppler and Wyllie, 1991; Keppler 1996; Bai and Koster Van Groos 1999; Zajacz et al., 2008). Although the coefficients vary with the chemical composition of the system, pressure and temperature, it is clear that Cu, Zn and Pb prefer the MVP relative to the silicate melt, an observation which explains the common concentration of these metals as magmatic hydrothermal ore deposits (e.g., Baker et al., 2004; Williams-Jones et al., 2010).

In this paper, we build on the results of a previous study in which we showed that Fe, Cu, Co and Ni at Merapi volcano were transferred from a mafic melt to an immiscible sulfide melt, and that an exsolving MVP originating from the mafic melt dissolved the sulfide melt and transferred Fe, Cu, Ni and Co to the surface (Nadeau et al., 2010). Here, we shed light on the pathways taken by the MVP en route to the surface and on the behaviour of Cu, Zn and Pb in the upper part of the magmatic-hydrothermal system. Based on the composition of a suite of silicate melt inclusions from Merapi volcano, we show that the more mafic magma underwent little mixing with the more felsic, resident magma. We also explain why Cu and Pb appear to be gradually enriched in more evolved melts at Merapi, a trend for Pb that is observed in other arc rocks but is more marked at Merapi, and for Cu which is opposite to that normally observed. In order to explain these results, we modelled the evolution of the silicate liquid through fractional crystallization (FC) and combined assimilation and fractional crystallization (AFC) to determine if these processes could account for the behaviour of Cu, Zn and Pb. Both processes were simulated using the thermodynamic program, MELTS (Ghiorso and Sack, 1995). We determined that FC, with or without small amounts of assimilation, can reproduce the trends observed for the major elements and for Zn in the silicate melt inclusions, but cannot explain the enrichments observed in Cu and Pb. The only process that appears capable of simulating the observed evolution of Cu and Pb is the percolation of the MVP (the fluid that dissolved the sulfide melt) through the felsic magma and the transfer of its metals to the latter.

3. Geological Setting

Merapi is an active calc-alkaline stratovolcano located in Central Java, Indonesia, and is a product of the ongoing subduction of the Australian oceanic plate under the Eurasian continental plate. The volcano appears to have begun erupting during the Pliocene (the oldest volcanic rocks are dated at 3.44 Ma; Newhall et al., 2000), but most of its activity occurred within the last 40,000 years (Camus et al., 2000).

In its lifetime, the volcano has experienced frequent plinian- to sub-plinian explosive eruptions (Newhall et al., 2000; Andreastuti et al., 2000, Camus et al., 2000). However, at the beginning of the 20th century, Merapi underwent a change in its style of activity that has continued to the present day, namely the eruption of viscous lava domes, which grow and collapse. These eruptions have been interspersed with occasional St-Vincent-type explosions, generating incandescent pyroclastic flows and associated surges. Eruptive periods, which usually last several months, are separated by periods of quiescent degassing typically lasting a few years. The lavas are of calc-alkaline affinity, range in SiO₂ content from 49.5 to 60.5 wt. %, and contain abundant normally and reversely zoned plagioclase (An₃₄₋₉₃), which coexists with fresh, resorbed and zoned clinopyroxene (augite) and amphibole (pargasite, magnesio-hornblende and magnesio-hastingsite), titanomagnetite, and occasional olivine, orthopyroxene and apatite (Camus et al., 2000). Alkali feldspar occurs as microlites or rim the plagioclase phenocrysts (Hammer et al., 2000). In some cases, fragments of scoria contain light, rhyolitic glass dispersed in darker dacitic glass (Camus et al., 2000). The eruptive products also contain gabbroic, volcano-sedimentary and calc-silicate enclaves (Camus et al., 2000; Chadwick et al., 2007). The melt inclusions analyzed and discussed in this paper come from three major outcrops located at Kaliadem, Ngipik Sari and Windusabrang. Kaliadem was the locus of the 2006 eruption, and this is where we sampled the 2006 lavas. Ngipik Sari is a major roadside outcrop where we were able to sample 19 distinct stratigraphic layers consisting of layas and fine ash. At Windusabrang, we sampled scoria in a quarry. Since at least 1978 (Allard and Tazieff, 1979), three high-temperature fumarole fields have been active at the summit of the volcano, namely the Dome, Gendol and Woro fields. Temperatures have been highest at Gendol, reaching 900°C in 1978 (LeGuern and Bernard., 1982).

4. Methodology

4.1 Analytical Methods

A total of 160 silicate melt inclusions in five lava and nine scoria hand samples were analyzed. They were hosted in phenocrysts of plagioclase, clinopyroxene and amphibole in the lava and scoria samples, and in megacrysts of clinopyroxene and amphibole, which occur only in the scoria samples. Melt inclusions were analyzed either in regular 30 micron thick polished thin sections or in polished grain mounts. The compositions of these inclusions and those of their hosts were analyzed using a JEOL JXA-8900L electron microprobe with a twenty micron defocused beam in the Geochemical Laboratories at McGill University, Montreal, Quebec. The instrument was calibrated using a set of glass standards of basaltic and rhyolitic composition. Relative errors were generally less than 1 percent (e.g., SiO_2 60 ± 0.6 wt.%). A subset of 76 of these inclusions was analyzed by laser ablation ICP-MS, also at McGill University. The system consists of a New-Wave UP-213 laser coupled to a PerkinElmer/SCIEX ELAN 6100 DRCplus ICP-MS, and was calibrated using glass standards similar to those employed with the electron microprobe; Si and Ca analyzed with the electron microprobe were used as internal standards. One sigma relative standard deviations were 10% or less for most analyses and rarely exceeded 20%. Finally, for the purpose of comparing our data to those of bulk volcanic rocks sampled at convergent margins, we made use of the Georoc geochemical database (Sarbas et al., accessed online 20 October 2009; http://georoc.mpch-mainz.gwdg.de/georoc/Start.asp).

4.2 Thermodynamic Modelling

The program MELTS (Ghiorso and Sack, 1995) was used to model the magmatic evolution at Merapi and determine if the concentrations of major and trace elements in the melt inclusions can be explained by fractional crystallization (FC) or combined assimilation and fractional crystallization (AFC). We were

particularly interested to determine if these processes could explain the high concentrations of Cu and Pb and the observation that Cu concentration increases with magma evolution at Merapi volcano, which is opposite to the trend observed for other volcanic arc rocks. Both FC and AFC were simulated isobarically and the magmas cooled from their calculated water-saturated liquidus. The water content of the melt was calculated using VolatileCalc (Newman and Lowenstern, 2002) for a degassing basalt containing 49 wt.% SiO₂, at 1000°C, in a closed system with 2 wt.% H₂O initially exsolved. The simulations were done using a single mafic starting composition for both more mafic and more felsic melt inclusions and separate starting compositions for the two inclusion suites. Starting melt compositions were those of the most primitive mafic and more felsic melt inclusions. In order to ensure that the simulations considered pressure and fO₂ conditions likely to have prevailed at Merapi volcano, fractional crystallization was simulated from 450 MPa (4.5 kbar) to 50 MPa (0.5 kbar) in 100 MPa (1 kbar) intervals at the nickel/nickel-oxide (NNO) oxygen buffer, and at a fixed pressure of 250 MPa (2.5 Kbar) for log fO₂ corresponding to NNO-2 to log fO₂ corresponding to NNO+2, in log 1 intervals. Three assimilant compositions were used in the AFC model: (1) that of the mafic component, calculated from the average composition of 551 gabbros and basalts of the Banda-Sunda arc (Georoc database; Sarbas et al., 2009; accessed online 29 March 2011); (2) the composition of volcano-sedimentary enclaves and (3) the composition of calcsilicate enclaves. These enclaves were from Merapi volcano and were collected and analyzed by J. Chadwick et al. (2007; personal communication). The rates of assimilation were allowed to vary among values of 2, 0.2 and 0.00002 grams per degree Celsius cooling, at a fixed pressure of 250 MPa (2.5 kbar) and a fO₂ corresponding to that of the NNO buffer. The simulations were initiated with a total mass of 100 grams of liquid at a temperature equivalent to a few degrees above the liquidus of the assimilating melt. These rates of assimilation cover a broad spectrum from greater than the rate of crystallization to a rate so low that the results of AFC are very similar to those of FC. Consequently, it was possible to confidently evaluate the role of AFC (if there was one) in the evolution of the

magmas at Merapi volcano. As the program MELTS considers both reduced and oxidized iron, we calculated total iron FeO* as FeO + 0.8998 • (Fe₂O₃) in order to compare the predicted total FeO concentration to that measured in our melt inclusions. The program can also simulate the behaviour of trace elements if their partition coefficients (D) are known. We therefore supplied these data to MELTS for the partitioning of Cu, Zn and Pb between crystals and melt, which we obtained from the GERM database (Staudigel et al., 1998; consulted online 11 April 2011). The simulations were stopped when the proportion of melt remaining was about 40 wt.%. This value is similar to the proportion of phenocrysts observed in our samples of scoria and lava, which averaged ~ 35% and ~50%, respectively, and is consistent with the MgO and SiO₂ contents of our melt inclusions.

5. Results

5.1 Compositions of Melt Inclusions

Results of the analyses of the silicate melt inclusions are presented in Figures 1 to 3, in which MgO is employed as an index of magmatic evolution. Melt inclusions and groundmass glass are grouped by host mineral in Fig. 1a, by rock type in Fig. 1b and by outcrop in Fig. 1c. All melt inclusion compositions are also reported in Table 1. The three diagrams illustrate the variation of SiO₂ content with MgO content. In these diagrams, more mafic melt inclusions, which range in MgO content from ~ 1.6 to 1 wt.%, plot separately from the more felsic melt inclusions, which contain between ~1.4 to 0 wt.% MgO. More mafic melt inclusions were observed only in megacrysts of clinopyroxene and amphibole, found in scoria. By contrast, the more felsic melt inclusions were hosted in megacrysts from scorias as well as in phenocrysts of clinopyroxene, amphibole and plagioclase from scorias and lavas. The compositions of groundmass glasses illustrated in Figures 1 to 3 are more evolved than those of melt inclusions in the same samples. Lithophile element concentrations (SiO₂, FeO*, Al₂O₃, CaO, Na₂O, K₂O and Zr)

are illustrated in Figure 2. The melt inclusions, which have SiO₂ concentrations between 51.6 to 70.8 wt.% SiO₂, are depleted in MgO compared to other arc rocks with similar SiO₂ concentrations. The same is true for the compositions of the bulk rocks reported by Gertisser and Keller (2003b), which are much lower in MgO than those of rocks from other arc volcanoes. As is the case for SiO₂, the concentrations of the other major element oxides in more mafic and more felsic melt inclusions form distinctly separate populations (Fig. 2). In addition, two populations of felsic melt inclusions can be distinguished based on their K₂O concentration, a main population and a small population characterized by high K₂O concentrations (Fig. 2). This latter population could not be related to a particular host mineral, rock type, or outcrop, nor correlated with the concentration of any other major or trace element. The significance of this population is explored further in the discussion of the simulations.

In contrast to the major element concentrations, those of the chalcophile (Cu, Zn and Pb) and volatile elements (S and Cl) in the more mafic and more felsic melt inclusions form single populations of continuously increasing (Cu, Pb, Cl) or decreasing (Zn, S) element concentration (Fig. 3). Groundmass glass was not analyzed for its trace element composition. The progressive enrichment of Pb, from 15 to 70 ppm, and of Cl, from 1600 to about 4000 ppm, in melt inclusions of more evolved composition is consistent with the behaviour of these elements in other arc rocks and likely reflects their incompatible behaviour (Stanton, 1994). However, the behaviour of Cu is opposite to that normally observed in arc magmas. At Merapi, Cu is more concentrated in melts of lower MgO content, increasing from about 15 ppm in the least evolved melt inclusions to 70 ppm in those that are most evolved. In contrast to Cu and Pb, Zn is progressively depleted with evolution of melt inclusion composition, ranging in concentration from 150 to 100 ppm in the more mafic melt inclusions to between 100 and 45 ppm in the felsic melt inclusions. This probably reflects the compatibility of Zn in oxide and ferromagnesian minerals. Sulfur is most concentrated in the mafic melt inclusions, reaching a content of ~ 650 ppm, is depleted in inclusions of intermediate composition, with a content of ~ 220 ppm, and is least concentrated in the most

felsic melt inclusions, with a concentration as low as 124 ppm. The concentration of S in the groundmass glass (28 to 40 ppm) is much lower than in the melt inclusions (~ 124 to 650 ppm), but the concentration of Cl in both types of glass (groundmass and inclusions) is similar, ranging from 1600 to 4150 ppm. There is considerable scatter in the melt inclusion data, which could be due to the complex magmatic history of the volcano (this is a general feature of subduction zone volcanoes). This scatter is more obvious for the more mafic melt inclusions, possibly because of the smaller size of the dataset. The greatest scatter in the more mafic melt inclusion population is for sulfur, and this may be related to an earlier loss of sulfur to an exsolving sulfide melt (Nadeau et al., 2010). Chlorine concentration also displays a great deal of scatter, particularly among felsic melt inclusions. This may be the result of a complex plumbing system and variable degrees of degassing and / or fluxing by an aqueous phase. Despite the scatter, it is still possible to identify trends in the concentration of most elements or their oxides with respect to MgO.

5.2 FC and AFC Simulations of Melt Composition

As mentioned previously, the evolution of the melts through fractional crystallization (FC) and fractional crystallization with assimilation (AFC) was simulated for a variety of pressure and fO_2 conditions. Results of these simulations are shown in Figures 4 to 7 and Appendix Figures A1 to A4 together with the measured melt inclusion compositions. In general, fractional crystallization alone and FC with low assimilation rates were successful in reproducing the concentration of major elements and Zn in the more mafic and more felsic melt inclusions, using separate starting melt compositions for each suite of inclusions. However, MELTS could not produce melts equivalent in composition to both more mafic and more felsic melt inclusions by evolution (FC or AFC) of a melt from a single primitive mafic melt starting composition. Furthermore, the program could not reproduce the concentrations of Cu and Pb observed in more mafic and more felsic melt inclusions using FC or AFC with

either a single mafic starting composition or separate starting compositions for both families. The results of the simulations are described in more detail below.

5.2.1 Mafic melt

For purposes of clarity and space limitations, it is not possible to show and discuss distributions of all major elements for each simulation. We therefore selected SiO₂, FeO* and K₂O because they encompass the full range of behaviour displayed by all the major elements. The simulation of FC for the more mafic melt at multiple pressures (Fig. 4 and Fig. A1a) satisfactorily reproduces the major element oxide composition of all melt inclusions except for CaO and FeO*. By 'multiple pressure' crystallization we infer that there are multiple magma reservoirs beneath Merapi in which FC or AFC proceed simultaneously, resulting in superposed trends of FC or AFC. Such a scenario is suggested by the complex plumbing systems of arc volcanoes and more specifically by the magmatic system at Merapi (Deegan et al., 2010; Chadwick et al., 2005). It also reproduces the concentration of Zn in these inclusions, but fails to do so for Pb. The small number of melt inclusions containing detectable Cu (five inclusions) precludes meaningful evaluation of the simulation for this element. Varying the oxygen fugacity did not improve the simulations (Fig. A1b).

Simulations involving application of the AFC model to a starting mafic melt composition also satisfactorily reproduced the distribution of all major elements and zinc in the more mafic melt inclusions, irrespective of whether the assimilant was mafic (Fig. A2a) or a calc-silicate enclave (Fig. 5 and A2c). The best fits to the data were obtained where the assimilation rate was set at 0.00002 g/°C. However, the use of AFC does not improve the fits for Cu and Pb.

5.2.2 Felsic melt

Fractional crystallization of a melt equivalent in composition to the most primitive of the felsic melt inclusions satisfactorily reproduced the trends in the major oxide

compositions and Zn of the felsic melt inclusions, except for that of K₂O in the small population of inclusions characterized by high concentrations of this oxide (Figs. 6 and Fig. A3). The best results were obtained using multiple-pressure FC (Fig 6 and A3a). Although the FC model failed to reproduce the high K₂O population, at very low pressure (50 MPa) it produced an enrichment in K₂O that could have reproduced this population if alkali feldspar had not started crystallizing at 0.75 wt.% MgO, leading to a depletion in K₂O. Unfortunately, we were unable to suppress the crystallization of alkali feldspar in MELTS (the program does not allow plagioclase and alkali feldspar to be suppressed separately). However, alkali feldspar is a very minor phase in Merapi rocks, occurring as microlites or rimming pre-existing plagioclase, and is thought to form only during eruptions (Hammer et al., 2000). It is thus possible that the high K₂O melt inclusion population reflects low-pressure fractional crystallization. Fractional crystallization failed to reproduce the trends for Cu and Pb in the felsic melt inclusion data at any of the pressures considered. For simulations in which pressure was fixed (Fig. A3b), increasing fO₂ leads to a rapid depletion of FeO* as a result of the crystallization of iron oxides. It also promotes enrichment of K₂O, except, as is the case for low pressure, that early crystallization of alkali feldspar depletes subsequent melts in this oxide. However, there was no need to vary fO₂, as the trend for this oxide is satisfactorily reproduced with multiplepressure FC. Changing fO₂ also did not help reproduce the trends for Cu and Pb. Varying initial H₂O content changes the evolution of the major elements appreciably. At low H₂O content, there is an enrichment in K₂O that could explain the high-K₂O melt-inclusion population, were it not for the early crystallization of alkali feldspar. Thus it is also possible that instead of low pressure or elevated fO_2 , the high-K₂O felsic melt-inclusion population reflects low H₂O content. We note that low pressure, low H₂O content and more oxidizing conditions are commonly linked in shallow magmas.

In general, the phenocrysts formed in our MELTS runs matched those observed at Merapi, although biotite appeared in our simulations and is absent in Merapi rocks. The main factor responsible for the formation of biotite appears to

be the initial H_2O content of the melt. Hence, its appearance may be due to the fact that the program does not consider CO_2 and thus overestimates the solubility of H_2O . The only other phases that crystallized in the models and are not found at Merapi are garnet, titanite and quartz. Garnet appeared in the FC of mafic melt at 450 MPa (4.5 Kbar), and thus its crystallization can be suppressed by keeping pressure lower than 450 MPa. Titanite and garnet both formed in the AFC simulations when the assimilant was calc-silicate host rock and the rate of assimilation was $0.2 \, \text{g/}^{\circ}\text{C}$; at lower rates of assimilation, neither phase formed. Finally, quartz formed in both the more mafic and more felsic melts when the assimilant was siliceous volcano-sedimentary rock and the rate of assimilation was $\geq 0.2 \, \text{g/}^{\circ}\text{C}$.

AFC simulations would produce very good fits for most major elements (Fig. 7 and Fig. A4) if the changes related to polybaric crystallization were superposed and the rates of assimilation were low. However, as FC satisfactorily predicts the evolution of the felsic melt (Fig. 6 and A3), assimilation, if it occurred, likely would have been minor. As with FC, AFC prevents the enrichment of K₂O because of early crystallization of alkali feldspar (see earlier discussion) and does not help explain the formation of the small population of high K₂O melt inclusions. Lastly and most importantly, AFC failed to reproduce the trends in Cu and Pb, owing undoubtedly to the very low concentrations of these metals in the assimilants.

In summary, fractional crystallization, possibly accompanied by minor assimilation of a mafic component, volcano-sedimentary or calc-silicate wallrocks, can satisfactorily reproduce the distribution of the major elements and Zn observed in the more mafic and more felsic melt inclusions, provided that the latter are treated separately. The H₂O-saturated starting melt compositions employed in the simulations also successfully predicted crystallization of the minerals that are present in Merapi volcanic rocks. However, FC and AFC could not reproduce the sharp discordance in the major-element trends for the two families of melt inclusions from a starting mafic melt composition (Fig. 2). They also were not able to reproduce the trends for Cu and Pb in the melt inclusion

suites, irrespective of whether the evolution of the two suites was modelled using a single mafic starting composition or separate mafic and felsic starting compositions.

6. Discussion

Based on the distributions of lithophile elements, we have demonstrated that the more mafic and more felsic melts sampled as inclusions in crystals at Merapi did not mix significantly, their lithophile element compositions forming two distinctly separate populations (Fig. 1 and 2). By contrast, the continuity in the trends of the ore metals and volatile elements from the mafic melt to the felsic melt requires transfer of these elements between the two melts (Fig. 3). Furthermore, whereas the trend for Pb is consistent with that generally observed in arc magmas and predicted by fractional crystallization, the trend for Cu is opposite to the general trend, suggesting that Cu behaviour in the melt was controlled by another mechanism (Fig. 8).

The most plausible explanation for the continuous distribution of ore metals in the felsic melt inclusions is that the metals were exchanged between the two melts by a magmatic volatile phase, and this is supported by the observation that both melts were volatile-saturated (Fig. 9 and Nadeau et al., 2010). As the Cu content of felsic melt reaches a maximum of 70 ppm, and since $D_{Cu}^{(fl/melt)} \approx 11$ -20 (Table 2), this MVP would have contained between 770 and 1400 ppm Cu. Using the same reasoning for Zn, which has a maximum concentration in the melt inclusions of 150 ppm, and since $D_{Zn}^{(fl/melt)} \approx 7.6$ -44 (Table 2), it follows that the MVP would have contained 1140 to 6600 ppm Zn. Finally, the maximum Pb concentration of 70 ppm in the melt inclusions and a $D_{Pb}^{(fl/melt)} \approx 4.2$ -20 (Table 2) would have corresponded to a Pb concentration in the MVP of 294 to 1400 ppm. In Figure 10, we compare these concentrations to those of fluid inclusions from porphyry and skarn deposits and associated barren intrusives in volcanic arcs (Baker et al., 2004; Klemm et al., 2007; Kouzmanov et al., 2010; Landtwing et al., 2005; Pudack et al., 2009; Rusk et al., 2004; Ulrich et al., 1999; 2001; Williams-

Jones et al., 2010). From this comparison, we can see that the concentration of Cu, Zn and Pb in the MVP inferred to have equilibrated with the melt is remarkably similar to the average concentration of fluid inclusions commonly analyzed from porphyry and skarn deposits and associated barren intrusives in volcanic arc environments. Moreover, the concentration of Cu and Pb in the fluid inclusions ranges to significantly higher values. Hence, a MVP could have contributed the Cu and Pb needed to explain the high concentrations of these metals in the felsic melt inclusions.

We propose that the MVP originated in the mafic magma and was enriched in metals during its exsolution as a result of the strong preference of metals for the aqueous phase. Furthermore, we propose that the MVP underwent substantial additional enrichment in Cu by dissolving immiscible sulfide liquid prior to entering the more felsic magma (Fig. 9). Nadeau et al. (2010; unpublished data) showed that the mafic magma exsolved a sulfide melt containing ~ 5 wt.% Cu with hundreds of ppm Zn and < 270 ppm Pb. This MVP then percolated up through the more felsic melt transferring Cu and possibly small amounts of Zn and Pb to the latter. However, as Zn partitions strongly into titanomagnetite, its concentration was buffered to lower values as a result of crystallization of this mineral, thereby explaining the overall depletion of Zn with magma evolution. The MVP thus served to facilitate communication and exchange of elements between two magmas that otherwise mixed very poorly.

Given the density and viscosity contrasts between magmas and MVPs, it is likely that the MVP ascended in the felsic magma by rising as bubbles. According to Ratdomopurbo and Poupinet (2000), a magma chamber is present below the crater of Merapi volcano at a depth of between 2.5 and 1.5 km. A rhyolitic melt under 2 km lithostatic pressure and at 1000°C can dissolve about 2.5 wt. % H₂O (Newman and Lowenstern, 2002). Using Stokes law (equation 4) and the Hess and Dingwell (1996) equation for melt viscosity (equation 5):

$$U = d^2(\rho_{hubble} - \rho_{melt})g/18\mu \tag{4}$$

where U is the bubble rise speed, d its diameter, ρ the density of the melt, μ its viscosity, and

$$\log \eta = \left[-3.545 + 0.833 \ln(w) \right] + \frac{\left[9601 - 2368 \ln(w) \right]}{\left\{ T - \left[195.7 + 32.25 \ln(w) \right] \right\}}$$
 (5)

where η is viscosity, w the water content of the melt in wt. % and T the temperature in Kelvin, our calculations show that bubbles 1 mm in diameter should rise at approximately 7 meters per day in a melt at 1000 °C with a density of 3 grams per cm³ and a H₂O content of 2.5 wt. %.

The data presented in Figures 3 could imply that the enrichment of Cu and Pb is correlated to MgO or the evolution of the melt, and that the percolation must have been concomitant with fractional crystallization. Given that the total height of the magma reservoir is approximately 1 km (Ratdomopurbo and Poupinet, 2000), this corresponds to a travel time for a 1 mm bubble of about 5 months through the entire vertical extent of the magma reservoir. This is very different to the general timescale reported for fractional crystallization, which is on the order of a few thousand to tens of thousands of years (e.g., Hawkesworth et al., 2000; Condomines et al., 2003) and on the order of hundred of years at Merapi, according to Gertisser et al (2003a). We therefore argue that the bubbles must have risen through and fluxed a magma chamber that was previously stratified in composition from about 60 wt. % and 1 wt. % MgO at its base to about 70 wt. % and 0 wt. % near its top. Since this magma was volatile-saturated, by fluxing we infer that the MVP circulated through- and partitioned certain elements towards the melt, although water was not being absorbed by- or dissolved in the melt. This is illustrated in Figure 11, in which fluxing is schematically shown to enrich the melt in Cu and Pb from the concentration predicted by the AFC model to the compositions of the melt inclusion. In this diagram, small amounts of fractional crystallization was assumed to accompany fluxing so the arrows are somewhat tilted towards more evolved composition.

In summary, the concentration of Cu is greater in more evolved magmas, which, as discussed above, is opposite to its behaviour in most arc magmas (Fig. 8). As also discussed earlier, we attribute this behaviour to the exsolution of a Curich sulfide melt from the mafic melt, dissolution of this melt by a MVP also originating in the mafic melt and transfer of the Cu to the felsic melt by this MVP.

Lead is also enriched in melts of more evolved composition at Merapi volcano, but in contrast to copper, this behaviour is similar to that of other arc magmas, although absolute Pb concentrations are higher at Merapi (Fig. 8). The enrichment of Pb was due in part to the incompatible behaviour of this element during magma evolution (Fig. 6). However, our modelling of fractional crystallization indicates that this process was insufficient to account for the observed Pb concentrations in the felsic melt inclusions. This suggests that the MVP may also have contributed Pb to the melt, although the source of this Pb is unclear because the sulfide melt contained less than 270 ppm Pb.

7. Conclusions

Although it is commonly thought that the Cu, Zn and Pb in magmatic hydrothermal deposits originate in magmas of intermediate to felsic composition from which they partition directly into exsolving aqueous fluids, we have shown that they may originate from primitive magmas that have subsequently interacted with these more evolved magmas. Previously, we showed that an immiscible sulfide melt was exsolved from a mafic magma at Merapi volcano, and that this magma exsolved a magmatic volatile phase, which then dissolved the Cu-rich sulfide melt (Nadeau et al., 2010). In this companion paper, we have shown that this magmatic volatile phase percolated upward through the more felsic, resident magma exchanging metals between two magmas that otherwise mixed poorly. We have also shown that in the case of Cu there was also an important net addition of metal to the felsic magma, explaining why, in contrast to other arc volcanoes, magma evolution was accompanied by enrichment in copper. Arc magmatic systems may be characterized by injections of primitive mafic magma accompanied by exsolution of an immiscible metal-rich sulfide liquid, and subsequently a magmatic volatile phase that facilitates transfer of the metals to the more evolved resident magma. Hence arc magmas are favourable environments for the formation of porphyry Cu ore deposits.

Acknowledgement

This study was funded by a SEG student grant to ON, scholarships to ON by the Natural Sciences and Engineering Research Council (NSERC) and the Fond Québécois de la Recherche sur la Nature et les Technologies (FQRNT), and research grants to AEWJ and JS from NSERC and FQRNT. Assistance in the analysis of the melt inclusions was provided by L. Shi and W. Minarik. The final version of the manuscript benefitted from constructive reviews by J. Lowenstern and an anonymous referee.

References

- Adam, J. and T. Green (2006). "Trace element partitioning between mica- and amphibole-bearing garnet lherzolite and hydrous basanitic melt; 1, Experimental results and the investigation of controls on partitioning behaviour." <u>Contributions to Mineralogy and Petrology</u> **152**(1): 1-17.
- Aignertorres, M., Blundy, J., Ulmer, P., Pettke, T. (2007). "Laser Ablation ICPMS study of trace element partitioning between plagioclase and basaltic melts: an experimental approach." <u>Contributions to Mineralogy and Petrology</u> **153**: 647-667.
- Allard, P., Tazieff H. (1979). "Volcanologie. Phénoménologie et cartographie thermique des principales zones fumeroliennes du volcan Mérapi (Indonésie)." <u>Comptes-Rendus de l'Académie des Sciences de Paris Série D 288</u>: 747-750.
- Andreastuti, S. D., B. V. Alloway, et al. (2000). "A detailed tephrostratigraphic framework at Merapi Volcano, central Java, Indonesia; implications for eruption predictions and hazard assessment." <u>Journal of Volcanology and Geothermal Research</u> **100**(1-4): 51-67.
- Bacon, C. R. and T. H. Druitt (1988). "Compositional evolution of the zoned calcalkaline magma chamber of Mount Mazama, Crater Lake, Oregon."

 <u>Contributions to Mineralogy and Petrology</u> **98**(2): 224-256.

- Bai, T. B. and A. F. Koster van Groos (1999). "The distribution of Na, K, Rb, Sr, Al, Ge, Cu, W, Mo, La, and Ce between granitic melts and coexisting aqueous fluids." <u>Geochimica et Cosmochimica Acta</u> **63**(7-8): 1117-1131.
- Baker, T., van Achterberg, E., Ryan, C. G., Lang, J. R. (2004). "Composition and evolution of ore fluids in a magmatic-hydrothermal skarn deposit." Geology **32**(2): 117-120.
- Beattie, P. (1993). "Uranium-thorium disequilibria and partitioning on melting of garnet peridotite." <u>Nature</u> **363**(6424): 63-65.
- Bindeman, I. N., Davis, A. M., and Drake, M. J. (1998). "Ion microprobe study of plagioclase-basalt partition experiments at natural concentration levels of trace elements." Geochimica et Cosmochimica Acta **62**(7): 1175-1193.
- Bougault, H. and R. Hekinian (1974). "Rift valley in the Atlantic Ocean near 36 degrees 50'N; petrology and geochemistry of basalt rocks." <u>Earth and Planetary Science Letters</u> **24**(2): 249-261.
- Brenan, J. M., H. F. Shaw, et al. (1995). "Experimental determination of traceelement partitioning between pargasite and a synthetic hydrous andesitic melt." <u>Earth and Planetary Science Letters</u> **135**(1-4): 1-11.
- Camus, G., Gourgaud, A., Mossand-Berthommier, P. C., Vincent, P. M. (2000). "Merapi (central Java, Indonesia); an outline of the structural and magmatological evolution, with a special emphasis to the major pyroclastic events." <u>Journal of Volcanology and Geothermal Research</u> **100**(1-4): 139-163.
- Candela, P. A. (1989). "Magmatic ore-forming fluids; thermodynamic and mass transfer calculations of metal concentrations." Reviews in Economic Geology 4: 203-221.
- Candela, P. A. and Picolli, P.M. (1995). Model ore-metal partitioning from melts into vapor and vapor/brine mixtures. <u>Magmas, fluids, and ore deposits</u>. J.
 F. H. Thompson. Victoria, British Columbia. Mineralogical Association of Canada Short Course Series, 23: 101-127.

- Chadwick, J. P., E. C. McCourt, et al. (2005). "Petrology and geochemistry of plutonic inclusions in recent Merapi lavas; implications for magmatic evolution in arc settings." <u>Irish Journal of Earth Sciences</u> **23**: 128.
- Chadwick, J. P., V. R. Troll, et al. (2007). "Carbonate assimilation at Merapi Volcano, Java, Indonesia; insights from crystal isotope stratigraphy."

 <u>Journal of Petrology</u> **48**(9): 1793-1812.
- Condomines, M., Gauthier, P.-J., and Sigmarsson, O. (2003). "Timescales of magma chamber processes and dating of young volcanic rocks." <u>Reviews</u> in Mineralogy and Geochemistry **52**: 125-174.
- Deegan, F. M., V. R. Troll, et al. (2010). "Magma-carbonate interaction processes and associated CO (sub 2) release at Merapi Volcano, Indonesia; insights from experimental petrology." <u>Journal of Petrology</u> **51**(5): 1027-1051.
- Dostal, J., Dupuy, C., Carron, J. P., Le Guen de Kerneizon, M., and Maury, R. C. (1983). "Partition coefficients of trace elements; application to volcanic rocks of St. Vincent, West Indies." Geochimica et Cosmochimica Acta 47(3): 525-533.
- Esperança, S., Carlson, R. W., Shirey, S. B., and Smith, D. (1997). "Dating crust-mantle separation; Re-Os isotopic study of mafic xenoliths from central Arizona." Geology **25**(7): 651-654.
- Ewart, A. and W. L. Griffin (1994). "Application of proton-microprobe data to trace-element partitioning in volcanic rocks." <u>Chemical Geology</u> **117**(1-4): 251-284.
- Gertisser, R. and Keller J. (2003a). "Temporal variations in magma composition at Merapi Volcano (Central Java, Indonesia): magmatic cycles during the past 2000 years of explosive activity." <u>Journal of Volcanology and Geothermal research</u> **123**: 1-23.
- Gertisser, R., Keller J. (2003b). "Trace element and Sr, Nd, Pb, O isotope variations in medium-K and high-K volcanic rocks from Merapi volcano, Central Java, Indonesia: Evidence for the involvement of subducted sediments in Sunda Arc magma genesis." <u>Journal of Petrology</u> **44**(3): 457-489.

- Ghiorso, M. S., Sack, R. O. (1995). "Chemical Mass Transfer in Magmatic Processes. IV. A Revised and Internally Consistent Thermodynamic Model for the Interpolation and Extrapolation of Liquid-Solid Equilibria in Magmatic Systems at Elevated Temperatures and Pressures."

 Contributions to Mineralogy and Petrology 119: 197-212.
- Halter, W. E., Heinrich, C. A., Pettke, T., Bierlein, F. P., Foster, D. A., Gray, D.
 R., Davidson, G. J. (2005). "Magma evolution and the formation of porphyry Cu-Au ore fluids; evidence from silicate and sulfide melt inclusions." Mineralium Deposita 39(8): 845-863.
- Hammer, J. E., Cashman, K. V., Voight, B. (2000). "Magmatic processes revealed by textural and compositional trends in Merapi dome lavas." <u>Journal of Volcanology and Geothermal Research</u> **100**(1-4): 165-192.
- Hart, S. R. and T. Dunn (1993). "Experimental cpx/melt partitioning of 24 trace elements." <u>Contributions to Mineralogy and Petrology</u> **113**(1): 1-8.
- Hauri, E. H., T. P. Wagner, et al. (1994). "Experimental and natural partitioning of Th, U, Pb and other trace elements between garnet, clinopyroxene and basaltic melts." <u>Chemical Geology</u> **117**(1-4): 149-166.
- Hawkesworth, C. J., Blake, S., Evans, P., Hughes, R., MacDonald, R., Thomas, L. E., Turner, S. P., Zellmer, G. (2000). "Time scales of crystal fractionation in magma chambers; integrating physical, isotopic and geochemical perspectives." Journal of Petrology 41(7): 991-1006.
- Heinrich, C. A., Ryan, C. G., Mernagh, T. P., and Eadington, P. J. (1992). "Segregation of ore metals between magmatic brine and vapor; a fluid inclusion study using PIXE microanalysis." <u>Economic Geology and the Bulletin of the Society of Economic Geologists</u> **87**(6): 1566-1583.
- Heinrich, C. A., Guenther, D., Audetat, A., Ulrich, T., Frischknecht, R. (1999). "Metal fractionation between magmatic brine and vapor, determined by microanalysis of fluid inclusions." <u>Geology</u> **27**(8): 755-758.
- Heinrich, C. A., Pettke T., Halter W.E., Aigner-Torres M., Audetat A., Günther D., Hattendorf B., Bleiner D., Guillong M., Horn I. (2003). "Quantitative multi-element analysis of mineral, fluid and melt inclusions by laser-

- ablation inductively-coupled-plasma mass-spectrometry." <u>Geochimica et</u> Cosmochimica Acta **67**(18): 3473-3496.
- Hemley, J. J., G. L. Cygan, et al. (1992). "Hydrothermal ore-forming processes in the light of studies in rock-buffered systems; I, Iron-copper-zinc-lead sulfide solubility relations." <u>Economic Geology and the Bulletin of the Society of Economic Geologists</u> **87**(1): 1-22.
- Hess, K. U. and D. B. Dingwell (1996). "Viscosities of hydrous leucogranitic melts; a non-Arrhenian model." <u>American Mineralogist</u> **81**(9-10): 1297-1300.
- Keppler, H. (1996). "Constraints from partitioning experiments on the composition of subduction-zone fluids." <u>Nature</u> **380** (6571): 237-240.
- Keppler, H. and P. J. Wyllie (1991). "Partitioning of Cu, Sn, Mo, W, U, and Th between melt and aqueous fluid in the systems haplogranite-H₂O-HCl and haplogranite-H₂O-HF." <u>Contributions to Mineralogy and Petrology</u> **109**(2): 139-150.
- Klemm, L. M., Pettke, T., Heinrich, C. A., Campos, E. (2007). "Hydrothermal evolution of the El Teniente Deposit, Chile; porphyry Cu-Mo ore deposition from low-salinity magmatic fluids." <u>Economic Geology and the</u> Bulletin of the Society of Economic Geologists **102**(6): 1021-1045.
- Kouzmanov, K., T. Pettke, et al. (2010). "Direct analysis of ore-precipitating fluids; combined IR microscopy and LA-ICP-MS study of fluid inclusions in opaque ore minerals." <u>Economic Geology and the Bulletin of the Society of Economic Geologists</u> **105**(2): 351-373.
- Kravchuk, I. K., I. V. Chernysheva, et al. (1980). "Element distribution between plagioclase phenocrysts and groundmass as an indicator for crystallization conditions of the basalts in the southern vent of Tolbachik." <u>Geochemistry</u> International **17**(4): 18-24.
- Landtwing, M. R., Pettke, T., Halter, W. E., Heinrich, C. A., Redmond, P. B., Einaudi, M. T., Kunze, K. (2005). "Copper deposition during quartz dissolution by cooling magmatic-hydrothermal fluids; the Bingham porphyry." Earth and Planetary Science Letters **235**(1-2): 229-243.

- Le Guern, F., Bernard A. (1982). "A new method for sampling and analyzing volcanic sublimates application to Merapi volcano." <u>Journal of Volcanology and Geothermal research</u> **12**: 133-146.
- Lemarchand, F., Villemant, B., and Calas, G. (1987). "Trace element distribution coefficients in alkaline series." <u>Geochimica et Cosmochimica Acta</u> **51**(5): 1071-1081.
- Luhr, J. F. and I. S. E. Carmichael (1980). "The Colima volcanic complex, Mexico; I, Post-caldera andesites from Volcan Colima." <u>Contributions to Mineralogy and Petrology</u> **71**(4): 343-372.
- MacLean, W. H. and H. Shimazaki (1976). "The partition of Co, Ni, Cu, and Zn between sulfide and silicate liquids." <u>Economic Geology and the Bulletin of the Society of Economic Geologists</u> **71**(6): 1049-1057.
- Matsui, Y., Onuma, N., Nagasawa, H., Higuchi, H., and Banno, S. (1977).

 "Crystal structure control in trace element partition between crystal and magma." Bulletin de la Société Française de Minéralogie et de Cristallographie 100(6): 315-324.
- McKenzie, D. and R. K. O'Nions (1991). "Partial melt distributions from inversion of rare earth element concentrations." <u>Journal of Petrology</u> **32**(5): 1021-1091.
- Mengason, M. J., P. Piccoli, et al. (2006). "Partitioning of ore metals among Fe-S-O melt, rhyolite melt, and pyrrhotite." <u>Abstracts with Programs -</u> Geological Society of America **38**(7): 245.
- Nadeau, O., Williams-Jones, A. E., Stix, J. (2010). "Sulphide magma as a source of metals in arc-related magmatic hydrothermal ore fluids." <u>Nature Geoscience</u> **3**(7): 501-505.
- Newhall, C. G., S. Bronto, et al. (2000). "10,000 years of explosive eruptions of Merapi Volcano, central Java; archaeological and modern implications." <u>Journal of Volcanology and Geothermal Research</u> **100**(1-4): 9-50.
- Newman, S. and J. B. Lowenstern (2002). "VolatileCalc; a silicate melt-H₂O-CO₂ solution model written in Visual Basic for Excel." <u>Computers & Geosciences</u> **28**(5): 597-604.

- Paster, T. P., Schauwecker, D. S., and Haskin, L. A. (1974). "The behavior of some trace elements during solidification of the Skaergaard layered series." Geochimica et Cosmochimica Acta 38(10): 1549-1577.
- Pudack, C., Halter, W. E., Heinrich, C. A., and Pettke, T. (2009). "Evolution of magmatic vapor to gold-rich epithermal liquid; the porphyry to epithermal transition at Nevados de Famatina, northwest Argentina." <u>Economic Geologists</u> 104(4): 449-477.
- Ratdomopurbo, A. and G. Poupinet (2000). "An overview of the seismicity of Merapi Volcano (Java, Indonesia); 1983-1994." <u>Journal of Volcanology and Geothermal Research</u> **100**(1-4): 193-214.
- Ripley, E. M., J. G. Brophy, et al. (2002). "Copper solubility in a basaltic melt and sulfide liquid/silicate melt partition coefficients of Cu and Fe."

 <u>Geochimica et Cosmochimica Acta</u> **66**(15): 2791-2800.
- Rusk, B. G., Reed, M. H., Dilles, J. H., Klemm, L. M., and Heinrich, C. A. (2004). "Compositions of magmatic hydrothermal fluids determined by LA-ICP-MS of fluid inclusions from the porphyry copper-molybdenum deposit at Butte, MT." Chemical Geology **210**(1-4): 173-199.
- Sarbas, B., U. Nohl, et al. (2009). "The GEOROC database; a decade of "online geochemistry"." Geochimica et Cosmochimica Acta 73(13S): A1158.
- Shimazaki, H. and W. H. Maclean (1976). "An experimental study on the partition of zinc and lead between the silicate and sulfide liquids." <u>Mineralium Deposita</u> **11**(2): 125-132.
- Simon, A., Candela, P., Pettke, T., Piccoli, P., and Heinrich, C. (2005). "The effect of sulfur on melt-volatile phase partitioning of copper." <u>Abstracts with Programs Geological Society of America</u> **37**(7): 163.
- Spera, F. J. (2000). Physical properties of magma. <u>Encyclopedia of volcanoes</u>. H. Sigurdsson, Academic Press: 171.
- Stanton, R. L., 1994, <u>Ore elements in arc lavas</u>, Oxford Monographs on Geology and Geophysics, 391 p.

- Staudigel, H., Albarede, F., Blichert-Toft, J., Edmond, J., McDonough, B., Jacobsen, S. B., Keeling, R., Langmuir, C. H., Nielsen, R. L., Plank, T., Rudnick, R., Shaw, H. F., Shirey, S. B., Veizer, J., and White, W. (1998). "Geochemical Earth Reference Model (GERM); description of the initiative." Chemical Geology 145(3-4): 153-159.
- Ulrich, T., Guenther, D., and Heinrich, C. A. (1999). "Gold concentrations of magmatic brines and the metal budget of porphyry copper deposits." Nature **399**(6737): 676-679.
- Ulrich, T., Guenther, D., and Heinrich, C. A. (2001). "The evolution of a porphyry Cu-Au deposit, based on LA-ICP-MS analysis of fluid inclusions; Bajo de la Alumbrera, Argentina." <u>Economic Geology and the Bulletin of the Society of Economic Geologists</u> **96**(8): 1743-1774.
- Urabe, T. (1987). "The effect of pressure on the partitioning ratios of lead and zinc between vapor and rhyolite melts." <u>Economic Geology and the Bulletin of the Society of Economic Geologists</u> **82**(4): 1049-1052.
- Williams-Jones, A. E., I. M. Samson, et al. "The genesis of distal zinc skarns; evidence from the Mochito Deposit, Honduras." <u>Economic Geology and</u> the Bulletin of the Society of Economic Geologists 105(8): 1411-1440.
- Zajacz, Z., Halter, W. E., Pettke, T., and Guillong, M. (2008). "Determination of fluid/melt partition coefficients by LA-ICPMS analysis of co-existing fluid and silicate melt inclusions; controls on element partitioning."

 <u>Geochimica et Cosmochimica Acta</u> 72(8): 2169-2197.

Table 1. Major and trace element concentrations in matrix glasses and silicate melt inclusions from Merapi volcano.

SiO_2	MgO	Al_2O_3	FeO	Na ₂ O	CaO	K ₂ O	P ₂ O5	MnO	TiO ₂	Cl	S	Total	Cu	Zn	Pb	Zr	Sample	Rock	Host	Name
64.07	0.00	16.07	2.51	4.1.4	2.11	5.00	0.14	0.14	0.22		afic ground									
64.97	0.90	16.07	3.51	4.14	2.11	5.28	0.14	0.14	0.32	2890	40	97.81					ps	S		M6.WD.3.1.9E
66.26	0.70	16.45	3.27	4.48	2.33	4.70	0.13	0.20	0.37		c 1. ·	99.07					ps	S		II.WD.3.3(1).GL2
51.64	1.40	19.89	8.23	3.05	10.37	2.08	0.44	0.28	0.47	1850	nafic melt in 645	98.15	38	149	22	82	ps	S	ma	M6.WD.3.4(1).4A
51.97	1.35	19.92	7.78	3.11	10.18	2.07	0.45	0.21	0.56	1820	489	97.86	38	149	22	82	ps	s	ma	M6.WD.3.4(1).4B
52.02	1.10	20.19	7.88	3.12	9.89	2.05	0.48	0.23	0.46	1890	469	97.69	19	116	21	77	ps	s	ma	M6.WD.3.3(1).1B
52.50	1.47	19.93	7.46	3.19	9.80	2.18	0.46	0.26	0.54	1620	605	98.07	23	110	19	88	ps	S	ma	M6.WD.3.4(1).2
53.23	1.11	20.15	7.84	2.97	9.84	2.10	0.49	0.26	0.50	2000	485	98.75	19	116	21	77	ps	s	ma	M6.WD.3.3(1).1A
53.51	1.57	21.34	7.20	3.64	7.71	2.39	0.48	0.20	0.62	1840	433	98.90		97	28	99	ps	S	mc	M6.WD.3.3(1).5A
54.11	1.60	21.56	7.08	3.61	7.54	2.46	0.44	0.21	0.63	1600	280	99.43		96	16	63	ps	S	mc	M6.WD.3.3(1).5B
54.99	1.03	20.81	5.86	3.90	6.87	2.29	0.36	0.28	0.67	1840	212	97.25		99	24	85	ps	S	mc	M6.WD.3.3(1).7A
55.31	1.25	21.51	6.46	3.95	7.18	2.20	0.36	0.18	0.75	1930	429	99.40	16	120	24	111	ps	S	mc	M6.WD.3.3(1).7B
56.97	0.98	19.52	6.40	4.25	6.53	3.69	0.47	0.20	0.40	2280	188	99.63		110	34	94	ps	S	ma	M6.WD.3.4(1).7B
57.71	1.05	19.02	6.85	4.75	6.34	2.69	0.43	0.26	0.46	2700	228	99.82		157	41	77	ps	S	ma	M6.WD.3.4(1).7A
										more fel	lsic groundi	nass glass								
71.01	0.211	14.33	2.48	3.75	0.728	6.14	0.074	0.066	0.502	n/a	n/a	99.46	n/a	n/a	n/a	n/a	ps	d		II.KALI06.1.GL1
											elsic melt ir									
60.89	1.30	19.15	5.59	4.85	3.59	4.24	0.59	0.25	0.45	1870	172	101.08		110	25	62	ps	S	mc	M6.WD.3.3(1).9A
62.29	0.46	16.93	3.18	4.44	2.02	4.80	0.24	0.10	0.37	2740	176	95.07					ps	S	С	M6.NSB.1.3(2).11A
62.51	1.30	17.94	3.39	5.57	2.98	4.51	0.39	0.10	0.25	2270		99.10		61	42	50	im	S	ma	WD.3.2.MGCX3.MT1.CX1.MI3
62.60	0.79	16.16	3.61	4.19	1.99	4.41	0.19	0.16	0.46	2640	284	94.81					ps	S	С	M6.NSB.1.3(2).11B
62.82	0.55	17.59	3.92	4.51	2.09	6.40	0.18	0.18	0.50	2510	296	99.00					ps	S	С	M6.NS.2.6(1).15C
63.29	1.25	16.62	5.52	3.76	3.04	4.71	0.33	0.18	0.54	2740	152	99.48					ps	S	p	M6.WD.3.3(1).30
63.29	0.98	16.37	3.98	4.71	2.36	5.11	0.19	0.16	0.60	2455		97.97		68	43	190	ps	S	c	M6.NS.6-10.1.13A3bis
63.37	0.60	16.45	2.80	4.45	1.90	4.46	0.20	0.12	0.46	3020	196	95.09					ps	S	c	M6.NSB.1.3(2).8B
63.48	0.57	16.72	3.83	4.21	2.14	6.29	0.16	0.14	0.48	2490	140	98.24					ps	S	С	M6.NS.2.6(1).7
63.67	0.45	15.46	2.68	3.80	1.85	4.65	0.13	0.03	0.29	2750	312	93.30					ps	S	С	M6.WD.1.4(2).16A
63.95	0.80	16.71	3.69	4.75	2.38	4.57	0.16	0.15	0.53	2620	240	97.94					ps	S	С	M6.NSB.1.3(2).4D
64.03	0.91	15.69	5.47	3.92	3.25	4.43	0.13	0.24	0.57	2680	204	98.87					ps	S	a	M6.WD.3.3(2).11A
64.03	0.70	16.05	3.02	4.10	2.33	4.52	0.15	0.14	0.41	2800	204 272	95.71					ps	S	a	M6.WD.1.4(2).5A1
64.09 64.12	0.40	15.38 16.12	2.59 2.92	3.65 4.00	1.80	4.79 4.54	0.10 0.16	0.15	0.31 0.38	2590	188	93.50 95.58					ps	S	c	M6.WD.1.4(2).16B
64.12	0.68 0.63	17.83	3.08	4.00 5.17	2.24 1.73	4.54 6.04	0.16	0.14 0.16	0.38	2830 2590	252	95.58 99.76					ps	s d	a	M6.WD.1.4(2).5A2
64.13	0.63	17.83	2.24	4.00	2.27	5.20	0.34	0.16	0.40	3010	252	99.76 95.51					ps	d d	a	M6.KALI06.1.19
64.21	0.70	16.93	3.75	4.00	2.67	4.50	0.17	0.07	0.65	2580	168	98.83					ps ps		c	M6.KALI06.1.17A
04.21	0.72	10.93	3.13	4.93	2.07	4.30	0.17	0.17	0.55	2380	108	90.03					ps	S	c	M6.NSB.1.3(2).4C

64.28	0.72	16.88	3.23	4.51	2.07	4.61	0.19	0.11	0.44	2740	272	97.30					ps	s	c	M6.NSB.1.3(2).11C
64.33	0.41	16.48	3.04	4.44	1.98	4.70	0.22	0.12	0.50	2900	240	96.50					ps	S	a	M6.NSB.1.3(2).3
64.35	0.81	16.75	3.66	4.67	2.56	4.34	0.19	0.20	0.54	2400	268	98.32					ps	S	c	M6.NSB.1.3(2).4A
64.37	0.64	16.77	3.96	4.22	2.13	5.86	0.19	0.12	0.48	2620	244	99.00					ps	S	c	M6.NS.2.6(1).2
64.39	0.93	16.92	3.96	4.82	2.69	4.51	0.20	0.15	0.48	2360	272	99.29					ps	S	c	M6.NSB.1.3(2).4E
64.52	0.70	16.31	3.77	4.12	3.33	4.70	0.17	0.20	0.35	2380		98.38					ps	S	a	M6.WD.3.1.3A
64.54	0.82	16.47	3.91	4.69	2.50	4.86	0.18	0.11	0.50	2690	280	98.84					ps	S	c	M6.NSB.1.3(2).13C
64.63	0.95	16.05	4.09	4.26	2.70	4.46	0.16	0.13	0.40	2600		98.05					ps	S	a	M6.WD.1.4(2).8B
64.70	0.82	14.87	4.08	4.60	1.98	4.79	0.18	0.18	0.45	3000		96.88	34	106	37	223	im	S	c	WD.3.2.mt1.cx2.mi3
64.73	0.33	17.98	2.06	4.63	2.40	4.64	0.29	0.14	0.44	3020	264	97.94					ps	d	c	M6.KALI06.1.2C
64.74	0.93	15.88	3.08	4.86	2.61	4.90	0.10	0.14	0.38	2710		97.84					ps	s	a	M6.WD.3.4(2).17A
64.75	1.04	15.64	4.83	4.31	2.95	4.53	0.22	0.24	0.41	2110		99.08					ps	s	a	M6.WD.3.3(2).11B
64.75	0.29	15.81	2.74	5.92	1.38	5.55	0.09	0.12	0.46	2500	136	97.33					ps	d	c	M6.KALI06.1.16D2
64.76	0.89	16.03	3.67	4.07	2.17	5.27	0.11	0.15	0.40	3180		97.76					ps	s	a	M6.WD.3.1.9B
64.83	0.73	16.51	3.63	4.96	2.31	4.75	0.19	0.21	0.47	2690	260	98.86					ps	s	c	M6.NSB.1.3(2).13B
64.84	0.67	16.76	3.56	4.50	2.15	5.73	0.20	0.16	0.41	2660	136	99.22					ps	s	c	M6.NS.2.6(1).12
64.85	0.77	16.47	3.21	4.19	2.48	4.52	0.09	0.17	0.39	2600		97.37					ps	s	c	M6.WD.3.4(1).8B
65.00	0.88	15.98	4.07	3.92	2.23	5.04	0.13	0.15	0.39	2450		97.98					ps	s	a	M6.WD.3.1.9A
65.02	0.42	15.48	2.69	5.22	1.54	5.16	0.11	0.16	0.30	3120	156	96.38					ps	s	c	M6.WD.3.4(2).7A1
65.03	0.69	16.35	3.62	4.09	3.44	4.85	0.14	0.18	0.36	2460		98.94					ps	s	a	M6.WD.3.1.3B
65.07	0.06	16.10	1.65	4.50	2.06	4.00	0.15	0.11	0.38	3000	168	94.35					ps	s	c	M6.WD.3.3(2).13
65.10	0.60	16.37	2.08	4.22	1.98	4.91	0.14	0.07	0.55	2800	180	96.28					ps	d	c	M6.KALI06.1.2B
65.12	1.09	15.32	3.31	5.10	1.81	4.25	0.15	0.13	0.29	2590		96.77	26	156	17	121	im	s	ma	WD.3.3.mt6.cx3.mi7
65.14	0.98	16.09	3.53	4.10	2.87	4.80	0.13	0.19	0.45	2680		98.50					ps	s	a	M6.WD.3.4(2).11
65.22	0.85	15.92	3.25	4.74	2.66	4.86	0.11	0.22	0.35	2670		98.40					ps	s	a	M6.WD.3.4(2).17B
65.26	0.93	16.20	3.84	4.10	2.34	5.05	0.10	0.15	0.45	3260		98.67					ps	s	a	M6.WD.3.1.9D
65.27	0.49	16.10	2.24	4.56	1.79	5.21	0.08	0.11	0.57	2610	156	96.67					ps	d	c	M6.KALI06.1.16F
65.41	0.44	16.15	2.23	4.68	1.71	5.10	0.10	0.08	0.52	2810	212	96.67					ps	d	c	M6.KALI06.1.16E
65.43	0.84	15.80	3.61	5.18	2.67	4.69	0.11	0.12	0.53	2780	220	99.25					ps	S	ma	M6.WD.3.3(2).4C1
65.53	0.45	15.11	2.89	3.85	1.85	4.67	0.16	0.18	0.34	3840		95.35					ps	S	c	M6.WD.1.4(2).17
65.61	0.92	15.62	3.40	4.90	2.26	5.31	0.12	0.22	0.50	2860		99.10					ps	S	a	M6.WD.3.3(2).5
65.61	0.83	15.20	3.25	4.73	2.00	4.63	0.19	0.12	0.45	2830		97.22		79	39	255	im	S	c	WD.3.2.mt1.cx2.mi1(a)
65.62	0.31	15.44	2.39	3.32	1.85	5.26	0.10	0.14	0.27	2460		94.91					ps	S	c	M6.WD.1.4(1).8
65.63	0.40	14.55	2.40	3.91	1.49	5.75	0.10	0.10	0.36	3040		94.92		89	45	210	im	S	c	WD.3.3.mt3.cx20.mi6b
65.68	0.98	16.00	3.52	4.02	2.26	5.14	0.13	0.17	0.36	3080		98.49					ps	S	a	M6.WD.3.1.9C
65.68	0.54	15.46	3.36	4.86	1.84	4.59	0.19	0.13	0.47	3490		97.38	39	94	35	137	im	S	c	wd.3.2.mt1.cx18.mi1
65.70	0.22	15.84	2.64	5.25	1.46	5.16	0.10	0.16	0.31	3110	212	97.13					ps	S	c	M6.WD.3.4(2).7A2
65.72	0.08	19.13	1.23	0.26	2.44	1.71	0.21	0.05	0.24	2580	496	91.39					ps	S	a	M6.WD.3.3(2).3
65.73	0.32	15.63	2.81	4.46	1.48	4.89	0.13	0.07	0.41	3100	180	96.21					ps	S	c	M6.WD.3.3(2).12A

65.85	0.76	15.82	3.40	5.15	2.66	4.56	0.11	0.21	0.54	2760	168	99.31					ps	S	ma	M6.WD.3.3(2).4C2
65.88	0.39	15.46	2.79	5.42	1.42	4.94	0.06	0.13	0.23	3760		96.99	66	36	68	206	im	S	a	WD.3.3.mt5.cx19.mi1
65.97	1.09	16.13	3.53	4.31	2.77	4.46	0.16	0.17	0.52	2180		99.30					ps	S	ma	M6.WD.3.3(2).4A2
65.98	0.70	15.70	3.12	4.89	1.96	4.61	0.15	0.13	0.48	2930		97.94	22	84	50	176	im	S	a	WD.3.3.MT3.CX5.MI4
66.06	0.57	15.35	3.18	4.57	1.53	4.89	0.15	0.15	0.45	2960		97.13	46	79	56	238	im	S	c	WD.3.3.mt4.cx5.mi1
66.09	1.24	16.21	3.89	2.77	3.01	4.41	0.12	0.09	0.56	2390	140	98.61					ps	S	ma	M6.WD.3.3(2).4A1
66.11	0.76	15.84	2.20	3.99	1.99	4.95	0.13	0.11	0.45	2490	244	96.79					ps	d	c	M6.KALI06.1.17D
66.12	0.31	15.59	2.37	4.82	1.94	4.93	0.14	0.11	1.47	2640	136	98.04					ps	d	c	M6.KALI06.1.16B
66.25	0.37	15.94	3.46	4.53	0.81	6.46	0.23	0.08	0.54	4150	172	99.01					ps	d	c	BV.1(1).12C
66.26	0.41	16.97	2.76	4.23	1.35	6.54	0.12	0.13	0.45	2130		99.41		64	64	203	ps	d	c	M6.KALI06.2.5A
66.33	0.57	16.20	2.09	4.13	1.95	5.03	0.14	0.11	0.67	2640	152	97.46					ps	d	c	M6.KALI06.1.2A
66.34	0.44	15.74	3.05	5.13	1.52	5.06	0.08	0.21	0.33	2920	152	98.15					ps	S	c	M6.WD.3.4(2).18
66.52	0.54	16.17	3.52	4.31	2.26	5.42	0.12	0.17	0.37	2650		99.62					ps	S	c	M6.WD.1.4(1).4
66.55	0.61	15.18	2.69	4.75	1.41	4.94	0.12	0.15	0.35	3020		96.99		89	45	210	im	S	c	wd.3.3.mt3.cx20.mi6a
66.55	0.29	14.86	2.36	4.88	1.50	4.84	0.12	0.13	0.33	3190		96.09	57	80	58	200	im	S	c	WD.3.3.MT2.CX17.MI2
66.65	0.11	15.56	2.00	4.73	1.83	4.39	0.12	0.06	0.37	3450		96.09	65	66	56	206	im	S	c	WD.3.3.MT5.CX22.MI1A
66.71	0.69	15.48	2.25	3.92	1.71	5.13	0.16	0.10	0.47	2650	132	96.85					ps	d	c	M6.KALI06.1.1A
66.72	0.84	15.21	3.23	4.89	2.05	4.54	0.15	0.22	0.39	2990		98.46		104	38	231	im	S	c	WD.3.2.mt1.cx2.mi1(b)
66.77	0.82	15.59	3.14	5.49	2.34	4.55	0.12	0.15	0.42	2850		99.61					im	S	a	WD.3.3.MT5.CX23.MI1
66.79	0.84	15.67	3.67	4.83	2.34	4.67	0.14	0.13	0.48	2960		99.78	44	144	36	221	im	S	c	WD.3.2.MT1.CX10.MI1
66.81	0.85	15.33	3.19	3.66	1.61	6.39	0.08	0.12	0.39	2730		98.65					ps	S	a	M6.NS.2.6(1).16
66.84	0.12	15.78	1.99	4.87	1.74	4.35	0.12	0.15	0.34	3720		96.59	26	65	66	193	im	S	c	wd.3.3.MT4.CX8.MI2
66.93	0.72	15.13	3.22	4.96	1.97	4.63	0.19	0.20	0.36	2860		98.52		82	45	251	im	S	c	WD.3.2.MT1.CX10.MI4
66.95	0.24	15.70	2.23	4.96	1.66	4.56	0.14	0.20	0.37	3470		97.28	61	74	66	169	im	S	c	WD.3.3.mt4.cx8.mi4
66.95	0.05	16.80	1.33	5.21	1.97	4.66	0.11	0.09	0.33	3160		97.74	40	80	70	162	im	S	c	WD.3.3.mt3.cx20.mi11
66.97	0.80	15.30	3.05	4.94	2.04	4.40	0.15	0.14	0.41	3020		98.42					im	S	c	WD.3.2.mt1.cx10.mi3
66.98	0.51	15.33	2.08	4.08	1.39	4.90	0.11	0.06	0.45	2430	120	96.11					ps	d	c	M6.KALI06.1.1B
67.13	0.14	15.49	1.96	4.82	1.88	4.36	0.14	0.10	0.34	3350		96.63	62	78	53	182	im	S	c	WD.3.3.MT5.CX22.MI1B
67.18	0.14	14.76	2.06	3.84	1.90	4.13	0.13	0.14	0.27	2940	184	94.82					ps	S	c	M6.WD.1.4(2).20
67.23	0.35	16.42	2.91	4.65	1.06	6.37	0.14	0.13	0.42	2650		99.89					ps	d	c	M6.KALI06.2.7A
67.28	0.22	17.47	1.36	4.78	2.17	4.40	0.39	0.15	0.42	2130	332	98.88					ps	d	c	BV.1(1).9
67.31	0.16	15.59	1.86	4.08	1.60	4.69	0.15	0.06	0.38	2790	144	96.12					ps	d	c	M6.KALI06.2.9B
67.42	0.55	15.42	2.06	4.17	1.32	4.77	0.15	0.03	0.74	2540	216	96.87					ps	d	c	M6.KALI06.1.1C
67.47	0.33	15.97	2.67	4.22	1.10	6.53	0.10	0.11	0.33	2440		99.04		49	37	168	ps	d	c	M6.KALI06.2.13C
67.47	0.33	15.97	2.67	4.22	1.10	6.53	0.10	0.11	0.33	2440		99.04		75	48	224	ps	d	c	M6.KALI06.2.13C2bis
67.53	0.51	16.45	2.23	4.50	1.59	4.84	0.20	0.08	0.58	2600	348	98.80					ps	d	c	M6.KALI06.1.5
67.65	0.17	15.54	1.73	4.09	1.53	4.70	0.12	0.12	0.40	2860	124	96.28					ps	d	c	M6.KALI06.2.9A
67.68	0.20	16.05	2.59	5.50	0.92	6.24	0.10	0.00	0.50	2740		100.02					ps	d	c	M6.KALI06.2.11
67.72	0.01	16.30	1.07	5.28	2.39	3.84	0.16	0.13	0.33	2920		97.43	73	52	46	222	im	S	c	WD.3.3.MT3.CX12.MI8

67.75	0.30	16.23	2.57	4.68	1.15	6.50	0.14	0.10	0.39	2590		100.01		51	57	232	ps	d	c	M6.KALI06.2.13B
67.76	0.06	15.56	1.41	5.03	1.85	4.22	0.15	0.07	0.41	3420							im	S	ma	WD.3.3.mt6.cx3.mi11x
67.83	0.37	16.22	2.91	4.14	1.05	6.54	0.11	0.13	0.37	2640		99.90	58	49	64	173	ps	d	c	M6.KALI06.2.15A
67.85	0.43	15.54	2.70	5.84	2.00	5.17	0.10	0.18	0.39	3100		100.44		68	47	224	im	S	ma	WD.3.3.mt6.cx3.mi4
67.92	0.13	15.82	1.76	4.98	1.59	4.73	0.07	0.09	0.46	3320		97.79	29	76	48	232	im	S	c	WD.3.3.mt2.cx17.mi1
67.94	0.05	16.02	1.10	4.88	1.90	4.85	0.10	0.12	0.42	3020		97.61	71	102	46	178	im	S	ma	WD.3.3.mt6.cx3.mi5
67.96	0.58	15.08	2.78	4.62	1.46	4.99	0.13	0.12	0.40	3470		98.40	29	81	49	221	im	S	c	WD.3.2.MT1.CX18.MI2
67.96	0.16	16.12	1.80	4.52	1.49	4.58	0.13	0.11	0.53	2710	124	97.63					ps	d	c	M6.KALI06.2.10A
67.96	0.66	15.71	3.41	4.57	2.19	4.88	0.11	0.15	0.33	2750	264	100.25					ps	S	c	M6.WD.3.3(1).28
67.96	0.06	15.88	1.68	5.07	1.63	4.79	0.15	0.13	0.39	3420		97.99	54	80	65	234	im	S	c	WD.3.3.MT2.CX17.MI3
67.98	0.09	15.50	1.81	4.87	1.64	4.99	0.10	0.10	0.32	3380		97.67	62	78	53	182	im	S	c	WD.3.3.MT5.CX22.MI2
68.00	0.23	14.84	2.20	4.62	1.32	4.98	0.15	0.06	0.34	3560		97.02	38	62	57	240	im	S	ma	WD.3.3.mt6.cx3.mi12.pt1
68.10	0.20	15.66	1.90	4.27	1.40	4.94	0.14	0.08	0.42	2760	196	97.37					ps	d	c	M6.KALI06.2.12A
68.14	0.33	15.61	2.73	4.48	0.95	6.42	0.26	0.14	0.52	3050		99.83					ps	d	c	M6.KALI06.2.17A
68.21	0.21	14.91	1.76	3.89	1.33	4.82	0.17	0.14	0.37	2110	156	96.00					ps	d	c	M6.KALI06.2.16A4
68.24	0.47	15.82	2.74	6.00	1.62	4.76	0.15	0.19	0.35	3040		100.57	56	124	41	193	im	S	c	WD.3.3.mt4.cx8.mi3
68.29	0.29	15.84	3.02	4.29	1.13	6.38	0.15	0.12	0.47	2750	152	100.23					ps	d	c	M6.KALI06.2.15B
68.45	0.15	15.18	1.71	4.15	1.20	4.82	0.16	0.07	0.41	2710	148	96.54					ps	d	c	M6.KALI06.2.7C
68.59	0.03	15.94	1.07	5.14	1.70	4.52	0.15	0.10	0.33	3070		97.81	54	45	53	211	im	S	a	WD.3.3.mt3.cx11.mi5
68.59	0.15	15.38	1.65	3.94	1.42	4.93	0.12	0.10	0.41	2540	176	96.92					ps	d	c	M6.KALI06.2.16A3
68.61	0.34	15.79	2.66	6.04	1.32	5.11	0.12	0.17	0.34	3020		100.75	51	60	41	173	im	S	c	WD.3.3.MT4.CX8.MI5
68.62	0.31	15.26	2.70	3.95	1.03	6.09	0.14	0.12	0.31	2840		98.77					ps	d	c	M6.KALI06.2.13A
68.76	0.14	14.91	1.69	4.22	1.24	4.49	0.16	0.04	0.44	2300	224	96.32					ps	d	c	M6.KALI06.2.16D3
68.98	0.00	15.68	0.93	5.02	1.71	4.46	0.12	0.10	0.33	2780		97.54	41	54	41	263	im	S	a	WD.3.3.mt3.cx11.mi6
69.70	0.03	16.12	1.06	1.22	2.34	3.52	0.14	0.14	0.38	2930		94.87					im	S	ma	WD.3.3.mt6.cx3.mi6
69.81	0.28	14.68	2.77	4.05	0.80	6.55	0.20	0.08	0.54	2820		99.99		53	62	296	ps	d	c	M6.KALI06.2.17B
70.81	0.49	13.92	3.08	3.84	0.76	5.95	0.18	0.17	0.58	2130		99.94					ps	d	p	M6.KALI06.1.4
														138	47	249	im	S	a	wd.3.3.mt3.cx11.mi4
														79	33	119	ps	S	ma	M6.NS.11.3(1).2
													25	78	34	145	ps	S	ma	M6.NS.11.3(1).6A
														64	44	247	im	S	ma	WD.3.3.mt6.cx3.mi11
													47	45	55	227	im	S	ma	WD.3.3.mt6.cx3.mi12.pt1bis
														23	54	266	ps	d	c	M6.KALI06.2.13B2bis
														65	76	234	ps	d	c	M6.Kali06.2.17B3bis
																	ps	S	c	M6.NS.11.3(1).1
													29	81	50	188	ps	S	c	M6.NS.11.3(1).13A
															68	207	ps	S	c	M6.NS.6-10.1.11A
														76	37	198	ps	S	c	M6.NS.6-10.1.13A1
														52	44	240	ps	S	c	M6.NS.6-10.1.13A2

	34	41	167	ps	S	c	M6.NS.6-10.1.13A4bis
	126	37	175	ps	S	c	M6.NS.6-10.1.16B2
	116	47	291	ps	S	c	M6.NS.6-10.1.7B
	47	37	173	ps	1	c	M6.NSB.1.4.10A1
	149	26	187	ps	1	c	M6.NSB.1.4.10A2
	86	41	166	ps	1	c	M6.NSB.1.4.7A1
61	95	52	152	ps	1	c	M6.NSB.1.4.7A2
	60	48	236	im	S	c	WD.3.2.MT1.CX2.MI2
	89		47	im	S	c	WD.3.3.mt3.cx26.mi2
	57	69	213	im	S	c	WD.3.3.MT3.CX4.MI2
		37	244	im	S	c	WD.3.3.MT3.CX5.MI5
5	122	20	112	ps	S	mc	M6.WD.3.3(1).7B2bis
23	108	17	99	ps	S	mc	M6.WD.3.3(1).7B3bis
45	63	38	102	ps	S	р	M6.NS.6-10.1.3B

All major oxides are in wt.% and trace elements are in ppm. Sample column indicates the type of sample in which the inclusion was analyzed (ps refers to polished section and im refers to indium mount). Rock column indicates the type of rock in which the inclusion was found (s stands fro scoria, d for dome lava and l for lava). Symbols a stands for amphibole, c for clinopyroxene, p for plagioclase, ma for amphibole megacryst and mc for clinopyroxene megacryst.

Table 2. Partition coefficients for sulfide melt-silicate melt, MVP-silicate melt, crystal-sulfide melt, crystal-mafic silicate melt and crystal-felsic silicate melt.

Elem	Partition Coefficient	Chemical	T (°C)	P (MPa)	Reference(s)					
ent		System	10.1							
~		titioning between su								
Cu	30-69	FeS-FeO-SiO2	1150	0.1	MacLean & Shimazaki,1976;					
	480-1303	basalt	1245	nd	Ripley et al., 2002;					
	200-500	rhyolite	1000-1070	nd	Mengason et al., 2006					
Zn	0.1-0.5	FeS-FeO-SiO2	1150	0.1	MacLean & Shimazaki, 1976;					
	0.1-0.5	FeS-FeO-SiO2	1016-1140	nd	Shimazaki & MacLean, 1976;					
	50-130	Rhyolite	1000-1070	nd	Mengason et al., 2006					
Pb	>10	Basic	1016-1140	nd	Shimazaki & MacLean, 1976;					
	3-7	Rhyolite	1000-1070	nd	Mengason et al., 2006					
		ng between magmat								
Cu	11-20, up to 215 in vapor	Rhyolite	750-850	50-140	Candela & Piccoli, 1995					
Zn	7.6-44	Rhyolite	800	200-350	Candela, 1989; Candela &					
DI.	4.2-20	Rhyolite to	000	200.250	Piccoli, 1995; Keppler, 1996					
Pb	4.2-20		800	300-350	Urabe, 1987; Candela, 1989;					
	Destition	Andesite	-1040	. C ::1:4	Keppler, 1996					
-		ning between crysta								
Cu	0.087	Plagioclase			Adam and Green, 2006; Bougault					
	0.204	Clinopyroxene			and Dunn, 1993; Paster et al.,					
	1.3175	Oxide	1974; Lemarchand et al., 1987; Esperanza et al., 1997							
7	1.475	Amphibole	D 1D	'44 1000 T	1 10 :1 1 1000					
Zn	0.14	Plagioclase			uhr and Carmichael, 1980;					
	0.467	Clinopyroxene			ult and Hekinian, 1974; Matsui					
	2.6	Oxide			1974; Lemarchand et al., 1987;					
701	2.3175	Amphibole	Kravchuk et a		1001 11 1001 7					
Pb	1.09325	Plagioclase			1991; Hauri et al., 1994; Beattie,					
	0.009	Clinopyroxene			98; Kravchuk et al., 1981;					
	1.805	Oxide	Aignertorres	et al., 2007;	Ewart and Griffin, 1994					
	0.1	Amphibole			_					
~		ning between crysta								
Cu	0.37	Plagioclase	Luhr and Car	michael, 198	30; Ewart and Griffin, 1994					
	0.66	Clinopyroxene								
	1.6	Oxide								
	11.6	Amphibole	·		20.5					
Zn	0.18	Plagioclase	Luhr and Car	michael, 198	30; Ewart and Griffin, 1994;					
	5.375	Clinopyroxene								
	12.35	Oxide								
	6.85	Amphibole								
Pb	0.61	Plagioclase	Brenan et al.,	1995; Ewar	t and Griffin, 1994					
	0.87	Clinopyroxene								
	2.9	Oxide								
	0.12	Amphibole								

The symbols fl. stand for hydrothermal fluid, m. for silicate melt and sulf. for sulfide melt.

Table 3. Bulk composition of enclaves found in Merapi rocks (Chadwick, J., personal communication). All data are in ppm.

Trace element	Calc-silicate 1	Calc-silicate 1	Calc-silicate 2	Volcano-	Volcano-
	(rim)	(core)		sedimentary 1	sedimentary 2
Cu	160	4.0	7.0	116	214
Zn	91	14	35	88	94
Pb	3.1	0.7	4.1	9.3	3.6

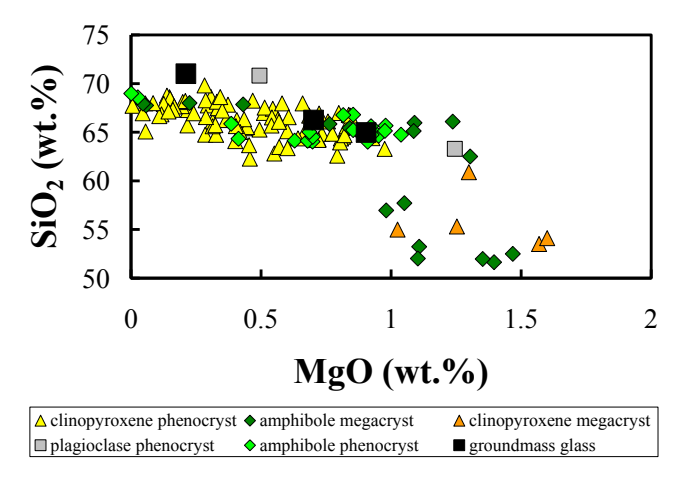
Table 4. Initial melt compositions used in MELTS (Ghiorso and Sack, 1995).

		moi	e mafic	melt			moi	re felsic		VS	CS	Mafic	
P (MPa)	450	350	250	150	50	450	350	250	150	50			
SiO_2	50.02	50.36	50.76	51.22	51.91	61.16	61.42	61.78	62.31	63.15	76.62	55.05	45.30
TiO_2	0.45	0.45	0.46	0.46	0.47	0.56	0.56	0.57	0.57	0.58	0.51	0.33	1.10
Al_2O_3	19.26	19.40	19.55	19.73	19.99	15.80	15.87	15.96	16.10	16.31	8.50	8.13	17.40
FeO*	7.97	8.02	8.09	8.16	8.27	4.18	4.20	4.22	4.26	4.32	3.11	4.97	9.60
MgO	1.35	1.36	1.37	1.38	1.40	1.33	1.33	1.34	1.35	1.37	1.38	2.56	13.10
CaO	10.05	10.11	10.19	10.29	10.42	3.16	3.17	3.19	3.22	3.26	8.22	26.54	9.80
Na ₂ O	2.95	2.98	3.00	3.03	3.07	4.08	4.09	4.12	4.15	4.21	0.94	0.91	2.40
K_2O	2.01	2.03	2.04	2.06	2.09	4.08	4.09	4.12	4.15	4.21	0.12	0.55	0.80
P_2O_5	0.42	0.43	0.43	0.43	0.44	0.24	0.25	0.25	0.25	0.25	0.08	0.12	0.20
MnO	0.27	0.27	0.27	0.28	0.28	0.23	0.24	0.24	0.24	0.24	0.11	0.27	0.30
H_2O	5.24	4.59	3.84	2.96	1.66	5.18	4.78	4.22	3.40	2.00	0.00	0.00	0.00
Cu	15	15	15	15	15	25	25	25	25	25	165	57	80
Zn	100	100	100	100	100	100	100	100	100	100	91	47	80
Pb	15	15	15	15	15	35	35	35	35	35	6	3	3

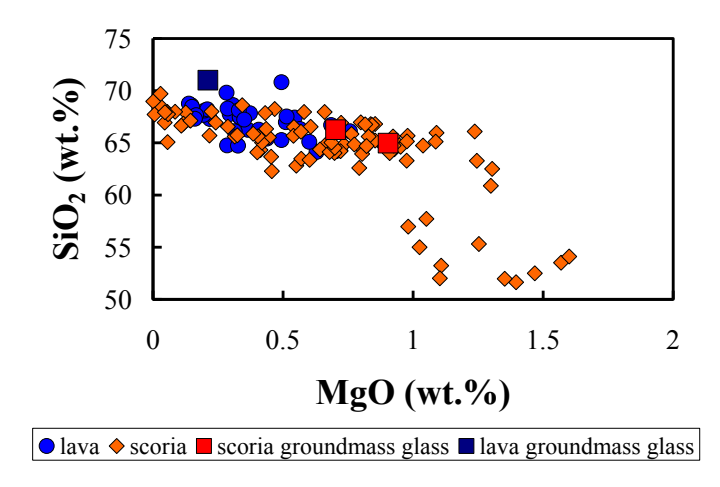
The VS, CS, and Mafic column report the composition of the assimilants used in the models. Symbol 'VS' stands for 'volcano-sedimentary assimilant, 'CS' for 'calc-silicate assimilant', and 'Mafic' for a mafic assimilant.

Figure 1. SiO₂ versus MgO for melt inclusions and matrix glass organized by host mineral (a), rock types (b) and according to element concentrations and by outcrop (c). Note the discontinuity between the trends for the more mafic and more felsic melt inclusions.

a)



b)



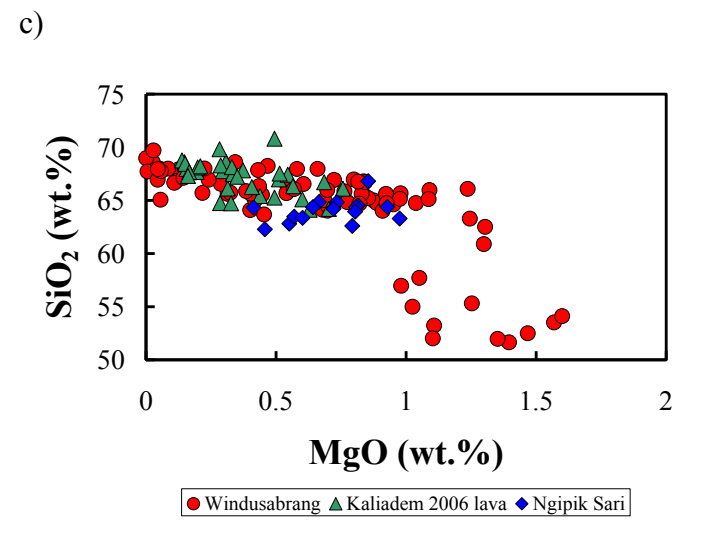
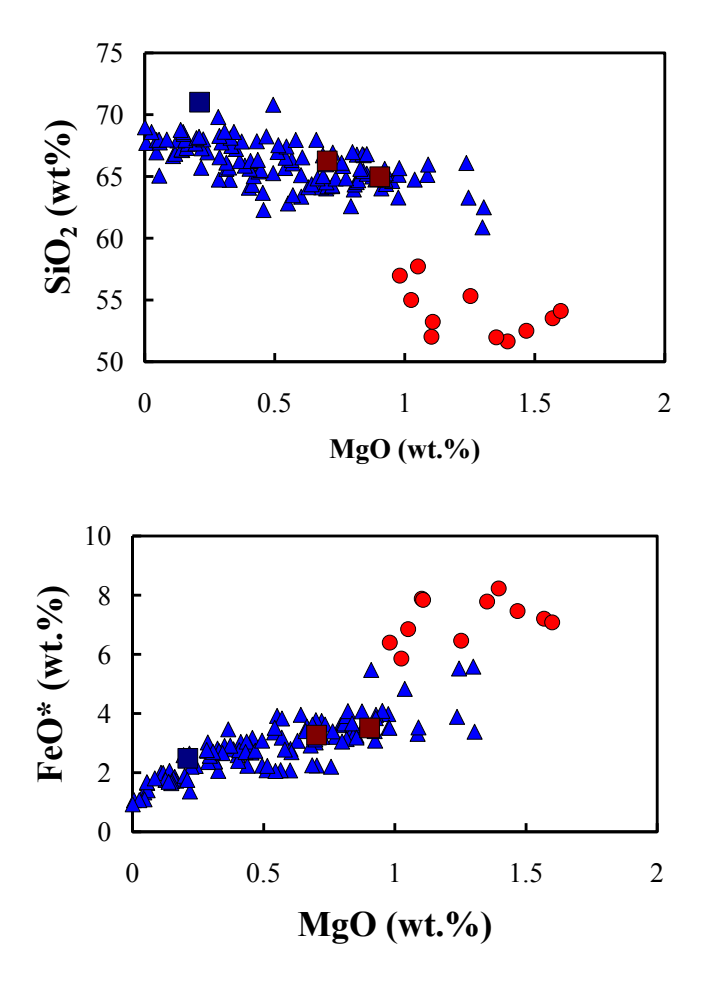
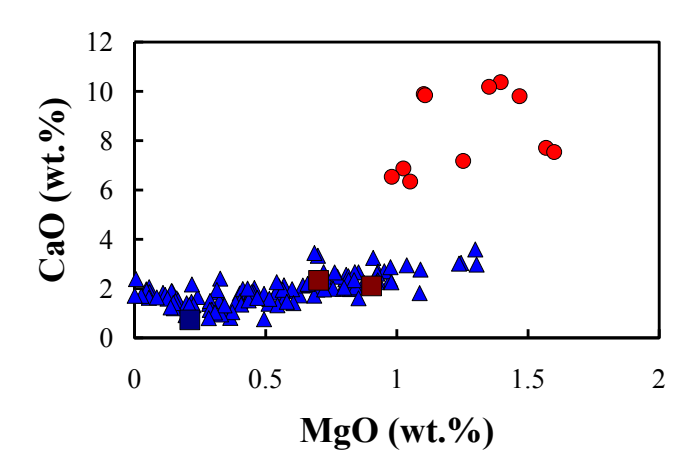
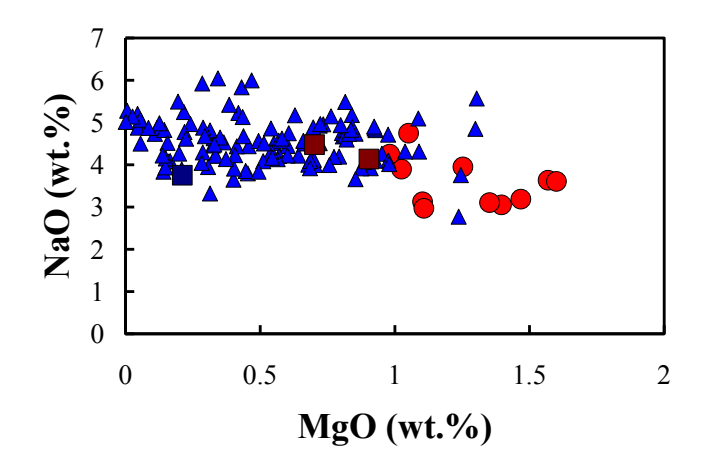
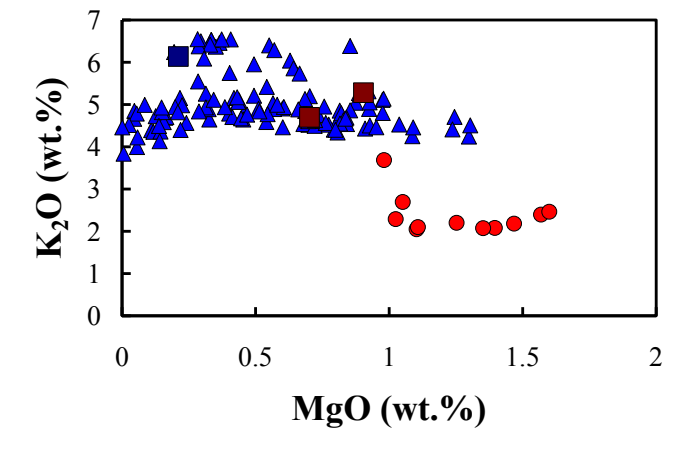


Figure 2. Lithophile element concentrations of silicate melt inclusions and matrix glasses as a function of MgO (used as an index of magmatic evolution). Note the discontinuity between the trends for the more mafic and more felsic melt inclusions.









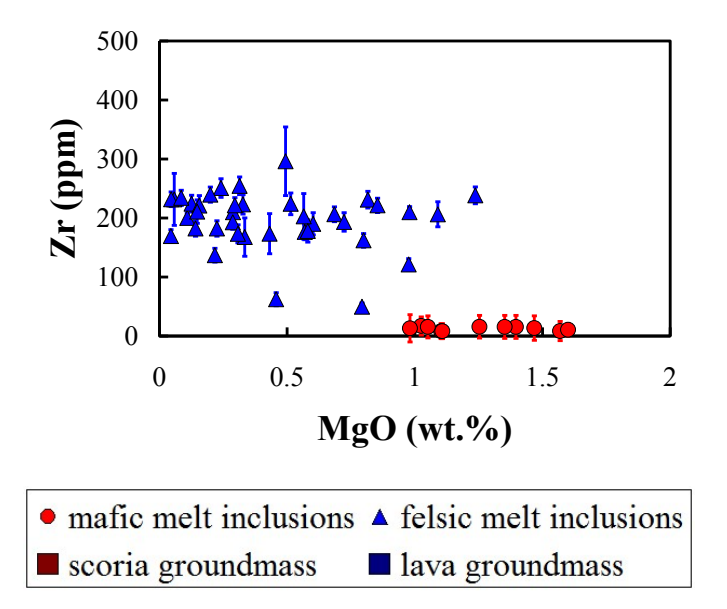
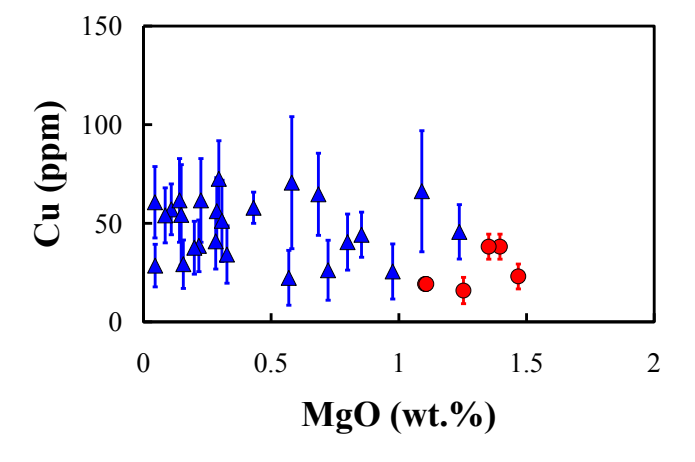
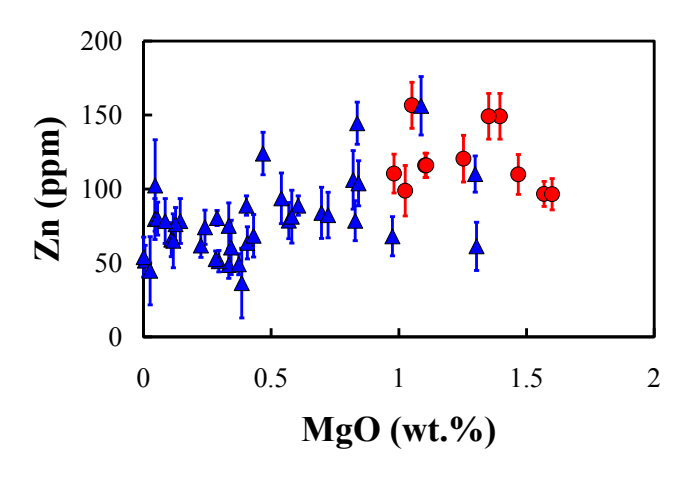
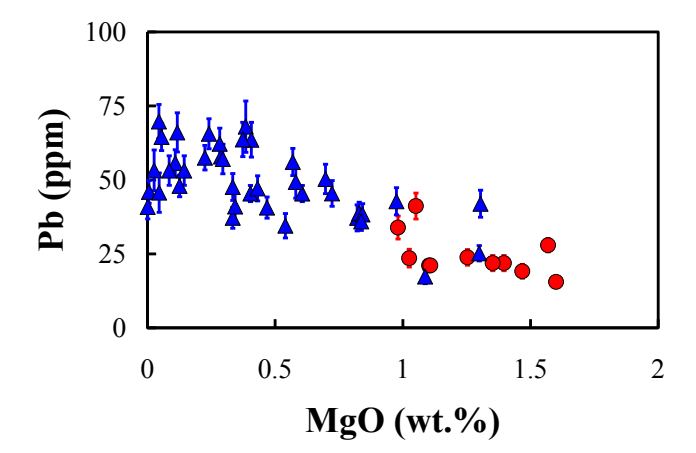
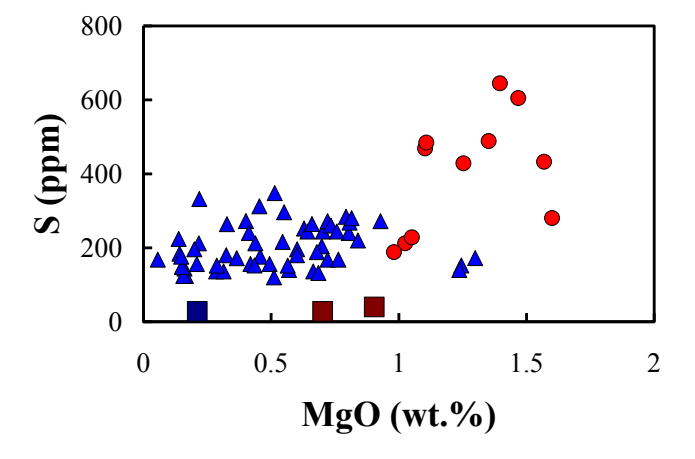


Figure 3. Ore and volatile element (Cu, Zn, Pb, Cl and S) concentrations in silicate melt inclusions and matrix glasses as a function of MgO (used as an index of magmatic evolution). Notice the continuity between the trends for more mafic and more felsic melt inclusions.









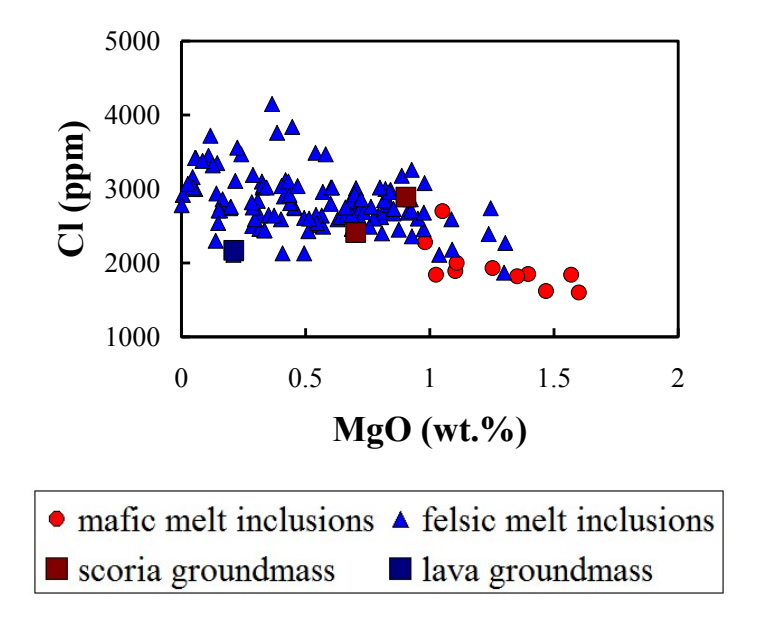
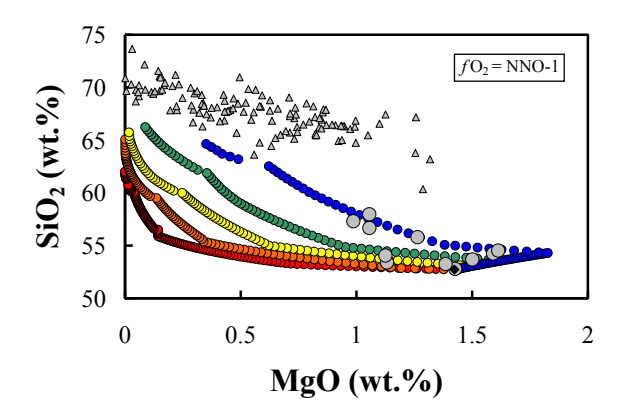


Figure 4. Concentrations of SiO_2 , Cu, and Pb versus MgO concentration using the MELTS model for fractional crystallization of the most primitive mafic melt inclusion at a buffered oxygen fugacity of NNO-1 and pressure varying from 450 MPa to 50 MPa at 100 MPa intervals. Also shown are the concentrations of both more mafic and more felsic melt inclusions. FeO* stands for total iron and was calculated as FeO + 0.8998 • (Fe₂O₃).



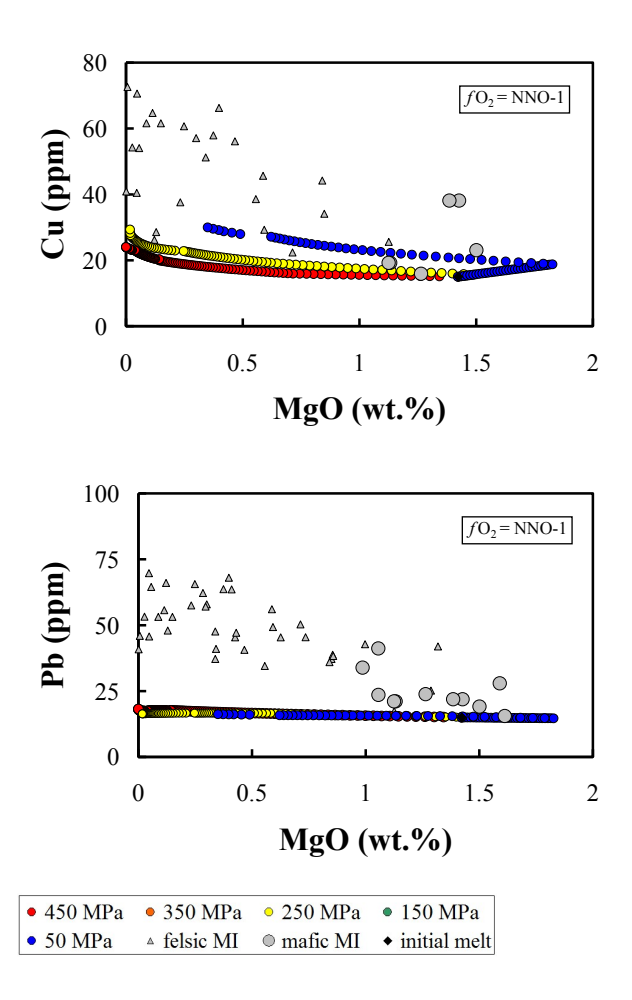


Figure 5. Concentrations of SiO_2 , Cu and Pb versus MgO concentrations using the MELTS model for assimilation of calc-silicate rocks (Table 4) and fractional crystallization of the most primitive mafic melt inclusion. Oxygen fugacity was buffered at NNO and pressure kept constant at 250 MPa while calc-silicate rocks were assimilated at rates varying between 2, 0.2 and 0.00002 g/ \mathbb{C} of cooling. Also shown are the concentrations of both mafic and more felsic melt inclusions. FeO* stands for total iron and was calculated according to FeO + 0.8998 • (Fe₂O₃).

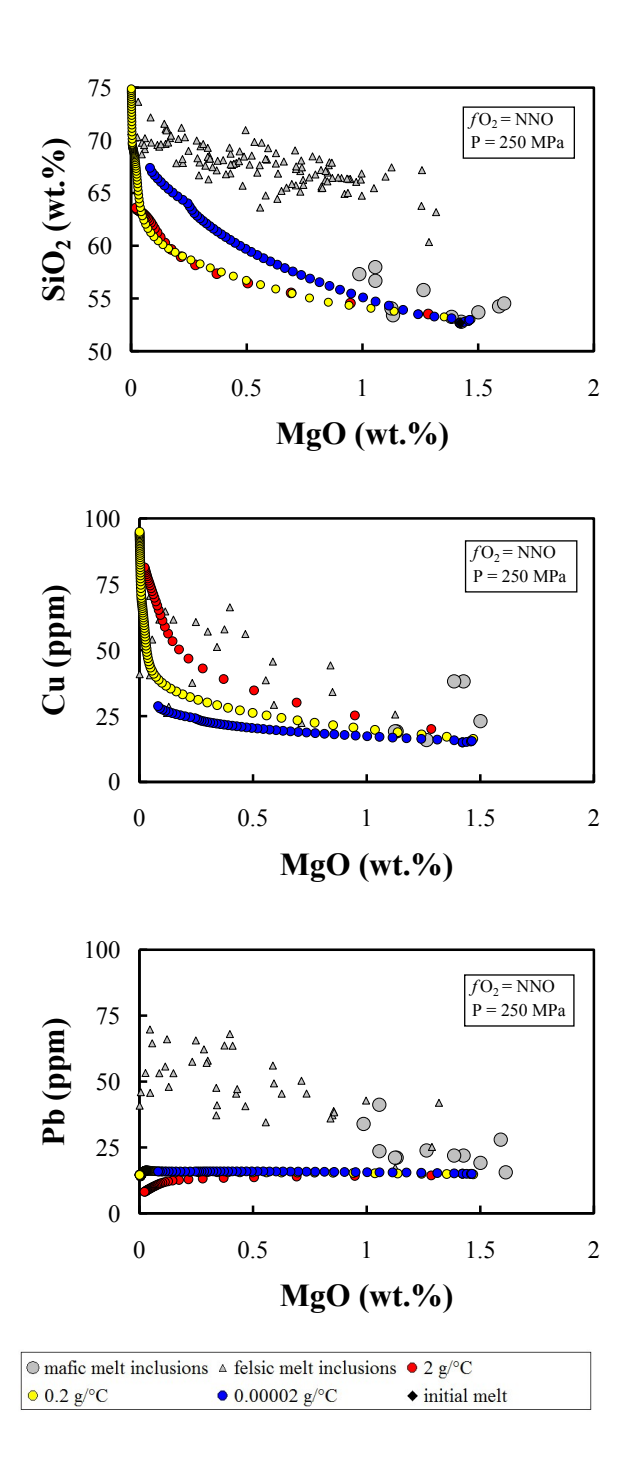
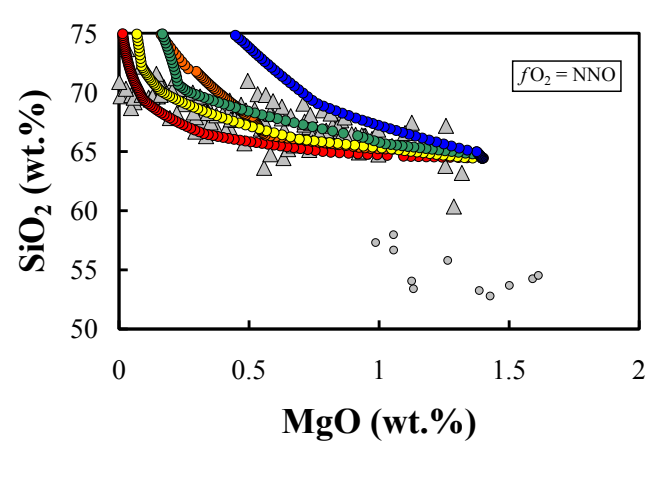
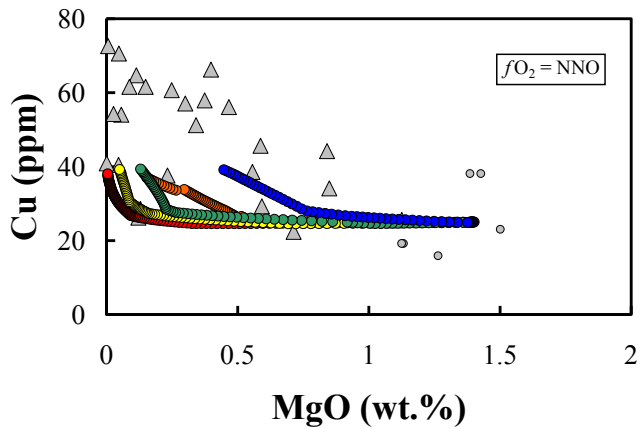
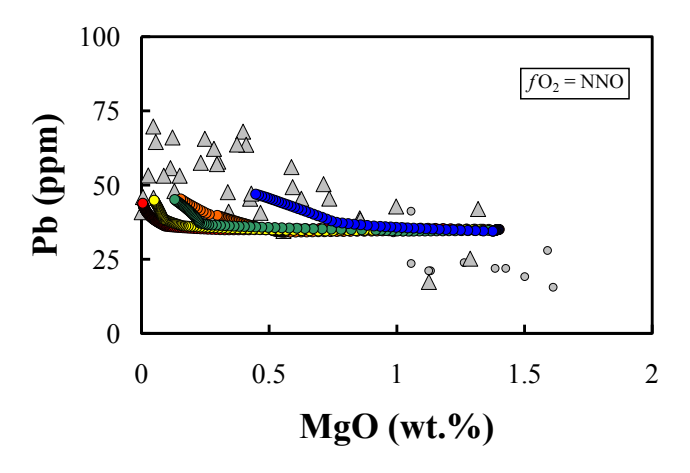


Figure 6. Concentrations of SiO2, Cu, and Pb versus MgO concentration using the MELTS model for fractional crystallization of the most primitive of the more felsic melt inclusions at a buffered oxygen fugacity of NNO and pressure varying from 450 MPa to 50 MPa at 100 MPa intervals. Also shown are the concentrations of both more mafic and

more felsic melt inclusions. FeO* stands for total iron and was calculated as FeO \pm 0.8998 \bullet (Fe2O3).







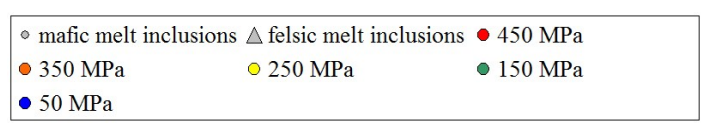
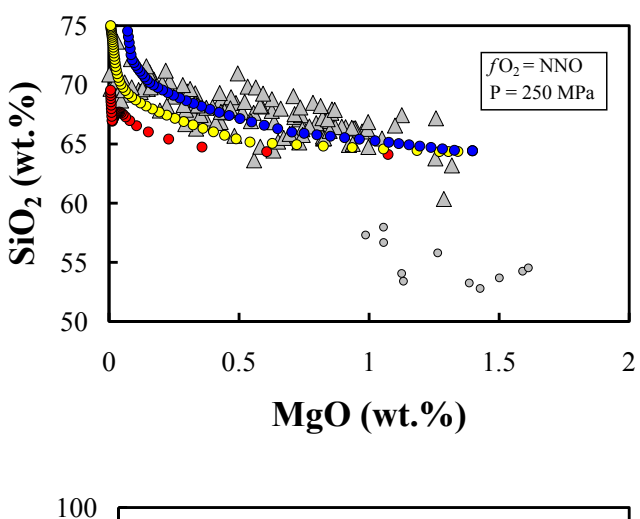
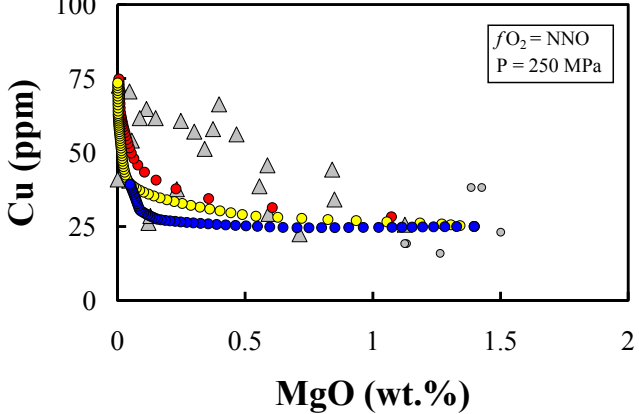


Figure 7. Concentrations of SiO2, Cu and Pb versus MgO concentrations using the MELTS model for assimilation of calc-silicate rocks (Table 4) and fractional crystallization of the most primitive of the more felsic melt inclusions. Oxygen fugacity was buffered at NNO and pressure kept constant at 250 MPa while calc-silicate rocks were assimilated at rates varying between 2, 0.2 and 0.00002 grams per degree Celsius of cooling. Also shown are the concentrations of both more mafic and more felsic melt inclusions. FeO* stands for total iron and was calculated according to FeO + 0.8998 • (Fe2O3).





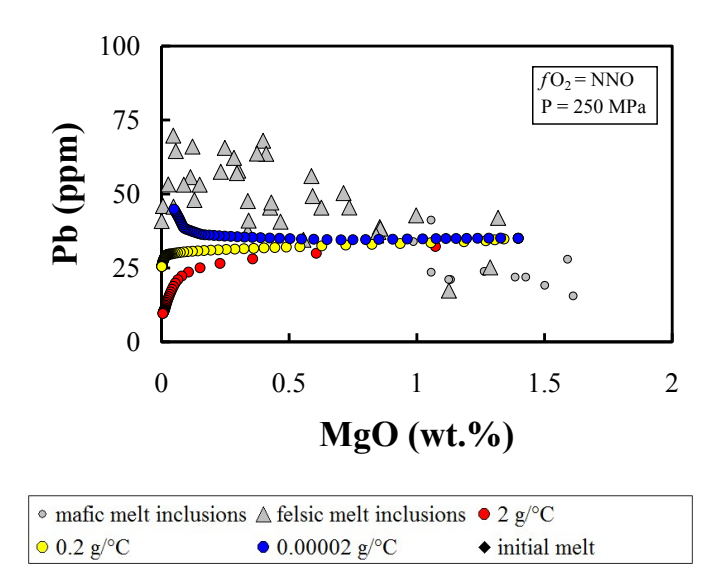


Figure 8. Concentration of Cu, Zn and Pb in Merapi bulk rocks and melt inclusions compared to other bulk arc rocks. Global arc data were obtained from the Georoc database (Sarbas et al., 2009; http://georoc.mpch-mainz.gwdg.de/georoc/Start.asp).

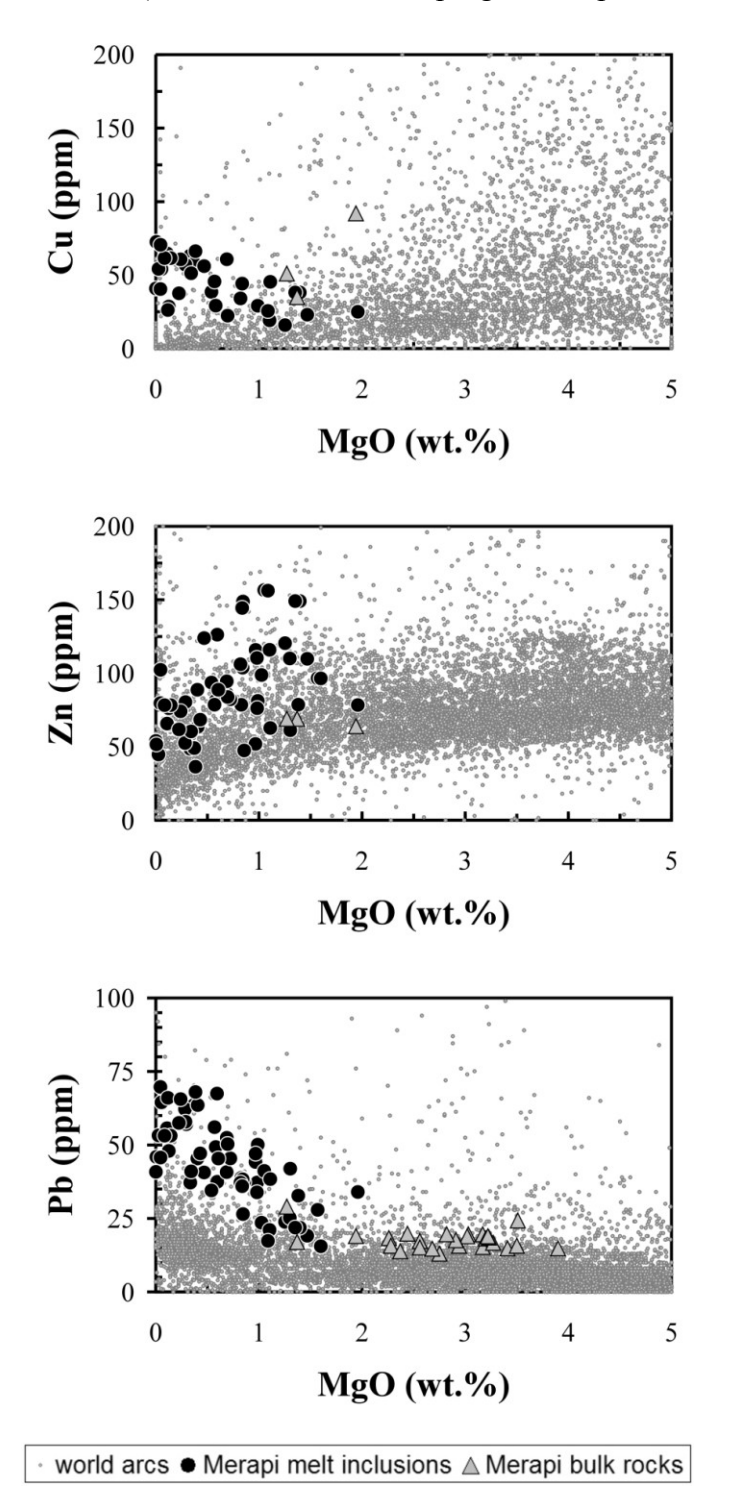


Figure 9. Photomicrographs of selected silicate melt inclusions. More mafic melt inclusions (8a, 8b and 8c) are hosted by megacrysts found in scorias, volatile-saturated and heterogeneously trapped with sulfide globules. More felsic melt inclusions (8d, 8e and 8f) are hosted by clinopyroxene phenocrysts and are also volatile saturated. All images except 8d and 8f were taken in reflected light, whereas 8d and 8f were taken in transmitted light. Note that that 8b is a closed system and that the sulfide has been partially dissolved by vapour (the bubble, formerly MVP).

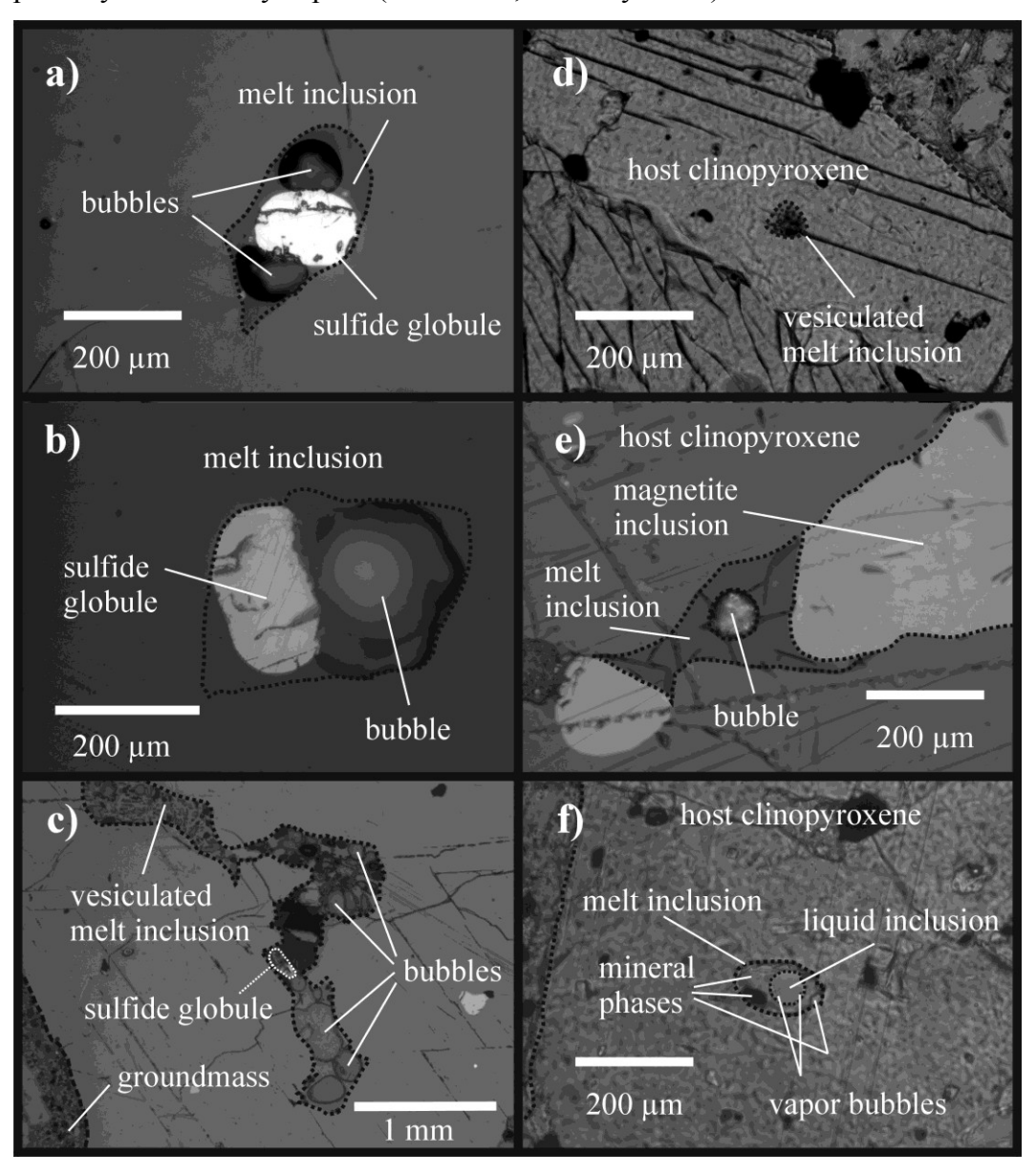


Figure 10. Concentration of Cu, Zn and Pb in fluid inclusions (Baker et al., 2004; Klemm et al., 2007; Kouzmanov et al., 2010; Landtwing et al., 2005; Pudack et al., 2009; Rusk et al., 2004; Ulrich et al., 1999; 2001; Williams-Jones et al., 2010) compared to that of the magmatic volatile phase (MVP) at Merapi, as calculated in the text. The black dot represents the average concentration of fluid inclusions and the Merapi MVP. The black vertical line represents the interquartile values, ranging from the 25th to the 75th percentile, for fluid inclusions and the full range of calculated concentrations of the Merapi MVP. The gray envelope shows the range of possible concentrations of fluid inclusions and the width of the envelope shows the relative number of values, in this case indicating a normal statistical distribution of the data. The calculated concentrations of Cu, Zn and Pb of the Merapi MVP are very similar to those of typical fluid inclusions.

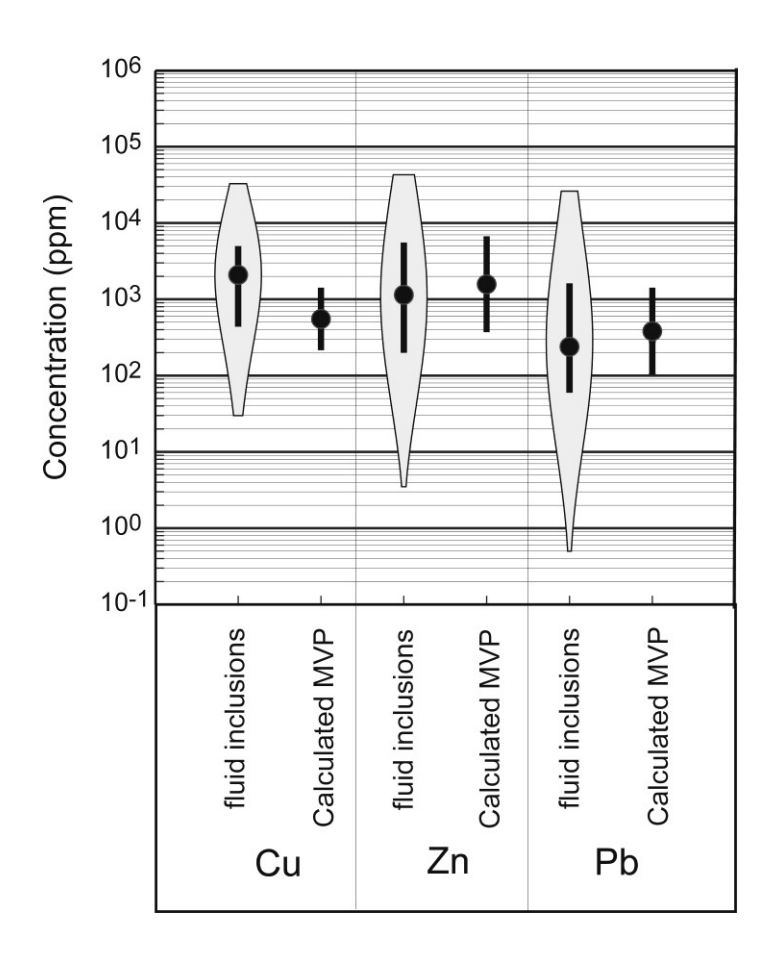
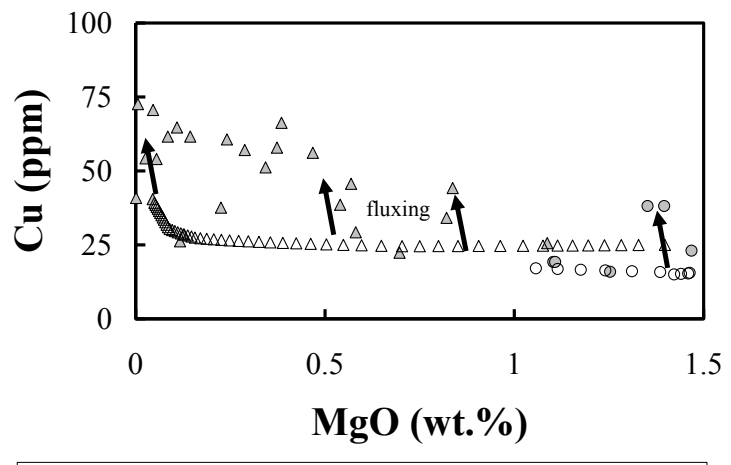
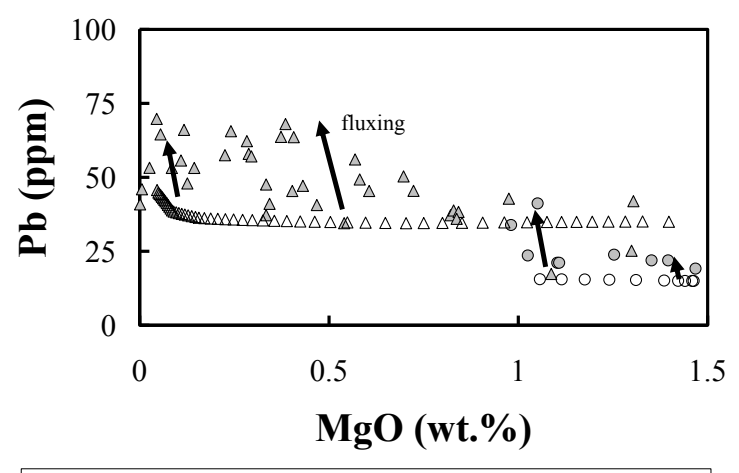


Figure 11. Plots of Cu and Pb versus MgO comparing AFC modelled concentrations of these elements versus the measured concentrations in melt inclusions. Also shown are arrows illustrating the amount of volatile fluxing required to explain the difference between the modelled and measured compositions. Empty and gray circles refer to mafic AFC and more mafic inclusions, whereas empty and gray triangles refer to felsic AFC and more felsic melt inclusions. The AFC model used is that of the assimilation of a mafic component at a rate of 0.00002 grams per degree Celsius, at fO2 = NNO and P = 250 MPa.



■ mafic melt inclusions △ felsic melt inclusions ○ mafic AFC △ felsic AFC

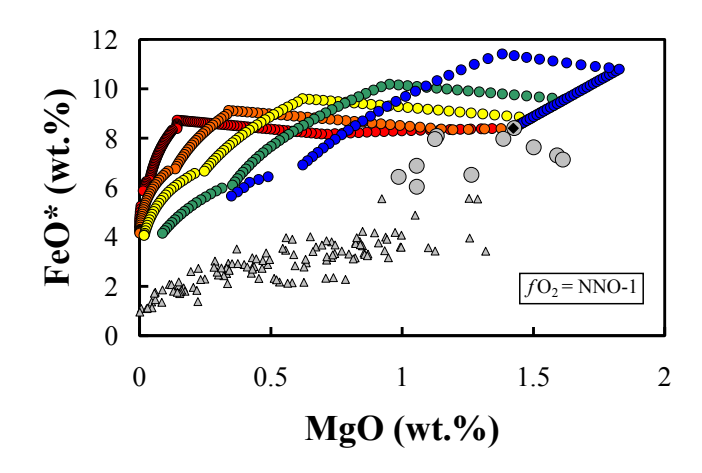


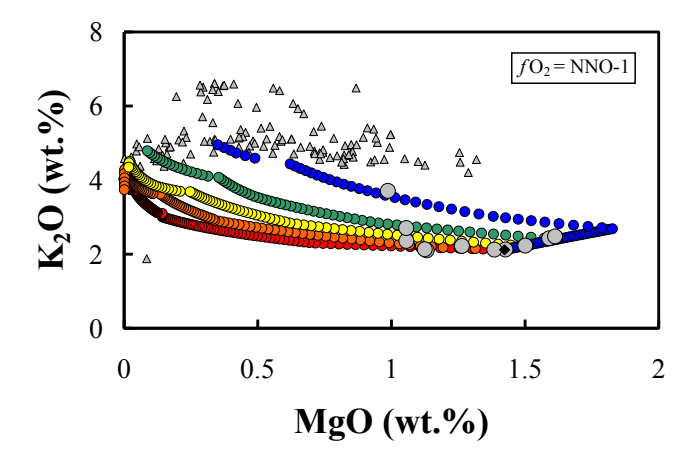
© mafic melt inclusions △ felsic melt inclusions ○ mafic AFC △ felsic AFC

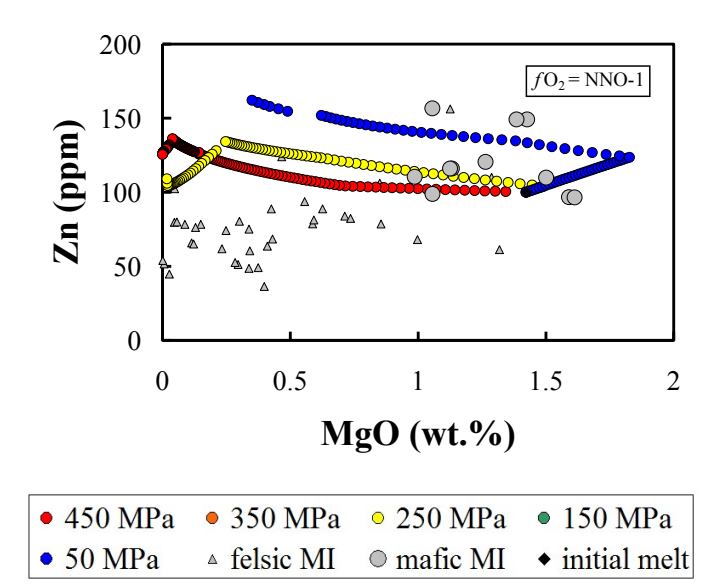
Appendices

Appendix 1. MELTS model for fractional crystallization of the most primitive mafic melt inclusion. Also shown are the concentrations of both mafic and felsic melt inclusions. a) Concentrations of FeO*, K_2O and Z_1 versus MgO concentrations. fO_2 is buffered at NNO-1 whereas pressure varies from 450 MPa to 50 MPa at 100 MPa intervals. b) Concentrations of SiO₂, FeO*, K_2O , Cu, Z_1 and Pb versus MgO concentrations . Pressure is fixed at 250 MPa whereas fO_2 varies from NNO-2 to NNO. FeO* stands for total iron and was calculated according to FeO + 0.8998 • (Fe₂O₃).

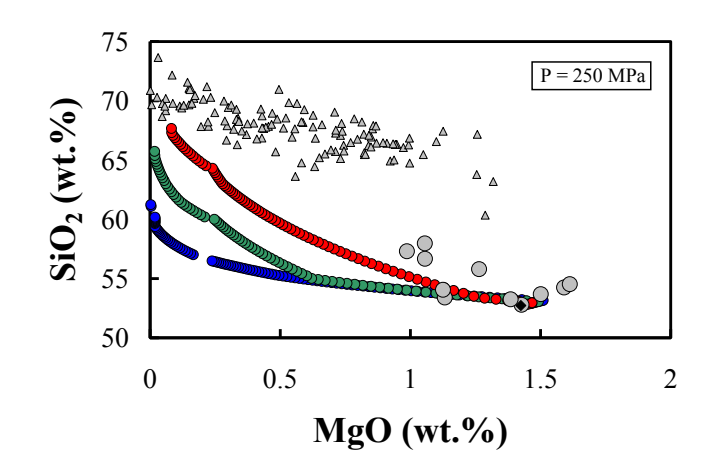
a) At fixed fO_2

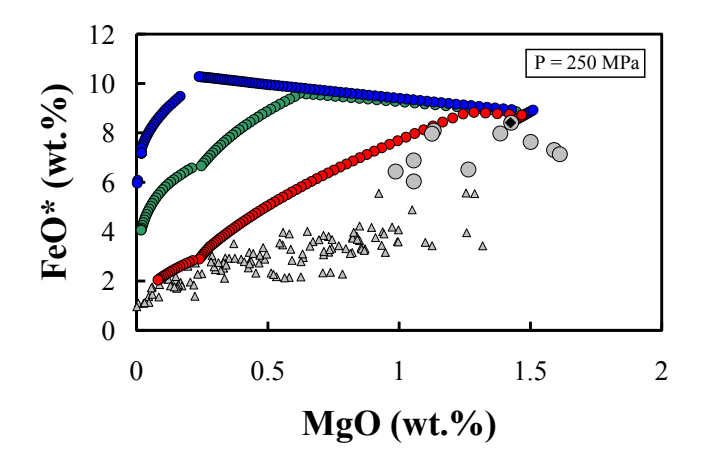


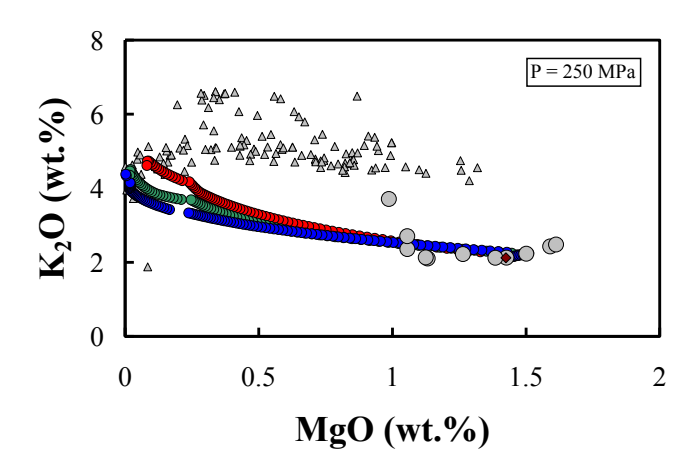


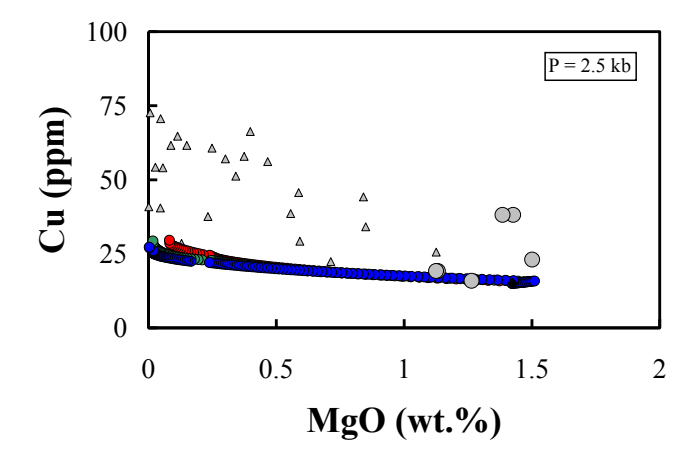


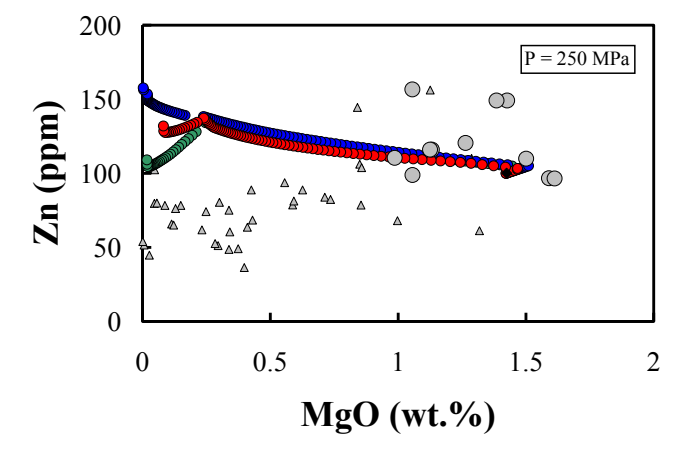
b) At fixed pressure

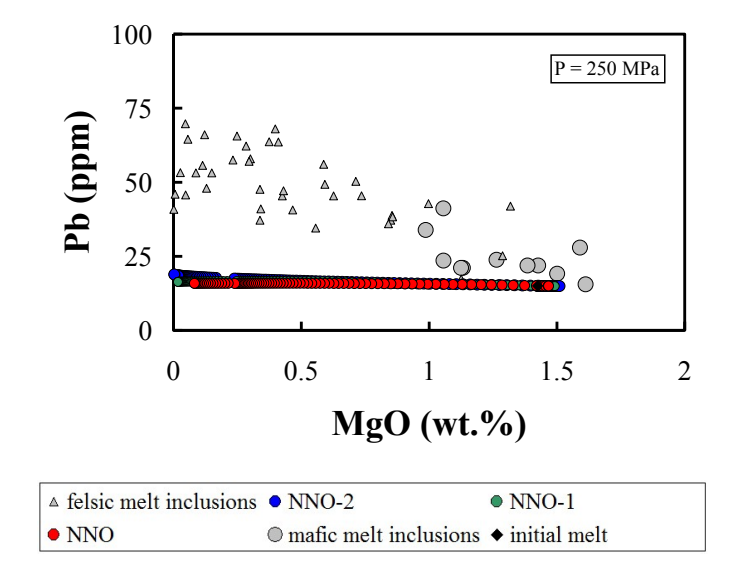






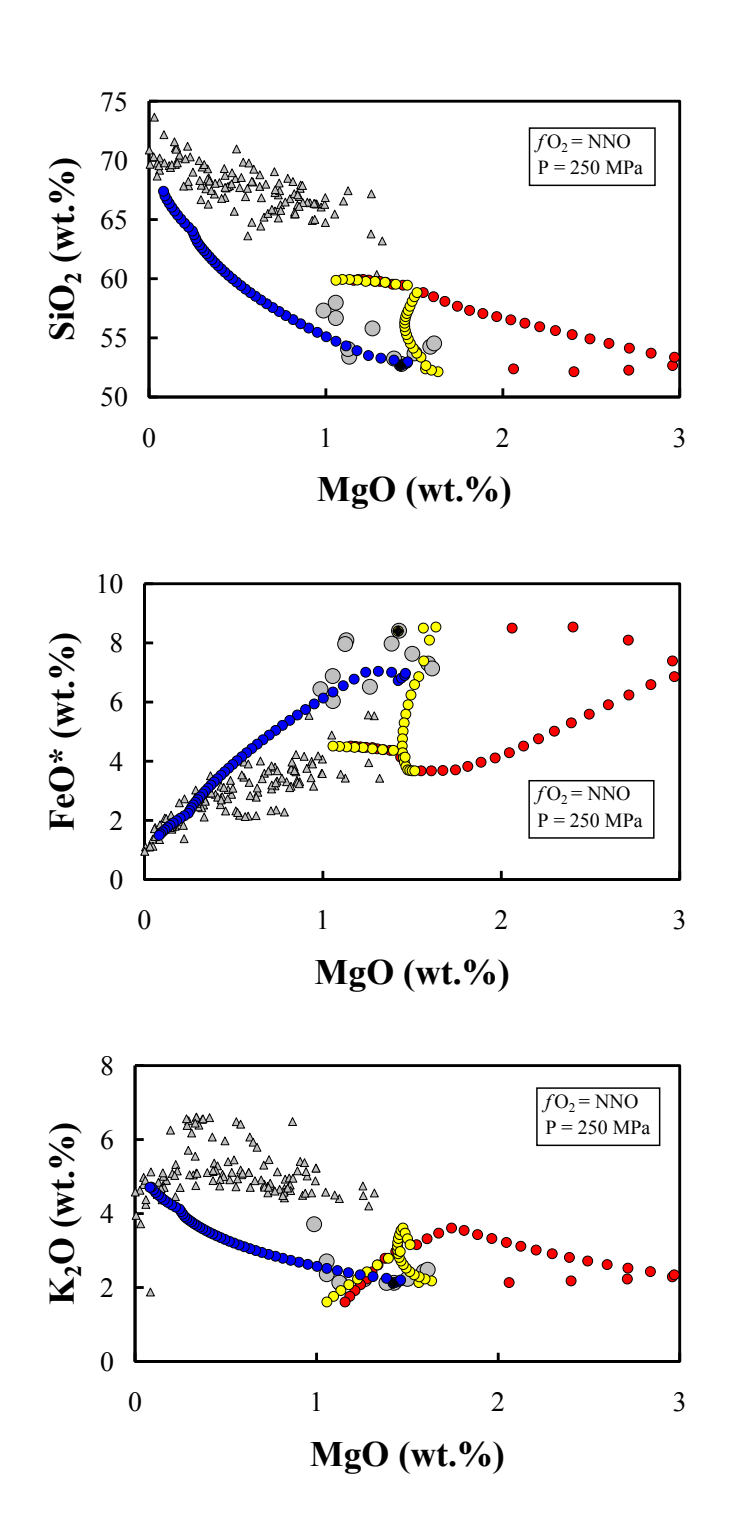


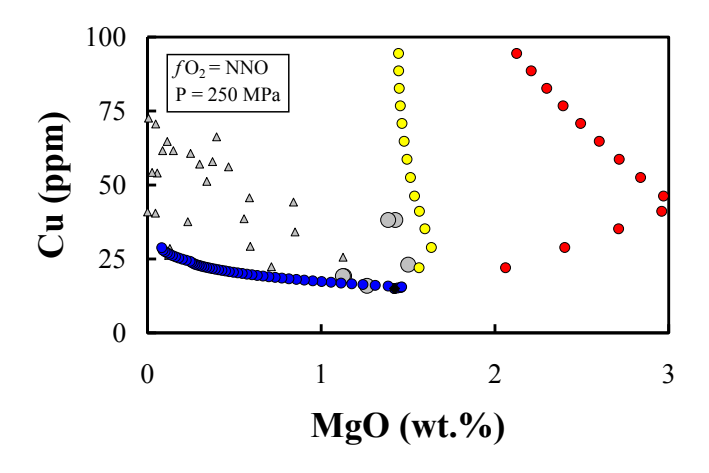


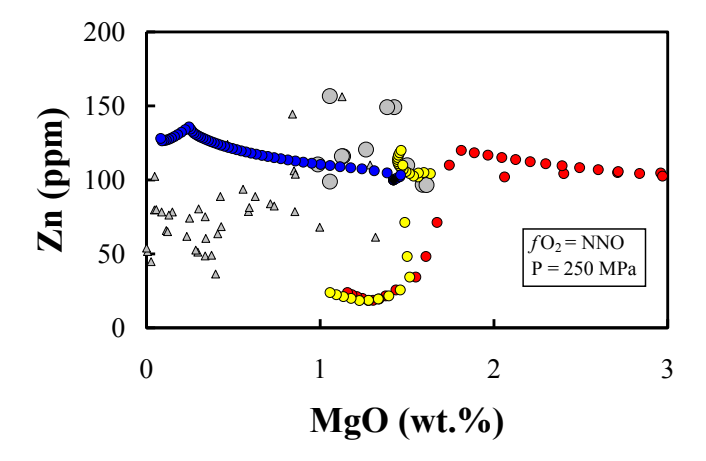


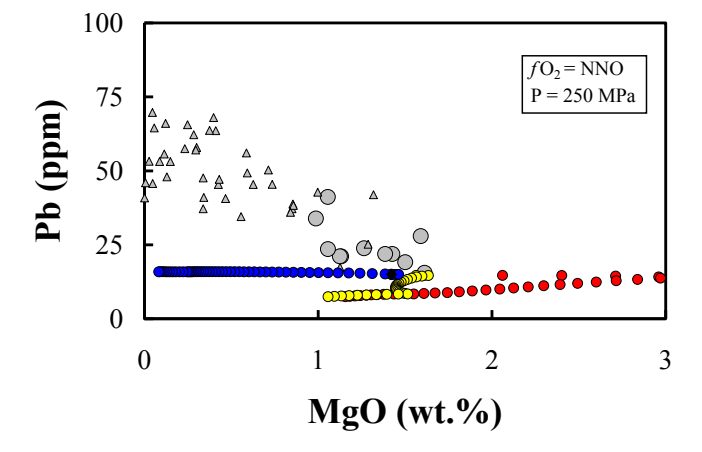
Appendix 2. MELTS model for assimilation and fractional crystallization in the mafic melt. Shown are rates of assimilation of 2, 0.2 and 0.00002 grams per degree Celsius of cooling. fO_2 is buffered at NNO and pressure is fixed at 250 MPa. Also shown are the concentrations of both mafic and felsic melt inclusions a) Concentrations of SiO₂, FeO*, K₂O, Cu, Zn and Pb versus MgO concentrations for assimilation of a mafic component. b) Concentrations of SiO₂, FeO*, K₂O, Cu, Zn and Pb versus MgO concentrations for assimilation of volcano-sedimentary rocks. c) Concentrations of FeO*, K₂O and Zn versus MgO concentrations for assimilation of calc-silicate rocks. FeO* stands for total iron and was calculated according to FeO + 0.8998 • (Fe₂O₃).

a) Assimilation of a mafic component

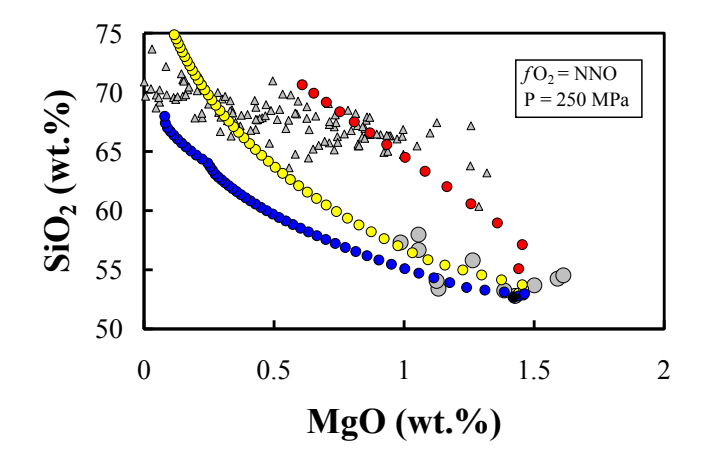


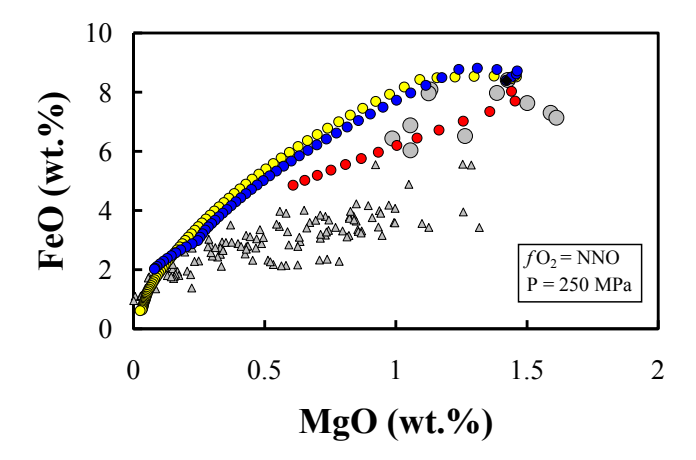


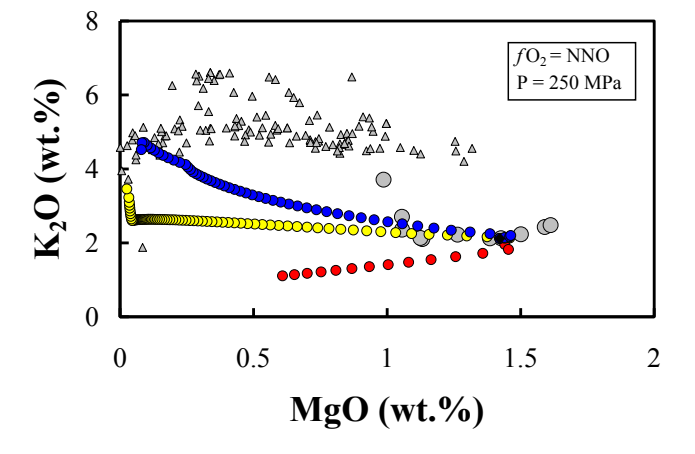


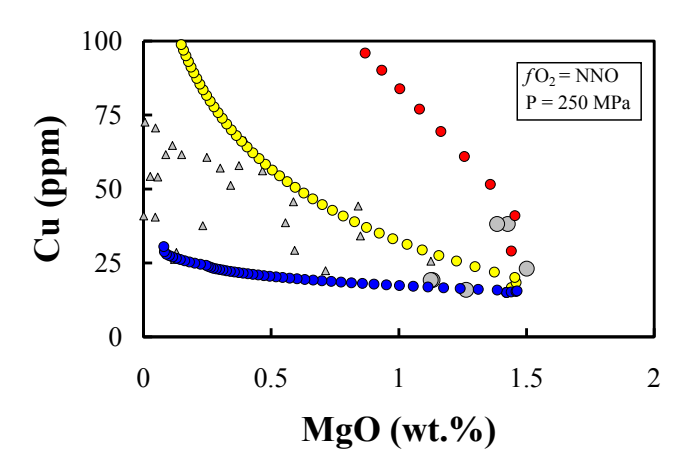


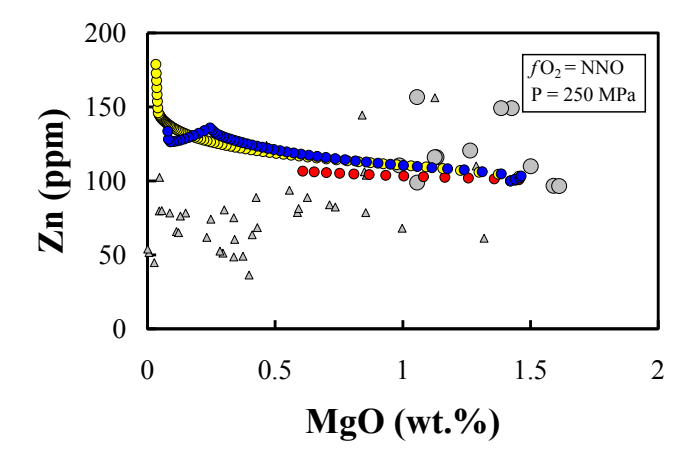
b) Assimilation of volcanosediments

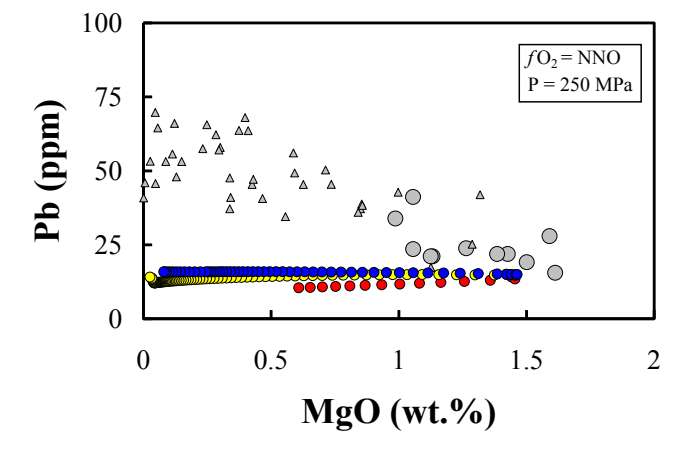




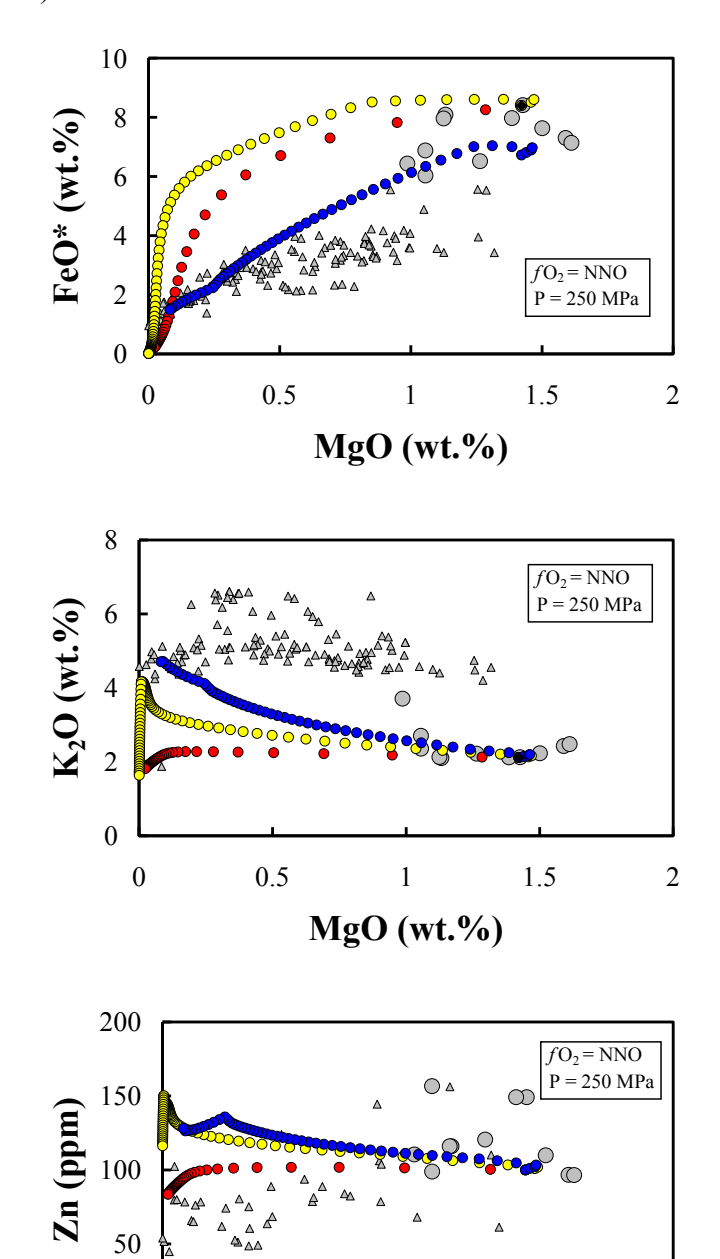


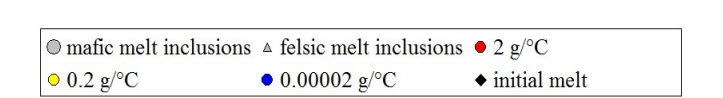






c) Assimilation of calc-silicates





MgO (wt.%)

0.5

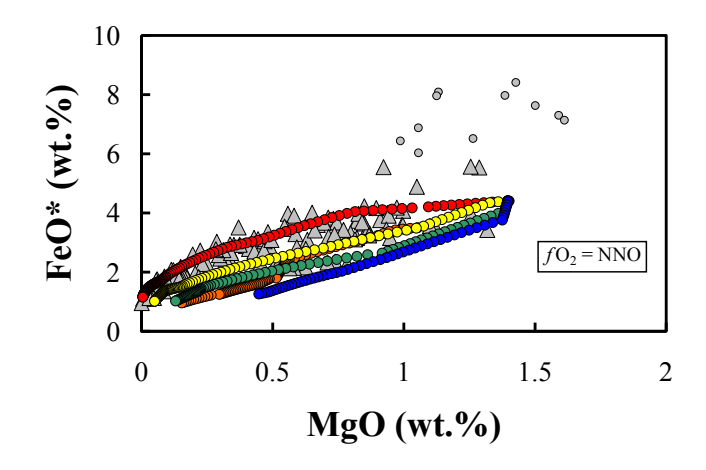
0

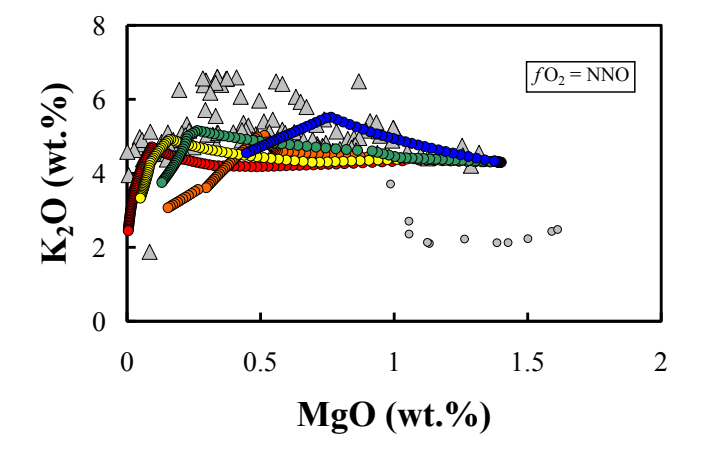
1.5

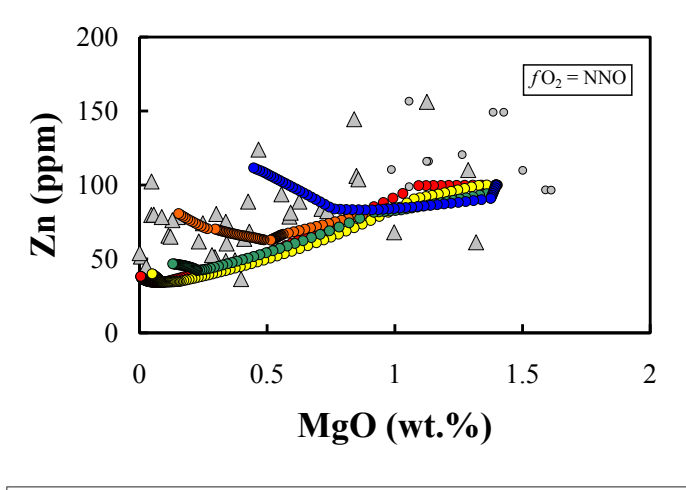
2

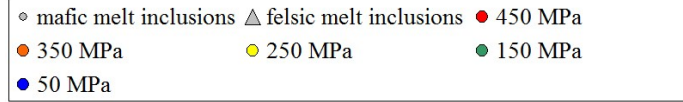
Appendix 3. MELTS model for fractional crystallization of the most primitive felsic melt inclusion. Also shown are the concentrations of both mafic and felsic melt inclusions. a) Concentrations of FeO*, K_2O and Z_1 versus MgO concentrations. fO_2 is buffered at NNO-1 whereas pressure varies from 450 MPa to 50 MPa at 100 MPa intervals. b) Concentrations of SiO₂, FeO*, K_2O , Cu, Z_1 and Pb versus MgO concentrations. Pressure is fixed at 250 MPa whereas fO_2 varies from NNO-1 to NNO+2 by log 1 intervals. c) Concentrations of SiO₂, FeO*, K_2O , Cu, Z_1 and Pb versus MgO concentrations. Pressure is fixed at 150 MPa and fO_2 buffered at NNO whereas initial water concentrations in the melt are varied between 1, 3 and 6 wt.%. FeO* stands for total iron and was calculated according to FeO + 0.8998 • (Fe₂O₃).

a) At fixed fO_2

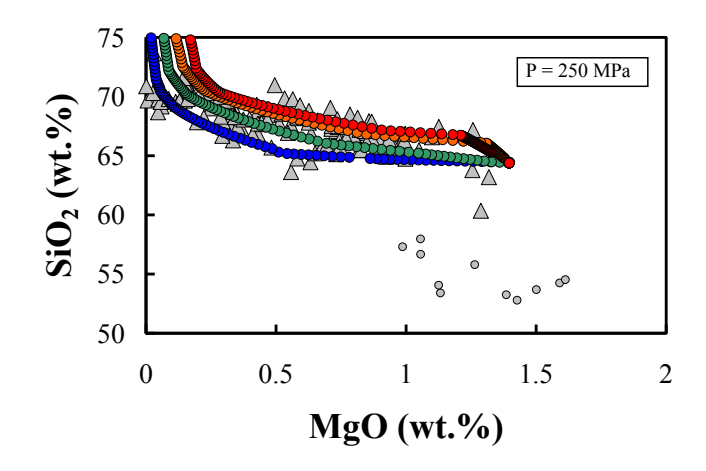


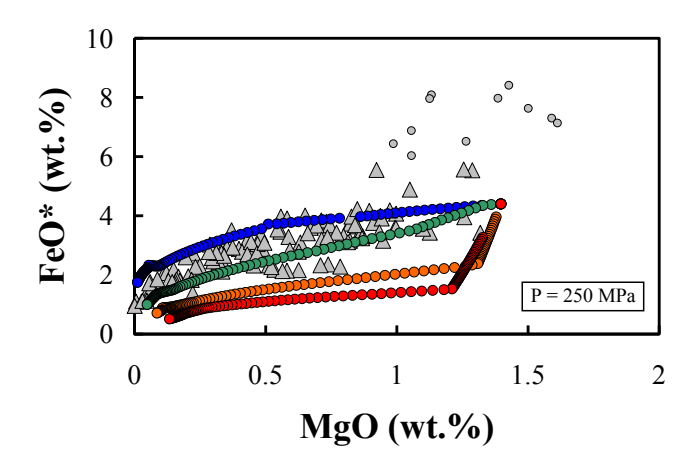


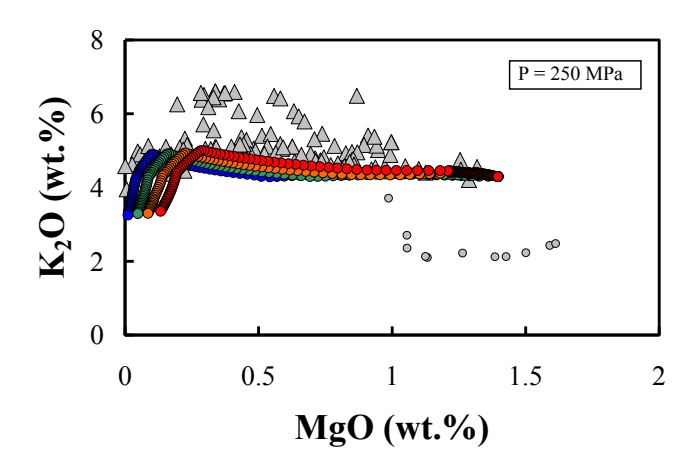


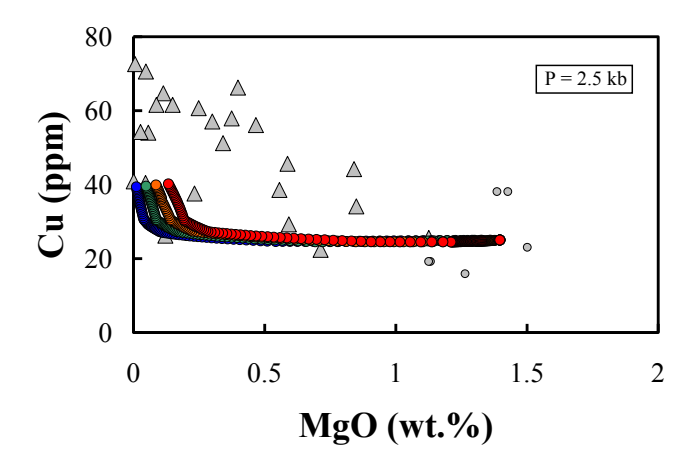


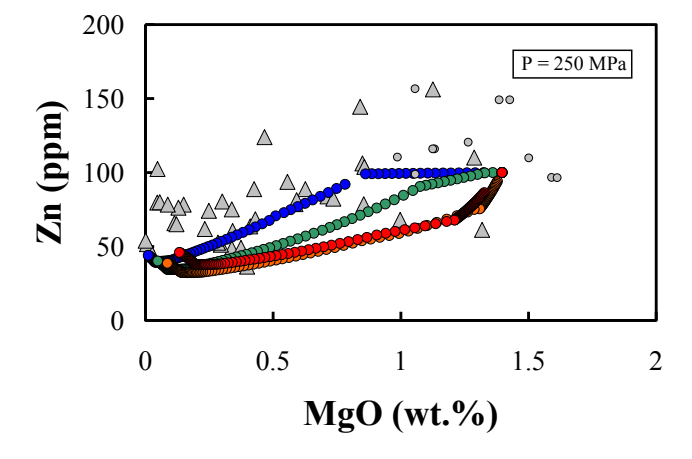
b) At fixed pressure

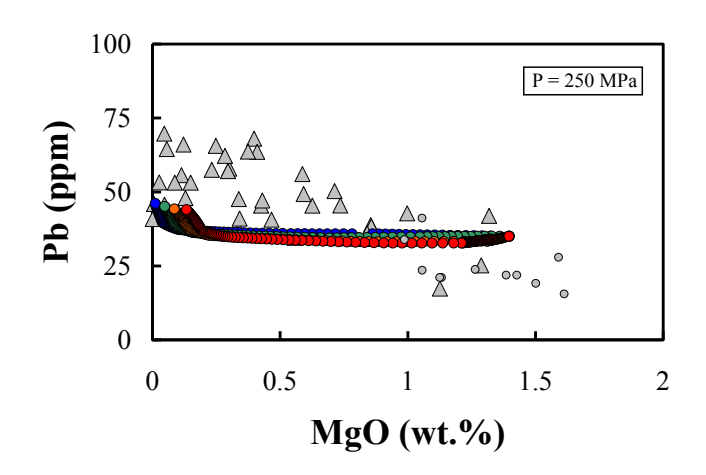


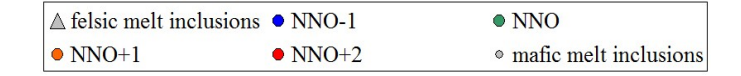




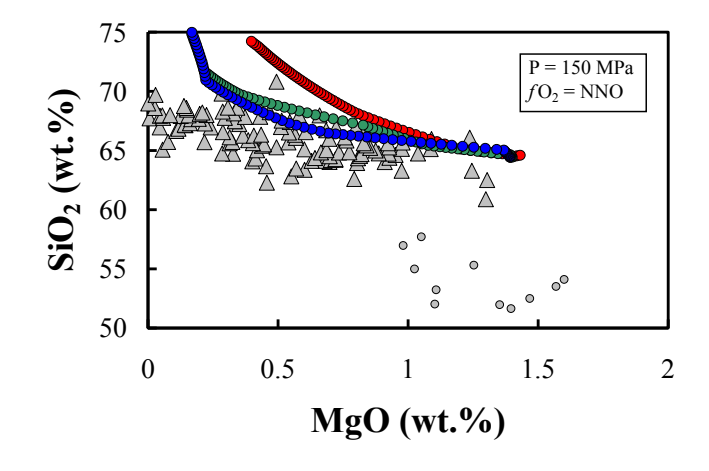


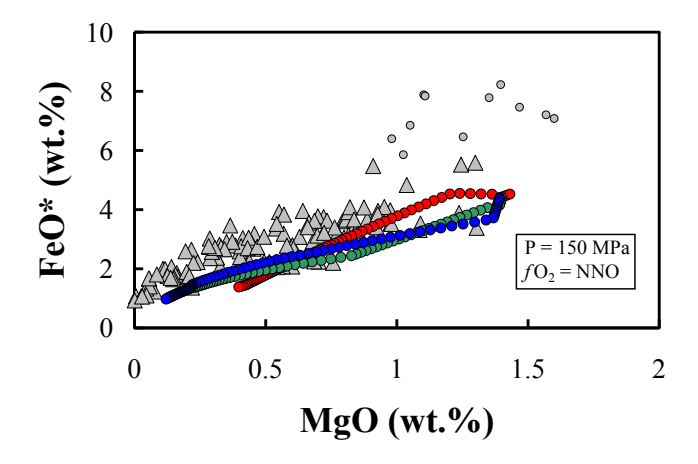


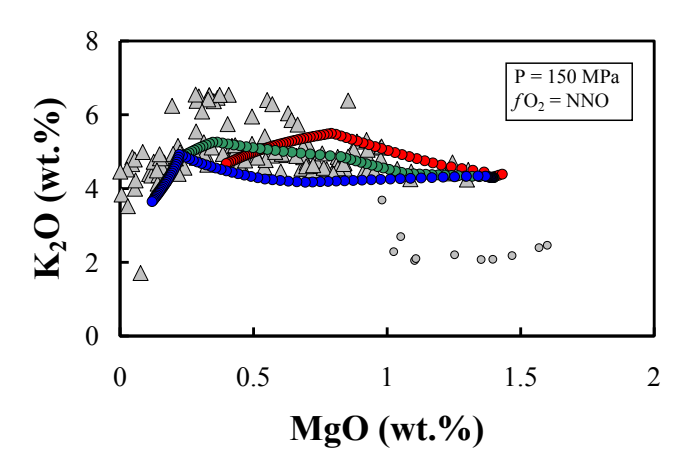


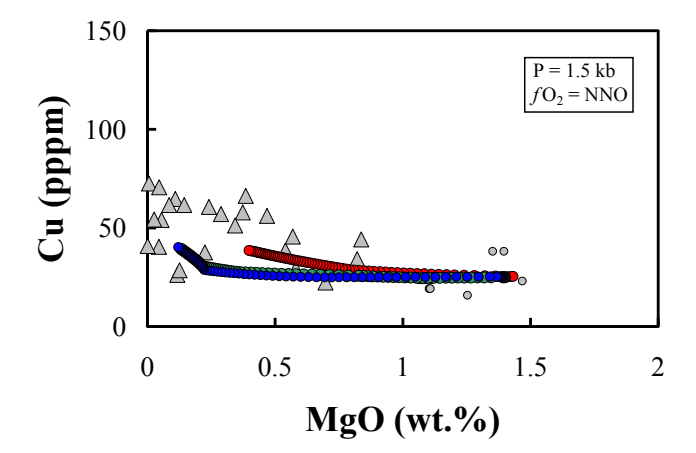


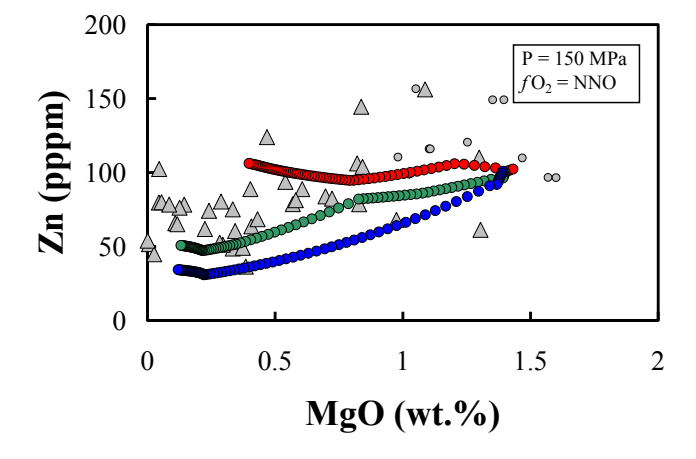
c) at different water content

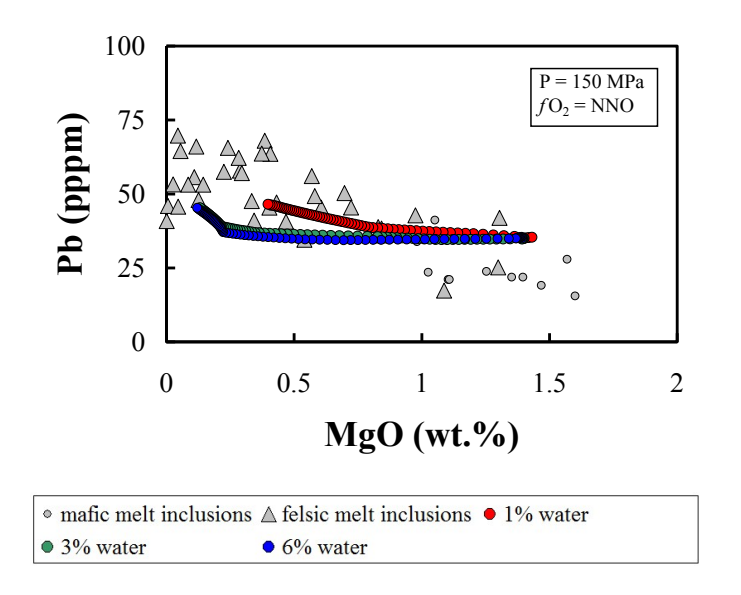






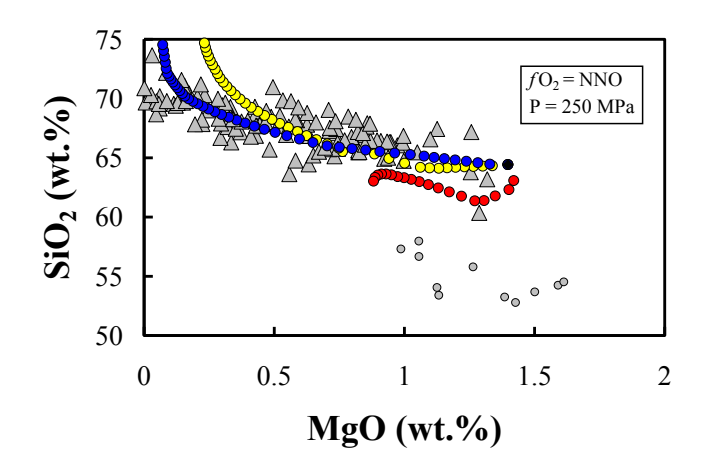


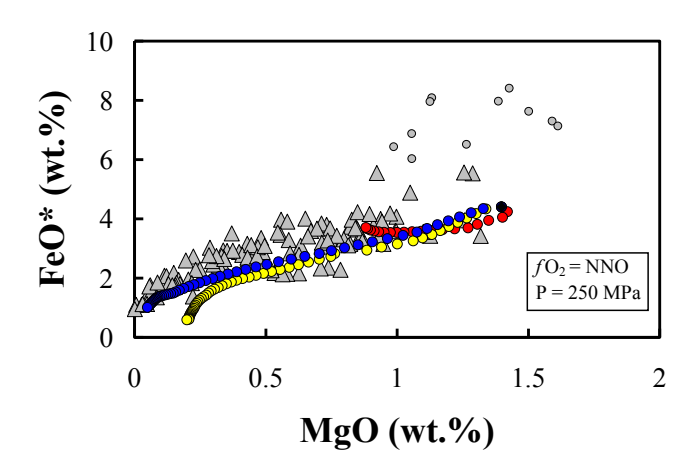


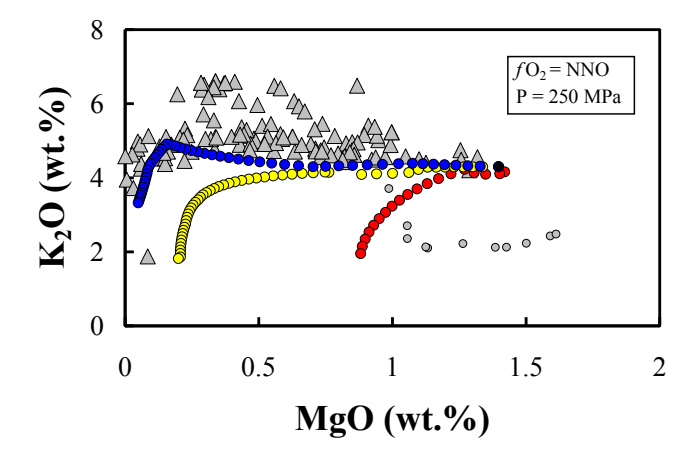


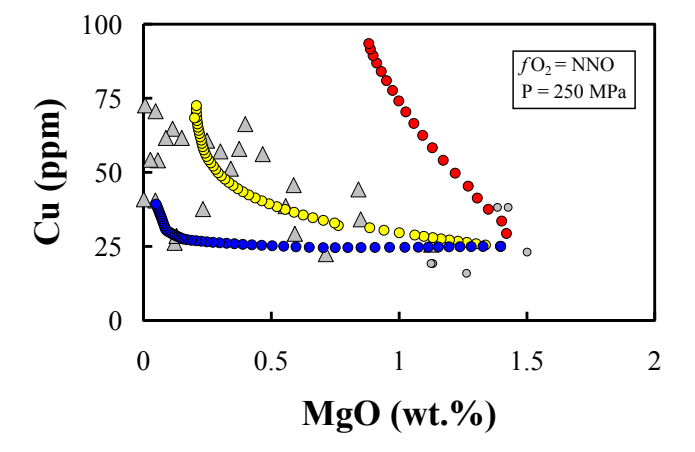
Appendix 4. MELTS model for assimilation and fractional crystallization in the felsic melt. Shown are rates of assimilation of 2, 0.2 and 0.00002 grams per degree Celsius of cooling. fO_2 is buffered at NNO and pressure is fixed at 250 MPa. Also shown are the concentrations of both mafic and felsic melt inclusions a) Concentrations of SiO₂, FeO*, K₂O, Cu, Zn and Pb versus MgO concentrations for assimilation of a mafic component. b) Concentrations of SiO₂, FeO*, K₂O, Cu, Zn and Pb versus MgO concentrations for assimilation of volcano-sedimentary rocks. c) Concentrations of FeO*, K₂O and Zn versus MgO concentrations for assimilation of calc-silicate rocks. FeO* stands for total iron and was calculated according to FeO + 0.8998 • (Fe₂O₃).

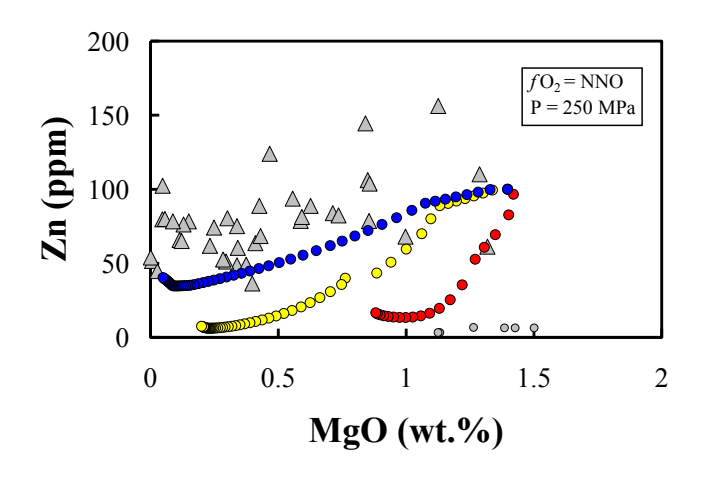
a) Assimilation of mafic component

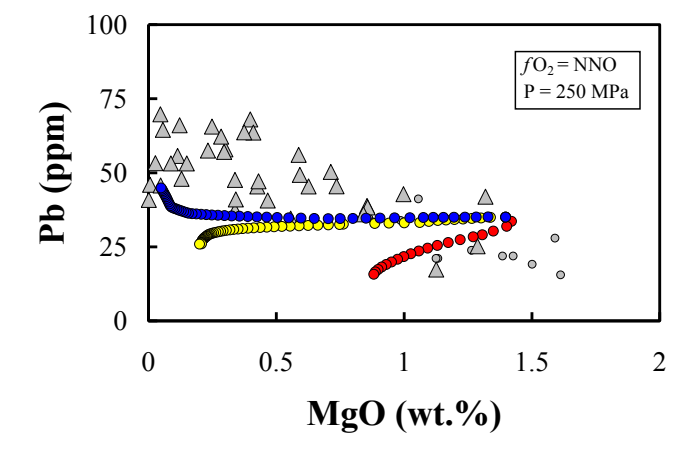




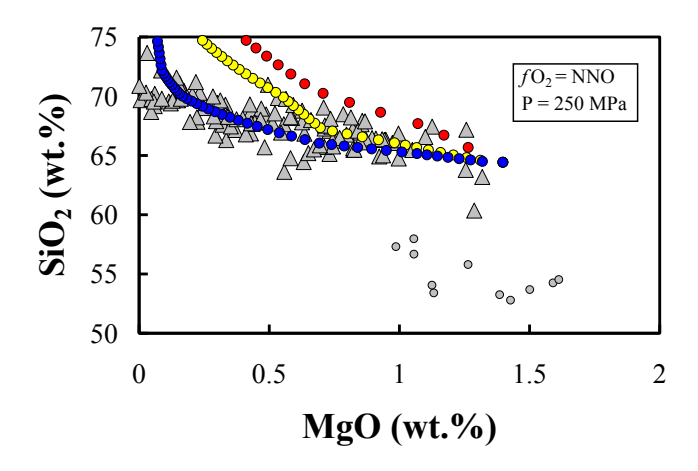


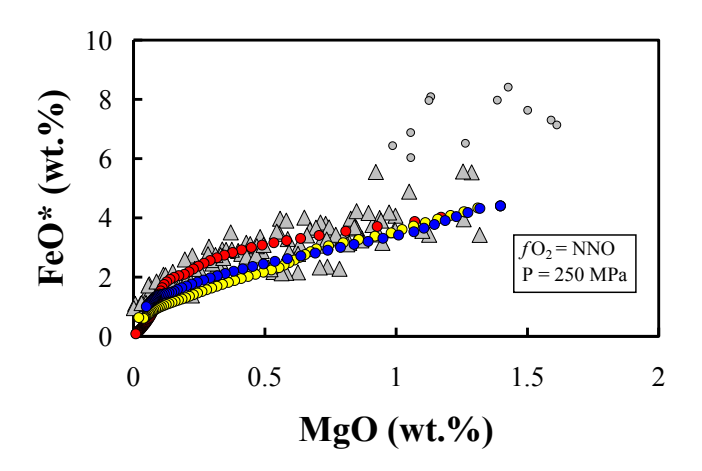


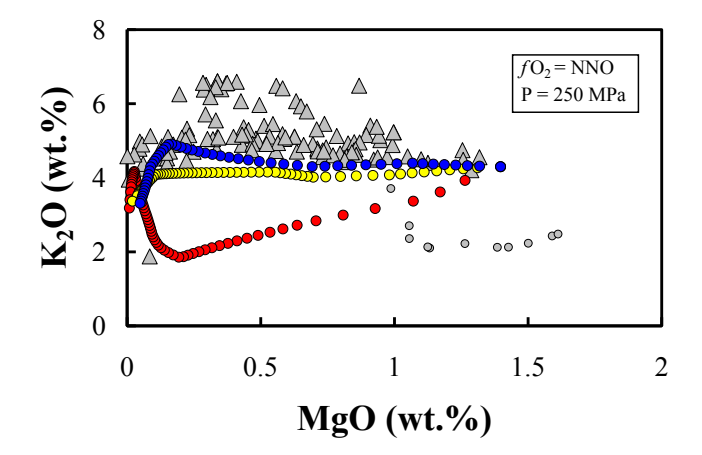


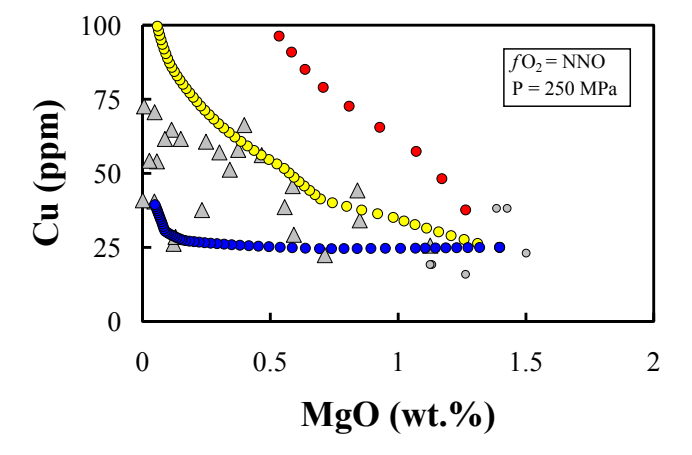


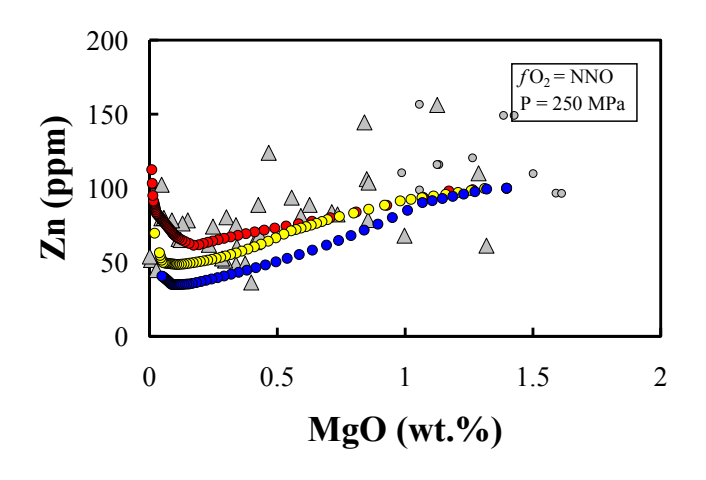
b) Assimilation of volcanosediments

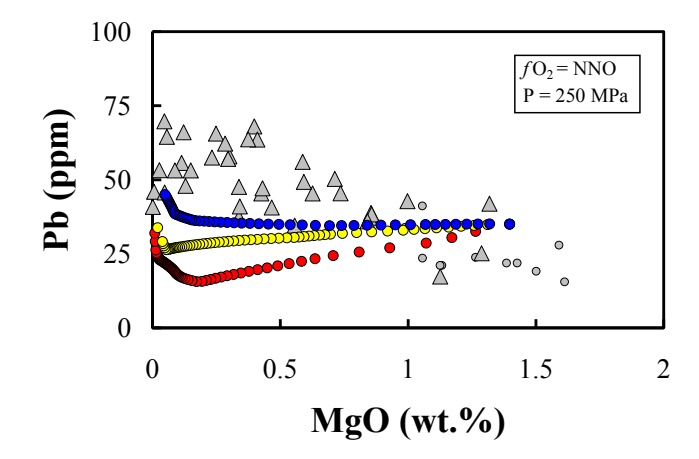




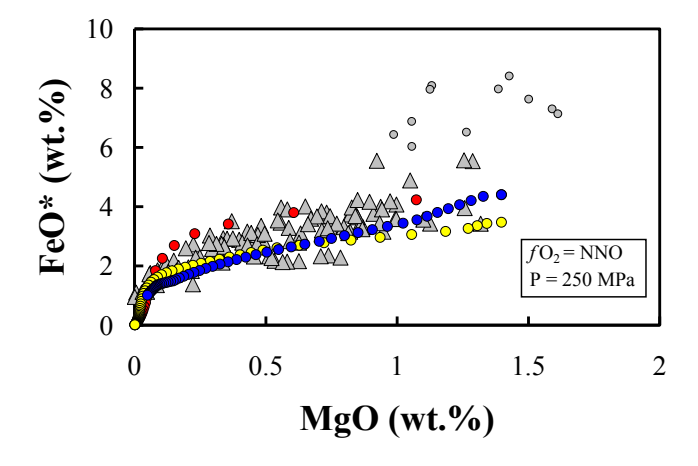


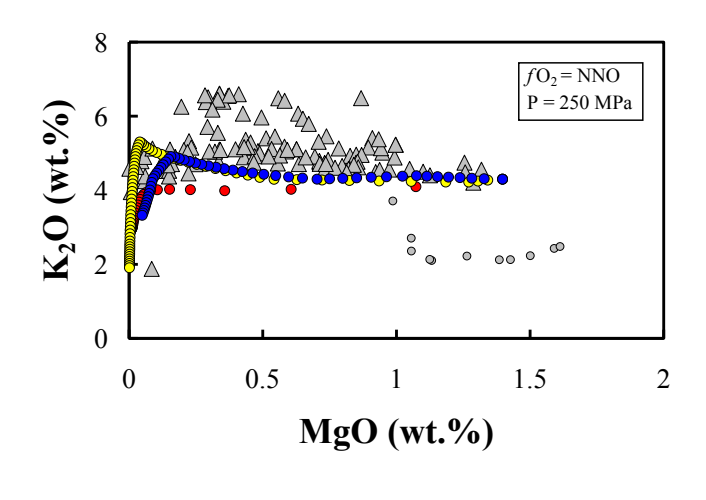


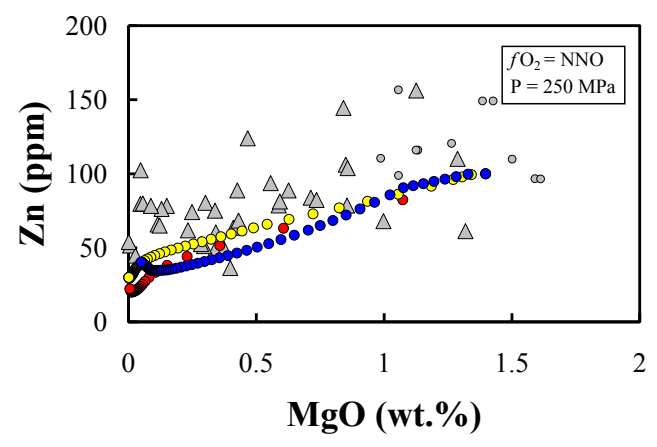




c) Assimilation of calc-silicates







mafic melt inclusions △ felsic melt inclusions
2 g/°C
0.2 g/°C
0.00002 g/°C
initial melt

Preface to chapter 3

The links that exist between volcanism and metallogenesis, the most direct being the existence of volcanogenic ore deposits and the presence of ore deposits within cogenetic volcanic rocks, are here examined. Although it is generally agreed that porphyryepithermal deposits form during the waning stages of volcanic activity, and that volcanic activity must be low when the magmatic-hydrothermal ores form, in the third and last main chapter of this thesis I compare the chemistry of these fluids, represented by fluid inclusions and volcanic gases, to shed light on the processes that occur within the porphyry-epithermal environment. By synthesizing the ratios of Cu, Zn, Pb and Mo to Na in fluid inclusions found in porphyry Cu (Mo) and comparing these to those from volcanic gases I show that these metals are zoned in the porphyry-epithermal environment, with Cu being deposited proximally to the magma, with gradual transitions to zones of Zn and Pb. Based on the fact that at Merapi (1) injections of reduced mafic magma result in explosive eruptions and in volcanic gases that are more reduced and enriched in Cu and Pb, and (2) periods of volcanic quiescence are related to fractional crystallization, enrichment of incompatible elements such as Mo in the shallow reservoir and to the quiescent degassing of more oxidized, Cu- and Pb-depleted and Mo-enriched gases, I build a model for the construction of porphyry-epithermal deposits.

Chapter 3

The Nature of Ore-forming (Cu, Mo, Pb, Zn)

Magmatic-Hydrothermal Systems: Insights from the

Compositions of Volcanic Gases and Fluid Inclusions

Olivier Nadeau, Anthony E. Williams-Jones and John Stix

Manuscript under review in Economic Geology and the Bulletin of the Society of Economic Geologists

1. Abstract

Strong links exist between arc-type stratovolcanoes and porphyry-epithermal magmatichydrothermal systems, the most direct being the occurrence of porphyry Cu and epithermal Au deposits in cogenetic volcanic rocks. Despite this, the nature of oreforming processes under active volcanoes has remained elusive. In principle, important insights into these processes can be gained from the trace metal composition of volcanic gases, which has been analyzed at numerous volcanoes for approximately fifty years. Recently, as a result of the development of micro-analytical techniques, it has also been possible to obtain similar information for the proximal volatile phases by analyzing inclusions of these fluids trapped close to the source magma. Consequently, there is now a sizeable body of data on the concentration of Cu, Zn, Pb and Mo in magmatichydrothermal fluids sampled both at depth below the volcano (proximal) and on its surface (distal). In this paper, we evaluate these two sets of data in order to determine the changes that occur between the environment of porphyry ore formation and the fumarolic or epithermal environment. We show that Cu, Zn and Pb are deposited in concentric zones around the magma reservoir upon injection of reduced mafic magma, with Cu deposited earlier and closer to the magma and Zn and Pb later and more distal from it. Molybdenum only deposits once the magma has evolved and oxidized through fractional crystallization and degassing. Using volcanic gas samples collected at Merapi volcano, Indonesia, immediately after an explosive eruption and during periods of quiescent degassing, we also consider the processes operating in magmatic-hydrothermal systems during the eruptive cycle. We show that injections of mafic magma and associated eruptions are accompanied by pulses of reducing, Cu-, Zn-, and Pb-rich fluids, by strong decompression of the system, and by large-scale deposition of a Cu-enriched, reduced mineral assemblage, whereas intervening periods of quiescent degassing are dominated by assimilation and fractional crystallization and by circulation of fluids, which become progressively more oxidized, more depleted in Cu, Zn and Pb, and more enriched in Mo.

2. Introduction

It is now widely recognized that active arc-type subvolcanic environments host magmatic-hydrothermal systems which may be forming porphyry- and epithermal-type ore deposits (e.g., Sillitoe, 1973; Henley and Ellis, 1983; Hedenquist and Lowenstern, 1994). Also, it is commonly accepted that magmatic-hydrothermal ores deposit when magmatic volatile phases (MVP) exsolve from intermediate to felsic magmas and cross steep physico-chemical gradients caused, for example, by cooling, decompression, fluid-mixing, boiling, and reaction with the wall-rock (e.g., Lowell and Guilbert, 1970; Gustafson and Hunt, 1975; Henley and McNabb, 1978; Reynolds and Beane, 1985; Hedenquist et al., 1998; Hezarkhani and Williams-Jones, 1998; Ulrich and Heinrich, 2001; Rusk et al., 2004; Klemm et al., 2007). As a result of recent advances in micro-analytical techniques, new insights into the nature of these magmatic-hydrothermal fluids are possible by analyzing trace elements in fluid inclusions trapped in minerals that grew at depth in these systems.

Volcanic gases are the surface expressions of these magmatic volatile phases (MVP) and record the changes that occur in magmatic-hydrothermal systems as volcanoes cycle through episodes of eruption and quiescence. The chemical composition of these gases can be determined by analyzing samples collected at volcanic fumaroles. Volcanic gases are thus related to MVP trapped as fluid inclusions, although the relationship between them and the MVP has remained elusive. We explore this relationship in this paper.

Here we establish a link between porphyry-epithermal-type magmatic-hydrothermal systems and arc-type volcanic systems by comparing volcanic gases from calc-alkaline stratovolcanoes and fluid inclusions from porphyry Cu (Au-Mo) ore deposits. We summarize and compare the concentrations of Cu, Zn, Pb and Mo and their ratios to Na in fluid inclusions (Ulrich et al., 1999; 2001; Rusk et al., 2004; Landtwing et al., 2005; Klemm et al., 2007; Pudack et al., 2009; Seo et al., 2009; Kouzmanov et al., 2010) and in volcanic gases (Oana, 1962; Mizutani, 1970; Stoiber and Rose, 1970; Menyailov and Nikitina, 1980; Menyailov, 1986; Gemmell, 1987; Symonds et al., 1987; 1990; 1996; Hedenquist et al., 1994; Taran et al., 1995; 2001; Wahrenberger et al., 2002;

Zelenski and Bortnikova, 2005; van Hinsberg et al., in press; and this study). Evidence is presented for a concentric zonation of metals depositing from fluids around a shallow magma chamber, with Cu being deposited earlier and proximal to the magma, followed by Zn and Pb at progressively greater distances. Our synthesis of the volcanic gas data and particularly our data from Merapi volcano show further that reducing Cu-rich fluids are associated with injections of reduced mafic magma into shallow, oxidized porphyry systems and that these fluids evolve during Cu-mineral deposition towards more oxidized, Cu-depleted and Mo-rich compositions, culminating in the deposition of a Mo-enriched, oxidized mineral assemblage.

3. Geological setting of Merapi Volcano

Merapi is an active calc-alkaline stratovolcano located in Central Java, Indonesia, and a product of the ongoing subduction of the Indo-Australian plate under the Eurasian plate. The volcano appears to have begun erupting during the Pliocene, with its oldest volcanic rocks having been dated at 3.44 Ma (Newhall et al., 2000), although most of its activity appears to have occurred in the last 40,000 years (Camus et al., 2000). Within its lifetime, the volcano has experienced frequent plinian to sub-plinian explosive eruptions (Andreastuti et al., 2000; Camus et al., 2000; Newhall et al., 2000). At the beginning of the 20th century, Merapi underwent a change in its style of activity that has continued to the present day. During the current phase of activity, Merapi has been erupting viscous lava domes, which grow and collapse. These eruptions have been interspersed with occasional St-Vincent-type explosions, generating incandescent pyroclastic flows and associated surges (e.g., in 2006 and in 2010). The eruptive periods, which are usually of several months' duration, are separated by periods of quiescent degassing, typically lasting a few years.

Merapi lavas are of calc-alkaline affinity, range in composition from 49.5 to 60.5 wt. % SiO₂, and contain abundant normally and reversely zoned plagioclase (An₃₄₋₉₃) crystals, which coexist with fresh and resorbed crystals of clinopyroxene (augite), amphibole (pargasite, magnesio-hornblende and magnesio-hastingsite), titanomagnetite, and rare

olivine, orthopyroxene and apatite (Camus et al., 2000). Alkali feldspar occurs as microlites or rims plagioclase phenocrysts (Hammer et al., 2000). In some cases, fragments of scoria contain light, rhyolitic layers among darker dacitic layers (Camus et al., 2000). Eruptive products include gabbroic enclaves and calc-silicate xenoliths interpreted to be partially assimilated products of calcareous wall-rock (Camus et al., 2000; Chadwick et al., 2007).

Three high-temperature fumarole fields have been active at the summit of the volcano since at least 1978, namely the Dome, Gendol and Woro fields (Allard and Tazieff, 1979). Temperatures have been highest at the Gendol fumarole field, reaching 900°C in 1978 (LeGuern and Bernard, 1982). In 2004, we measured temperatures at Gendol reaching 754°C. The temperatures of the gases emanating at Woro are somewhat lower; we measured temperatures up to 580°C in 2004, and up to 515°C in 2006.

4. Methodology

4.1 Fluid inclusions

The ranges and average concentrations of Cu, Zn, Pb and Mo in fluid inclusions reported in this paper were compiled from data for a suite of selected fluid inclusions found in samples from the Bajo de la Alumbrera Cu-Au porphyry deposit, Argentina (Seo et al., 2009; Ulrich et al., 1999; 2001), the Bingham Cu-Au-Mo porphyry deposit, USA (Landtwing et al., 2005), the Butte Cu-Mo porphyry deposit, USA (Rusk et al., 2004), the El Teniente Cu-Mo porphyry deposit, Chile (Klemm et al., 2007), the Famatina Cu-Au-Mo porphyry deposit and the La Mejicana Cu-Au high sulfidation epithermal deposit, Argentina (Pudack et al., 2009) and the Rosiea-Poieni Cu-Au porphyry deposit, Romania (Kouzmanov et al., 2010). These data are presented in Figure 1 and reported in Appendix 1. We have chosen these fluid inclusion data because they are from well-known research groups, are published in very reputable journals, are derived from a suite of subduction-zone-related calc-alkaline magmatic-hydrothermal environments such as that now present beneath Merapi, and the authors have classified the inclusions into physically distinct groups, i.e., supercritical or subcritical single-phase fluids, vapors and brines.

Unfortunately, data are not available for Cu, Zn, Pb and Mo concentrations in fluid inclusions originating from barren intrusions in equivalent environments.

4.2 Volcanic gas condensates

The concentrations of Cu, Zn, Pb and Mo in volcanic gas condensates reported in this paper are from samples analyzed from Satsuma Iwojima (Hedenquist et al., 1994), Showashinzan (Oana, 1962; Mizutani, 1970; Symonds et al, 1996), Kawa Ijen (van Hinsberg et al., in press), New Tolbachik (Menyailov and Nikitina, 1980), Momotombo (Menyailov et al., 1986), Cerro Negro (Stoiber and Rose, 1970), Augustine (Symonds et al., 1990), Kudryavy (Taran et al, 1995; Wahrenberger et al., 2002), Colima (Taran et al., 2001), Mutnovsky (Zelenski and Bortnikova, 2005) and Merapi (Symonds et al., 1987; this study). These volcanoes were selected because of the considerable time span over which they were sampled, the quality of the methods used for sampling and because they are located in subduction zones.

We also collected gas condensates at Merapi volcano. This involved sampling fumaroles in the Gendol (2004 and 2005) and Woro (2004 and 2006) fields using a meter-long fused silica tube connected to an ice-trap condenser via a short silicon rubber tube; gases could not be sampled at Gendol in 2006 because the field was destroyed by the 2006 eruption. The ice-trap condenser was filled with ice, gases were hand-pumped slowly through the condenser, and liquid that collected in the ice trap was stored in Teflon bottles. Some condensates were visually clear, whereas others contained yellow precipitates. The precipitates were filtered, weighed and analyzed separately. Solid and liquid fractions of the condensates were analyzed at Actlabs Inc., Ontario, Canada, by ICP-MS, ICP-OES, neutron activation (INAA), ion chromatography and conductivity.

4.3 Volcanic gas sublimates

Our sampling of gas condensates at Merapi volcano was complemented by sampling of the corresponding sublimates. This involved inserting meter-long, fused silica tubes into the fumaroles immediately after the condensates had been collected and waiting until

sufficient solid had precipitated on the inner walls of the tubes to permit them to be sampled. In 2004, tubes were inserted in six fumaroles in the Gendol field and two in fumaroles in the Woro field, for periods varying between four and six days. In 2006, tubes were placed in two fumaroles in the Woro field, for a period of 22 days. The sampling was done during the dry season to avoid dissolution and redistribution of sublimates by rain. After insertion of the tubes in the fumaroles but prior to sublimate accumulation, temperatures were measured along the tube centerlines at 10 cm intervals using a meter-long thermocouple. In Montreal, the tubes were cut into sections representing increments of 10 to 20°C. The sublimates were scraped off and a fraction of each sublimate was mounted on thin sections and polished. As several of the sublimate phases are water-soluble (e.g., halite and sylvite), the polishing agent (aluminum oxide or diamond paste) was suspended in alcohol rather than water. The phases in the polished sections were analyzed chemically using a JEOL JXA-8900L electron microprobe (EMPA) at McGill University. A second fraction of sublimate was scanned using a Siemens D500 X-ray diffractometer equipped with a Co tube and a Si detector at the Université du Québec à Montréal. The diffraction patterns were analyzed using Jade software at McGill University for identification of major phases.

4.4 Data analysis

NCSS statistical software was used to display the fluid inclusion and volcanic gas data as 'violin plots' showing the range of base metal concentrations. As violin plots also display interquartile values from the 25th to the 75th percentile and a 'density trace' showing the relative number of data points for each concentration, it was possible to reliably visualize the distribution of the data. Most of the data points are normally distributed, although for populations in which the number of data points was small (e.g., Mo concentrations in volcanic gas condensates, which are often below the limit of detection), this is not the case. We thus focused and placed most emphasis on normal values, from the 25th to the 75th percentile, for our generalizations of fluid inclusion and volcanic gas concentrations in Cu, Zn, Pb and Mo.

5. Results

5.1 Fluid inclusions

The concentrations of Cu, Zn, Pb and Mo in fluid inclusions from the studies cited above are shown in Figure 1 and tabulated in Appendix 1. In the presentation that follows, concentration ranges refer to those between the 25th and 75th percentiles (the majority of the data). These fluid inclusions are subdivided into three categories: single-phase supercritical fluid inclusions (Fig. 1a), brine inclusions (Fig. 1b) and vapor inclusions (Fig. 1c). Supercritical fluid inclusions represent deeper, more primitive fluids. Brine and vapor inclusions represent both phases of a fluid that has unmixed. Copper concentration reaches its maximum value in supercritical fluid inclusions, in which it ranges from about 2000 to 8000 ppm, and in which Zn and Pb have their lowest values, Zn ranging from 100 to 300 ppm and Pb from 20 to 60 ppm. Concentrations of Mo are low and range from 7 to 40 ppm. Zinc, lead and molybdenum have their highest concentrations in brine inclusions; Zn concentration ranges from 3000 to 9000 ppm, Pb from 1000 to 3000 ppm and Mo from 30 to 300 ppm. In these inclusions, Cu concentration is generally lower than that of Zn, ranging from about 300 to 3000 ppm. By contrast, the concentration of Cu in vapor inclusions is almost as high as in supercritical fluid inclusions, ranging from about 500 to 6000 ppm, whereas Zn and Pb concentrations are much lower, ranging from 40 to 700 ppm and from 10 to 100 ppm, respectively, and Mo has its lowest concentration, i.e., between 6 and 30 ppm.

In general, supercritical fluid and vapor inclusions are most enriched in Cu, most depleted in Mo and have intermediate values of Zn and Pb, with Zn being more enriched than Pb. However, brine inclusions are noticeably different in having concentrations of Zn, Pb and Mo approximately one order of magnitude higher than in the other types of fluid inclusions.

5.2 Volcanic gas condensates

The concentrations of Cu, Zn, Pb and Mo in volcanic gas condensates from the volcanoes referred to above are shown in Figure 2 and reported in Appendix 2. Concentrations for Merapi are also reported in Table 1. The concentrations of each of the four base metals under study vary in gas condensates by about three to four orders of magnitude. However, their normal statistical distribution allows us to treat them as we did the fluid inclusion data, by using the interquartile values in the violin plots as the significant ranges. Figure 2a shows the concentration of Cu, Zn, Pb and Mo for all volcanic gas samples gathered from the literature and for gases for Merapi volcano analyzed in this study. In all volcanic gas condensates, Cu is more depleted than the other base metals considered in this study, with values from about 0.01 to 0.2 ppm, whereas the other metals (Zn, Pb, Mo) vary from about 0.1 to 1 ppm, which is about one order of magnitude higher. Gas condensates from Merapi volcano have very similar Pb and Mo concentrations to those of other arc volcanoes (approximately 0.1 to 1 ppm and 0.1 to 0.3 ppm, respectively). At Merapi, Zn is somewhat depleted (0.1 to 0.2 ppm) as is Cu (0.005 to 0.03 ppm) (Fig. 2a) and the corresponding ranges for other arc volcanoes are 0.1 to 1 ppm and 0.01 to 0.2 ppm, respectively. In general, volcanic gas condensate concentrations of Cu, Zn, Pb and Mo range from about 10⁻³ to 10¹ ppm, whereas concentrations of these metals in fluid inclusions range from about 10⁰ to 10⁵ ppm, i.e., about 3 to 4 orders of magnitude higher.

In order to understand the reasons for the great variability of metal concentration in volcanic gases, we first looked for a correlation between the concentrations of Cu, Zn, Pb and Mo in gas condensates and the silica or alkali content of the associated volcanic rocks, and found none. We then subdivided the volcanic gas data into five temperature groups 85°C to 200°C, 201°C to 400°C, 401°C to 600°C, 601°C to 800°C and 801°C to 1020°C. After confirming that metal concentrations in the Merapi gases are similar to those of gases from other volcanoes at equivalent temperatures, we included the data for Merapi with the data for the other volcanoes (Figs 2b to 2e). Figure 2b displays the concentration of Cu in volcanic gas condensates with respect to temperature for all the volcanoes considered, and Figures 2c, 2d and 2e do the same for Zn, Pb and Mo, respectively. In general, volcanic gases sampled at temperatures below 400 or 500°C

represent mixtures of magmatic gases with gases from other sources, e.g., groundwater (Symonds et al., 1994). Copper concentration is substantially higher in the 801°C to 1020°C temperature group than in the lower-temperature groups, with values reaching 2 ppm. In the other temperature groups, its concentration is at least an order of magnitude lower, reaching up to 0.2, and there is no obvious correlation with temperature; condensates in the 201°C to 400°C group actually have slightly higher Cu concentrations than the 401°C to 600°C and 601°C to 800°C groups. By contrast, the concentrations of Zn and Pb correlate strongly with temperature, in the case of Zn reaching up to 8 ppm and in the case of Pb, up to 3 ppm. In general, Zn is hence more concentrated in volcanic gases than is Pb. The distributions for Mo generally behave irregularly, as is evident from the anomalous shapes of the gray envelopes and the highly variable length of the interquartile bars of Fig. 2e. This is due to the fact that the Mo concentration is commonly below the analytical limit of detection. Consequently the distributions are more difficult to interpret than those for the other metals. The average concentration of Mo is approximately constant at about 0.2 ppm for gases at temperatures higher than 200°C. If we neglect the exaggerated downward extension of the interquartile bar for gases in the 401-600°C group, we observe that the interquartile lines gradually extend towards higher concentrations with increasing temperature of the gases. This suggests that there also may be a positive correlation of Mo concentration with temperature.

As discussed earlier, fumarolic gases at Merapi volcano were sampled during periods of quiescent degassing as well as immediately after an eruption (this study). We report here the concentrations of Cu, Zn, Pb and Mo and their ratios to K in individual gas condensates sampled from the Woro field at Merapi in 1984 (quiescent degassing; Symonds et al., 1987) and 2004 (quiescent degassing), and immediately after the explosive eruption of 2006 (Fig. 3). Sodium could not be used as a basis of normalization because Symonds et al. (1987) did not report its concentration. The concentrations of Cu, Zn, Pb and Mo in condensates from the Gendol field and their ratios to Na and K, as well as the concentrations of these metals ratioed to Na for condensates from the Woro field, are reported in Appendix 3. The concentration of Cu in gas condensates from the Woro field was significantly higher after the explosive eruption in 2006, reaching about 0.1 ppm as compared to 0.003 ppm in a sample collected during quiescent degassing in 2004;

the other 2004 sample had a Cu concentration below the limit of detection. The concentration of Pb was also higher in 2006 (up to 8.5 ppm) than in 2004 (up to 1.4 ppm) or in 1984 (up to 0.8 ppm). Concentrations of Cu and Zn in gas condensates from Merapi in 1984 (Symonds et al., 1987) could not be used in this comparison because of contamination with Cu and Zn from the pump (Symonds et al., 1990). The destruction of the Gendol fumarole field during the eruption of 2006 prevented us from sampling it after the eruption, and thus comparing the concentration of base metals at Gendol before and after this explosive event. The concentration of Mo in the condensate from Woro in 2006 was below the limit of detection for one sample, and very low (0.6 ppb) in the other, compared to samples collected at Woro during quiescent degassing in 1984 and 2004; these concentrations reached 0.18 and 0.02 ppm, respectively. The trends in the ratios of Cu, Zn, Pb and Mo to K in the gas condensates are very similar to the trends of absolute concentrations, demonstrating that the variations in metal concentrations are not simply the result of dilution of the gases, but instead reflect internal variations caused by changes in the magmatic-hydrothermal system (Fig. 3b).

5.3 Comparison of fluid inclusion and volcanic gas data

In order to facilitate comparison of fluid inclusions and volcanic gases, both data sets were normalized to the concentration of Na and are compared in Figure 4, where distributions of Cu/Na, Zn/Na, Pb/Na and Mo/Na ratios for supercritical fluid inclusions (Fig. 4a), brine inclusions (Fig. 4b) and vapor inclusions (Fig. 4c) are shown together with those for volcanic gas condensates. We also carried out the same normalization using K. However, as the resulting distributions of data points are very similar to those obtained with Na, and as Na is the dominant metal in most fluids, thereby providing a more reliable basis for normalization than K, we have limited our comparison to data ratioed to Na.

Volcanic gas condensates have substantially lower Cu/Na ratios than supercritical fluid and vapor inclusions. However, the Cu/Na ratio is very similar in brine inclusions and in volcanic gas condensates. By contrast, ratios of Zn/Na, Pb/Na and Mo/Na in volcanic gas condensates are much higher than those of all three types of fluid inclusions.

Hence, with respect to Na (and K), Cu behaves in a manner that is opposite to Zn, Pb and Mo. Metal/Na ratios in supercritical fluid and vapor inclusions decrease in the order: $(Cu/Na)_{fl.incl.} > (Zn/Na)_{fl.incl.} > (Pb/Na)_{fl.incl.} > (Mo/Na)_{fl.incl.}$, whereas in brine inclusions, they decrease in the order: $(Zn/Na)_{fl.incl.} > (Pb/Na)_{fl.incl.} > (Cu/Na)_{fl.incl.} > (Mo/Na)_{fl.incl.}$ Ratios of volcanic gases increase in the order $(Cu/Na)_{volc.gas} < (Mo/Na)_{volc.gas} < (Zn/Na)_{volc.gas} < (Pb/Na)_{volc.gas}$. This suggests a fundamental difference in the behaviour not only of Cu but also of Zn and Pb in volcanic gases compared to higher density fluids. Using the relationship:

$$R_{Me}^{Na} = \frac{\left(\frac{Me}{Na}\right)_{fl.incl.}}{\left(\frac{Me}{Na}\right)_{volc.gas}} \tag{1}$$

where 'Me' can be either Cu, Zn, Pb or Mo, fl.incl. stands for 'fluid inclusions' and 'volc.gas' for 'volcanic gas condensates', it can also be shown that in supercritical fluid and vapor inclusions, $R_{Cu}^{Na} > 1$ and $R_{Zn,Pb,Mo}^{Na} < 1$, and in brine inclusions, $R_{Cu}^{Na} \approx 1$ and $R_{Zn,Pb,Mo}^{Na} < 1$, indicating that Cu prefers the supercritical fluids and vapor to the brine, and Zn, Pb and Mo appear to prefer the volcanic gas to the supercritical fluid and vapor.

5.4 Volcanic gas sublimates

In Figure 5 and Table 2, we list the minerals identified in volcanic gas sublimates precipitated in silica tubes at Merapi volcano in 2004 and 2006 as a function of temperature. The striking feature of these data is that sublimates collected during 2004, a period of quiescent degassing, consist mainly of sulfates and oxides, and minor proportions of chlorides and native elements, whereas those collected immediately after the explosive eruption in 2006 consist mainly of sulfides, chlorides and native elements. The only oxide identified in 2006 was hematite, which was found at the cold end of one tube and probably formed as a result of atmospheric oxidation. Copper was present only in trace amounts in pyrite, and only in sublimates collected in 2006. Zinc occurred in the form of wurtzite-greenockite (ZnS-CdS solid solution) in 2006 and as zincovoltaite (a hydrated Zn, Fe, K, Al sulfate) in 2004. Lead precipitated as galena (sulfide), tsugaruite (arseno-sulfide) or cotunite (chloride) in 2006, but as anglesite (sulfate), palmierite

(sulfate) or penfieldite (chloro-hydroxide) in 2004. Finally, molybdenum was only observed in 2004 and as powellite (oxide).

The silica tube experiments referred to above were first conducted at Merapi in 1979 by Le Guern and Bernard (1982). At that time, minerals sublimated from the gases were relatively reduced and included sulfides of Fe, Zn, Pb and Mo, chlorides of Na and K, and cristobalite, magnetite and hercynite. Sulfides were dominant and sulfates absent. Although this sampling was not conducted immediately after an explosive eruption, seismicity was increasing in 1979, and fumarole temperatures were relatively high (Global Volcanism Program of the Smithsonian National Museum of Natural History (GVP) website consulted online in August 2010). Silica tubes were also inserted in fumaroles at Merapi in 1984 by Symonds et al. (1987); at that time the minerals precipitated appeared to have had a level of oxidation intermediate between the oxidized and reduced groups reported above. Sublimates included cristobalite and magnetite, sulfates of K-Ca and K-Na, K-Na-Fe, K-Cs, K-Pb, Zn and Cu, chlorides of Na, K, Pb-K, and sulfides of Fe, Zn and Pb. Merapi was in a period of quiescence in 1984 according to information reported to the GVP website (consulted online in August 2010) by the Merapi Volcano Observatory (MVO). It thus appears that the proportions of sulfides, sulfates and oxides precipitating from Merapi gases and, by extension, from hydrothermal fluids at depth, vary with the activity of the volcano.

6. Discussion

The fluid inclusion data summarized above were interpreted by their authors to represent magmatic fluids that were supercritical, brines or vapors. Complemented by knowledge of phase relationships in the H₂O-NaCl system and metal speciation in aqueous fluids (Pearson, 1963; Seward, 1981; Candela and Holland, 1984; Crerar et al., 1985; Seward and Barnes, 1997), these data provide important clues about the behaviour of Cu, Zn, Pb and Mo in magmatic-hydrothermal ore-forming (porphyry) systems. Moreover, the Cu/Na, Zn/Na, Pb/Na and Mo/Na data, when compared to those for volcanic gases, also provide clues about the changes occurring between the level of porphyry ore formation, the intervening epithermal environment and the surface of the volcano.

6.1 Physico-chemical evolution of magmatic-hydrothermal fluids

Depending on the pressure, temperature and chemical composition of the system, a MVP can evolve along different paths. To a first approximation, this evolution can be illustrated on a pressure-temperature-composition phase diagram for the system H₂O-NaCl (Fig. 1; Geiger et al., 2005). The starting point will depend on the conditions of exsolution of the MVP from the magma, particularly the pressure. This also determines whether the exsolved fluid comprises one or two phases. The reservoirs hosting the magmas supplying the fluids responsible for porphyry and epithermal deposits typically occur at depths of ~2 to ~9 km (Sillitoe, 2010; Seedorff et al., 2005). The upper end of this range also represents the depth inferred for the shallow reservoir at Merapi volcano, based on seismic evidence (1.5 to 2.5 km; Ratdomopurbo and Poupinet, 2000). At these depths (2 to 9 km), the corresponding lithostatic pressures are 2.5 kbar (250 MPa) to 0.6 kbar (60 MPa), and the hydrostatic pressures are 0.8 kbar (80 MPa) to 0.2 kbar (20 MPa). Assuming that the magma is saturated with an aqueous phase at these depths and given the position of the solvus on Figure 6 (the black curved grid), it follows that deeper porphyry magmas will tend to exsolve supercritical fluids, particularly if the pressure is dominantly lithostatic, whereas the shallow magmas will exsolve subcritical fluids. However, the saturation pressure will depend on the H₂O content of the magma. For example, a magma of intermediate composition with 6 wt. % H₂O will saturate with an aqueous fluid at a pressure of ~ 3 Kbar (300 MPa), whereas one with 2 wt. % H₂O will saturate with this fluid at a pressure of ~ 0.4 Kbar (40 MPa); these pressures will be modified by the presence of other volatiles, e.g., CO₂. The salinity of the fluids is a function of pressure and the extent of crystallization of the magma (Cline and Bodnar, 1991). At greater depth, higher degrees of crystallization are required to reach water saturation through second boiling and magmas exsolve higher salinity fluids, whereas at shallower depths, the opposite is the case (Cline and Bodnar, 1991). In Figure 6, point A represents a porphyry fluid containing 20 wt. % NaCl at 7 km depth in a 2 kbar lithostatic pressure regime.

Volcanic gases emitted in open systems that degas quiescently, i.e., in which the rock overlying the magma is highly fractured, porous and permeable, allowing the

magma to be connected to the atmosphere through the hydrothermal system, are in regimes in which pressure is close to or even below hydrostatic pressure. At such low pressure, exsolution is subcritical, i.e., the gas is accompanied by a brine and, on cooling, this fluid will deposit minerals, notably quartz, that will seal the system. As a result, pressure will climb, in some cases to values exceeding the confining capacity of the rock, triggering an explosive eruption, and opening the system to hydrostatic- or even vaporstatic conditions. For example, as mentioned above, the shallow magma chamber at Merapi volcano is about 2 km below the surface. Hence, during quiescent degassing, the magma will be under a hydrostatic regime corresponding to a pressure of about 0.2 kbar (20 MPa), and will exsolve two fluids, low salinity vapor (dominant), accompanied by a very high salinity liquid (minor). Point B on Figure 6 represents the combined fluid at 0.2 kbar containing 5 wt. % NaCl, at 900°C. As they rise, these fluids (vapor and brine) decompress at near constant temperature and thus gradually condense small amounts of liquid and evaporate even smaller amounts of vapor, respectively. Point B on Figure 6 extends laterally along a dotted gray tie-line to the solvus surface, where the compositions of the vapor and the liquid are illustrated by smaller gray dots. Upon decompression, the vapor will gradually condense liquid of more saline composition, and thus become gradually less saline. On its arrival at the surface, its composition will be represented by point B'. However, when the system seals, pressure in the shallow reservoir may rise to a value in excess of 0.6 kbar (60 MPa).

Deeper parts of the complex magmatic-hydrothermal system at Merapi volcano (Deegan et al., 2010; Nadeau et al., under review) are exposed to much higher pressures that the shallow parts (4 to 4.5 kbar according to Nadeau et al., under review and up to 5 kbar for the more felsic magma according to Chadwick et al., 2005), and consequently represent supercritical conditions for any exsolving hydrothermal fluid. Upon opening of the system and during the explosive eruption, this overpressurized fluid will undergo catastrophic phase separation into a great amount of low salinity vapor and a small amount of high salinity brine (flash boiling). Since the solubility of metals in hydrothermal fluids is sensitive to the physical state of these fluids, flash boiling will have important consequences for metal transportation and deposition. This is discussed further below.

Porphyry fluids are thought to exsolve from magmas emplaced in systems that are 'closed', i.e., underlying a relatively impermeable crustal carapace which is isolated from the surface and exposed to a higher pressure, lithostatic regime (Sillitoe, 2010; Seedorff et al., 2005). These porphyry fluids thus usually evolve under lithostatic pressure conditions. However, in contrast to volcanic gases, porphyry fluids commonly are at much lower temperatures than magmatic volcanic gases (i.e., 350° to 700°C according to Sillitoe, 2010, versus 400° to > 900°C). The combined effects of the lithostatic regime and lower temperature result commonly in the evolution of porphyry fluids from conditions above the solvus towards much lower pressure. The bold dashed black line A-A' on Fig. 6 represents a 20 wt. % NaCl porphyry fluid evolving above the solvus, with its projection shown for clarity as dotted black lines on the solvus, on the pressurecomposition plane and on the temperature-composition plane. This fluid will be exposed to gradually decreasing pressure and its temperature will decrease adiabatically, but its salinity will remain constant. Given the shift of the critical curve (red line) towards less saline composition at lower P-T conditions, the fluid will gradually contract from a single low density supercritical phase to a liquid, without a change in phase (Heinrich, 2005; Williams-Jones and Heinrich, 2005). However, if the path of the critical fluid was such that it retained more heat during decompression, it would intersect the solvus and unmix into brine and vapor. Furthermore, if there was an abrupt transition to a hydrostatic regime, due to fluid overpressure-induced failure of the carapace during exsolution of the supercritical fluid from the magma, the unmixing into brine and vapor could occur early in the evolution of the magmatic-hydrothermal system.

Magmatic aqueous liquids (brines) are of high-density and usually are highly saline, alkaline, and Cl-rich, whereas magmatic vapors are of low-density and salinity, and are acidic and S-rich (Webster and Mandeville, 2007). Pearson's rule (Pearson, 1963; Crerar et al., 1985) states that hard metals (e.g., Mo) prefer to form complexes with hard ligands (e.g., OH⁻, SO₄²⁻), whereas soft metals (e.g., Cu⁺, Au⁺) prefer to do so with soft ligands (e.g., HS⁻, H₂S, S₂O₃²⁻). In between these two extremes lies a gray area where borderline metals (e.g., Zn²⁺ and Pb²⁺) prefer complexing with borderline ligands (e.g., Cl⁻). Given that S-species are more volatile and thus partition preferentially into a vapor, whereas Cl-species are less volatile and partition preferentially in the liquid, Pearson's

rule helps explains why Cu is preferentially enriched in vapor inclusions and Zn and Pb are more concentrated in brine inclusions; Cu will follow sulphur and Zn and Pb chlorine (Fig. 1; Heinrich et al., 1999). Molybdenum is also enriched in brines, where it forms oxyacids due to the availability of hydroxide ions; the electrically neutral nature of the vapor precludes formation of OH⁻. However, there is experimental evidence that Mo may favour the vapor phase as the critical point of the system is approached (Rempel et al., 2008). Oxygen fugacity may also play a role with the formation of hard ligands such as SO₄²⁻ in the liquid and solvation of the metal by SO₂ (the dominant form of S volcanic gases) in the vapor.

6.2 Relationship between magmatic-hydrothermal fluids and volcanic gases

Volcanic gases are thought to be magmatic (or juvenile), and thus not to have mixed appreciably with other crustal fluids when they are at temperatures above 500°C (Symonds et al., 1994). The above discussion pertaining to the trend B-B' in Fig. 6, as well as observations of Delmelle et al. (2000) and Webster and Mandeville (2007), suggest that volcanic gases constitute the gaseous fraction resulting from unmixing of a MVP into brine and vapor, although they could expand directly from a supercritical fluid. Vapor and brine inclusions, which are commonly found as boiling or condensation assemblages within the same samples, are also the results of unmixing or phase separation. By contrast, volcanic gases emitted during quiescent degassing (for obvious reasons, they are usually sampled during periods of quiescent degassing and not during explosive eruptions) usually condense only minor amounts of liquid. This, combined with the fact that they and supercritical fluids have the highest temperature, suggests that the best comparison that can be made between deep and surface fluids is between supercritical fluids and volcanic gases. In order to better understand the processes that occur in MVP within the porphyry-epithermal environment, it is therefore most helpful to compare the ratios of the concentrations of Cu, Zn, Pb and Mo to Na in supercritical fluid inclusions with those in high temperature magmatic volcanic gases (Fig. 4a).

The fact that $R_{Cu}^{Na} > 1$ and $R_{Zn,Pb,Mo}^{Na} < 1$ (the ratio of the metal to Na in fluid inclusions over the same ratio in volcanic gases) in supercritical fluid and vapor

inclusions, and that that $R_{Cu}^{Na} \approx 1$ in brine inclusions, as discussed earlier, indicates that Cu prefers the medium salinity supercritical fluid and the lower density, low salinity vapor over the high density, high salinity brine. However, the fact that $R_{Cu}^{Na} > 1$ and $R_{Zn,Pb,Mo}^{Na}$ < 1 also seems to suggest that the depletion in Cu and enrichment in Zn, Pb and Mo in the volcanic gases is greater even than those in the brine inclusions. This is very unexpected, given our understanding of the behaviour of these metals in aqueous fluids, which predicts that Cu should favour the vapor phase and that Zn, Pb and Mo should favour the brine (see earlier discussion of metal speciation). Indeed, studies of coexisting fluid inclusions from porphyry systems have shown that Cu partitions preferentially into the vapor, whereas Zn, Pb and Mo partition into the brine (e.g., Ulrich et al., 1999). We suggest that the contrary behaviour of volcanic gases results from deposition of Cuminerals earlier and closer to the magma than Zn, Pb and Mo-bearing minerals. According to this interpretation, the composition of the supercritical fluid inclusions reflects conditions immediately prior to deposition of porphyry copper ores, whereas the composition of the volcanic gases represents a later more distal signature. However, the Cu content of supercritical fluid inclusions normalized to Na is only somewhat higher than that of vapor inclusions, suggesting that vapor inclusions also reflect the conditions prior to deposition of porphyry copper mineralization, although after those represented by the supercritical fluid inclusions (Fig. 4). This interpretation is also suggested by the observation that in the liquid phase, at least, the solubility of the copper ore-forming minerals is much lower than that of lead and zinc ore-forming minerals; equivalent data are currently not available for the vapor phase but similar behaviour is expected (e.g., Crerar and Barnes, 1976; Seward, 1984; Ruaya and Seward, 1986; and Xiao et al., 1998). Thus, it is reasonable to argue that Cu should be the first of these metals to be depleted from the vapor (by deposition at the level of the porphyry), and that the vapor should continue to mobilize Pb and Zn to higher crustal levels. The result would be a zonation analogous to the concentric zonation of Cu, Zn and Pb in porphyry ore systems, with Cuminerals deposited earlier and closer to the intrusion, and Zn and Pb at progressively greater distances (Babcock et al., 1997; Lang and Eastoe, 1998; Sillitoe, 2010). The reason that R_{Mo}^{Na} is lower than for other metals, suggesting that it should deposit later and

at greater distance from the porphyry than Cu, Zn and Pb, is unclear (a possible explanation is suggested later). This behaviour is inconsistent with the observation that in porphyry systems, Mo is usually deposited at high temperature, although where both Cu and Mo deposit, the position of Cu and Mo relative to the porphyry is highly variable (Seedorff et al., 2005).

Deep mafic melt at Merapi volcano was saturated with respect to a Cu-rich, immiscible sulfide melt containing 5 wt. % Cu that was dissolved by an exsolving MVP (Nadeau et al., 2010). Despite this, Merapi gases are depleted in Cu, even compared to gases emitted by other volcanoes (Fig. 2a). We propose that this depletion reflects earlier deposition of Cu minerals and that this occurred, not in response to a decrease in temperature, but rather a decrease in pressure (as the regime changed from lithostatic to atmospheric conditions), which sharply reduced the solubility of Cu in the gas phase (Archibald et al., 2002).

6.3 Cyclic deposition of ores in porphyry systems

We have shown previously that the 2006 explosive eruption at Merapi volcano was triggered by the injection of sulfide-melt-saturated mafic magma upward into cooler, more oxidized and more felsic resident magma (Nadeau et al, 2010). The resulting decrease in pressure on the mafic magma caused exsolution of a MVP (first boiling), which in turn dissolved the sulfide melt. Evidence of the latter is provided by the composition of the volcanic gases immediately after the eruption. These gases were enriched in Cu and Pb and depleted in Mo (Fig. 3), but the concentration of Zn in the gas after the explosive 2006 eruption was very similar to that during quiescent degassing in 2004 (Fig. 2a). The behaviour of Zn probably resulted from the crystallization of Zn-bearing titanomagnetite, which is present as phenocrysts in the more felsic resident magma, and must have buffered the concentration of Zn in the volcanic gases. Experiments conducted after the 2006 eruption showed that upon cooling, the gases precipitated a reduced, Cu-, Zn- and Pb-rich mineral assemblage (Fig. 5c). By contrast, the periods of quiescent degassing which follow eruptions at Merapi are accompanied by assimilation and fractional crystallization (AFC) of the magmas and fluxing of the

shallow resident magma by a Cu-, Zn- and Pb-rich MVP that originated in the mafic melt (Nadeau et al., under review). It is evident from Figure 3 that the gases were enriched in Mo during quiescent degassing in 2004 and in 1984. Upon cooling, these gases sublimated a more oxidized, Cu- and Zn-depleted and Mo-enriched paragenesis.

Using the sublimates as proxies for mineral parageneses in a porphyry deposit, it is attractive to speculate that the alternation of phases of eruptive activity triggered by injections of sulfide-saturated mafic magma, and phases of quiescence related to AFC and fluxing, has its parallel in processes occurring at depth in the porphyry environment. Thus the alternations in mineralogy of crack-and-seal veins and multiply brecciated breccia dykes observed in porphyry deposits are a deeper manifestation of the explosive and quiescent degassing that occurs in the volcanic edifice. In both environments, overpressures caused by exsolution of aqueous magmatic fluids lead to failure of the carapace, large-scale escape of fluids, mineral deposition and partial re-sealing of the system, and eventually a repetition of the cycle. Using the analogy of volcanic systems, we propose that minerals precipitating at the beginning of a cycle in the porphyry environment are equivalent to those of the eruptive stage, and those precipitating later but before the next cycle are equivalent to those of the quiescent stage. Finally we propose, that as for the volcanic environment, the repetition in mineral assemblages is one controlled dominantly by changing redox conditions and by injections of reduced mafic magma into a more oxidized felsic resident magma.

6.4 Model for the formation of porphyry deposits

We thus propose a model (Fig. 7) in which the injection of reduced mafic magmas into shallow resident magma reservoirs results in a pulse of reducing, Cu-, Zn- and Pb-rich ore fluid (Fig. 7a). The metals deposit in the sequence the Cu→Zn→Pb as deduced from the observed zonation of these metals in porphyry systems (e.g., Babcock et al., 1997; Lang and Eastoe, 1998; Sillitoe, 2010) and by comparing deep (supercritical fluid inclusions) and shallow (volcanic gases) representatives of the magmatic volatile phase. During periods of quiescence (Fig. 7b), the system is open and the pressure hydrostatic, the magmas evolve through AFC (Nadeau et al., under review), gradually degas, become

more oxidized (degassing H₂ oxidizes the remaining magma), and exsolve fluids with more oxidized ligands that are enriched in incompatible metals such as Mo. The presence of Cu only in the 2006 sublimates (as traces in pyrite) and Mo only in 2004 sublimates (in powellite) is consistent with this model. Porphyry deposits are thus considered by us to be the products of multiple episodes of fluid overpressure triggered by injections of reduced mafic magma, cyclic deposition of minerals from reduced to oxidized assemblages (Cu-rich to Mo-rich), and an overall evolution of magmatic hydrothermal systems from early and proximal Cu mineral saturation to progressively later and more distal Zn and Pb mineral saturation.

7. Conclusions

We have compared the ratio of Cu, Zn, Pb and Mo to Na in fluid inclusions found in porphyry Cu (Au, Mo) deposits to that of volcanic gas condensates. From these data, it is evident that the behaviour of the metals in supercritical porphyry fluids is different from that of volcanic gases, i.e., Cu is dominant in the former and Zn, Pb and Mo predominate in the latter. Related conclusions are: 1) the compositions of the supercritical fluid inclusions and volcanic gases record compositions in the hydrothermal system prior to and after Cu mineral deposition, respectively; 2) mineral deposition in volcanic gases is caused by decreasing pressure, whereas in higher density porphyry-related fluids, it results from decreasing temperature; and 3) the metal distribution in porphyry-related fluids and volcanic gases reflects a zonation of porphyry systems from early and proximal Cu deposition, to progressively later and more distal Zn and Pb mineral deposition.

The compositions of condensates and sublimates of volcanic gases sampled during an eruptive cycle at Merapi volcano, Indonesia, show that during eruptions the fluids are more reducing due to the injection of more reduced magmas (Nadeau et al., 2010), and during periods of quiescence they are more oxidized. This is reflected in a gradual enrichment of incompatible metals such as Mo in the fluid, gradual oxidation of the MVP and deposition of a more oxidized, Cu-, Zn- and Pb-depleted, and Mo-enriched mineral assemblage. We believe that these observations mirror processes occurring in the

porphyry environment. Finally, we suggest that variations in the permeability of the hydrothermal system results in pressure fluctuations from values greater than lithostatic to hydrostatic or even vaporstatic values, and that these variations satisfactorily explain the nature of porphyry Cu and related mineral deposits.

Acknowledgements

This study was funded scholarships to ON by the Natural Sciences and Engineering Research Council (NSERC), the Fond Québécois de la Recherche sur la Nature et les Technologies (FQRNT) and by McGill University, and research grants to AEWJ and JS from NSERC and FQRNT.

References

- Allard, P., and Tazieff, H., (1979) Phenomenologie et cartographie thermique des principales zones fumerolliennes du volcan Merapi (Indonesie): Phenomenology and thermal mapping of the principal furmarole zones of Merapi Volcano, Indonesia, v. 288, no. 8, p. 747-750.
- Andreastuti, S. D., Alloway, B. V., Smith, I. E. M., (2000). "A detailed tephrostratigraphic framework at Merapi Volcano, central Java, Indonesia; implications for eruption predictions and hazard assessment." <u>Journal of Volcanology</u> and Geothermal Research **100**(1-4): 51-67.
- Archibald, S. M., Migdisov A.A., Williams-Jones A.E. (2002). "An experimental study of the stability of copper chloride complexes in water vapor at elevated temperatures and pressures." Geochimica et Cosmochimica Acta 66(9): 1611-1619.
- Babcock, R. C., Jr., G. H. Ballantyne, and Phillips, C. H., (1997). "Summary of the geology of the Bingham District, Utah." <u>Guidebook Series (Society of Economic Geologists (U. S.)</u> **29**: 113-132.
- Camus, G., A. Gourgaud, et al. (2000). "Merapi (central Java, Indonesia); an outline of the structural and magmatological evolution, with a special emphasis to the major

- pyroclastic events." <u>Journal of Volcanology and Geothermal Research</u> **100**(1-4): 139-163.
- Candela, P. A., and Holland, H. D., 1984, The partitioning of copper and molybdenum between silicate melts and aqueous fluids: <u>Geochimica et Cosmochimica Acta</u>, v. 48, no. 2, p. 373-380.
- Chadwick, J. P., McCourt, E. C., Troll, V. R., Waight, T. E. (2005). "Petrology and geochemistry of plutonic inclusions in recent Merapi lavas; implications for magmatic evolution in arc settings." <u>Irish Journal of Earth Sciences</u> **23**: 128.
- Chadwick, J. P., V. R. Troll, et al. (2007). "Carbonate assimilation at Merapi Volcano, Java, Indonesia; insights from crystal isotope stratigraphy." <u>Journal of Petrology</u> **48**(9): 1793-1812.
- Cline, J. S. and R. J. Bodnar (1991). "Can economic porphyry copper mineralization be generated by a typical calc-alkaline melt?" <u>Journal of Geophysical Research</u> **96**(B5): 8113-8126.
- Crerar, D. A. and H. L. Barnes (1976). "Ore solution chemistry; V, Solubilities of chalcopyrite and chalcocite assemblages in hydrothermal solution at 200 degrees to 350 degrees C." <u>Economic Geology and the Bulletin of the Society of Economic Geologists</u> **71**(4): 772-794.
- Crerar, D., S. Wood, et al. (1985). "Chemical controls on solubility of ore-forming minerals in hydrothermal solutions." The Canadian Mineralogist **23**(3): 333-352.
- Deegan, F. M., Troll, V. R., Freda, C., Misiti, V., Chadwick, J. P., McLeod, C. L., and Davidson, J. P. (2010). "Magma-carbonate interaction processes and associated CO (sub 2) release at Merapi Volcano, Indonesia; insights from experimental petrology." Journal of Petrology **51**(5): 1027-1051.
- Delmelle, P., Bernard A., Kusakabe M., Fischer T.P., Takano B. (2000). "Geochemistry of the magmatic-hydrothermal system of Kawah Ijen volcano, East Java, Indonesia." <u>Journal of Volcanology and Geothermal research</u> **97**: 31-53.
- Driesner, T. and C. A. Heinrich (2007). "The system H₂O-NaCl; Part I, Correlation formulae for phase relations in temperature-pressure-composition space from 0 to 1000 degrees C, 0 to 5000 bar, and 0 to 1 X_{NaCl}." <u>Geochimica et Cosmochimica</u> Acta **71**(20): 4880-4901.

- Geiger, S., Driesner, T., Heinrich, C. A., and Matthaei, S. K. (2005). "On the dynamics of NaCl-H₂O fluid convection in the Earth's crust." <u>Journal of Geophysical Research</u> **110**: no.B7, 23.
- Gemmell, J. B. (1987). "Geochemistry of metallic trace elements in fumarolic condensates from Nicaraguan and Costa Rican volcanoes." <u>Journal of Volcanology and Geothermal Research</u> **33**(1-3): 161-181.
- Gustafson, L. B. and J. P. Hunt (1975). "The porphyry copper deposit at El Salvador, Chile." Economic Geology and the Bulletin of the Society of Economic Geologists **70**(5): 857-912.
- Hammer, J. E., K. V. Cashman, and Voight, B. (2000). "Magmatic processes revealed by textural and compositional trends in Merapi dome lavas." <u>Journal of Volcanology and Geothermal Research</u> **100**(1-4): 165-192.
- Hedenquist, J. W. and J. B. Lowenstern (1994). "The role of magmas in the formation of hydrothermal ore deposits." <u>Nature</u> **370**(6490): 519-527.
- Hedenquist, J. W., M. Aoki, et al. (1994). "Flux of volatiles and ore-forming metals from the magmatic-hydrothermal system of Satsuma Iwojima Volcano; with Suppl. Data 9430." Geology **22**(7): 585-588.
- Hedenquist, J. W., A. Arribas, Jr., et al. (1998). "Evolution of an intrusion-centered hydrothermal system; Far Southeast-Lepanto porphyry and epithermal Cu-Au deposits, Philippines." <u>Economic Geology and the Bulletin of the Society of Economic Geologists</u> **93**(4): 373-404.
- Heinrich, C. A., Guenther, D., Audetat, A., Ulrich, T., Frischknecht, R. (1999) Metal fractionation between magmatic brine and vapor, determined by microanalysis of fluid inclusions: <u>Geology</u>, v. 27, no. 8, p. 755-758.
- Heinrich, C. A. (2005). "The physical and chemical evolution of low-salinity magmatic fluids at the porphry to epithermal transition; a thermodynamic study."

 <u>Mineralium Deposita</u> **39**(8): 864-889.
- Henley, R. W. and A. J. Ellis (1983). "Geothermal systems ancient and modern; a geochemical review." <u>Earth-Science Reviews</u> **19**(1): 1-50.
- Henley, R. W., McNabb, A. (1978). "Magmatic vapor plumes and ground-water interaction in porphyry copper emplacement." <u>Economic Geology</u> **73**(1): 1-20.

- Hezarkhani, A. and A. E. Williams-Jones (1998). "Controls of alteration and mineralization in the Sungun porphyry copper deposit, Iran; evidence from fluid inclusions and stable isotopes." <u>Economic Geology and the Bulletin of the Society of Economic Geologists</u> **93**(5): 651-670.
- Klemm, L. M., T. Pettke, et al. (2007). "Hydrothermal evolution of the El Teniente Deposit, Chile; porphyry Cu-Mo ore deposition from low-salinity magmatic fluids." Economic Geology and the Bulletin of the Society of Economic Geologists 102(6): 1021-1045.
- Kouzmanov, K., Pettke, T., Heinrich, C. A., Bodnar, R., Cline, J. (2010). "Direct analysis of ore-precipitating fluids; combined IR microscopy and LA-ICP-MS study of fluid inclusions in opaque ore minerals." <u>Economic Geology and the Bulletin of the Society of Economic Geologists</u> **105**(2): 351-373.
- Landtwing, M. R., Pettke, T., Halter, W. E., Heinrich, C. A., Redmond, P. B., Einaudi, M. T., Kunze, K. (2005). "Copper deposition during quartz dissolution by cooling magmatic-hydrothermal fluids; the Bingham porphyry." <u>Earth and Planetary Science Letters</u> **235**(1-2): 229-243.
- Lang, J. R. and C. J. Eastoe (1988). "Relationships between a porphyry Cu-Mo deposit, base and precious metal veins and Laramide intrusions, Mineral Park, Arizona."
 <u>Economic Geology and the Bulletin of the Society of Economic Geologists</u> 83(3): 551-567.
- Le Guern, F., Bernard A. (1982). "A new method for sampling and analyzing volcanic sublimates application to Merapi volcano." <u>Journal of Volcanology and</u> Geothermal research **12**: 133-146.
- Lowell, J. D. and J. M. Guilbert (1970). "Lateral and vertical alteration-mineralization zoning in porphyry ore deposits." <u>Economic Geology and the Bulletin of the Society of Economic Geologists 65(4)</u>: 373-408.
- Menyailov, I. A. and L. P. Nikitina (1980). "Chemistry and metal contents of magmatic gases; the new Tolbachik volcanoes case (Kamchatka)." <u>Bulletin Volcanologique</u> **43**(1): 197-205.
- Menyailov, I. A., L. P. Nikitina, et al. (1986). "Temperature increase and chemical change of fumarolic gases at Momotombo Volcano, Nicaragua, in 1982-1985; are

- these indicators of a possible eruption?" <u>Journal of Geophysical Research</u> **91**(B12): 12,199-12,214.
- Mizutani, Y. (1970). "Copper and zinc in fumarolic gases of Showashimzan volcano, Hokkaido, Japan." <u>Geochemical Journal</u> **4**(2): 87-91.
- Nadeau, O., Williams-Jones, A. E., Stix, J. (2010). "Sulfide magma as a source of metals in arc-related magmatic hydrothermal ore fluids." <u>Nature Geoscience</u> **3**(7): 501-505.
- Nadeau, O., Williams-Jones, A.E., Stix, J. (under review). "The Behaviour of Copper, Zinc and Lead during Magmatic-Hydrothermal Activity at Merapi Volcano, Indonesia." <u>Economic Geology and the Bulletin of the Society of Economic Geologists</u>.
- Newhall, C. G., Bronto, S., Alloway, B. V., Banks, N. G., Bahar, I., del Marmol, M. A., Hadisantono, R. D., Holcomb, R. T., McGeehin, J. P., Miksic, J. N., Rubin, Meyer, Sayudi, D. S., Sukhyar, R., Andreastuti, S. D., Tilling, R. I., Torley, R., Trimble, D. A., Wirakusumah, A. D. (2000). "10,000 years of explosive eruptions of Merapi Volcano, central Java; archaeological and modern implications." Journal of Volcanology and Geothermal Research 100(1-4): 9-50.
- Oana, S. (1962). "Volcanic gases and sublimates from Showashinzan." <u>Bulletin of Volcanology</u> **24**: 49-57.
- Pearson, R. G. (1963). "Hard and soft acids and bases." <u>Journal of the American</u>
 <u>Chemical Society</u> **85**: 3533-3539.
- Pudack, C., Halter, W. E., Heinrich, C. A., and Pettke, T. (2009). "Evolution of magmatic vapor to gold-rich epithermal liquid; the porphyry to epithermal transition at Nevados de Famatina, northwest Argentina." <u>Economic Geology and the Bulletin of the Society of Economic Geologists</u> **104**(4): 449-477.
- Ratdomopurbo, A. and G. Poupinet (2000). "An overview of the seismicity of Merapi Volcano (Java, Indonesia); 1983-1994." <u>Journal of Volcanology and Geothermal Research</u> **100**(1-4): 193-214.
- Rempel, K. U., A. E. Williams-Jones, et al. (2008). "The solubility of molybdenum dioxide and trioxide in HCl-bearing water vapour at 350 degrees C and pressures up to 160 bars." <u>Geochimica et Cosmochimica Acta</u> **72**(13): 3074-3083.

- Reynolds, T. J. and R. E. Beane (1985). "Evolution of hydrothermal fluid characteristics at the Santa Rita, New Mexico, porphyry copper deposit." <u>Economic Geology and the Bulletin of the Society of Economic Geologists</u> **80**(5): 1328-1347.
- Ruaya, J. R. and T. M. Seward (1986). "The stability of chlorozinc(II) complexes in hydrothermal solutions up to 350 degrees C." Geochimica et Cosmochimica Acta **50**(5): 651-661.
- Rusk, B. G., Reed, M. H., Dilles, J. H., Klemm, L. M., and Heinrich, C. A. (2004). "Compositions of magmatic hydrothermal fluids determined by LA-ICP-MS of fluid inclusions from the porphyry copper-molybdenum deposit at Butte, MT." Chemical Geology **210**(1-4): 173-199.
- Seedorff, E., J. H. Dilles, et al. (2005). Porphyry deposits; characteristics and origin of hypogene features. <u>Economic Geology; one hundredth anniversary volume, 1905-2005</u>.
 J. W. T. Hedenquist, John F H; Goldfarb, Richard J; Richards, Jeremy P, Society of Economic Geologists, Littleton, CO, United States (USA).
- Seo, J. H., Guillong, M., and Heinrich, C. A. (2009). "The role of sulfur in the formation of magmatic-hydrothermal copper-gold deposits." <u>Earth and Planetary Science Letters</u> **282**(1-4): 323-328.
- Seward, T. M. (1984). "The formation of lead(II) chloride complexes to 300 degrees C; a spectrophotometric study." <u>Geochimica et Cosmochimica Acta</u> **48**(1): 121-134.
- Seward, T. M., and Barnes, H. L., 1997, Metal transport by hydrothermal ore fluids, *in* Barnes, H. L., ed., <u>Geochemistry of hydrothermal ore deposits</u>, John Wiley and Sons Inc., p. 465-486.
- Sillitoe, R. H. (1973). "The tops and bottoms of porphyry copper deposits." <u>Economic</u> Geology and the Bulletin of the Society of Economic Geologists **68**(6): 799-815.
- Sillitoe, R. H. (2010). "Porphyry copper systems." <u>Economic Geology and the Bulletin of</u> the Society of Economic Geologists **105**(1): 3-41.
- Stoiber, R. E., Rose, W.I. (1970). "The geochemistry of Central American volcanic gas condensates." <u>Geological Society of America Bulletin</u> **81**: 2891-2912.
- Symonds, R. B., Rose W.I., Reed M.H., Lichte F.E. (1987). "Volatilization, transport and sublimation of metallic and non-metallic elements in high temperature gases at Merapi Volcano, Indonesia." <u>Geochimica et Cosmochimica Acta</u> **51**: 2083-2101.

- Symonds, R. B., Rose, W. I., Gerlach, T. M., Briggs, P. H., and Harmon, R. S. (1990). "Evaluation of gases, condensates, and SO (sub 2) emissions from Augustine Volcano, Alaska; the degassing of a Cl-rich volcanic system." <u>Bulletin of Volcanology</u> **52**(5): 355-374.
- Symonds, R. B., Rose W.I., Bluth G.J.S., Gerlach T.M. (1994). Volcanic-gas studies: Methods, results, and applications. <u>Volatiles in Magma</u>. M. S. o. America. **30:** 1-66.
- Symonds, R. B., Y. Mizutani, et al. (1996). "Long-term geochemical surveillance of fumaroles at Showa-Shinzan Dome, Usu Volcano, Japan." <u>Journal of Volcanology</u> and Geothermal Research **73**(3-4): 177-211.
- Taran, Y. A., J. W. Hedenquist, et al. (1995). "Geochemistry of magmatic gases from Kudryavy Volcano, Iturup, Kuril Islands." <u>Geochimica et Cosmochimica Acta</u> **59**(9): 1749-1761.
- Taran, Y. A., Bernard, A., Gavilanes, J. C., Lunezheva, E., Cortes, A., and Armienta, M. A. (2001). "Chemistry and mineralogy of high-temperature gas discharges from Colima Volcano, Mexico; implications for magmatic gas-atmosphere interaction." Journal of Volcanology and Geothermal Research 108(1-4): 245-264.
- Ulrich, T., Guenther, D., and Heinrich, C. A. (1999). "Gold concentrations of magmatic brines and the metal budget of porphyry copper deposits." <u>Nature</u> **399**(6737): 676-679.
- Ulrich, T., Guenther, D., and Heinrich, C. A., (2001). "The evolution of a porphyry Cu-Au deposit, based on LA-ICP-MS analysis of fluid inclusions; Bajo de la Alumbrera, Argentina." Economic Geology and the Bulletin of the Society of Economic Geologists **96**(8): 1743-1774.
- Ulrich, T. and C. A. Heinrich (2001). "Geology and alteration geochemistry of the porphyry Cu-Au-deposit at Bajo de la Alumbrera, Argentina." <u>Economic Geology</u> and the Bulletin of the Society of Economic Geologists **96**(8): 1719-1741.
- van Hinsberg, V. J., Berlo, K., Palmer, S., Scher, S., Williams-Jones, A.E., Vigouroux, N., Mauri, G., Williams-Jones, G. (in press). "Kawah Ijen: Geochemical, geophysical and hydrological survey of the Kawah Ijen volcanic system." <u>Bulletin of the Global Volcanism Network</u>.

- Wahrenberger, C., Seward T.M., Dietrich V. (2002). Volatile trace-element transport in high-temperature gases from Kudryavy volcano (Iturup, Kurile Islands, Russia. <u>A tribute to A. Crerar.</u> R. H. a. S. A. Wood, The Geochemical Society. **Special Publication No. 7:** 307-327.
- Webster, J. D. and C. W. Mandeville (2007). "Fluid immiscibility in volcanic environments." Reviews in Mineralogy and Geochemistry **65**(1): 313-362.
- Williams-Jones, A. E. and C. A. Heinrich (2005). "Vapor transport of metals and the formation of magmatic-hydrothermal ore deposits." <u>Economic Geology and the Bulletin of the Society of Economic Geologists</u> **100**(7): 1287-1312.
- Xiao, Z., C. H. Gammons, et al. (1998). "Experimental study of copper(I) chloride complexing in hydrothermal solutions at 40 to 300 degrees C and saturated water vapor pressure." Geochimica et Cosmochimica Acta 62(17): 2949-2964.
- Zelenski, M. and S. Bortnikova (2005). "Sublimate speciation at Mutnovsky Volcano, Kamchatka." <u>European Journal of Mineralogy</u> **17**(1): 107-118.

Table 1. Concentration of selected elements in volcanic gas condensates at Merapi

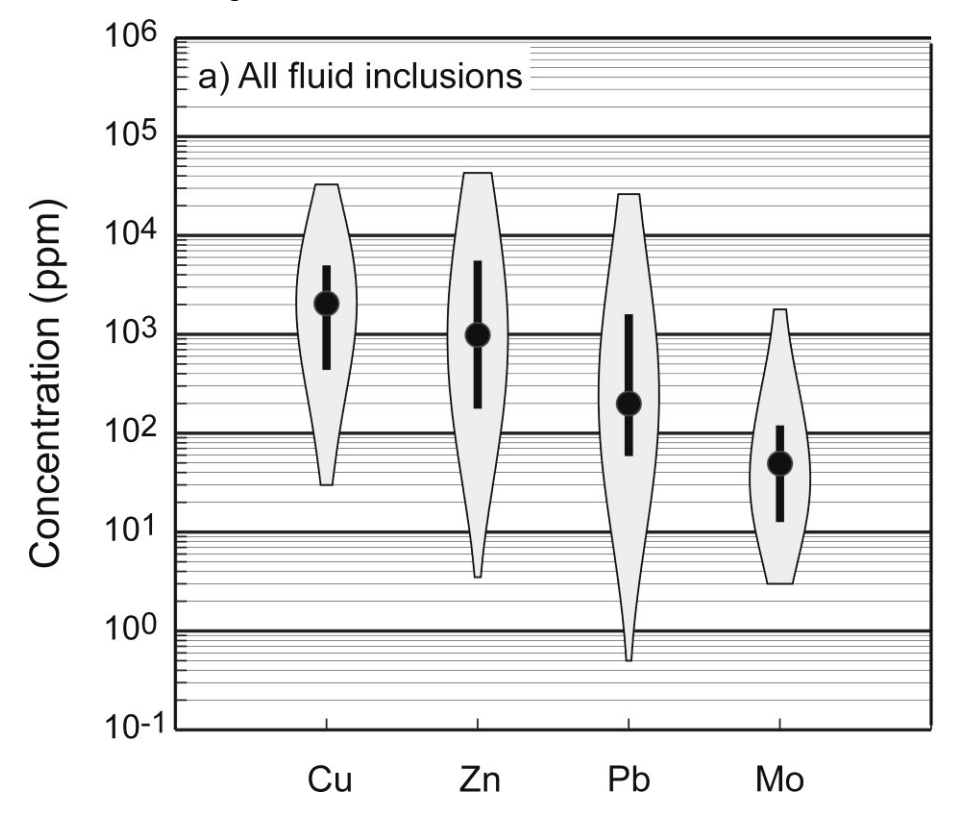
T (°C)	Na	K	Cu	Zn	Pb	Мо	CI	S	Sample	Reference
515	2.3	2.27	0.16	0.42	8.53		4849	9060	2006 Woro 1	this study
417	1.2	0.63	0.28	0.15	8.01	0.0006	7193	12982	2006 Woro 2	this study
572	3.4	2.3		0.15	1.41	0.02	3030	496	2004 Woro 1	this study
266	0.6	1.13	0.003	0.06	0.07	0.004	893	1120	2004 Woro 3	this study
		6.2			0.83	80.0	3500	490	1984 Woro 1	Symonds et al., 1987
		2.6			0.32	0.16	3700	1000	1984 Woro 2	Symonds et al., 1987
		2.9			0.35	0.18	3300	590	1984 Woro 3	Symonds et al., 1987
705	1.1	0.44		0.13	0.08	0.357	7250	10300	2004 Gendol1 A	this study
593	12	2.99	0.00	0.52	0.07	0.256	3830	15900	2004 Gendol1 B	this study
754	0.7	0.31	0.01	0.14	0.26	0.182	6620	5400	2004 Gendol1 D	this study
526	2.1	2.83	0.01	0.17	0.03	0.783	6710	22900	2004 Gendol1 E	this study
515	1.2	0.65	0.01	0.1	0.36	0.477	5630	1100	2004 Gendol1 H	this study
602	2.7	1.05	0.01	0.14	0.42	0.148	5330	7780	2004 Gendol1 I	this study
604	9	4.99	0.03	0.18	1.31	0.161	5420	10900	2004 Gendol2 1	this study
588	2	1.21	0.01	0.15	0.44	0.346	6500	15600	2004 Gendol2 2	this study
		20			1.6	0.12	3600	520	1984 Gendol 1	Symonds et al., 1987
		6.8			1.5	0.11	3200	820	1984 Gendol 2	Symonds et al., 1987
		9.6			1	0.15	3800	2500	1984 Gendol 3	Symonds et al., 1987
		14			1	2.8	3100	540	1984 Gendol 4	Symonds et al., 1987

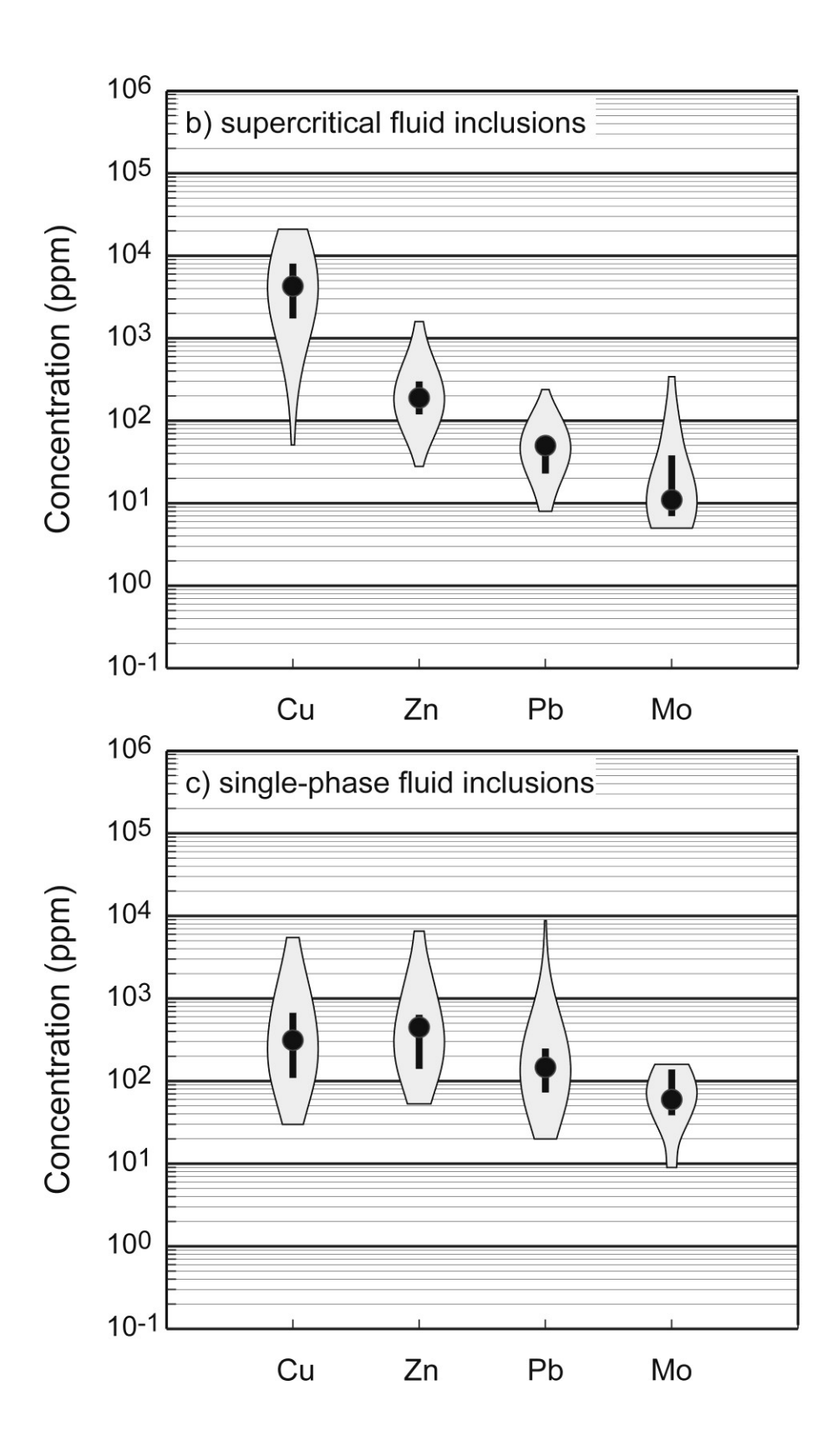
all data are in ppm except otherwise noted.

Table 2. Chemical formulae and depositional temperatures of minerals precipitated from Merapi volcanic gases in 2004 and 2006.

Mineral names	eral names Chemical Formulas		Temperature range (°C)				
		Gendol 2004	Woro 2004	Woro 2006			
anglesite	PbSO ₄	420-600	440-470				
anhydrite	CaSO ₄	450-600	225-500				
barite	BaSO ₄		460-470				
bismuthinite	Bi ₂ S ₃			340-500			
celestine	SrSO₄	440-460					
challacolloite	KPb ₂ Cl ₅			320-560			
cotunite	PbCl ₂			300-590			
galena	PbS			300-560			
halite	NaCl		420-580	520-540			
hematite	Fe ₂ O ₃	560-600	460-470	320-340			
ilmenite	FeTiO ₃		460-470				
iron-chromium	Fe-Cr			320-590			
palmierite	$K_2Pb(SO_4)_2$	560-600					
penfieldite	Pb ₂ Cl ₃ (OH)		380-450				
potassium-alum	KAI(SO ₄) ₂ .12H ₂ O	460-560					
powellite	CaMoO ₄		460-470				
pyrite	FeS ₂			300-590			
salamoniac	NH₄CI		190-420				
selenium	Se	400-460					
shcherbinaite	V_2O_5	440-450					
smythite	$(Fe,Ni)_9S_{11}$ or $(Fe,Ni)_{11}S_{13}$			380-480			
sodium-alum	$NaAl(SO_4)_2.12H_2O$	460-480					
sulfur	S (As)		190-350	300-520			
sylvite	KCI		440-580	520-580			
tamarugite	$NaAl(SO_4)_2.6H_2O$	450-560					
tellurium	Te	500-560					
tsugaruite	$Pb_4As_2S_7$			320-340			
voltaite	$K_2Fe_5AIFe_3 (SO_4)_{12}.18H_2O$	500-560					
wurtzite	(Zn,Fe,Cd)S			340-590			
zincovoltaite	$K_2Zn_5Fe_3Al(SO_4)_{12}.18H_2O$	420-460					

Figure 1. Violin plots displaying the concentrations of Cu, Zn, Pb and Mo in fluid inclusions from selected porphyry Cu (Mo) magmatic-hydrothermal systems. a) supercritical fluid inclusions; b) brine inclusions; c) vapor inclusions. Data from Klemm et al. (2007), Kouzmanov et al. (2010), Landtwing et al. (2005), Pudack et al. (2009), Rusk et al. (2004) and Ulrich et al. (1999; 2001). For each range of values, the central black dot represents the mean, the bold vertical bar extending from this dot represents the interquartile range linking values ranging from the 25th to the 75th percentile, and the broader, gray area covers the full range of values. Its lateral extent represents the relative number of data points.





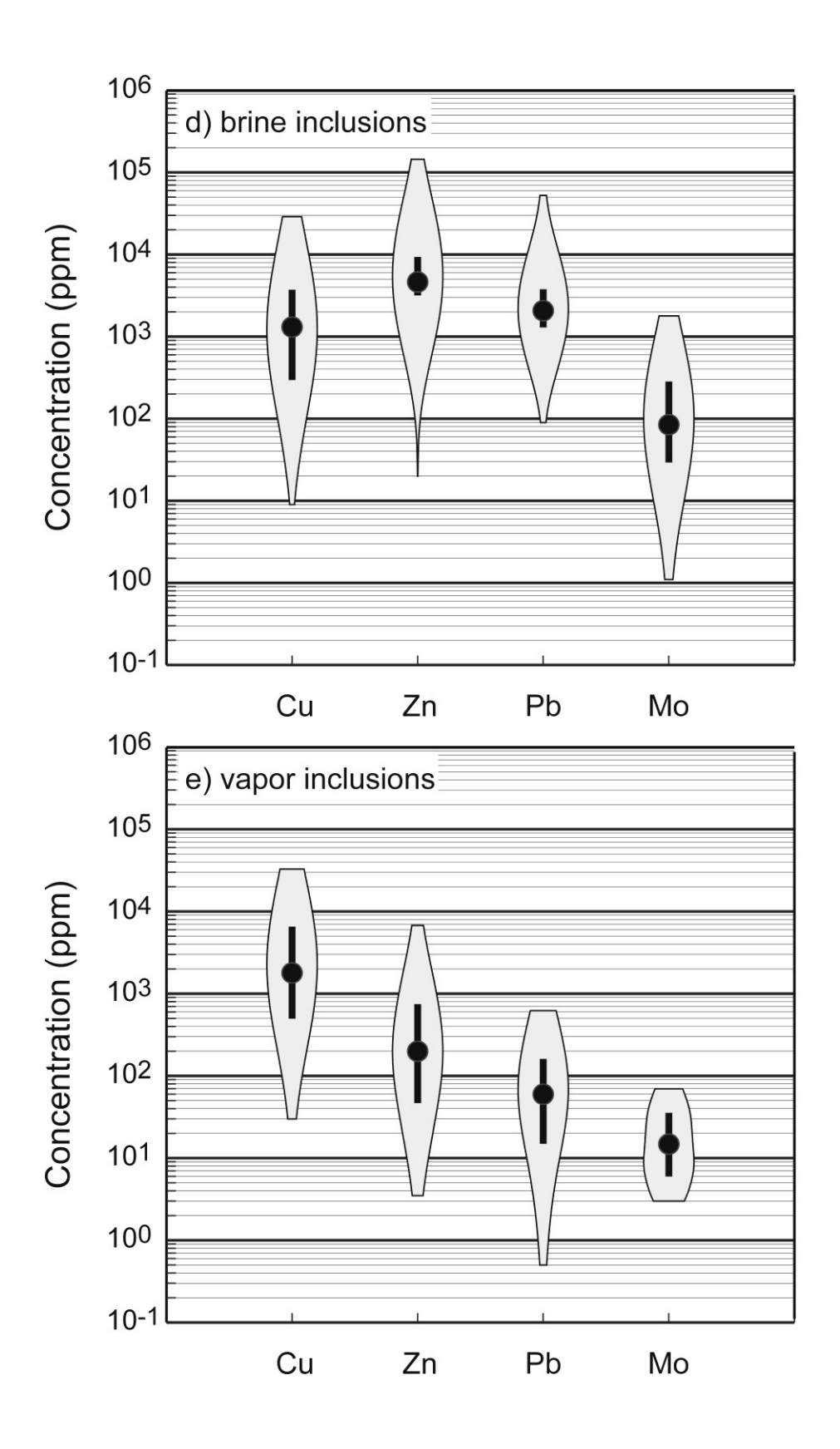
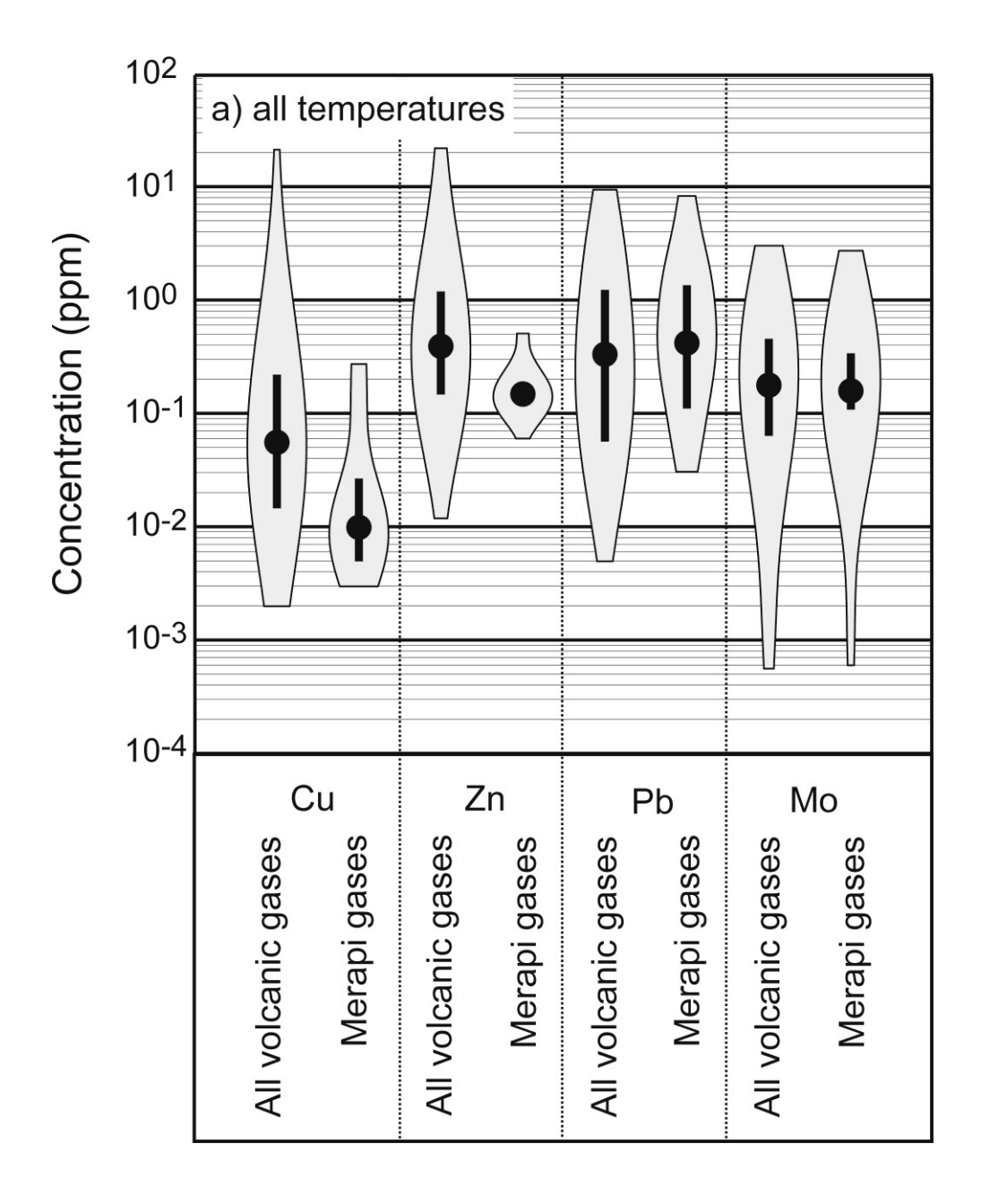
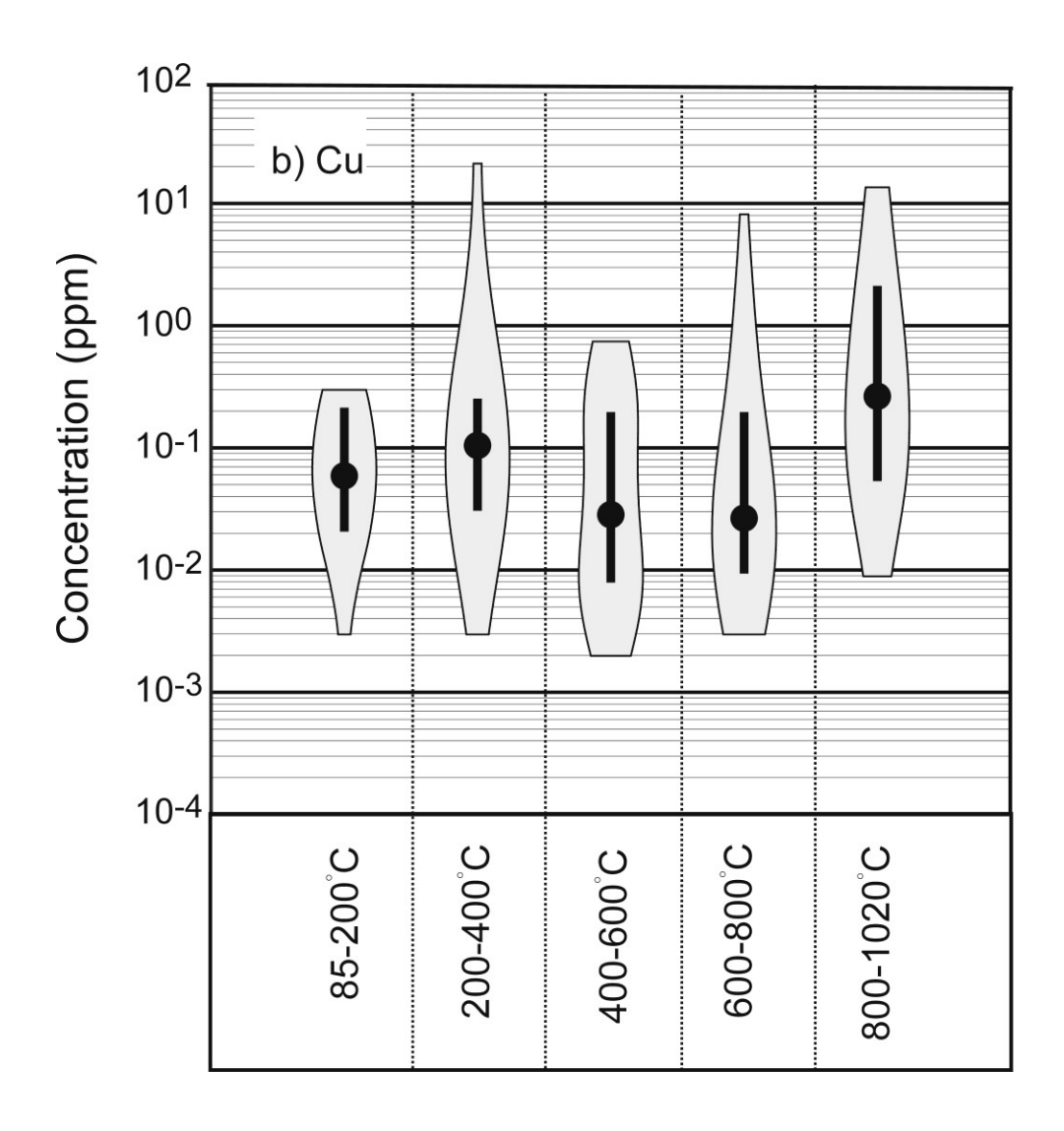
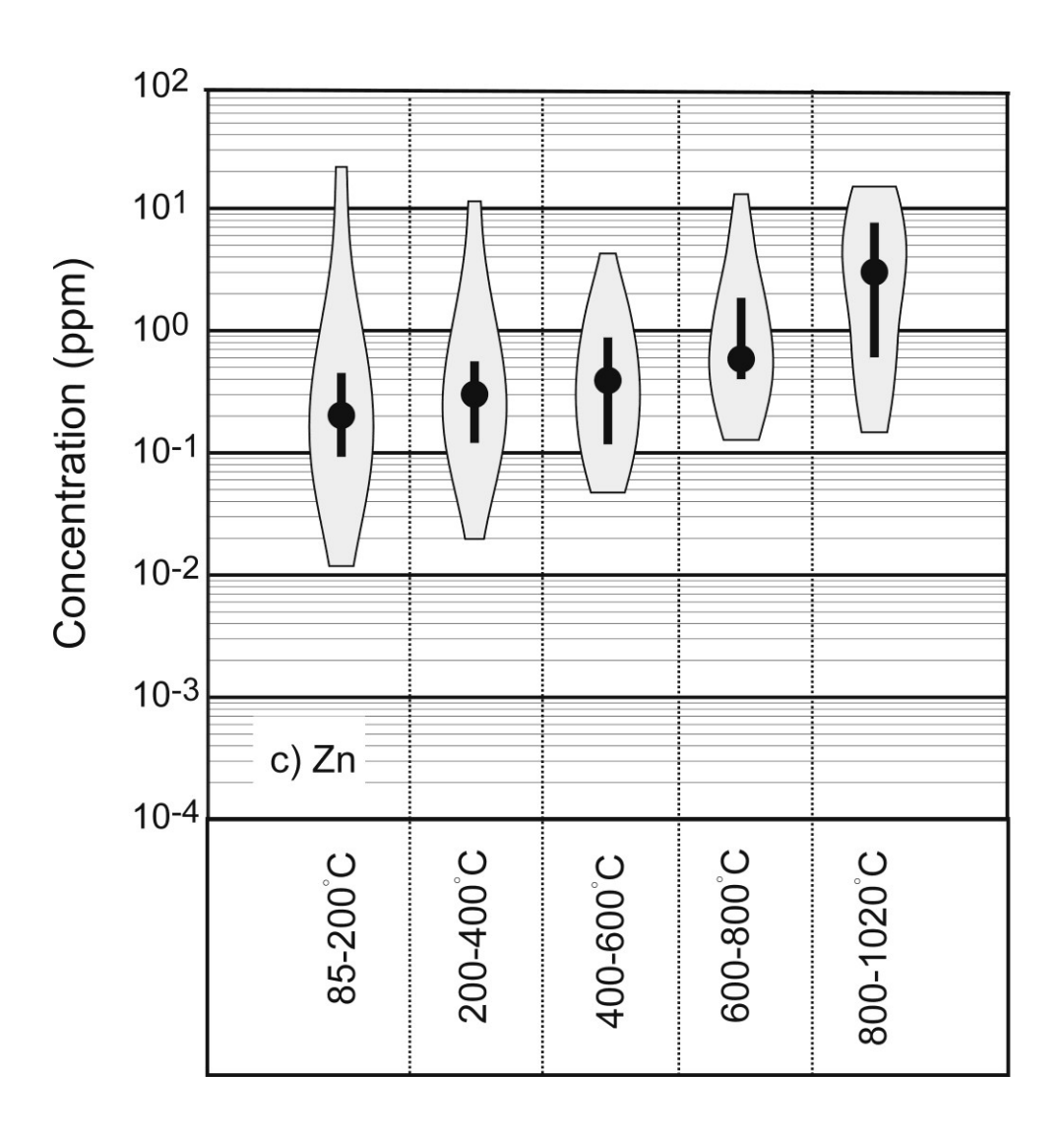
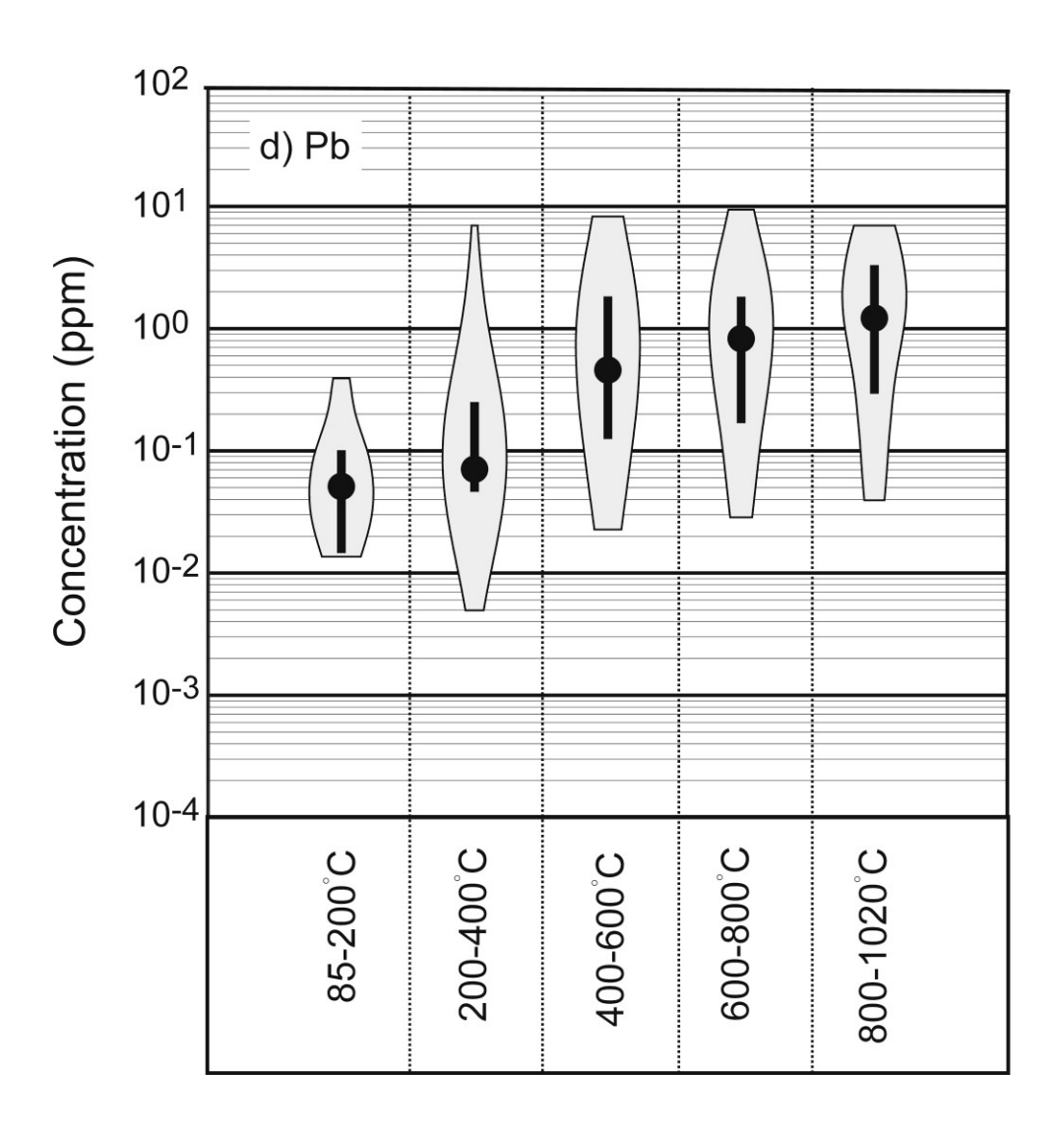


Figure 2. Violin plots displaying the concentrations of Cu, Zn, Pb and Mo in volcanic gas condensates from island arc volcanoes (Gemmel, 1987; Hedenquist et al., 1994; Menyailov and Nikitina, 1980; Menyailov et al., 1986; Mizutani, 1970; Oana, 1962; Stoiber and Rose, 1970; Symonds et al., 1987; 1990; 1996; Taran et al., 1995; 2001; Van Hinsberg et al., in press; Wahrenberger et al., 2002; Zelenski and Bortnikova, 2005) and from Merapi (this study). a) Concentrations of Cu, Zn, Pb and Mo in condensates of volcanic gases sampled at temperatures ranging from 85 to 1020 °C, b), c), d) and e) concentrations of Cu, Zn, Pb and Mo, respectively, in volcanic gases grouped according to temperature. The significance of the different features of the violin plots are described in the caption to Figure 1.









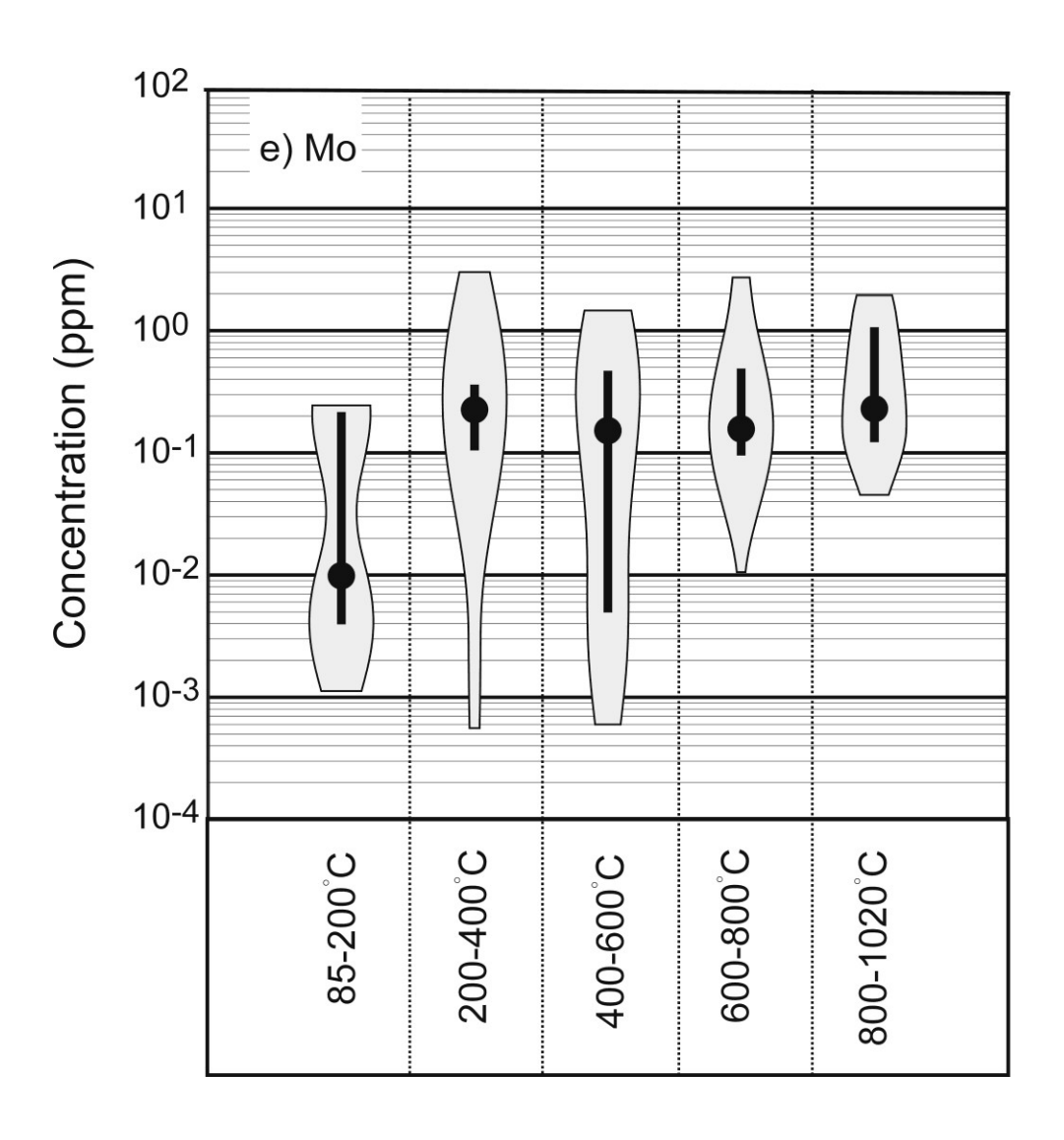


Figure 3. Histogram of concentrations of Cu, Zn, Pb and Mo (Fig 3a) and their ratios to K (Fig 3b) in volcanic gas condensates sampled at Woro in 1984 (Symonds et al., 1987), in 2004 and 2006 (this study).

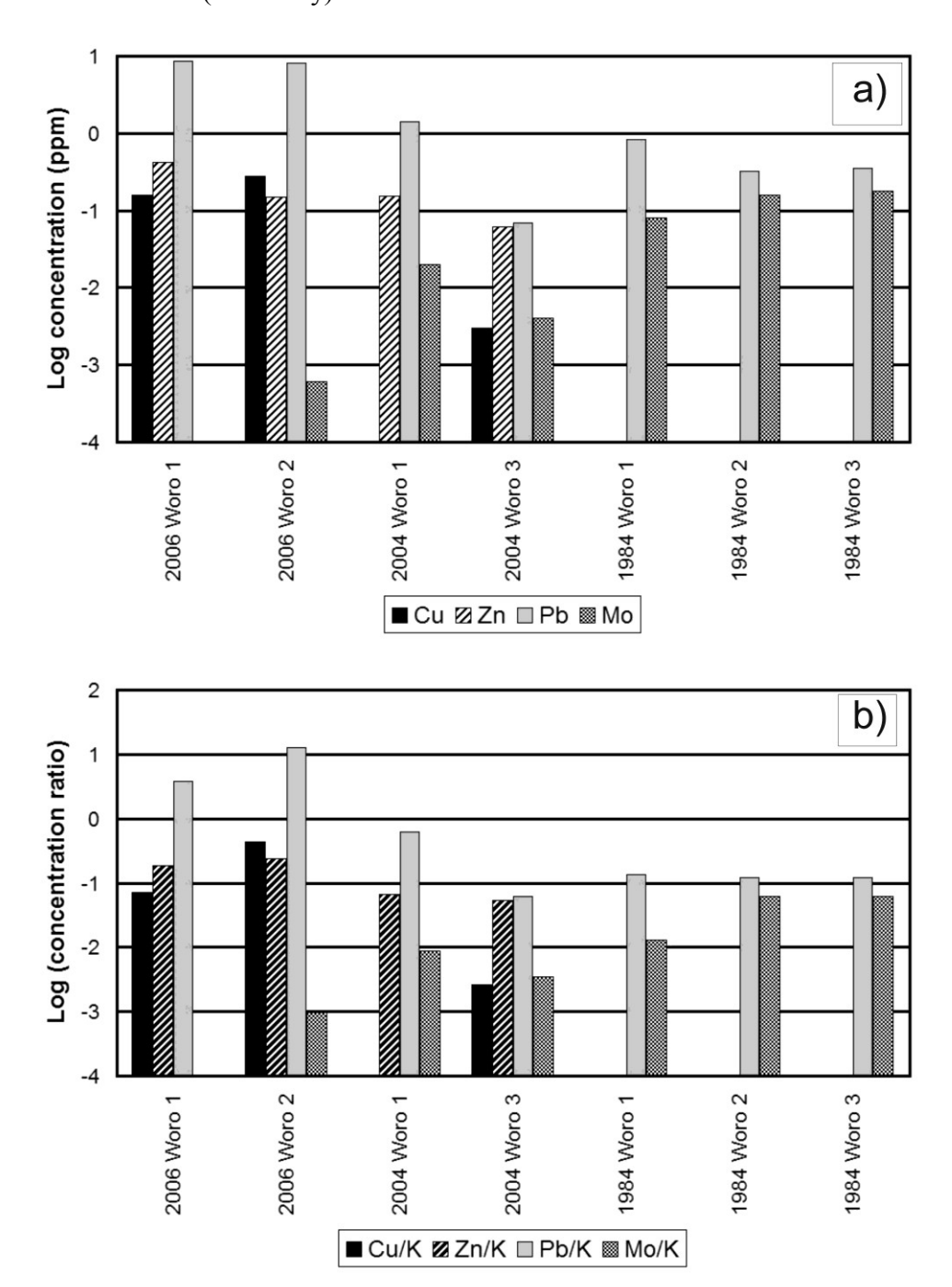
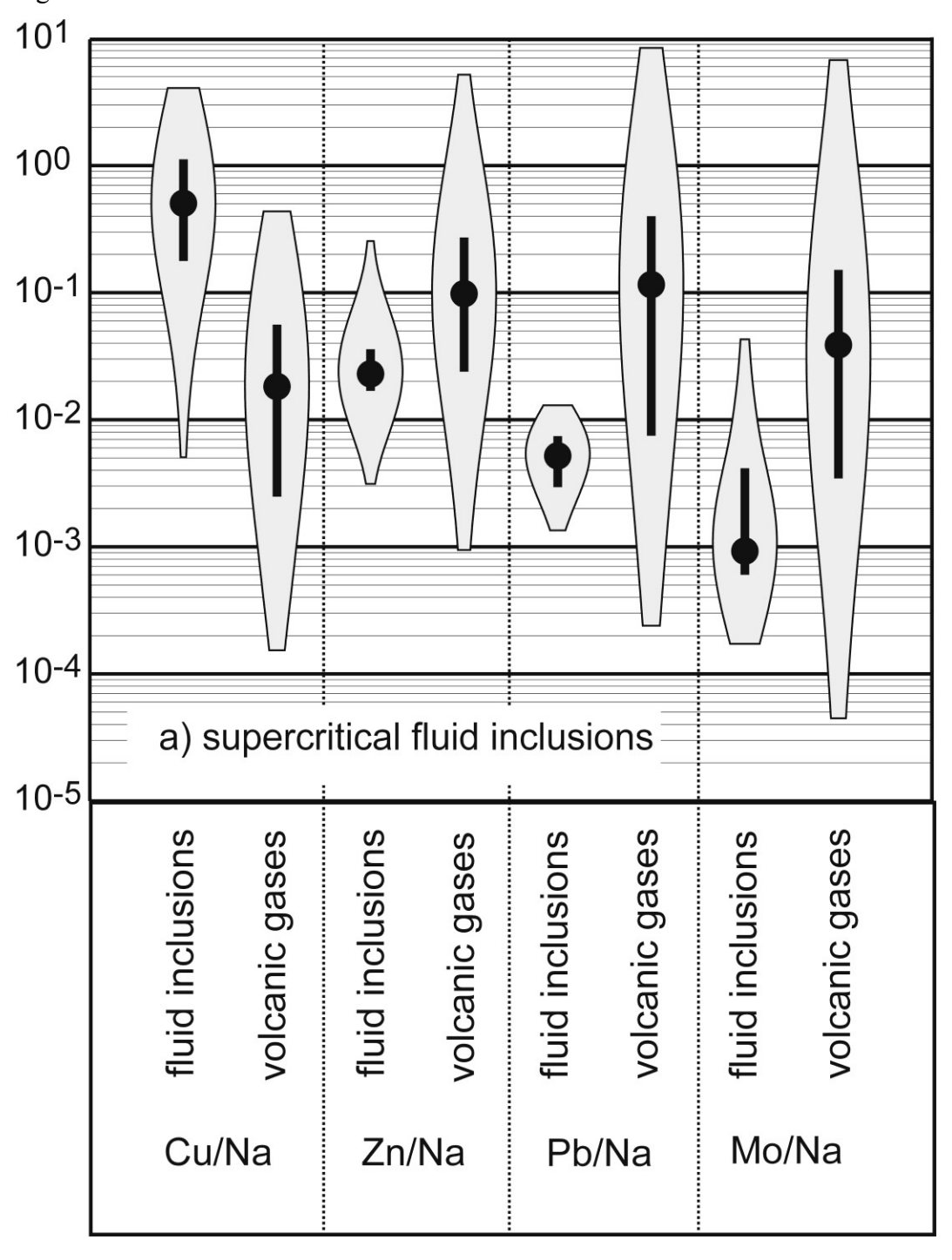
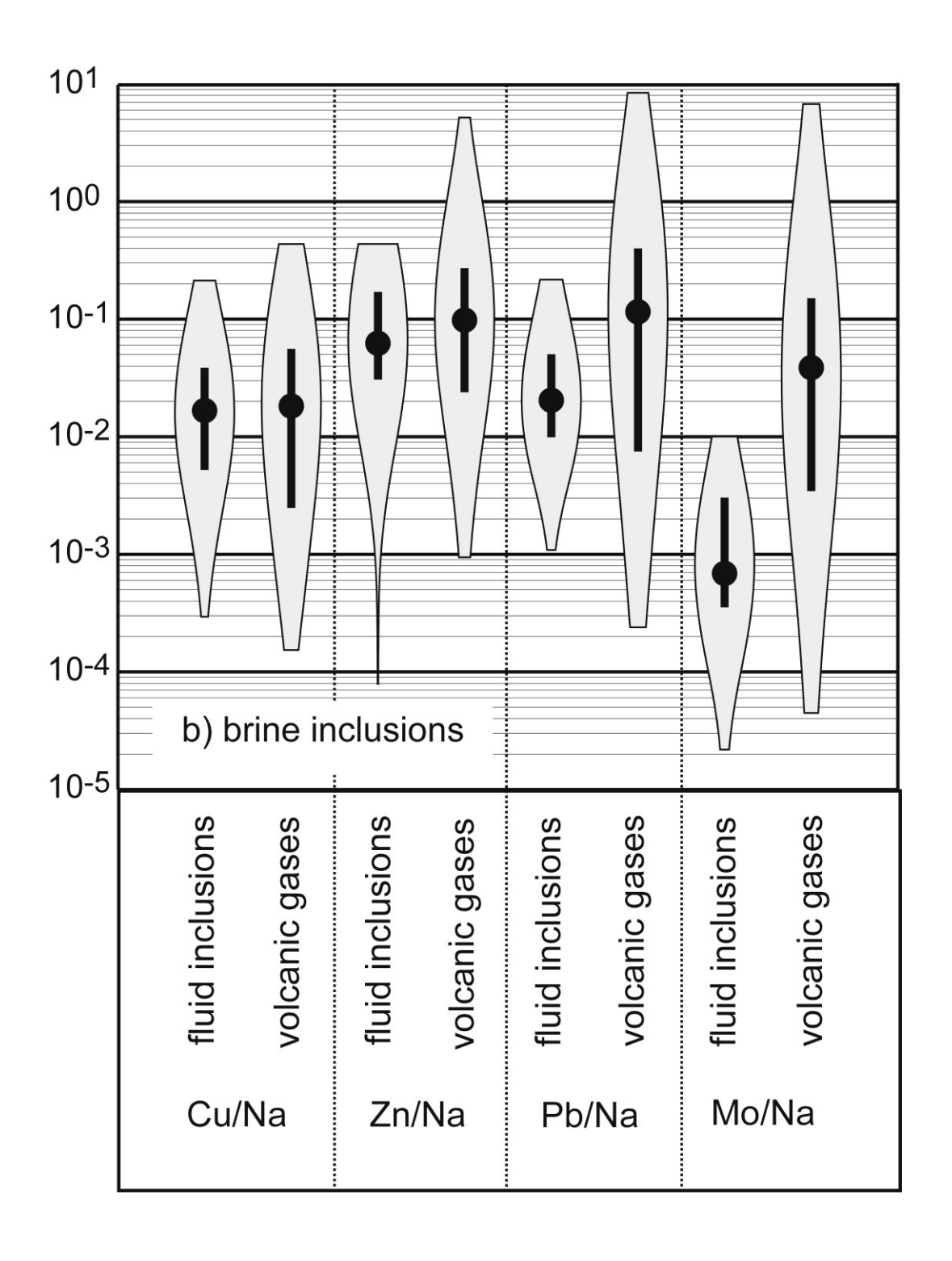


Figure 4. Violin plots comparing Cu/Na, Zn/Na, Pb/Na and Mo/Na ratios in supercritical fluid (a), brine (b) and vapor (c) inclusions and in volcanic gas condensates. The significance of the different features of the violin plots are described in the caption to Figure 1.





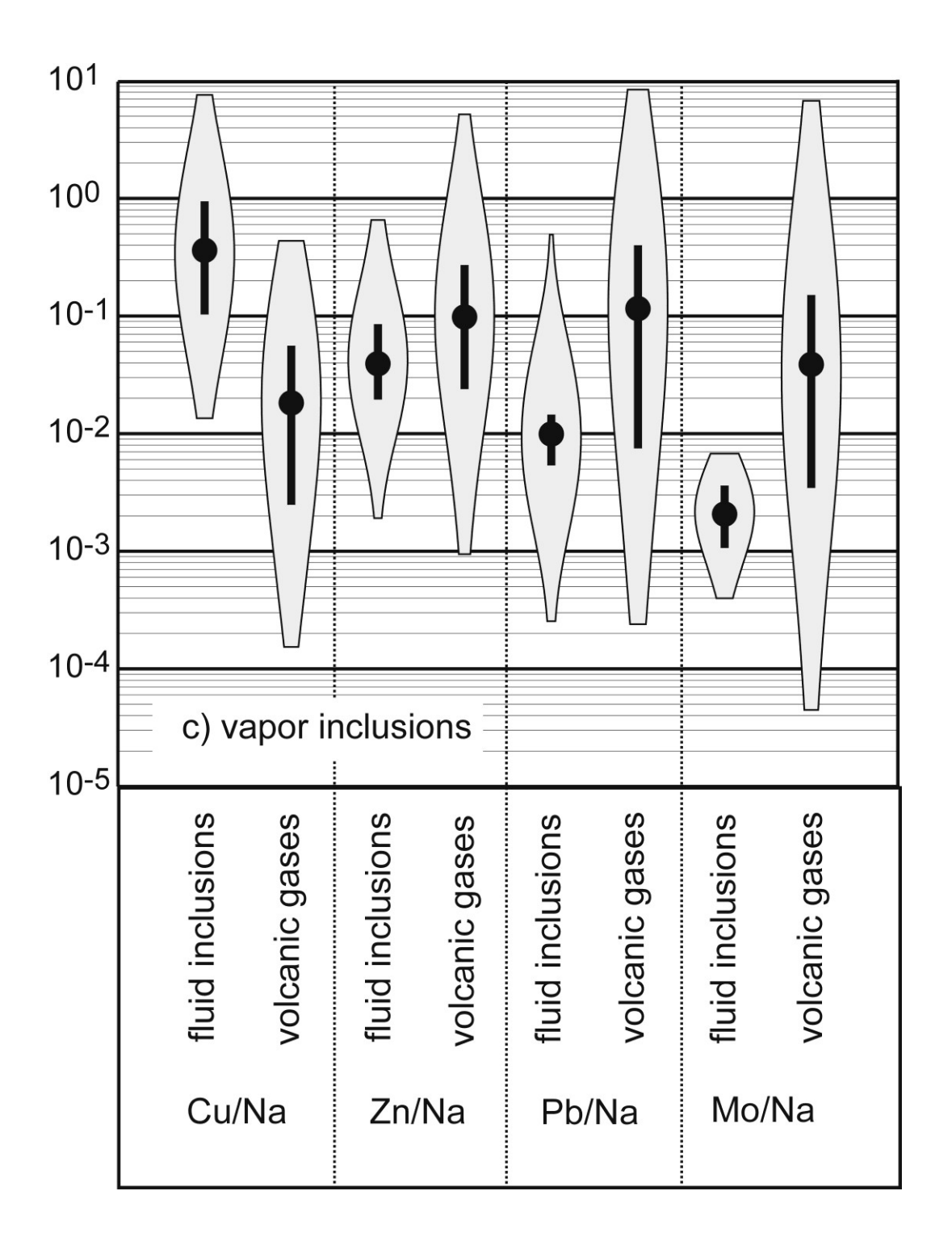
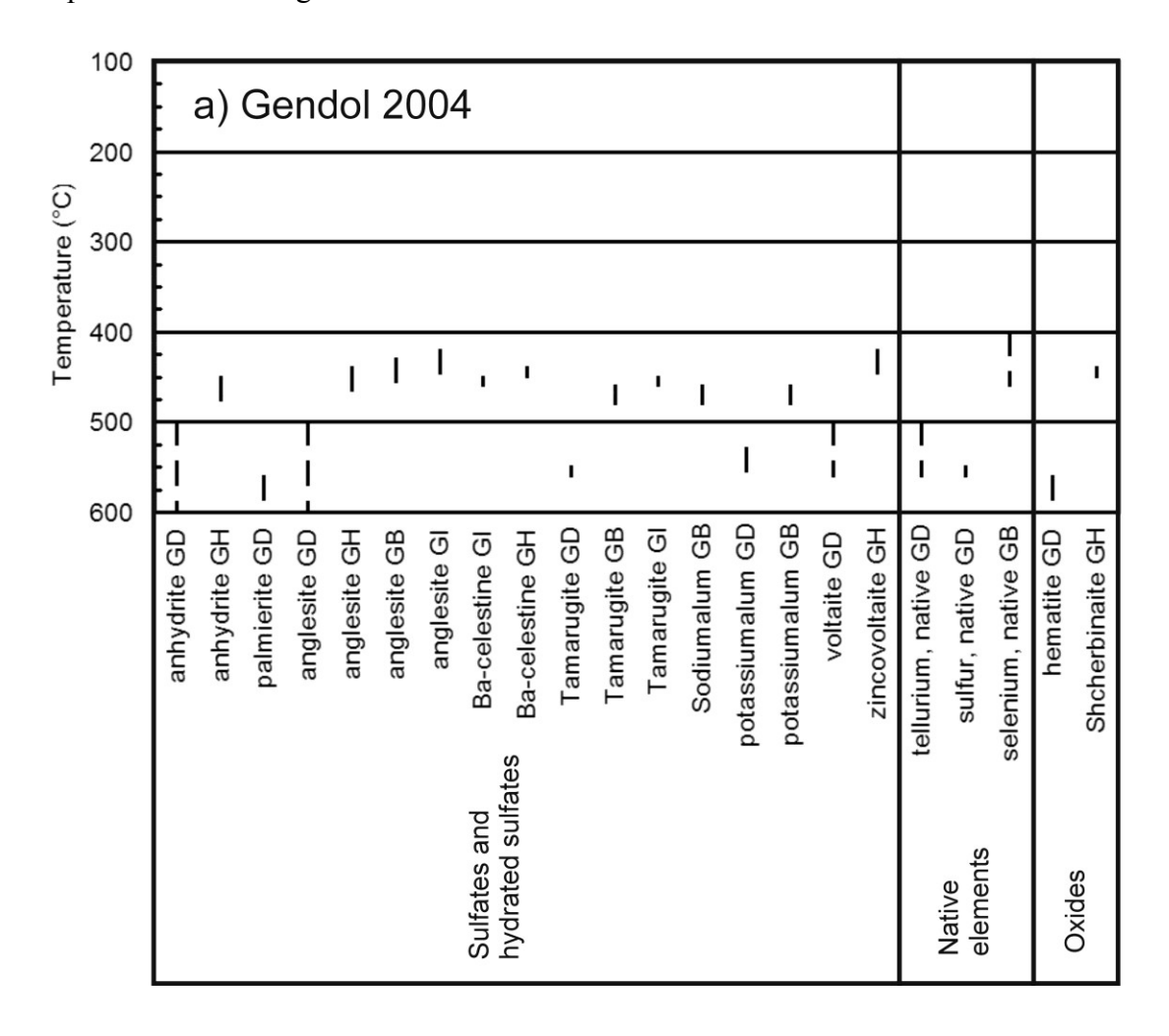
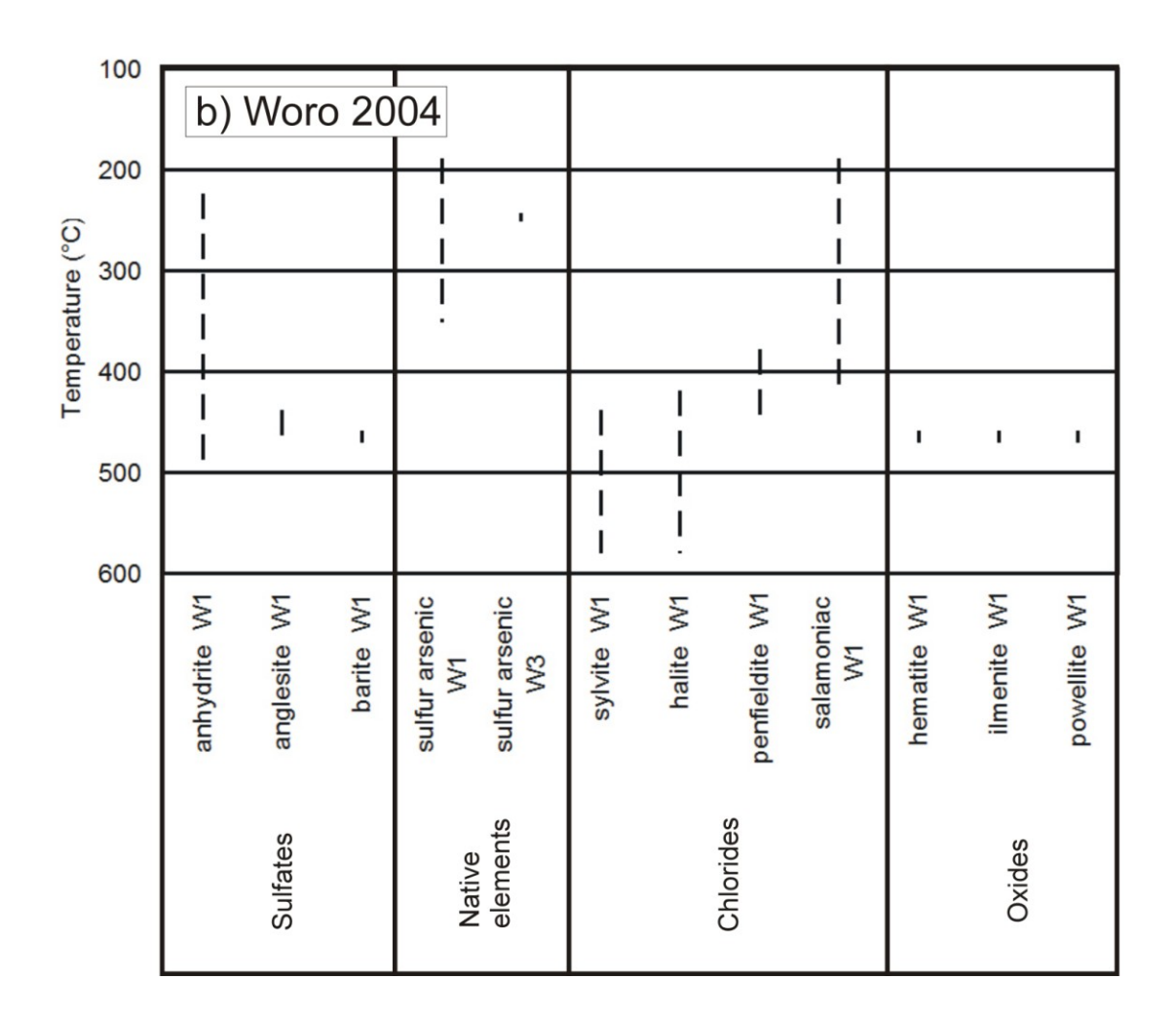


Figure 5. Volcanic gas sublimate mineralogy and precipitation temperatures in silica tubes inserted in fumaroles of the Gendol field (G) in 2004 and the Woro field (W) in 2004 and 2006. The minerals are grouped in families. a) Sublimates identified in tubes from Gendol in 2004; b) Sublimates identified in tubes from Woro in 2004; c) Sublimates identified in tubes from Woro in 2006. Mineral names, formulae and precipitation temperatures are also given in Table 2.





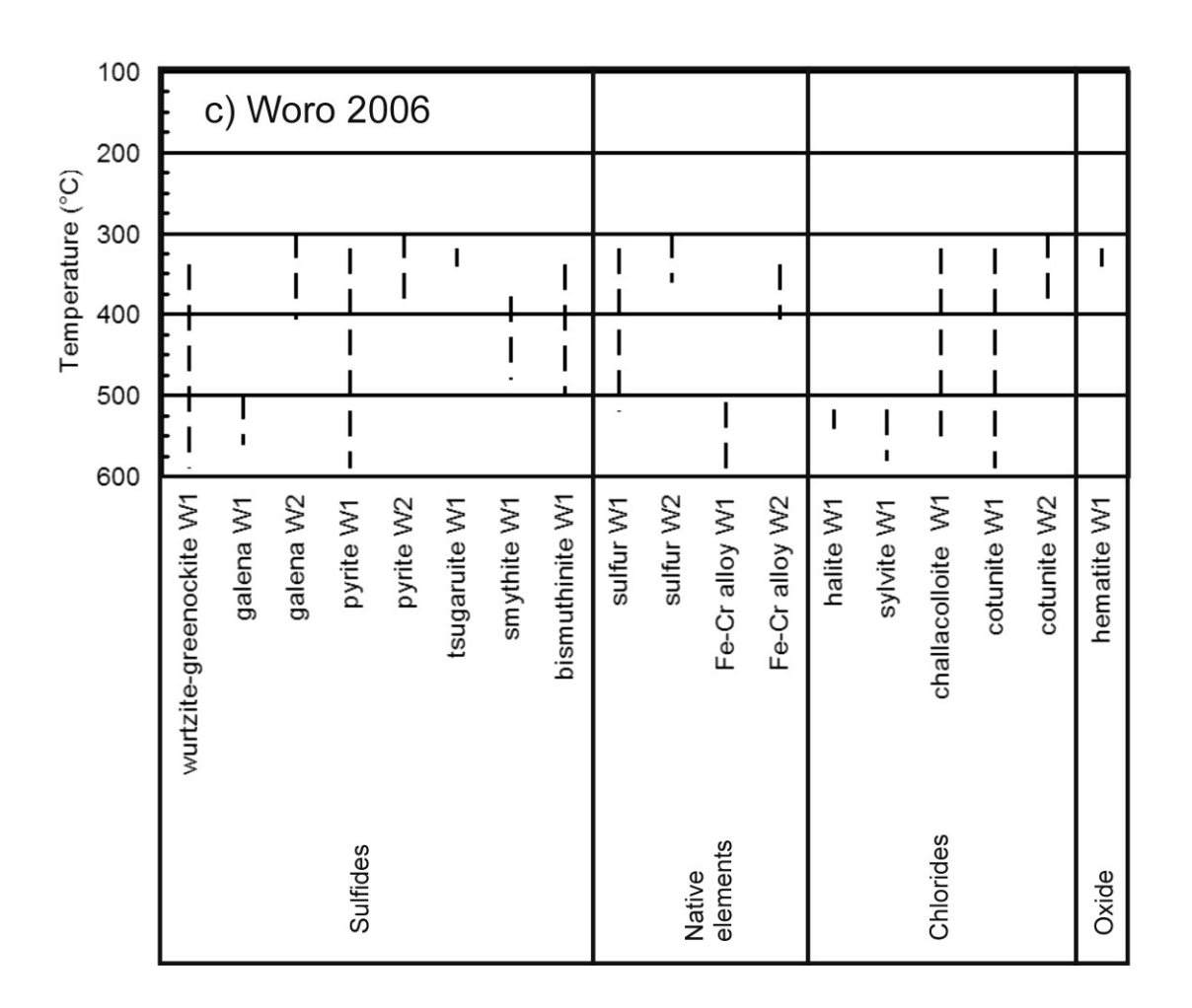


Figure 6. Phase diagram for the H₂O-NaCl system in pressure-temperature-composition space emphasising the liquid-vapor solvus present at magmatic-hydrothermal conditions. Modified from Geiger et al., 2005. Curve A represents the path taken by a porphyritic magmatic volatile phase under a lithostatic pressure gradient, at constant salinity, during decompression and adiabatic cooling. Curve B displays the path taken by a subvolcanic magmatic volatile phase from the magma to the surface, at constant temperature and decreasing pressure under a hydrostatic pressure gradient.

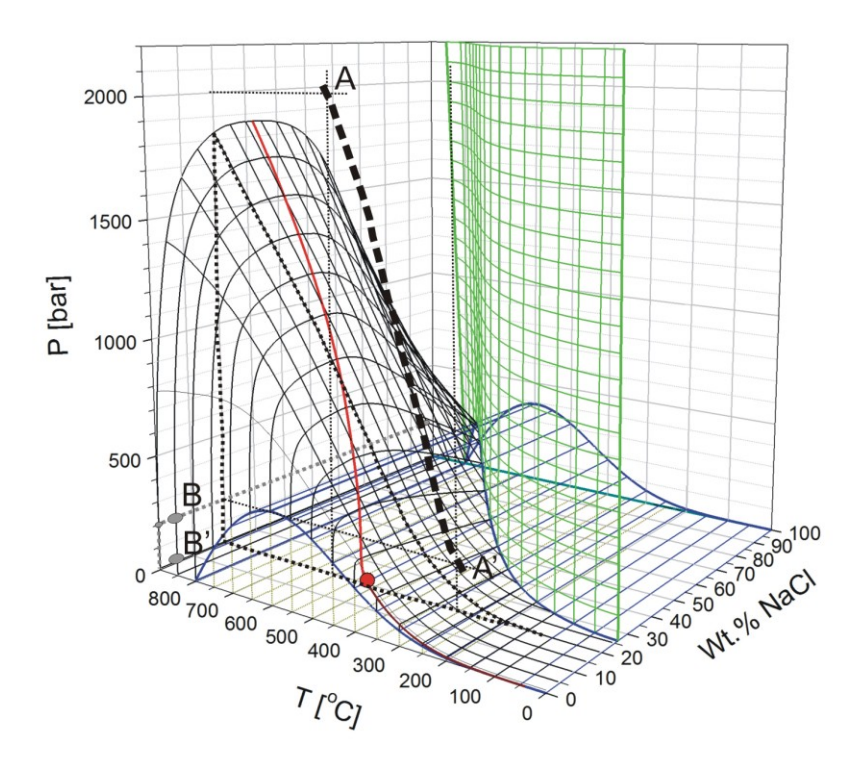
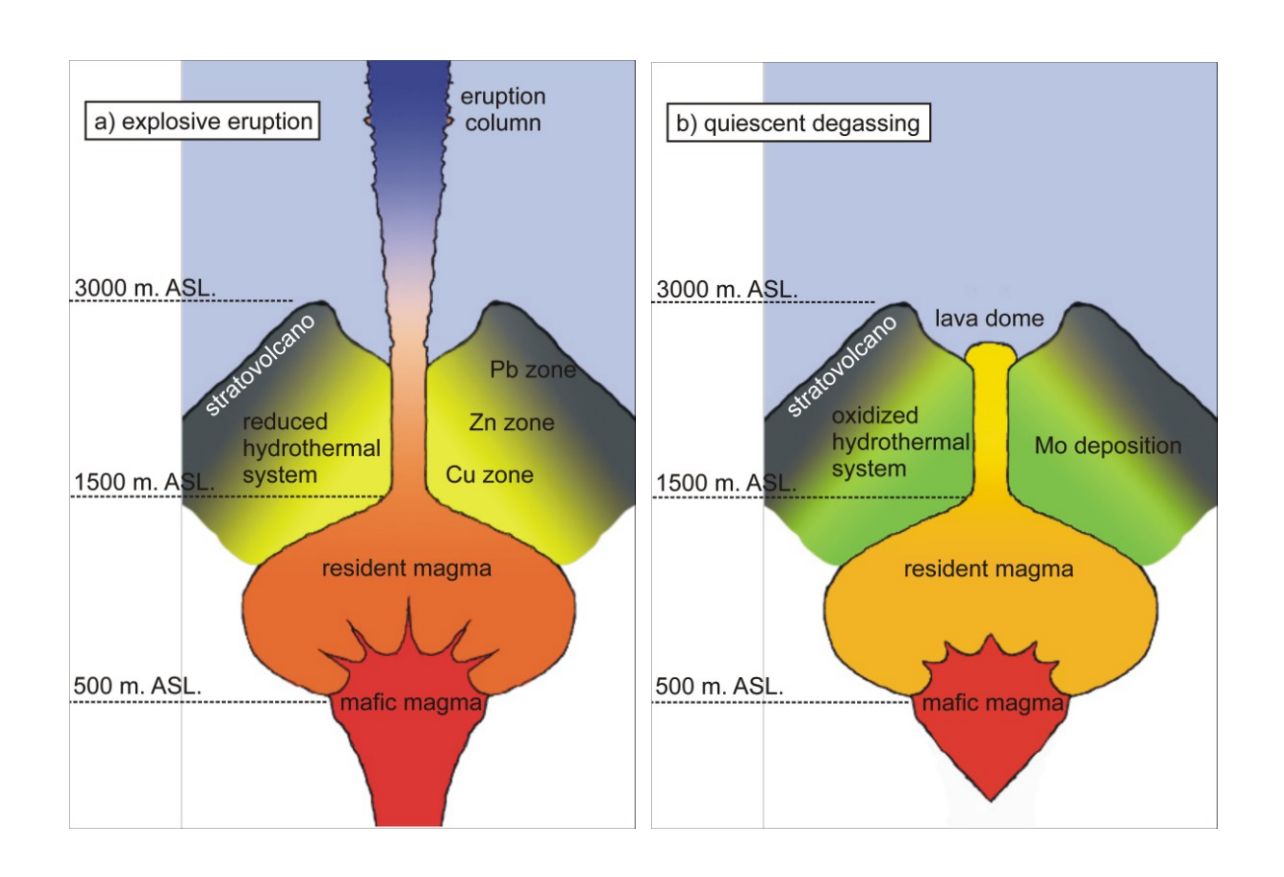


Figure 7. Schematic evolution of a subduction zone magmatic-hydrothermal system during eruptive cycles. a) Injection of sulfide-saturated mafic magma upward into shallower, more oxidized and more felsic resident magma triggers the exsolution of a magmatic volatile phase (MVP) from the mafic melt, which dissolves its sulfide melt, opens up the hydrothermal system and abruptly lowers its pressure from greater than lithostatic to hydrostatic or even vaporstatic. The MVP is volatilized (flash boiling) and the volcano explodes. The remaining volatile phase is transferred into the more felsic, resident magma. The hydrothermal fluid circulating during and after the explosive eruption is hotter, more reduced and enriched in Cu, Zn and Pb. The resulting hydrothermal mineral paragenesis is thus also more reduced, and sulfides of Cu (and Zn in the case of systems that are not buffered by Zn-bearing phenocrysts) and Pb are zoned from deeper to shallower levels. b) Once the eruption is over, the system is temporarily left open and the pressure regime remains hydrostatic or vaporstatic. The mafic magma does not immediately mix with the felsic resident magma although its MVP is transferred to-, percolates and equilibrates with the resident magma (Nadeau et al., under review). The resident magma evolves via the assimilation of different wall rocks (limestones in the case of Merapi, Chadwick et al., 2007) and fractional crystallization. Consequently, Cu, Zn and Pb become gradually depleted- and Mo and other incompatible metals become gradually enriched in the melt and its MVP. As the magma degasses, its magmatic-hydrothermal system and the resulting hydrothermal mineral paragenesis become gradually more oxidized, Cu-, Zn- and Pb-depleted and Mo- and other incompatible element-enriched. The hydrothermal system eventually seals and pressure starts increasing.



Appendix 1. Fluid inclusion data from the literature

magmatic system	type	NaCl eq. (%)	Na	Cu	Zn	Mo	Pb	Cu/Na	Zn/Na	Pb/Na	Mo/Na	Reference
El Teniente porphyry Cu-Mo	b	39.1	96900	820	2600	4	650	8.46E-03	2.68E-02	6.71E-03	4.13E-05	Klemm et al., 2007
El Teniente porphyry Cu-Mo	b	42.7	112400	450	2600	11	520	4.00E-03	2.31E-02	4.63E-03	9.79E-05	Klemm et al., 2007
El Teniente porphyry Cu-Mo	b	45.6	104600	260	6600	8	2100	2.49E-03	6.31E-02	2.01E-02	7.65E-05	Klemm et al., 2007
El Teniente porphyry Cu-Mo	b	48.1	139500	9600	4800	17	760	6.88E-02	3.44E-02	5.45E-03	1.22E-04	Klemm et al., 2007
El Teniente porphyry Cu-Mo	b	38.9	92400	4900	4400	12	1000	5.30E-02	4.76E-02	1.08E-02	1.30E-04	Klemm et al., 2007
El Teniente porphyry Cu-Mo	b	36.6	86600	2800	4100	55	750	3.23E-02	4.73E-02	8.66E-03	6.35E-04	Klemm et al., 2007
El Teniente porphyry Cu-Mo	b		114200	5000	4300	760	620	4.38E-02	3.77E-02	5.43E-03	6.65E-03	Klemm et al., 2007
El Teniente porphyry Cu-Mo	b	49.4	152000	4600	1300	660	460	3.03E-02	8.55E-03	3.03E-03	4.34E-03	Klemm et al., 2007
El Teniente porphyry Cu-Mo	b		159800	7900	1700	1200	610	4.94E-02	1.06E-02	3.82E-03	7.51E-03	Klemm et al., 2007
El Teniente porphyry Cu-Mo	b	60.3	200700	3900	1100	830	220	1.94E-02	5.48E-03	1.10E-03	4.14E-03	Klemm et al., 2007
El Teniente porphyry Cu-Mo	b	57.5	166200	29100	1400	1300	550	1.75E-01	8.42E-03	3.31E-03	7.82E-03	Klemm et al., 2007
El Teniente porphyry Cu-Mo	b	51.9	176400	7400	1300	1000	520	4.20E-02	7.37E-03	2.95E-03	5.67E-03	Klemm et al., 2007
El Teniente porphyry Cu-Mo	b		177600	4200		1800	400	2.36E-02		2.25E-03	1.01E-02	Klemm et al., 2007
El Teniente porphyry Cu-Mo	b		189700	730		610	610	3.85E-03		3.22E-03	3.22E-03	Klemm et al., 2007
El Teniente porphyry Cu-Mo	b	32.3	97800	400	1700	17	640	4.09E-03	1.74E-02	6.54E-03	1.74E-04	Klemm et al., 2007
El Teniente porphyry Cu-Mo	b		81000	420	2300		460	5.19E-03	2.84E-02	5.68E-03		Klemm et al., 2007
El Teniente porphyry Cu-Mo	b	30.7	75300	400	23700	8	800	5.31E-03	3.15E-01	1.06E-02	1.06E-04	Klemm et al., 2007
El Teniente porphyry Cu-Mo	b	31.8	98400	620	910	120	270	6.30E-03	9.25E-03	2.74E-03	1.22E-03	Klemm et al., 2007
El Teniente porphyry Cu-Mo	b	39.3	96100	2100	4500	60	1000	2.19E-02	4.68E-02	1.04E-02	6.24E-04	Klemm et al., 2007
El Teniente porphyry Cu-Mo	sc	13.0	37800	370	1600	80	220	9.79E-03	4.23E-02	5.82E-03	2.12E-03	Klemm et al., 2007
El Teniente porphyry Cu-Mo	sc	12.2	34700	1500	980	6	240	4.32E-02	2.82E-02	6.92E-03	1.73E-04	Klemm et al., 2007
El Teniente porphyry Cu-Mo	sc	2.1	5400	1400	220		50	2.59E-01	4.07E-02	9.26E-03		Klemm et al., 2007
El Teniente porphyry Cu-Mo	sc	4.0	8600	3300	240	15	40	3.84E-01	2.79E-02	4.65E-03	1.74E-03	Klemm et al., 2007
El Teniente porphyry Cu-Mo	sc	5.2	10200	14400	300	17	50	1.41E+00	2.94E-02	4.90E-03	1.67E-03	Klemm et al., 2007
El Teniente porphyry Cu-Mo	sc		13200	4300	220	8	50	3.26E-01	1.67E-02	3.79E-03	6.06E-04	Klemm et al., 2007
El Teniente porphyry Cu-Mo	sc	4.2	5100	21100	110		13	4.14E+00	2.16E-02	2.55E-03		Klemm et al., 2007
El Teniente porphyry Cu-Mo	sc		15400	4500	150	11	75	2.92E-01	9.74E-03	4.87E-03	7.14E-04	Klemm et al., 2007
El Teniente porphyry Cu-Mo	sc	5.1	15500	2500			50	1.61E-01		3.23E-03		Klemm et al., 2007
El Teniente porphyry Cu-Mo	sc	4.8	14400	2800	250		65	1.94E-01	1.74E-02	4.51E-03		Klemm et al., 2007
El Teniente porphyry Cu-Mo	sc	4.5	11800	6200	270	6	55	5.25E-01	2.29E-02	4.66E-03	5.08E-04	Klemm et al., 2007
El Teniente porphyry Cu-Mo	sc	5.8	17300	4600	460	8	75	2.66E-01	2.66E-02	4.34E-03	4.62E-04	Klemm et al., 2007
El Teniente porphyry Cu-Mo	sc	4.0	8100	8700	120	7	19	1.07E+00	1.48E-02	2.35E-03	8.64E-04	Klemm et al., 2007
El Teniente porphyry Cu-Mo	sc	6.1	20800	1700	190		59	8.17E-02	9.13E-03	2.84E-03		Klemm et al., 2007
El Teniente porphyry Cu-Mo	\mathbf{v}	3.9	8800	5800	260	60	35	6.59E-01	2.95E-02	3.98E-03	6.82E-03	Klemm et al., 2007
El Teniente porphyry Cu-Mo	v		900	260	12	6	9	2.89E-01	1.33E-02	1.00E-02	6.67E-03	Klemm et al., 2007
El Teniente porphyry Cu-Mo	v		2900	350	55	3	11	1.21E-01	1.90E-02	3.79E-03	1.03E-03	Klemm et al., 2007
El Teniente porphyry Cu-Mo	v	3.8	2200	3200			20	1.45E+00		9.09E-03		Klemm et al., 2007
El Teniente porphyry Cu-Mo	v	3.8	7500	9700	140	3	35	1.29E+00	1.87E-02	4.67E-03	4.00E-04	Klemm et al., 2007
El Teniente porphyry Cu-Mo	v	0.9	1200	3700				3.08E+00				Klemm et al., 2007
El Teniente porphyry Cu-Mo	v		1900	1500	100	4	16	7.89E-01	5.26E-02	8.42E-03	2.11E-03	Klemm et al., 2007
El Teniente porphyry Cu-Mo	v	2.3	2800	10900	80	8	15	3.89E+00	2.86E-02	5.36E-03	2.86E-03	Klemm et al., 2007

El Teniente porphyry Cu-Mo	v	3.5	3000	23200	90	5	14	7.73E+00	3.00E-02	4.67E-03	1.67E-03	Klemm et al., 2007
El Teniente porphyry Cu-Mo	v	4.3	6800	18800	270	19	50	2.76E+00	3.97E-02	7.35E-03	2.79E-03	Klemm et al., 2007
El Teniente porphyry Cu-Mo	v		14200	7200	290	55	70	5.07E-01	2.04E-02	4.93E-03	3.87E-03	Klemm et al., 2007
El Teniente porphyry Cu-Mo	v		6400	16200	220	25	35	2.53E+00	3.44E-02	5.47E-03	3.91E-03	Klemm et al., 2007
El Teniente porphyry Cu-Mo	v		8600	7900	220	12	60	9.19E-01	52 02	6.98E-03	1.40E-03	Klemm et al., 2007
El Teniente porphyry Cu-Mo	v	4.5	14400	3200		7	00	2.22E-01		0.702 03	4.86E-04	Klemm et al., 2007
Rosia-Poieni porphyry Cu-Au	b		111628	3009	29240		13251	2.70E-02	2.62E-01	1.19E-01		Kouzmanov et al., 2010
Rosia-Poieni porphyry Cu-Au	b		112692	2761	28718		13300	2.45E-02	2.55E-01	1.18E-01		Kouzmanov et al., 2010
Rosia-Poieni porphyry Cu-Au	b		109324	3161	31545		14192	2.89E-02	2.89E-01	1.30E-01		Kouzmanov et al., 2010
Rosia-Poieni porphyry Cu-Au	b		115614	3370	23792		11069	2.91E-02	2.06E-01	9.57E-02		Kouzmanov et al., 2010
Rosia-Poieni porphyry Cu-Au	b		117970	2571	20567		12104	2.18E-02	1.74E-01	1.03E-01		Kouzmanov et al., 2010
Rosia-Poieni porphyry Cu-Au	b		117141	1392	20818		9503	1.19E-02	1.78E-01	8.11E-02		Kouzmanov et al., 2010
Rosia-Poieni porphyry Cu-Au	b		118096	2366	20364		11002	2.00E-02	1.72E-01	9.32E-02		Kouzmanov et al., 2010
Rosia-Poieni porphyry Cu-Au	b		126933	16441	4370		2000	1.30E-01	3.44E-02	1.58E-02		Kouzmanov et al., 2010
Rosia-Poieni porphyry Cu-Au	b		119053	13997	3845		1453	1.18E-01	3.23E-02	1.22E-02		Kouzmanov et al., 2010 Kouzmanov et al., 2010
Rosia-Poieni porphyry Cu-Au	b		126294	10272	4176		1079	8.13E-02	3.31E-02	8.54E-03		Kouzmanov et al., 2010 Kouzmanov et al., 2010
Rosia-Poieni porphyry Cu-Au	b		116054	2102	22745		11145	1.81E-02	1.96E-01	9.60E-02		Kouzmanov et al., 2010 Kouzmanov et al., 2010
Rosia-Poieni porphyry Cu-Au	b		108437	8874	30565		14115	8.18E-02	2.82E-01	1.30E-01		Kouzmanov et al., 2010 Kouzmanov et al., 2010
Rosia-Poieni porphyry Cu-Au	b		110684	3970	31198		15865	3.59E-02	2.82E-01	1.43E-01		Kouzmanov et al., 2010 Kouzmanov et al., 2010
Rosia-Poieni porphyry Cu-Au	b		129053	1516	9976		4890	1.17E-02	7.73E-02	3.79E-02		Kouzmanov et al., 2010
Rosia-Poieni porphyry Cu-Au	b		113825	2621	24544		12579	2.30E-02	2.16E-01	1.11E-01		Kouzmanov et al., 2010
Rosia-Poieni porphyry Cu-Au	b		115400	1487	19633		16947	1.29E-02	1.70E-01	1.47E-01		Kouzmanov et al., 2010
Rosia-Poieni porphyry Cu-Au	b		113836	3170	25023		12461	2.78E-02	2.20E-01	1.47E-01 1.09E-01		Kouzmanov et al., 2010
Rosia-Poieni porphyry Cu-Au	b		117696	2019	22070		7277	1.72E-02	1.88E-01	6.18E-02		Kouzmanov et al., 2010
Rosia-Poieni porphyry Cu-Au Rosia-Poieni porphyry Cu-Au	b		120260	2314	16677		10056	1.72E-02 1.92E-02	1.39E-01	8.36E-02		Kouzmanov et al., 2010 Kouzmanov et al., 2010
Rosia-Poieni porphyry Cu-Au Rosia-Poieni porphyry Cu-Au	b		118632	1860	18853		10030	1.57E-02	1.59E-01 1.59E-01	8.82E-02		Kouzmanov et al., 2010
Rosia-Poieni porphyry Cu-Au Rosia-Poieni porphyry Cu-Au	b		119786	1000	13816		26325	1.3/E-02	1.35E-01 1.15E-01	2.20E-01		Kouzmanov et al., 2010
Rosia-Poieni porphyry Cu-Au Rosia-Poieni porphyry Cu-Au	b		122163	1885	17538		10794	1.54E-02	1.13E-01 1.44E-01	8.84E-02		Kouzmanov et al., 2010
Rosia-Poieni porphyry Cu-Au Rosia-Poieni porphyry Cu-Au	b		119590	1317	21814		11815	1.34E-02 1.10E-02	1.44E-01 1.82E-01	9.88E-02		Kouzmanov et al., 2010
Rosia-Poieni porphyry Cu-Au Rosia-Poieni porphyry Cu-Au	b		115808	1057	25452		14115	9.13E-03	2.20E-01	1.22E-01		Kouzmanov et al., 2010 Kouzmanov et al., 2010
Rosia-Poieni porphyry Cu-Au	b		105602	1748	39610		17722	1.66E-02	3.75E-01	1.68E-01		Kouzmanov et al., 2010
Rosia-Poieni porphyry Cu-Au Rosia-Poieni porphyry Cu-Au	b		97573	2581	43213		20343	2.65E-02	4.43E-01	2.08E-01		Kouzmanov et al., 2010
Rosia-Poieni porphyry Cu-Au	b		107373	2986	35954		19660	2.78E-02	3.35E-01	1.83E-01		Kouzmanov et al., 2010
Rosia-Poieni porphyry Cu-Au Rosia-Poieni porphyry Cu-Au	b		107373	3725	34765		19574	3.42E-02	3.33E-01 3.19E-01	1.80E-01		Kouzmanov et al., 2010 Kouzmanov et al., 2010
Rosia-Poieni porphyry Cu-Au Rosia-Poieni porphyry Cu-Au	b		109691	5232	34364		18912	4.77E-02	3.13E-01 3.13E-01	1.72E-01		Kouzmanov et al., 2010
Rosia-Poieni porphyry Cu-Au	b		105348	5147	33324		17606	4.77E-02 4.89E-02	3.16E-01	1.67E-01		Kouzmanov et al., 2010
Rosia-Poieni porphyry Cu-Au	b		94639	139	26504		10189	1.47E-03	2.80E-01	1.07E-01 1.08E-01		Kouzmanov et al., 2010
Rosia-Poieni porphyry Cu-Au Rosia-Poieni porphyry Cu-Au	b		101573	113	23176		10715	1.47E-03 1.11E-03	2.28E-01	1.05E-01		Kouzmanov et al., 2010
Rosia-Poieni porphyry Cu-Au Rosia-Poieni porphyry Cu-Au	b		101373	194	19817		11812	1.11E-03 1.92E-03	1.96E-01	1.03E-01 1.17E-01		Kouzmanov et al., 2010
Rosia-Poieni porphyry Cu-Au Rosia-Poieni porphyry Cu-Au	b		107724	244	30213		17146	2.27E-03	2.80E-01	1.17E-01 1.59E-01		Kouzmanov et al., 2010
Rosia-Poieni porphyry Cu-Au Rosia-Poieni porphyry Cu-Au	b b		107724	337	5946		3760	3.21E-03	5.66E-02	3.58E-02		Kouzmanov et al., 2010 Kouzmanov et al., 2010
Rosia-Poieni porphyry Cu-Au Rosia-Poieni porphyry Cu-Au	b		1011035	319	6591		4178	3.21E-03 3.16E-03	6.52E-02	4.14E-02		Kouzmanov et al., 2010 Kouzmanov et al., 2010
Rosia-Poieni porphyry Cu-Au Rosia-Poieni porphyry Cu-Au	b		101033	235	7808		4178	2.29E-03	7.63E-02	4.14E-02 4.09E-02		Kouzmanov et al., 2010 Kouzmanov et al., 2010
	b b		96803	233 167	16573		4189	1.73E-03	1.71E-01	4.09E-02 5.07E-02		•
Rosia-Poieni porphyry Cu-Au	D		90803	10/	103/3		4911	1./3E-03	1./1E-01	3.0/E-02		Kouzmanov et al., 2010

Rosia-Poieni porphyry Cu-Au	v		1675									Kouzmanov et al., 2010
Rosia-Poieni porphyry Cu-Au	v		1642	30	31		1.7	1.83E-02	1.89E-02	1.04E-03		Kouzmanov et al., 2010 Kouzmanov et al., 2010
Rosia-Poieni porphyry Cu-Au	v		1957	30	24		1./	1.03E-02	1.83E-02 1.23E-02	1.041.5		Kouzmanov et al., 2010
Rosia-Poieni porphyry Cu-Au	v		1821		3.5				1.92E-02			Kouzmanov et al., 2010 Kouzmanov et al., 2010
Rosia-Poieni porphyry Cu-Au	v		1961	47	3.3		0.5	2.40E-02	1.9215-03	2.55E-04		Kouzmanov et al., 2010
Rosia-Poieni porphyry Cu-Au	v		1935	1332	33		13	6.88E-01	1.71E-02	6.72E-03		Kouzmanov et al., 2010 Kouzmanov et al., 2010
Rosia-Poieni porphyry Cu-Au	v		1963	67	33		13	3.41E-02	1./1L-02	0.72L-03		Kouzmanov et al., 2010
Rosia-Poieni porphyry Cu-Au	v		1567	07	531		153	J.41L-02	3.39E-01	9.76E-02		Kouzmanov et al., 2010
Rosia-Poieni porphyry Cu-Au	v		1941		40		0.7		2.06E-02	3.61E-04		Kouzmanov et al., 2010
Rosia-Poieni porphyry Cu-Au	v		785		211		0.7		2.69E-01	J.01L-04		Kouzmanov et al., 2010
Rosia-Poieni porphyry Cu-Au	v		1664		172		33		1.03E-01	1.98E-02		Kouzmanov et al., 2010 Kouzmanov et al., 2010
Rosia-Poieni porphyry Cu-Au	v		1386		134		9.3		9.67E-02	6.71E-03		Kouzmanov et al., 2010 Kouzmanov et al., 2010
Rosia-Poieni porphyry Cu-Au	v		1617		809		23		5.00E-01	1.42E-02		Kouzmanov et al., 2010
Rosia-Poieni porphyry Cu-Au	v		1952		28		23		1.43E-02	1.4215-02		Kouzmanov et al., 2010
Rosia-Poieni porphyry Cu-Au	v		1014		20				1.43E-02			Kouzmanov et al., 2010
Rosia-Poieni porphyry Cu-Au	v		1870				1.4			7.49E-04		Kouzmanov et al., 2010
Rosia-Poieni porphyry Cu-Au	v		1936		4.1		1.5		2.12E-03	7.49E-04 7.75E-04		Kouzmanov et al., 2010 Kouzmanov et al., 2010
Rosia-Poieni porphyry Cu-Au	v		1967		4.1		1.3		2.12E-03	7.73E-04		Kouzmanov et al., 2010
Rosia-Poieni porphyry Cu-Au	v		1226		27		15		2.20E-02	1.22E-02		Kouzmanov et al., 2010
Rosia-Poieni porphyry Cu-Au			1816		21		13		2.20E-02	1.2215-02		Kouzmanov et al., 2010
Rosia-Poieni porphyry Cu-Au	v		1581	113	76		3.8	7.15E-02	4.81E-02	2.40E-03		Kouzmanov et al., 2010 Kouzmanov et al., 2010
	v		1252	303	832		625	7.13E-02 2.42E-01		4.99E-01		•
Rosia-Poieni porphyry Cu-Au Bingham Cu-Au-Mo porphyry	V	46.2			2900	45	2400	2.42E-01 2.11E-01	6.65E-01 2.36E-02		2.665.04	Kouzmanov et al., 2010
	b	46.2 46.1	123000	26000 22000	4100	45 270	3800	2.11E-01 2.16E-01	4.02E-02	1.95E-02 3.73E-02	3.66E-04 2.65E-03	Landtwing et al., 2005
Bingham Cu-Au-Mo porphyry	b b	44.6	102000 108000	15000	2800	270 94	3800	1.39E-01	4.02E-02 2.59E-02	3.73E-02 3.52E-02	2.05E-03 8.70E-04	Landtwing et al., 2005
Bingham Cu-Au-Mo porphyry								1.39E-01 1.14E-01		3.52E-02 2.35E-02		Landtwing et al., 2005
Bingham Cu-Au-Mo porphyry	b	48.7	132000	15000	2700	60	3100		2.05E-02		4.55E-04	Landtwing et al., 2005
Bingham Cu-Au-Mo porphyry	b	43.8	112000	6200	4400	10.00	3600	5.54E-02	3.93E-02	3.21E-02	0.205.02	Landtwing et al., 2005
Bingham Cu-Au-Mo porphyry	b	44.8	113000	3500	3500	1060	2900	3.10E-02	3.10E-02	2.57E-02	9.38E-03	Landtwing et al., 2005
Bingham Cu-Au-Mo porphyry	b	47.3	125000	3200	3300	400	3300	2.56E-02	2.64E-02	2.64E-02	3.20E-03	Landtwing et al., 2005
Bingham Cu-Au-Mo porphyry	b	44.8	110000	2500	4500	70	3700	2.27E-02	4.09E-02	3.36E-02	6.36E-04	Landtwing et al., 2005
Bingham Cu-Au-Mo porphyry	b	46.6	113000	2100	3800	140	3300	1.86E-02	3.36E-02	2.92E-02	1.24E-03	Landtwing et al., 2005
Bingham Cu-Au-Mo porphyry	b		107000	1300	4000	620	4100	1.21E-02	3.74E-02	3.83E-02	5.79E-03	Landtwing et al., 2005
Bingham Cu-Au-Mo porphyry	b	44.2	123000	700	2100		2100	5.69E-03	1.71E-02	1.71E-02		Landtwing et al., 2005
Bingham Cu-Au-Mo porphyry	b	42.5	116000	600	2100		1800	5.17E-03	1.81E-02	1.55E-02	4.21E 04	Landtwing et al., 2005
Bingham Cu-Au-Mo porphyry	b	41.7	102000	400	3700	44	2900	3.92E-03	3.63E-02	2.84E-02	4.31E-04	Landtwing et al., 2005
Bingham Cu-Au-Mo porphyry	b	45.2	116000	8100	2500	150	3800	6.98E-02	2.16E-02	3.28E-02	1.29E-03	Landtwing et al., 2005
Bingham Cu-Au-Mo porphyry	b	42.1	106000	7100	3100	49	3200	6.70E-02	2.92E-02	3.02E-02	4.62E-04	Landtwing et al., 2005
Bingham Cu-Au-Mo porphyry	b	38.9	980000	6520	3100		3600	6.65E-03	3.16E-03	3.67E-03		Landtwing et al., 2005
Bingham Cu-Au-Mo porphyry	b	39.9	105000	4500	3300		2500	4.29E-02	3.14E-02	2.38E-02		Landtwing et al., 2005
Bingham Cu-Au-Mo porphyry	b	38.9	115000	3000	2200		2000	2.61E-02	1.91E-02	1.74E-02		Landtwing et al., 2005
Bingham Cu-Au-Mo porphyry	b	40.9	960000	2000	3500	21	3200	2.08E-03	3.65E-03	3.33E-03	2.19E-05	Landtwing et al., 2005
Bingham Cu-Au-Mo porphyry	b	41	112000	1450	2100	40-	2600	1.29E-02	1.88E-02	2.32E-02	0.60= -	Landtwing et al., 2005
Famatina Cu-Au porphyry / HS epithermal	b		196000	1500		190	1700	7.65E-03		8.67E-03	9.69E-04	Pudack et al., 2009
Famatina Cu-Au porphyry / HS epithermal	b		128000	880		50	1100	6.88E-03		8.59E-03	3.91E-04	Pudack et al., 2009

Famatina Cu-Au porphyry / HS epithermal	b		169000	50		40	930	2.96E-04		5.50E-03	2.37E-04	Pudack et al., 2009
Famatina Cu-Au porphyry / HS epithermal	b		110000	240		360	1200	2.18E-03		1.09E-02	3.27E-03	Pudack et al., 2009
Famatina Cu-Au porphyry / HS epithermal	b		85000	820		30	940	9.65E-03		1.11E-02	3.53E-04	Pudack et al., 2009
Famatina Cu-Au porphyry / HS epithermal	b		96000	4600			610	4.79E-02		6.35E-03		Pudack et al., 2009
Famatina Cu-Au porphyry / HS epithermal	b		97000	3000			550	3.09E-02		5.67E-03		Pudack et al., 2009
Famatina Cu-Au porphyry / HS epithermal	b		114000	3800			540	3.33E-02		4.74E-03		Pudack et al., 2009
Famatina Cu-Au porphyry / HS epithermal	v		8000	670		40	90	8.38E-02		1.13E-02	5.00E-03	Pudack et al., 2009
Famatina Cu-Au porphyry / HS epithermal	V		5000	270		6	60	5.40E-02		1.20E-02	1.20E-03	Pudack et al., 2009
Famatina Cu-Au porphyry / HS epithermal	v		4000	1100			60	2.75E-01		1.50E-02		Pudack et al., 2009
Famatina Cu-Au porphyry / HS epithermal	v		9000	580			70	6.44E-02		7.78E-03		Pudack et al., 2009
Famatina Cu-Au porphyry / HS epithermal	v		34000	3300		70	200	9.71E-02		5.88E-03	2.06E-03	Pudack et al., 2009
Famatina Cu-Au porphyry / HS epithermal	v		8000	2100		20	110	2.63E-01		1.38E-02	2.50E-03	Pudack et al., 2009
Famatina Cu-Au porphyry / HS epithermal	v		9000	5500			70	6.11E-01		7.78E-03		Pudack et al., 2009
Famatina Cu-Au porphyry / HS epithermal	v		7000	390		10	90	5.57E-02		1.29E-02	1.43E-03	Pudack et al., 2009
Famatina Cu-Au porphyry / HS epithermal	v		7000	1500			90	2.14E-01		1.29E-02		Pudack et al., 2009
Famatina Cu-Au porphyry / HS epithermal	v		5000	5400			150	1.08E+00		3.00E-02		Pudack et al., 2009
Famatina Cu-Au porphyry / HS epithermal	v		10000	1300			110	1.30E-01		1.10E-02		Pudack et al., 2009
Famatina Cu-Au porphyry / HS epithermal	v		1000	440			8	4.40E-01		8.00E-03		Pudack et al., 2009
Butte Cu-Mo porphyry	b	38	68000	5900	12000		1200	8.68E-02	1.76E-01	1.76E-02		Rusk et al., 2004
Butte Cu-Mo porphyry	b	38	110000	170	3300		1000	1.55E-03	3.00E-02	9.09E-03		Rusk et al., 2004
Butte Cu-Mo porphyry	b	38	100000		5600		1000		5.60E-02	1.00E-02		Rusk et al., 2004
Butte Cu-Mo porphyry	b	38	55000		9500				1.73E-01			Rusk et al., 2004
Butte Cu-Mo porphyry	b	38	100000	380	4700		1000	3.80E-03	4.70E-02	1.00E-02		Rusk et al., 2004
Butte Cu-Mo porphyry	b	38	110000	81	4000		860	7.36E-04	3.64E-02	7.82E-03		Rusk et al., 2004
Butte Cu-Mo porphyry	b	38	110000	1000	4300		1100	9.09E-03	3.91E-02	1.00E-02		Rusk et al., 2004
Butte Cu-Mo porphyry	b	38	91000	800	5800		810	8.79E-03	6.37E-02	8.90E-03		Rusk et al., 2004
Butte Cu-Mo porphyry	b	38	100000	1100	4500		800	1.10E-02	4.50E-02	8.00E-03		Rusk et al., 2004
Butte Cu-Mo porphyry	b	38	80000	88	6900		1300	1.10E-03	8.63E-02	1.63E-02		Rusk et al., 2004
Butte Cu-Mo porphyry	b	38	100000	140	8300		1600	1.40E-03	8.30E-02	1.60E-02		Rusk et al., 2004
Butte Cu-Mo porphyry	b	38	97000	440	12000		2000	4.54E-03	1.24E-01	2.06E-02		Rusk et al., 2004
Butte Cu-Mo porphyry	b	38	83000	150	9800		1400	1.81E-03	1.18E-01	1.69E-02		Rusk et al., 2004
Butte Cu-Mo porphyry	b	38	96000	760	15000		1700	7.92E-03	1.56E-01	1.77E-02		Rusk et al., 2004
Butte Cu-Mo porphyry	b	38	97000		7900		1300		8.14E-02	1.34E-02		Rusk et al., 2004
Butte Cu-Mo porphyry	b	38	74000		6400		840		8.65E-02	1.14E-02		Rusk et al., 2004
Butte Cu-Mo porphyry	b	38	91000	850	7100	16	1500	9.34E-03	7.80E-02	1.65E-02	1.76E-04	Rusk et al., 2004
Butte Cu-Mo porphyry	b	38	100000	2400	2800		790	2.40E-02	2.80E-02	7.90E-03		Rusk et al., 2004
Butte Cu-Mo porphyry	sc	2.7	6300	4400	130		32	6.98E-01	2.06E-02	5.08E-03		Rusk et al., 2004
Butte Cu-Mo porphyry	sc	2.7	7800	2100				2.69E-01				Rusk et al., 2004
Butte Cu-Mo porphyry	sc	2.7	6100	3800	64			6.23E-01	1.05E-02			Rusk et al., 2004
Butte Cu-Mo porphyry	sc	2.7	7800	3400	170	5	20	4.36E-01	2.18E-02	2.56E-03	6.41E-04	Rusk et al., 2004
Butte Cu-Mo porphyry	sc	2.7	5900	5600	100		8	9.49E-01	1.69E-02	1.36E-03		Rusk et al., 2004
Butte Cu-Mo porphyry	sc	2.7	6500	5600	150		24	8.62E-01	2.31E-02	3.69E-03		Rusk et al., 2004
Butte Cu-Mo porphyry	sc	2.3	5200	3800	140		10	7.31E-01	2.69E-02	1.92E-03		Rusk et al., 2004
Butte Cu-Mo porphyry	sc	3.2	6300	10100	140		35	1.60E+00	2.22E-02	5.56E-03		Rusk et al., 2004

Butte Cu-Mo porphyry	sc	2.7	4000	13400	81			3.35E+00	2.03E-02			Rusk et al., 2004
Butte Cu-Mo porphyry	sc	2.3	5100	6600	120		19	1.29E+00	2.35E-02	3.73E-03		Rusk et al., 2004
Butte Cu-Mo porphyry	sc	2.7	8900	1100	28			1.24E-01	3.15E-03			Rusk et al., 2004
Butte Cu-Mo porphyry	sc	2.7	6500	6000	100		9	9.23E-01	1.54E-02	1.38E-03		Rusk et al., 2004
Butte Cu-Mo porphyry	sc	2.7	8200	1800	160		19	2.20E-01	1.95E-02	2.32E-03		Rusk et al., 2004
Butte Cu-Mo porphyry	sc	2.7	6700	2200				3.28E-01				Rusk et al., 2004
Butte Cu-Mo porphyry	sc	2.7	8100	1500	170			1.85E-01	2.10E-02			Rusk et al., 2004
Butte Cu-Mo porphyry	sc	2.7	8600	1200	150	8	14	1.40E-01	1.74E-02	1.63E-03	9.30E-04	Rusk et al., 2004
Butte Cu-Mo porphyry	sc	2.7	6900	5000	160		22	7.25E-01	2.32E-02	3.19E-03		Rusk et al., 2004
Butte Cu-Mo porphyry	sc	2.7	6600	3600	160		17	5.45E-01	2.42E-02	2.58E-03		Rusk et al., 2004
Butte Cu-Mo porphyry	sc	2.7	7800	2300	110		22	2.95E-01	1.41E-02	2.82E-03		Rusk et al., 2004
Butte Cu-Mo porphyry	sc	2.7	7900	2200	170		23	2.78E-01	2.15E-02	2.91E-03		Rusk et al., 2004
Butte Cu-Mo porphyry	sc	2.9	10000	51	43		30	5.10E-03	4.30E-03	3.00E-03		Rusk et al., 2004
Butte Cu-Mo porphyry	sc	2.4	4300	2000	140		11	4.65E-01	3.26E-02	2.56E-03		Rusk et al., 2004
Butte Cu-Mo porphyry	sc	2.5	8800	320	100		48	3.64E-02	1.14E-02	5.45E-03		Rusk et al., 2004
Butte Cu-Mo porphyry	sc	1.9	5200	2300	100		9	4.42E-01	1.92E-02	1.73E-03		Rusk et al., 2004
Butte Cu-Mo porphyry	sc	2.7	6400	160	90		15	2.50E-02	1.41E-02	2.34E-03		Rusk et al., 2004
Butte Cu-Mo porphyry	sc	2.5	8200	130	140		58	1.59E-02	1.71E-02	7.07E-03		Rusk et al., 2004
Butte Cu-Mo porphyry	sc	2.5	8000	1000				1.25E-01				Rusk et al., 2004
Butte Cu-Mo porphyry	sc	2.5	7600	1200	100			1.58E-01	1.32E-02			Rusk et al., 2004
Butte Cu-Mo porphyry	sc	4	13000		230		76		1.77E-02	5.85E-03		Rusk et al., 2004
Butte Cu-Mo porphyry	sc	2.4	7200	940	190		93	1.31E-01	2.64E-02	1.29E-02		Rusk et al., 2004
Butte Cu-Mo porphyry	sc	3.3	9400	600	340		62	6.38E-02	3.62E-02	6.60E-03		Rusk et al., 2004
Butte Cu-Mo porphyry	sc	3.3	5700	12000	200		50	2.11E+00	3.51E-02	8.77E-03		Rusk et al., 2004
Butte Cu-Mo porphyry	sc	3.4	7000	9900	140			1.41E+00	2.00E-02			Rusk et al., 2004
Butte Cu-Mo porphyry	sc	3.2	5800	10000	460	37	63	1.72E+00	7.93E-02	1.09E-02	6.38E-03	Rusk et al., 2004
Butte Cu-Mo porphyry	sc	3.3	9100	3100	560	38	83	3.41E-01	6.15E-02	9.12E-03	4.18E-03	Rusk et al., 2004
Butte Cu-Mo porphyry	sc	3.3	8700	2200	390		48	2.53E-01	4.48E-02	5.52E-03		Rusk et al., 2004
Butte Cu-Mo porphyry	sc	3.3	7900	5000	300	343	66	6.33E-01	3.80E-02	8.35E-03	4.34E-02	Rusk et al., 2004
Butte Cu-Mo porphyry	sc	3.3	6100	7300	240		42	1.20E+00	3.93E-02	6.89E-03		Rusk et al., 2004
Butte Cu-Mo porphyry	sc	3.3	10000	360			61	3.60E-02		6.10E-03		Rusk et al., 2004
Butte Cu-Mo porphyry	sc	3.3	6000	12000			77	2.00E+00		1.28E-02		Rusk et al., 2004
Butte Cu-Mo porphyry	sc	3.3	9800		60		26		6.12E-03	2.65E-03		Rusk et al., 2004
Butte Cu-Mo porphyry	sc	3.3	8100	4300	290		46	5.31E-01	3.58E-02	5.68E-03		Rusk et al., 2004
Butte Cu-Mo porphyry	sc	3.3	8600	1800	690		63	2.09E-01	8.02E-02	7.33E-03		Rusk et al., 2004
Butte Cu-Mo porphyry	sc	3.3	8600	4400	110		52	5.12E-01	1.28E-02	6.05E-03		Rusk et al., 2004
Butte Cu-Mo porphyry	sc	3.3	8100	5200			59	6.42E-01		7.28E-03		Rusk et al., 2004
Butte Cu-Mo porphyry	sc	3.3	7100	11000	70		35	1.55E+00	9.86E-03	4.93E-03		Rusk et al., 2004
Butte Cu-Mo porphyry	sc	3.3	8300	7900				9.52E-01				Rusk et al., 2004
Butte Cu-Mo porphyry	sc	3.3	8500	3400	1500		35	4.00E-01	1.76E-01	4.12E-03		Rusk et al., 2004
Butte Cu-Mo porphyry	sc	3.3	9700	330	470		100	3.40E-02	4.85E-02	1.03E-02		Rusk et al., 2004
Butte Cu-Mo porphyry	sc	3.3	10000				54			5.40E-03		Rusk et al., 2004
Butte Cu-Mo porphyry	sc	3.3	6500	11000	210		52	1.69E+00	3.23E-02	8.00E-03		Rusk et al., 2004
Butte Cu-Mo porphyry	sc	3.3	9600	890	300		88	9.27E-02	3.13E-02	9.17E-03		Rusk et al., 2004

Butte Cu-Mo porphyry	sc	3.3	6900	10000	210		44	1.45E+00	3.04E-02	6.38E-03		Rusk et al., 2004
Butte Cu-Mo porphyry	sc	3.3	8600	1300	640		81	1.51E-01	7.44E-02	9.42E-03		Rusk et al., 2004
Butte Cu-Mo porphyry	sc	3.7	8900	4600	040		40	5.17E-01	7.77L-02	4.49E-03		Rusk et al., 2004
Butte Cu-Mo porphyry	sc	4.6	6200	18000	1600		75	2.90E+00	2.58E-01	1.21E-02		Rusk et al., 2004
Butte Cu-Mo porphyry	sc	4.1	7200	12000	300		23	1.67E+00	4.17E-02	3.19E-03		Rusk et al., 2004
Butte Cu-Mo porphyry	sc	4.1	7700	13000	300	42	61	1.69E+00	4.17E-02	7.92E-03	5.45E-03	Rusk et al., 2004
Butte Cu-Mo porphyry		4.1	10000	5500		42	01	5.50E-01		7.92E-03	J.43L-03	Rusk et al., 2004
Butte Cu-Mo porphyry	sc sc	4.1	7100	15000	210			2.11E+00	2.96E-02			Rusk et al., 2004
Butte Cu-Mo porphyry		4.1	9900	7200	200		100	7.27E-01	2.90E-02 2.02E-02	1.01E-02		
Butte Cu-Mo porphyry	sc	4.1	12000	2100	200		100	1.75E-01	2.02E-02	1.01E-02		Rusk et al., 2004
Butte Cu-Mo porphyry	sc	4.1	9500	8100	330		68	8.53E-01	3.47E-02	7.16E-03		Rusk et al., 2004
	sc						59					Rusk et al., 2004
Butte Cu-Mo porphyry	sc	4.1	4500	18000	350 270			4.00E+00	7.78E-02	1.31E-02		Rusk et al., 2004
Butte Cu-Mo porphyry	sc	4.1	6400	14000			56	2.19E+00	4.22E-02	8.75E-03		Rusk et al., 2004
Butte Cu-Mo porphyry	sc	4.1	7900	8000	1100		1.420	1.01E+00	1.39E-01	1.025.02		Rusk et al., 2004
Bajo de la Alumbrera Cu-Au porphyry	b		78000	6500			1420	8.33E-02	0.00E+00	1.82E-02		Seo et al., 2009
Bajo de la Alumbrera Cu-Au porphyry	v		24000	1800		450	210	7.50E-02	0.00E+00	8.75E-03	4.645.02	Seo et al., 2009
Bingham Cu-Au-Mo porphyry	b		97000	7600		450	2800	7.84E-02	0.00E+00	2.89E-02	4.64E-03	Seo et al., 2009
Bingham Cu-Au-Mo porphyry	b		129000	18900		33	3000	1.47E-01	0.00E+00	2.33E-02	2.56E-04	Seo et al., 2009
Bingham Cu-Au-Mo porphyry	b		117000	1190		88	3800	1.02E-02	0.00E+00	3.25E-02	7.52E-04	Seo et al., 2009
Bingham Cu-Au-Mo porphyry	V		16800	4200		51	390	2.50E-01	0.00E+00	2.32E-02	3.04E-03	Seo et al., 2009
Bingham Cu-Au-Mo porphyry	V		23000	10800		18.3	440	4.70E-01	0.00E+00	1.91E-02	7.96E-04	Seo et al., 2009
Bingham Cu-Au-Mo porphyry	V		22000	300		21	540	1.36E-02	0.00E+00	2.45E-02	9.55E-04	Seo et al., 2009
Bajo de la alumbrera Cu-Au porphyry	b		160000	7600	14000	70	4500	4.75E-02	8.75E-02	2.81E-02	4.38E-04	Ulrich et al., 1999
Bajo de la alumbrera Cu-Au porphyry	v		17000	33000	1200		200	1.94E+00	7.06E-02	1.18E-02		Ulrich et al., 1999
Bajo de la alumbrera Cu-Au porphyry	b	46.5	106000	100	6000	140	1700	9.43E-04	5.66E-02	1.60E-02	1.32E-03	Ulrich et al., 2002
Bajo de la alumbrera Cu-Au porphyry	b	37.9	50000	300	6000		1800	6.00E-03	1.20E-01	3.60E-02		Ulrich et al., 2002
Bajo de la alumbrera Cu-Au porphyry	b	53.3	92000	200				2.17E-03				Ulrich et al., 2002
Bajo de la alumbrera Cu-Au porphyry	b	36.9	105000	100	6000	30	2000	9.52E-04	5.71E-02	1.90E-02	2.86E-04	Ulrich et al., 2002
Bajo de la alumbrera Cu-Au porphyry	b	58.5	219000	1700				7.76E-03				Ulrich et al., 2002
Bajo de la alumbrera Cu-Au porphyry	b	58.3	105000	10000	18300	220	4400	9.52E-02	1.74E-01	4.19E-02	2.10E-03	Ulrich et al., 2002
Bajo de la alumbrera Cu-Au porphyry	b	61.9	243000	3700				1.52E-02				Ulrich et al., 2002
Bajo de la alumbrera Cu-Au porphyry	b	63.8	252000	2300	20			9.13E-03	7.94E-05			Ulrich et al., 2002
Bajo de la alumbrera Cu-Au porphyry	b	63.8	124000	4800	7400	70	3300	3.87E-02	5.97E-02	2.66E-02	5.65E-04	Ulrich et al., 2002
Bajo de la alumbrera Cu-Au porphyry	b	65.5	100000	500	8900		2800	5.00E-03	8.90E-02	2.80E-02		Ulrich et al., 2002
Bajo de la alumbrera Cu-Au porphyry	b	71.1	107000	1200	12000	120	3600	1.12E-02	1.12E-01	3.36E-02	1.12E-03	Ulrich et al., 2002
Bajo de la alumbrera Cu-Au porphyry	b	52.7	123000	2200	4600		1600	1.79E-02	3.74E-02	1.30E-02		Ulrich et al., 2002
Bajo de la alumbrera Cu-Au porphyry	b	61.4	81000	3200	9500	40	2600	3.95E-02	1.17E-01	3.21E-02	4.94E-04	Ulrich et al., 2002
Bajo de la alumbrera Cu-Au porphyry	b	45.1	65000	3200	6000	80	1500	4.92E-02	9.23E-02	2.31E-02	1.23E-03	Ulrich et al., 2002
Bajo de la alumbrera Cu-Au porphyry	b	51.9	198000	1000				5.05E-03				Ulrich et al., 2002
Bajo de la alumbrera Cu-Au porphyry	b	49.9	80000	5500	9900	90	2400	6.88E-02	1.24E-01	3.00E-02	1.13E-03	Ulrich et al., 2002
Bajo de la alumbrera Cu-Au porphyry	b	48.3	110000	2600	5400	130	1700	2.36E-02	4.91E-02	1.55E-02	1.18E-03	Ulrich et al., 2002
Bajo de la alumbrera Cu-Au porphyry	b	44.0	104000	2000	9000	60	2000	1.92E-02	8.65E-02	1.92E-02	5.77E-04	Ulrich et al., 2002
Bajo de la alumbrera Cu-Au porphyry	b	44.0	100000	5200	5700	50	1800	5.20E-02	5.70E-02	1.80E-02	5.00E-04	Ulrich et al., 2002
Bajo de la alumbrera Cu-Au porphyry	b	42.1	97000	700	5000		1200	7.22E-03	5.15E-02	1.24E-02		Ulrich et al., 2002

Bajo de la alumbrera Cu-Au porphyry	b	41.4	100000	500	1200	1500	5.00E-03	1.20E-02	1.50E-02	Ulrich et al., 2002
Bajo de la alumbrera Cu-Au porphyry	b	17.6	33000		1000	200		3.03E-02	6.06E-03	Ulrich et al., 2002
Bajo de la alumbrera Cu-Au porphyry	b	7.1	20000	300	1300	1600	1.50E-02	6.50E-02	8.00E-02	Ulrich et al., 2002
Bajo de la alumbrera Cu-Au porphyry	b	3.0	9500	100	200	90	1.05E-02	2.11E-02	9.47E-03	Ulrich et al., 2002
Bajo de la alumbrera Cu-Au porphyry	b	1.4	4700		300	110		6.38E-02	2.34E-02	Ulrich et al., 2002
Bajo de la alumbrera Cu-Au porphyry	v		11000	500			4.55E-02			Ulrich et al., 2002
Bajo de la alumbrera Cu-Au porphyry	v		3000	1100	200	70	3.67E-01	6.67E-02	2.33E-02	Ulrich et al., 2002
Bajo de la alumbrera Cu-Au porphyry	v		7000	900	700	200	1.29E-01	1.00E-01	2.86E-02	Ulrich et al., 2002
Bajo de la alumbrera Cu-Au porphyry	v		11000	1200	400	140	1.09E-01	3.64E-02	1.27E-02	Ulrich et al., 2002
Bajo de la alumbrera Cu-Au porphyry	v		3000	300	100	30	1.00E-01	3.33E-02	1.00E-02	Ulrich et al., 2002
Bajo de la alumbrera Cu-Au porphyry	v		6000	3000	300	100	5.00E-01	5.00E-02	1.67E-02	Ulrich et al., 2002
Bajo de la alumbrera Cu-Au porphyry	v	3.6	14000	6000	800	170	4.29E-01	5.71E-02	1.21E-02	Ulrich et al., 2002
Bajo de la alumbrera Cu-Au porphyry	v	3.4	9800	2500	1000	250	2.55E-01	1.02E-01	2.55E-02	Ulrich et al., 2002
Bajo de la alumbrera Cu-Au porphyry	v	9.5	30000	30000	6800	620	1.00E+00	2.27E-01	2.07E-02	Ulrich et al., 2002
Bajo de la alumbrera Cu-Au porphyry	v	3.5	13000	29000	1000	40	2.23E+00	7.69E-02	3.08E-03	Ulrich et al., 2002
Bajo de la alumbrera Cu-Au porphyry	v	5.7	21000	26000	1300	180	1.24E+00	6.19E-02	8.57E-03	Ulrich et al., 2002
Bajo de la alumbrera Cu-Au porphyry	v	5.3	17000	33000	1200	230	1.94E+00	7.06E-02	1.35E-02	Ulrich et al., 2002
Bajo de la alumbrera Cu-Au porphyry	v	1.7	7900	5200			6.58E-01			Ulrich et al., 2002
Bajo de la alumbrera Cu-Au porphyry	v	1.3	3900	1800			4.62E-01			Ulrich et al., 2002
Bajo de la alumbrera Cu-Au porphyry	v	1	3900	500			1.28E-01			Ulrich et al., 2002
Bajo de la alumbrera Cu-Au porphyry	v	1	3900	1700			4.36E-01			Ulrich et al., 2002

^{&#}x27;Type' refers to 'fluid inclusion type': symbol 'sc' stands for 'supercritical', 'b' for 'brine' and 'v' for 'vapor'. All element concentrations are in ppm.

Appendix 2. Concentration of selected elements in volcanic gas condensates

Volcano	T (°C)	Na	K	Cu	Zn	Pb	Мо	Ref
Augustine	390	8.0				7.2	3.1	Symonds et al, 1990
Augustine	431	0.6				1.2	1.5	Symonds et al, 1990
Augustine	433	0.5				0.36	0.64	Symonds et al, 1990
Augustine	500	0.2				0.12	1.1	Symonds et al, 1990
Augustine	625	0.6				2.1	2.6	Symonds et al, 1990
Augustine	631	6.6	8			9.1	0.5	Symonds et al, 1990
Augustine	635	1.6	1			0.72	1.6	Symonds et al, 1990
Augustine	642	0.4				0.15	0.86	Symonds et al, 1990
Augustine	870	21	22			3.1	1.1	Symonds et al, 1990
Augustine	870	22	22			3.3	1.1	Symonds et al, 1990
Cerro Negro	170	3.5	3.4	0.3	0.7		0.18	Gemmell, 1987
Cerro Negro	250	1.9	1.7	0.3	0.5		0.28	Gemmell, 1987
Cerro Negro	260	1.5	1.3	0.2	0.8		0.29	Gemmell, 1987
Cerro Negro	272	1	1.5	0.2	0.4		0.2	Gemmell, 1987
Cerro Negro	274	3.5	3.2	0.4	0.3	0.4	0.26	Gemmell, 1987
Cerro Negro	300	4.4	1.5	0.8	1.6	0.1	0.19	Gemmell, 1987
Cerro Negro	315	1.1	1.4	0.2	0.4		0.2	Gemmell, 1987
Cerro Negro	216	53	5	V. <u>L</u>	₩.¬		V. <u>L</u>	Stoiber & Rose, 1970
Cerro Negro	275	48	50					Stoiber & Rose, 1970
Cerro Negro	343	18	8					Stoiber & Rose, 1970
Cerro Negro	427	3	3					Stoiber & Rose, 1970
Cerro Negro	570	6	8					Stoiber & Rose, 1970
Cerro Negro	610	16	7					Stoiber & Rose, 1970 Stoiber & Rose, 1970
Ū	740	34	43					,
Cerro Negro				0.07	4.07	0.40	0.007	Stoiber & Rose, 1970
Colima	738	29	17	0.87	4.97	0.48	0.097	Taran et al., 2001
Colima	742	36	22	0.931	5.3	0.451	0.091	Taran et al., 2001
Colima	828	24	26	0.44	8.14	0.078	0.182	Taran et al., 2001
Kawa Ijen	350	320	45	13.6	5.2	0.23	0.06	Van Hinsberg, unpublished data
Kawa Ijen	350	464	60	21.9	11.8	0.8	0.47	Van Hinsberg, unpublished data
Kawa Ijen	350	199	10	11.3	5.3	0.31	0.23	Van Hinsberg, unpublished data
Kudryavy	535	2.4	15.5	0.76	0.25	6.4	0.002	Taran et al., 1995
Kudryavy	585	23	12.8	0.032	0.58	1.84	0.004	Taran et al., 1995
						^ 7	0.46	
Kudryavy	605	2.6	20.5	0.91	13.5	9.7	0.16	Taran et al., 1995
Kudryavy Kudryavy			20.5 9.53	0.91	13.5 1	9.7 0.11	0.16	Taran et al., 1995 Taran et al., 1995
, ,	605	2.6	9.53 28.7				0.11 0.27	·
Kudryavy	605 825 870 940	2.6 5	9.53	0.09 0.13 0.27	1 1 3.1	0.11	0.11	Taran et al., 1995
Kudryavy Kudryavy	605 825 870	2.6 5 41	9.53 28.7	0.09 0.13	1 1	0.11 0.58	0.11 0.27	Taran et al., 1995 Taran et al., 1995
Kudryavy Kudryavy Kudryavy	605 825 870 940	2.6 5 41	9.53 28.7	0.09 0.13 0.27	1 1 3.1	0.11 0.58 1.25	0.11 0.27 0.2	Taran et al., 1995 Taran et al., 1995 Taran et al., 1995
Kudryavy Kudryavy Kudryavy Kudryavy	605 825 870 940 160	2.6 5 41	9.53 28.7	0.09 0.13 0.27 0.034	1 1 3.1 0.33	0.11 0.58 1.25 0.0138	0.11 0.27 0.2 0.00113	Taran et al., 1995 Taran et al., 1995 Taran et al., 1995 Wahrenberger et al., 2002
Kudryavy Kudryavy Kudryavy Kudryavy Kudryavy	605 825 870 940 160 300	2.6 5 41	9.53 28.7	0.09 0.13 0.27 0.034 0.0311	1 1 3.1 0.33 0.13	0.11 0.58 1.25 0.0138 0.109	0.11 0.27 0.2 0.00113 0.00056	Taran et al., 1995 Taran et al., 1995 Taran et al., 1995 Wahrenberger et al., 2002 Wahrenberger et al., 2002
Kudryavy Kudryavy Kudryavy Kudryavy Kudryavy Kudryavy	605 825 870 940 160 300 470	2.6 5 41 6.1	9.53 28.7	0.09 0.13 0.27 0.034 0.0311 0.0116	1 1 3.1 0.33 0.13 0.12	0.11 0.58 1.25 0.0138 0.109 0.561	0.11 0.27 0.2 0.00113 0.00056 0.00304	Taran et al., 1995 Taran et al., 1995 Taran et al., 1995 Wahrenberger et al., 2002 Wahrenberger et al., 2002 Wahrenberger et al., 2002
Kudryavy Kudryavy Kudryavy Kudryavy Kudryavy Kudryavy Kudryavy	605 825 870 940 160 300 470 680	2.6 5 41 6.1	9.53 28.7	0.09 0.13 0.27 0.034 0.0311 0.0116 0.0205	1 3.1 0.33 0.13 0.12 0.5	0.11 0.58 1.25 0.0138 0.109 0.561 0.47	0.11 0.27 0.2 0.00113 0.00056 0.00304 0.0107	Taran et al., 1995 Taran et al., 1995 Taran et al., 1995 Wahrenberger et al., 2002 Wahrenberger et al., 2002 Wahrenberger et al., 2002 Wahrenberger et al., 2002
Kudryavy Kudryavy Kudryavy Kudryavy Kudryavy Kudryavy Kudryavy Kudryavy	605 825 870 940 160 300 470 680 710	2.6 5 41 6.1	9.53 28.7 5.62	0.09 0.13 0.27 0.034 0.0311 0.0116 0.0205 0.0333	1 3.1 0.33 0.13 0.12 0.5 0.64	0.11 0.58 1.25 0.0138 0.109 0.561 0.47 0.668	0.11 0.27 0.2 0.00113 0.00056 0.00304 0.0107 0.127	Taran et al., 1995 Taran et al., 1995 Taran et al., 1995 Wahrenberger et al., 2002
Kudryavy Kudryavy Kudryavy Kudryavy Kudryavy Kudryavy Kudryavy Kudryavy Kudryavy	605 825 870 940 160 300 470 680 710 920	2.6 5 41 6.1 3 1.1	9.53 28.7 5.62	0.09 0.13 0.27 0.034 0.0311 0.0116 0.0205 0.0333 0.0544	1 1 3.1 0.33 0.13 0.12 0.5 0.64 1.28	0.11 0.58 1.25 0.0138 0.109 0.561 0.47 0.668 0.791	0.11 0.27 0.2 0.00113 0.00056 0.00304 0.0107 0.127 0.204	Taran et al., 1995 Taran et al., 1995 Taran et al., 1995 Wahrenberger et al., 2002
Kudryavy Merapi	605 825 870 940 160 300 470 680 710 920	2.6 5 41 6.1 3 1.1 13 0.6	9.53 28.7 5.62 13.2 1.13	0.09 0.13 0.27 0.034 0.0311 0.0116 0.0205 0.0333 0.0544	1 1 3.1 0.33 0.13 0.12 0.5 0.64 1.28	0.11 0.58 1.25 0.0138 0.109 0.561 0.47 0.668 0.791	0.11 0.27 0.2 0.00113 0.00056 0.00304 0.0107 0.127 0.204	Taran et al., 1995 Taran et al., 1995 Taran et al., 1995 Wahrenberger et al., 2002 this study
Kudryavy Kudryavy Kudryavy Kudryavy Kudryavy Kudryavy Kudryavy Kudryavy Kudryavy Merapi Merapi	605 825 870 940 160 300 470 680 710 920 266 417	2.6 5 41 6.1 3 1.1 13 0.6 1.2	9.53 28.7 5.62 13.2 1.13 0.63	0.09 0.13 0.27 0.034 0.0311 0.0116 0.0205 0.0333 0.0544 0.00 0.28	1 1 3.1 0.33 0.13 0.12 0.5 0.64 1.28 0.06 0.15	0.11 0.58 1.25 0.0138 0.109 0.561 0.47 0.668 0.791 0.07	0.11 0.27 0.2 0.00113 0.00056 0.00304 0.0107 0.127 0.204	Taran et al., 1995 Taran et al., 1995 Taran et al., 1995 Wahrenberger et al., 2002 this study this study
Kudryavy Kudryavy Kudryavy Kudryavy Kudryavy Kudryavy Kudryavy Kudryavy Merapi Merapi Merapi Merapi	605 825 870 940 160 300 470 680 710 920 266 417 515	2.6 5 41 6.1 3 1.1 13 0.6 1.2 2.3 1.2	9.53 28.7 5.62 13.2 1.13 0.63 2.27	0.09 0.13 0.27 0.034 0.0311 0.0116 0.0205 0.0333 0.0544 0.00 0.28 0.16 0.01	1 1 3.1 0.33 0.13 0.12 0.5 0.64 1.28 0.06 0.15 0.42	0.11 0.58 1.25 0.0138 0.109 0.561 0.47 0.668 0.791 0.07 8.01 8.53 0.36	0.11 0.27 0.2 0.00113 0.00056 0.00304 0.0107 0.127 0.204 0.0006	Taran et al., 1995 Taran et al., 1995 Taran et al., 1995 Wahrenberger et al., 2002 this study this study this study
Kudryavy Kudryavy Kudryavy Kudryavy Kudryavy Kudryavy Kudryavy Kudryavy Merapi Merapi Merapi Merapi Merapi	605 825 870 940 160 300 470 680 710 920 266 417 515 515	2.6 5 41 6.1 3 1.1 13 0.6 1.2 2.3 1.2 2.1	9.53 28.7 5.62 13.2 1.13 0.63 2.27 0.65 2.83	0.09 0.13 0.27 0.034 0.0311 0.0116 0.0205 0.0333 0.0544 0.00 0.28 0.16	1 1 3.1 0.33 0.13 0.12 0.5 0.64 1.28 0.06 0.15 0.42 0.1 0.17	0.11 0.58 1.25 0.0138 0.109 0.561 0.47 0.668 0.791 0.07 8.01 8.53 0.36 0.03	0.11 0.27 0.2 0.00113 0.00056 0.00304 0.0107 0.127 0.204 0.0006 0.477 0.783	Taran et al., 1995 Taran et al., 1995 Taran et al., 1995 Wahrenberger et al., 2002 this study this study this study this study this study
Kudryavy Kudryavy Kudryavy Kudryavy Kudryavy Kudryavy Kudryavy Kudryavy Merapi Merapi Merapi Merapi Merapi Merapi Merapi Merapi	605 825 870 940 160 300 470 680 710 920 266 417 515 515 526 572	2.6 5 41 6.1 3 1.1 13 0.6 1.2 2.3 1.2 2.1 3.4	9.53 28.7 5.62 13.2 1.13 0.63 2.27 0.65 2.83 2.3	0.09 0.13 0.27 0.034 0.0311 0.0116 0.0205 0.0333 0.0544 0.00 0.28 0.16 0.01 0.01	1 1 3.1 0.33 0.13 0.12 0.5 0.64 1.28 0.06 0.15 0.42 0.1 0.17 0.15	0.11 0.58 1.25 0.0138 0.109 0.561 0.47 0.668 0.791 0.07 8.01 8.53 0.36 0.03 1.41	0.11 0.27 0.2 0.00113 0.00056 0.00304 0.0107 0.127 0.204 0.0006 0.477 0.783 0.02	Taran et al., 1995 Taran et al., 1995 Taran et al., 1995 Wahrenberger et al., 2002 this study this study this study this study this study this study
Kudryavy Kudryavy Kudryavy Kudryavy Kudryavy Kudryavy Kudryavy Kudryavy Merapi	605 825 870 940 160 300 470 680 710 920 266 417 515 515 526 572 588	2.6 5 41 6.1 3 1.1 13 0.6 1.2 2.3 1.2 2.1 3.4 2	9.53 28.7 5.62 13.2 1.13 0.63 2.27 0.65 2.83 2.3 1.21	0.09 0.13 0.27 0.034 0.0311 0.0116 0.0205 0.0333 0.0544 0.00 0.28 0.16 0.01 0.01	1 1 3.1 0.33 0.13 0.12 0.5 0.64 1.28 0.06 0.15 0.42 0.1 0.17 0.15 0.15	0.11 0.58 1.25 0.0138 0.109 0.561 0.47 0.668 0.791 0.07 8.01 8.53 0.36 0.03 1.41 0.44	0.11 0.27 0.2 0.00113 0.00056 0.00304 0.0107 0.127 0.204 0.0006 0.477 0.783 0.02 0.346	Taran et al., 1995 Taran et al., 1995 Taran et al., 1995 Wahrenberger et al., 2002 this study
Kudryavy Kudryavy Kudryavy Kudryavy Kudryavy Kudryavy Kudryavy Kudryavy Merapi	605 825 870 940 160 300 470 680 710 920 266 417 515 515 526 572 588 593	2.6 5 41 6.1 3 1.1 13 0.6 1.2 2.3 1.2 2.1 3.4 2	9.53 28.7 5.62 13.2 1.13 0.63 2.27 0.65 2.83 2.3 1.21 2.99	0.09 0.13 0.27 0.034 0.0311 0.0116 0.0205 0.0333 0.0544 0.00 0.28 0.16 0.01 0.01 0.01	1 1 3.1 0.33 0.13 0.12 0.5 0.64 1.28 0.06 0.15 0.42 0.1 0.17 0.15 0.15 0.55 0.55	0.11 0.58 1.25 0.0138 0.109 0.561 0.47 0.668 0.791 0.07 8.01 8.53 0.36 0.03 1.41 0.44 0.07	0.11 0.27 0.2 0.00113 0.00056 0.00304 0.0107 0.127 0.204 0.0006 0.477 0.783 0.02 0.346 0.256	Taran et al., 1995 Taran et al., 1995 Taran et al., 1995 Wahrenberger et al., 2002 this study
Kudryavy Kudryavy Kudryavy Kudryavy Kudryavy Kudryavy Kudryavy Kudryavy Merapi	605 825 870 940 160 300 470 680 710 920 266 417 515 515 526 572 588	2.6 5 41 6.1 3 1.1 13 0.6 1.2 2.3 1.2 2.1 3.4 2	9.53 28.7 5.62 13.2 1.13 0.63 2.27 0.65 2.83 2.3 1.21	0.09 0.13 0.27 0.034 0.0311 0.0116 0.0205 0.0333 0.0544 0.00 0.28 0.16 0.01 0.01	1 1 3.1 0.33 0.13 0.12 0.5 0.64 1.28 0.06 0.15 0.42 0.1 0.17 0.15 0.15	0.11 0.58 1.25 0.0138 0.109 0.561 0.47 0.668 0.791 0.07 8.01 8.53 0.36 0.03 1.41 0.44	0.11 0.27 0.2 0.00113 0.00056 0.00304 0.0107 0.127 0.204 0.0006 0.477 0.783 0.02 0.346	Taran et al., 1995 Taran et al., 1995 Taran et al., 1995 Wahrenberger et al., 2002 this study

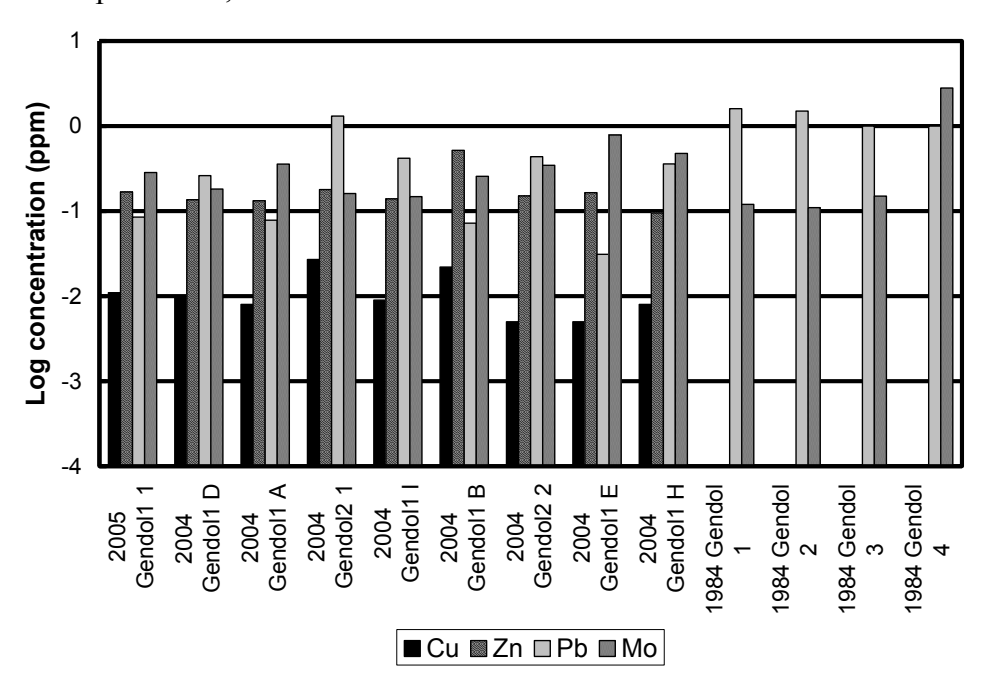
Merapi	705	1.1	0.44		0.13	80.0	0.357	this study
Merapi	754	0.7	0.31	0.01	0.14	0.26	0.182	this study
Merapi			6.2			0.83	0.08	Symonds et al., 1987
Merapi			2.6			0.32	0.16	Symonds et al., 1987
Merapi			2.9			0.35	0.18	Symonds et al., 1987
Merapi			20			1.6	0.12	Symonds et al., 1987
Merapi			6.8			1.5	0.11	Symonds et al., 1987
Merapi			9.6			1	0.15	Symonds et al., 1987
Merapi			14			1	2.8	Symonds et al., 1987
Momotombo	456	11	3.6	0.4	1.5	2.5		Gemmell, 1987
Momotombo	471	11	5.7	0.3	0.7	7	0.49	Gemmell, 1987
Momotombo	485	7.7	5.1	0.3	0.4	2	0.48	Gemmell, 1987
Momotombo	500	3.5	1.8	0.2	1.3	- 0	0.15	Gemmell, 1987
Momotombo	536	3.6	4.8	0.2	0.9	5.2	0.45	Gemmell, 1987
Momotombo	666 765	7.1	11	0.2	0.7	1.9	0.5	Gemmell, 1987
Momotombo	765 770	2.7	25	0.2 8.4	1.9	2.5		Gemmell, 1987
Momotombo Momotombo	770 790	19	41	0.4	7.6	5.1		Gemmell, 1987 Menyailov et al, 1986
Mutnovsky	410	4.6	1.6	0.003	0.06	0.025	0.001	Zelenski et al., 2005
Mutnovsky	450	4.0 8	1.6	0.003	0.00	0.025	0.001	Zelenski et al., 2005 Zelenski et al., 2005
Mutnovsky	480	18	2.2	0.008	0.07	0.04	0.005	Zelenski et al., 2005 Zelenski et al., 2005
Mutnovsky	507	2.3	1.5	0.008	0.03	0.14	0.005	Zelenski et al., 2005 Zelenski et al., 2005
New	301	2.0	1.0	0.020	0.10	0.10	0.000	ZCICHSKI Ct al., 2000
Tolbachik New	980	420	182	2.17	15.6	1.58		Menyailov & Nikitina, 1980
Tolbachik	1020	700	241	14	9.26	0.3		Menyailov & Nikitina, 1980
New Tolbachik New	1010	200	165	5.9	9.61	0.57		Menyailov & Nikitina, 1980
Tolbachik	950	29	10.2	3.5	0.38	0.04		Menyailov & Nikitina, 1980
Poas	344	13	4.8	0.2	8.6	0.8		Gemmell, 1987
Poas	561	3.4	4.1	0.2	4.4	1.1		Gemmell, 1987
Poas	711	1.6	4.4	0.2	0.5	1.1		Gemmell, 1987
Poas	724	5.4	13	0.1	1	3.7		Gemmell, 1987
Poas	819	9.2	17	0.6	3.3	3.7		Gemmell, 1987
Poas	830	6	11	0.2	4.6	4.2		Gemmell, 1987
Poas	851	29	79		6.9	3.4		Gemmell, 1987
Poas	852	7.1	14	0.3	1.3	5.4		Gemmell, 1987
Satsuma Iwojima Satsuma	102	2.8	0.2	0.003	0.03	0.014		Hedenquist (appendix), 1994
Iwojima Satsuma	105	6.9	1	0.02	0.06	0.038	0.01	Hedenquist (appendix), 1994
Iwojima Satsuma	165	8.3	1.5	0.013	0.01		0.005	Hedenquist (appendix), 1994
Iwojima	330	8.7	1.1	0.006	0.03	0.24		Hedenquist (appendix), 1994
Satsuma Iwojima	505	6.1	1.2	0.064	0.06	1.27	0.03	Hedenquist (appendix), 1994
Satsuma Iwojima Satsuma	705	15	4.8	0.036	0.24	1.77	0.16	Hedenquist (appendix), 1994
Iwojima Satsuma	877	12	2.1	0.03	0.15	1.04	0.43	Hedenquist (appendix), 1994
lwojima	877	6.3	1.3	0.009	0.17	1.43	1.07	Hedenquist (appendix), 1994
showa								
shinzan showa	750			0.005	0.6			Mizutani, 1970
shinzan showa	759			0.018	2			Mizutani, 1970
shinzan showa	722	3		0.007	0.49			Symonds et al., 1996
shinzan	830	130	9	0.02	0.32	0.065	0.046	Symonds et al., 1996

showa								
shinzan	336	6	2	0.034	0.58	0.23	0.61	Symonds et al., 1996
showa								, , , , , , , , , , , , , , , , , , , ,
shinzan	560	3		0.11	0.63	0.023		Symonds et al., 1996
showa								·
shinzan	588			0.006	0.25			Symonds et al., 1996
showa								
shinzan	600			0.002	0.11			Symonds et al., 1996
showa		_						
shinzan	635	9		0.004	2.9	0.065		Symonds et al., 1996
showa	007	2		0.004	4.0	0.05	0.005	Compande et al. 1000
shinzan showa	637	3		0.081	1.8	0.05	0.035	Symonds et al., 1996
shinzan	661	3		0.015	0.52			Symonds et al., 1996
showa	001	0		0.015	0.52			Cymonus et al., 1000
shinzan	662	7	3	0.003	0.41	0.029		Symonds et al., 1996
showa		-	-					
shinzan	194				0.14			Mizutani, 1970
showa								
shinzan	222				0.12			Mizutani, 1970
showa								
shinzan	300				0.28			Mizutani, 1970
showa	000				0.07			Minutes: 4070
shinzan	328				0.27			Mizutani, 1970
showa shinzan	430			0.009	1.2			Mizutani, 1970
showa	430			0.003	1.2			Mizatani, 1970
shinzan	460			0.011	1.6			Mizutani, 1970
showa				0.0				
shinzan	464				0.12			Mizutani, 1970
showa								·
shinzan	470			0.012	1.5			Mizutani, 1970
showa								
shinzan	645				1			Mizutani, 1970
showa	004			0.040	4.0			N
shinzan	661			0.019	1.3			Mizutani, 1970
showa shinzan	700			0.007	0.55			Mizutani, 1970
showa	700			0.007	0.55			wizutarii, 1970
shinzan	220	13	1.7	0.004	0.02	0.005		Oana, 1962
showa		.0		0.00-	0.02	0.000		33.13, 1002
shinzan	525	23	11.2	0.035	0.4	0.03		Oana, 1962
showa		-	_		-			,
shinzan	760	23	15.9	0.035	0.55	0.035		Oana, 1962

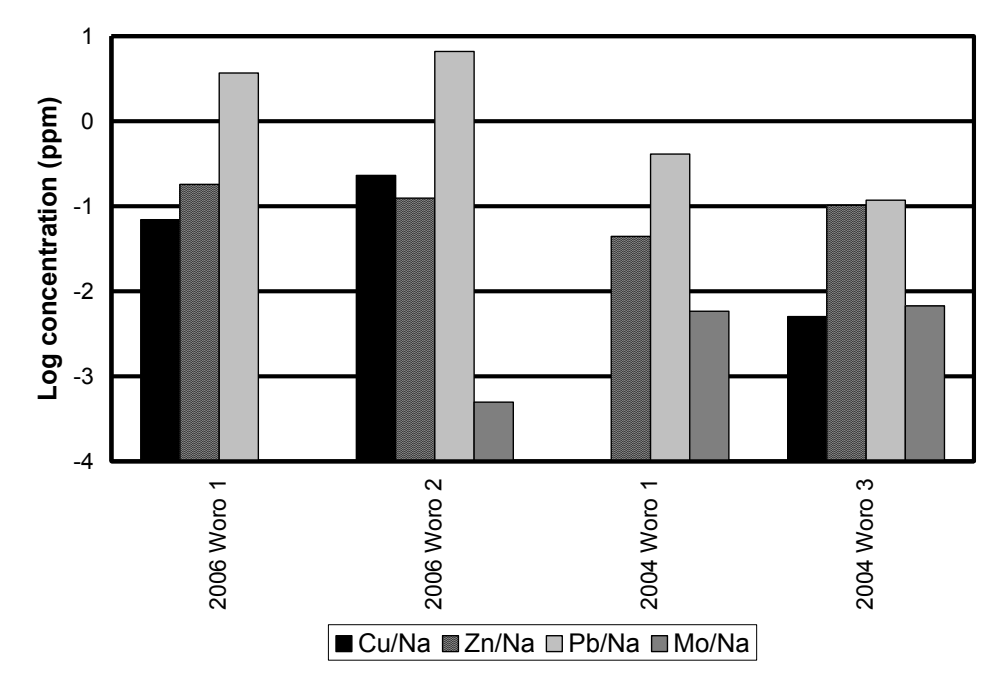
all data are in ppm except otherwise noted.

Appendix 3. Concentration of Cu, Zn, Pb and Mo and their ratios to Na and K at Gendol and Woro fields, Merapi, in 1984, 2004, 2005 and 2006.

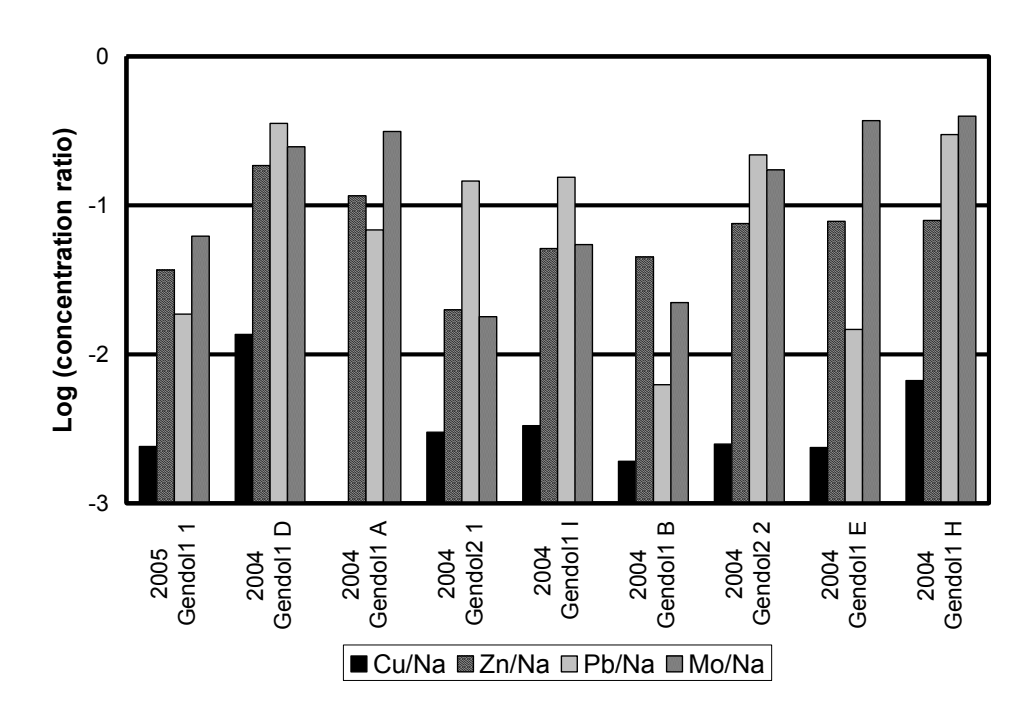
a) Concentrations of Cu, Zn, Pb and Mo in gas condensates from Gendol fumarole field at Merapi in 1984, 2004 and 2005.



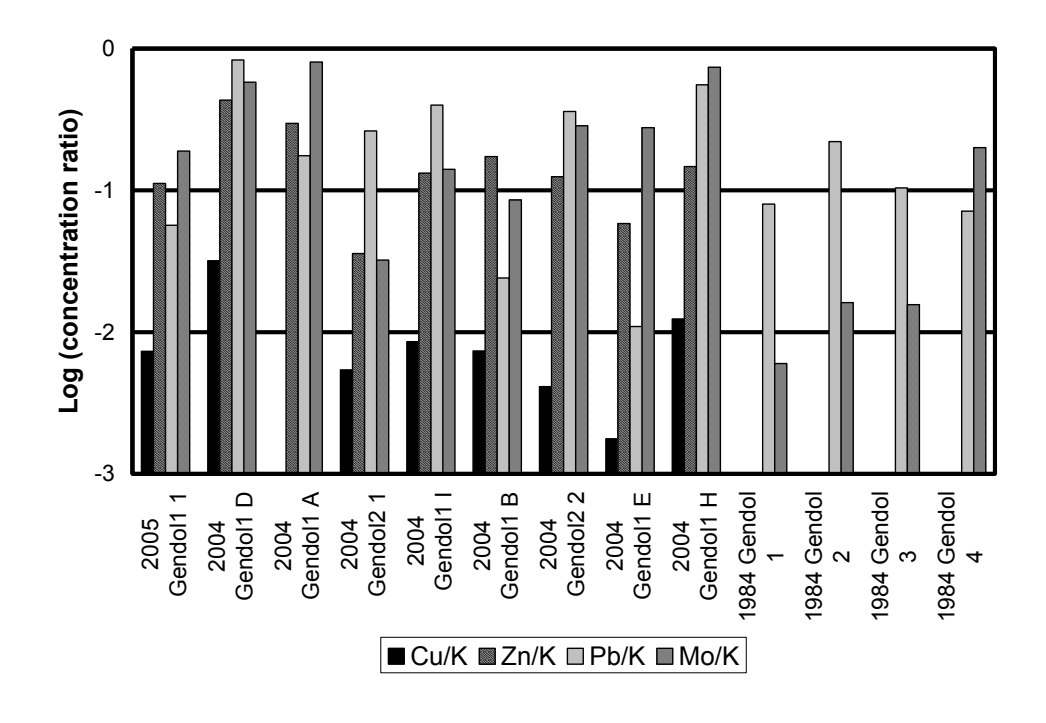
b) Ratios of Cu, Zn, Pb and Mo to Na in gas condensates from Woro fumarole field at Merapi in 2004 and 2006.



c) Ratios of Cu, Zn, Pb and Mo to Na in gas condensates from Gendol fumarole field at Merapi in 2004 and 2005.



d) Ratios of Cu, Zn, Pb and Mo to K in gas condensates from Gendol fumarole field at Merapi in 1984, 2004 and 2005.



Thesis Conclusions

1. Main findings

- 1. At Merapi volcano, and at similar arc volcanoes and magmatic-hydrothermal ore forming environments, injections of reduced, sulfide saturated mafic magma may result in the dissolution and subsequent degassing of the sulfide melt through the shallow magmatic-hydrothermal system to the atmosphere. The presence of these sulfide melts can be identified in volcanic gases emitted after mafic magma injections and resulting explosive eruptions.
- 2. The mafic magmas injected at Merapi and at other similar systems may or may not mix with shallower resident magma. If the magmas do not mix and if the sulfide melt associated with the mafic magma is dissolved by an exsolving magmatic volatile phase (MVP), the MVP may act as a vector of communication through which chalcophile (Cu, Zn and Pb) elements are transferred from the mafic to the shallower magma. These base metals will thus partition and exchange between MVP and the shallow magma through which they percolate.
- 3. The construction of certain porphyry-epithermal deposits may be determined by the alternation of reducing and oxidizing phases of mineral deposition. Injections of reduced mafic magma and dissolution of associated sulfide melt lead to pulses of reduced, Cu-, Zn- and Pb-rich fluids which accordingly deposits a reduced, Cu-, Zn- and Pb-bearing mineral assemblage. These metals are deposited in concentric zones around the shallow, resident magma (the porphyry), with Cu deposited earlier and closer, and with gradual shifts through zones rich in Zn and Pb. In volcanic systems these injections may be accompanied by explosive eruptions and degassing of reduced, Cu- and Pb-rich gases. By contrast, subsequent phases of mineral deposition are dominated by fractional crystallization and degassing, which promote enrichment of incompatible elements such as Mo and gradual oxidation of the magma. The related MVP are thus more oxidized, Cu-, Zn- and Pb-depleted and Mo-enriched, and accordingly deposit a more oxidized,

Mo-enriched mineral assemblage. In volcanic environments, these periods result in quiescent degassing.

2. Contribution to knowledge

The most significant finding in this thesis is the role played by reduced mafic magma injections in the construction of porphyry Cu and related epithermal deposits. Previous models for metallogenesis have generally ignored the role that these magmas play in the formation of these deposits. It has been discovered more recently that metals such as Cu may in fact originate from the deeper magma and avoid being trapped in phenocrystic phases by the physico-chemical pathways described above (Keith et al., 1991; 1997; Larocque et al., 2000; Halter et al., 2002; 2005; Nadeau et al., 2010). The links we have established between porphyry-epithermal and volcanic environments also contribute to the evolution of our understanding of the dynamics of subduction-zone environments.

3. Future work

Another source of information relevant to the present thesis resides in fluid inclusions. Although we have used literature data, significant advances can be made if cogenetic melt and fluid inclusions will be studied. Such data are rare currently, but more such studies should be conducted given advances in micro-analytical techniques. We have focussed on the bottom (melt inclusions) and tops (volcanic gases) of magmatic-hydrothermal systems. Studying the related fluid inclusions should enable a more thorough understanding of their mechanics and mechanisms of formation.

At most arc volcanoes, Cu is depleted with magmatic evolution (Nadeau et al., under review). However at Merapi, the opposite appears to be the case. It appears reasonable that this is caused by dissolution of the sulfide melt into a MVP and its percolation through and equilibration with shallow resident magma. Since we argue that this process is important to the genesis of porphyry Cu deposits, future research should test if this trend is reproduced in melt inclusions of mineralized systems, and opposite in melt inclusions of barren ones.

We have demonstrated in the second main chapter of this thesis that a Cu-, Zn- and Pb-rich MVP enriched the shallow resident magma in the metals (Nadeau et al., under review). Although we had shown in the first main chapter that Cu in the MVP originated from the sulfide melt (Nadeau et al., 2010), we were unable to identify a potential source for Pb. Future work pursued at Merapi should investigate this avenue. One way to investigate this is to seek enclaves and xenoliths in Merapi rocks and analyze them for Pb. Chadwick et al. (2005; 2007a; 2007b) and Deegan et al. (2010) investigated assimilation processes at Merapi but have not adopted this metallogenic point of view. The main assimilant they find at Merapi is a carbonate, and it is thus thought that there are carbonates in the basement of Merapi. Since it is recognized that porphyritic intrusions in limestone may form skarns, future metallogenically-oriented research conducted at Merapi should consider this avenue and observe, analyze and investigate these calc-silicate enclaves (Camus et al., 2000; Chadwick et al., 2005; 2007a; 2007b).

Thesis appendices

Appendix 1 – Major and trace element concentrations in sulfide melt inclusions. Symbol 'atom. %' stands for 'atomic proportion in percentage', 'wt. %' for 'weight percent', 'po' for pyrrhotite, 'py' for pyrite, 'cu' for cubanite, '?' for an unidentified mineral phase, '??' for an unidentified phase with $Fe_3Cu_2S_5$ stoichiometry, 'n/a' for 'not analyzed', and negative numbers mean they were not detected at that lower limit.

Fe	Cu	S	Fe	S	Cu	Total	Ag	As	Pd	Zn	Ni	Ti	Au	Co	Sn	Pb	Cu	Mo	Pt	W	mineral	Sample
	atom. %	1		wt. %										ppm								
39.8	7.5	52.5	49.2	37.2	10.5	97.3	n/a	-240	n/a	-200	1630	200	-66	1130	n/a	-270	105390	-160	-330	-400	?	BV.1(1).SG.1
46.0	0.1	53.6	58.0	38.9	0.2	97.5	n/a	-240	n/a	320	1860	-180	-66	1550	n/a	-270	1950	-160	-330	-400	po	BV.1(1).SG.7
46.3	0.0	53.5	58.8	39.0	0.0	98.1	n/a	-240	n/a	-200	1190	250	-66	1400	n/a	-270	450	-160	-330	-400	po	BV.1(2).SG.2
32.0	17.7	49.8	39.5	35.2	24.9	100.1	n/a	-240	n/a	1580	270	2980	-66	770	n/a	-270	248610	-160	-330	-400	cu	BV.2.SG.18A1
30.8	19.1	49.6	38.5	35.5	27.2	101.7	n/a	-240	n/a	1880	230	2960	-66	570	n/a	-270	271580	-160	-330	-400	??	BV.2.SG.18A2
14.4	36.3	49.3	16.4	32.2	47.0	95.6	n/a	-240	n/a	-200	150	-180	-66	-150	n/a	-270	469730	-160	-330	-400	?	BV.2.SG.6A1
15.6	39.8	42.4	1.3	2.0	3.7	7.3	n/a	-240	n/a	300	-110	-180	-66	-150	n/a	-270	37070	2310	-330	-400	?	BV.2.SG.6A2
29.7	20.4	49.7	33.4	32.1	26.2	92.0	n/a	-240	n/a	1210	600	-180	-66	490	n/a	-270	261910	-160	-330	-400	??	BV.2.SG.6A3
46.3	0.0	53.5	59.2	39.3	0.0	98.7	n/a	-240	n/a	-200	440	880	-66	1110	n/a	-270	-334	-160	-330	-400	po	M6.KALI06.1.SG.12A
45.4	1.1	53.3	57.7	38.9	1.6	98.5	n/a	-240	n/a	-200	420	840	-66	1270	n/a	-270	15860	-160	-330	-400	po	M6.KALI06.1.SG.12B
26.4	23.3	50.2	30.6	33.4	30.8	95.1	n/a	-240	n/a	670	550	-180	-66	220	n/a	-270	308140	-160	-330	-400	?	M6.KALI06.1.SG.14A1
31.2	19.3	49.5	36.2	33.0	25.4	94.7	n/a	-240	n/a	300	500	-180	-66	330	n/a	-270	254390	-160	-330	-400	??	M6.KALI06.1.SG.14B
46.3	0.0	53.4	59.2	39.2	0.1	98.8	n/a	-240	n/a	190	790	960	-66	1200	n/a	-270	660	-160	-330	-400	po	M6.KALI06.1.SG.20A
47.6	0.1	52.1	60.5	38.0	0.1	98.9	n/a	-240	n/a	-200	620	1290	-66	1280	n/a	-270	890	-160	-330	-400	po	M6.KALI06.1.SG.20B
29.8	19.9	50.1	36.4	35.2	27.7	99.6	n/a	-240	n/a	720	360	360	-66	620	n/a	-270	277330	-160	-330	-400	??	M6.KALI06.1.SG.7.1
29.3	20.5	50.0	35.7	35.1	28.5	99.6	n/a	-240	n/a	900	380	1510	-66	370	n/a	-270	284660	-160	-330	-400	??	M6.KALI06.1.SG.7.2
48.0	0.0	51.8	60.5	37.5	0.1	98.3	n/a	-240	n/a	-200	870	-180	-66	1340	n/a	-270	690	-160	-330	-400	po	M6.KALI06.2.SG.14A1
33.2	16.1	50.5	40.8	35.6	22.5	99.1	n/a	-310	n/a	730	400	-240	n/a	880	n/a	-290	224960	-220	-410	-800	cu	M6.NS.11.3(1).SG.10A
47.2	0.2	52.4	60.4	38.5	0.3	99.5	n/a	-310	n/a	-240	1320	-240	n/a	1090	n/a	-290	3360	-220	-410	-800	po	M6.NS.11.3(1).SG.10B
45.9	1.3	52.5	57.8	38.0	1.8	98.0	n/a	-310	n/a	-240	1350	970	n/a	1600	n/a	-290	18270	-220	-410	-800	po	M6.NS.11.3(1).SG.15B
46.2	0.4	53.1	58.7	38.7	0.6	98.5	n/a	-310	n/a	-240	1360	1020	n/a	1590	n/a	-290	5790	-220	-410	-800	po	M6.NS.11.3(1).SG.15C
46.9	0.3	52.7	60.3	38.9	0.4	99.8	n/a	-310	n/a	-240	660	-240	n/a	1260	n/a	-290	4110	-220	-410	-800	po	M6.NS.11.3(1).SG.3
46.7	0.1	52.9	60.2	39.1	0.2	99.8	n/a	-310	n/a	450	450	630	n/a	1390	n/a	-290	2070	-220	-410	-800	po	M6.NS.2.6(1).SG.10A

		i					i													i		
46.4	0.1	53.3	59.0	38.9	0.1	98.5	n/a	-310	n/a	250	1040	1060	n/a	1420	n/a	-290	-1240	-220	-410	-800	po	M6.NS.2.6(1).SG.6A
46.5	0.0	53.2	59.7	39.3	0.1	99.4	n/a	-310	n/a	-240	1020	740	n/a	1470	n/a	-290	-1240	-220	-410	-800	po	M6.NS.2.6(1).SG.6B
46.4	0.0	53.4	59.8	39.5	0.1	99.6	n/a	-310	n/a	-240	990	670	n/a	600	n/a	-290	-1200	-220	-410	-800	po	M6.NS.2.6(2).SG.10A
43.3	4.0	52.4	55.8	38.8	5.9	100.8	n/a	-310	n/a	280	810	740	n/a	1210	n/a	-290	58890	-220	-410	-800	po	M6.NS.2.6(2).SG.10B1
47.3	0.1	52.4	59.9	38.1	0.1	98.4	n/a	-310	n/a	-240	1120	680	n/a	1350	n/a	-290	-1200	-220	-410	-800	po	M6.NS.2.6(2).SG.10B2
46.5	0.1	53.1	60.0	39.4	0.1	99.8	n/a	-310	n/a	-240	1000	740	n/a	1530	n/a	-290	-1200	-220	-410	-800	po	M6.NS.2.6(2).SG.10C
46.7	0.3	52.8	59.8	38.8	0.4	99.3	n/a	-310	n/a	-240	930	830	n/a	1400	n/a	-290	4160	-220	-410	-800	po	M6.NS.2.6(2).SG.2A
46.7	0.0	52.8	60.6	39.3	0.0	100.6	n/a	-310	n/a	-240	1280	2910	n/a	1900	n/a	-290	-1200	-220	-410	-800	po	M6.NS.6-10.1.SG.15
35.4	16.6	47.8	37.9	29.4	20.2	87.9	n/a	-310	n/a	740	640	250	n/a	410	n/a	1130	202260	-220	-410	-800	cu	M6.NS.6-10.1.SG.17
46.7	0.0	52.9	60.1	39.1	0.1	99.8	n/a	-310	n/a	420	1180	2050	n/a	1950	n/a	-290	-1200	-220	-410	-800	po	M6.NS.6-10.1.SG.19A
46.3	0.0	53.2	59.9	39.5	0.0	100.0	n/a	-310	n/a	-240	2140	900	n/a	3080	n/a	-290	-1200	-220	-410	-800	po	M6.NS.6-10.1.SG.19B
46.8	0.0	52.8	60.1	38.9	0.0	99.6	n/a	-310	n/a	-240	2250	710	n/a	2840	n/a	-290	-1200	-220	-410	-800	po	M6.NS.6-10.1.SG.19C
46.6	0.0	53.1	59.9	39.2	0.0	99.3	n/a	-310	n/a	-240	1050	-240	n/a	1460	n/a	-290	-1200	-220	-410	-800	po	M6.NS.6-10.1.SG.8
42.5	2.2	55.1	52.8	39.3	3.1	95.4	n/a	-310	n/a	240	1390	-240	n/a	1430	n/a	-290	30670	-220	-410	-800	po	M6.NSB.1.3(2).SG.14A1
46.8	0.3	52.7	59.5	38.5	0.4	98.7	n/a	-310	n/a	-240	1620	240	n/a	1240	n/a	-290	4160	-220	-410	-800	po	M6.NSB.1.3(2).SG.5A
46.8	0.0	52.9	59.5	38.6	0.0	98.5	n/a	-310	n/a	-240	1410	310	n/a	1550	n/a	-290	-1200	-220	-410	-800	po	M6.NSB.1.3(2).SG.5B
46.6	0.1	53.0	59.7	38.9	0.1	99.1	n/a	-310	n/a	-240	1190	1040	n/a	1440	n/a	-290	-1200	-220	-410	-800	po	M6.NSB.1.4.SG.12
29.6	19.7	50.6	36.4	35.7	27.5	99.8	-400	190	-330	640	290	270	-66	300	-180	-270	275210	360	-330	-250	??	M6.WD.1.4(1).1A
46.7	0.1	53.0	58.9	38.3	0.1	97.5	-400	-165	-330	-200	890	-180	-66	1190	-180	-270	760	390	-330	-250	po	M6.WD.1.4(1).1B
44.3	3.4	52.1	54.4	36.8	4.8	96.2	n/a	-240	n/a	-200	700	420	-66	1050	n/a	-270	47640	-160	-330	-400	po	M6.WD.1.4(2).SG.11
46.6	0.1	53.1	58.7	38.4	0.1	97.5	n/a	-240	n/a	360	500	800	-66	1480	n/a	-270	820	-160	-330	-400	po	M6.WD.1.4(2).SG.9
45.4	1.4	53.0	56.4	37.8	2.0	96.5	-400	-165	-330	-200	570	840	-66	1230	-180	-270	20180	270	-330	-250	po	M6.WD.3.1.6
44.9	2.9	52.1	58.3	38.8	4.3	101.7	-400	-165	-330	-200	670	170	150	1350	-180	-270	42940	-160	360	-250	po	M6.WD.3.1.8
46.7	0.0	53.1	58.4	38.1	0.0	96.8	n/a	-240	n/a	190	820	-180	-66	1250	n/a	-270	490	-160	-330	-400	po	M6.WD.3.1.SG.REDO.8
32.4	16.9	50.5	39.7	35.5	23.6	99.0	-400	-165	-330	-200	-110	-180	-66	1220	-180	-270	235970	290	-330	-250	cu	M6.WD.3.3(1).10A
32.5	16.9	50.4	39.8	35.4	23.6	99.1	-400	-165	-330	640	-110	-180	-66	930	-180	-270	236050	340	-330	-250	cu	M6.WD.3.3(1).10B
34.0	15.3	50.5	41.5	35.4	21.3	98.5	-400	-165	-330	680	-110	-180	-66	1600	-180	-270	212900	300	360	-250	cu	M6.WD.3.3(1).11A
33.6	15.3	50.8	41.0	35.6	21.3	98.3	-400	-165	-330	320	140	300	-66	1510	-180	-270	213320	460	-330	-250	cu	M6.WD.3.3(1).11B
32.5	16.8	50.5	40.0	35.6	23.5	99.4	-400	-165	-330	1170	80	-180	-66	1570	-180	-270	234650	410	-330	-250	cu	M6.WD.3.3(1).12A.FULL
42.2	0.7	56.0	53.4	40.6	1.0	96.4	-400	-165	-330	-200	7150	-180	-66	6640	-180	-270	10390	370	-330	-250	po	M6.WD.3.3(1).12B.FULL
33.6	15.5	50.7	41.1	35.6	21.6	98.6	-400	-165	-330	500	-110	200	-66	1520	-180	-270	216430	520	-330	-250	cu	M6.WD.3.3(1).13B
32.5	0.2	66.6	43.8	51.5	0.4	96.7	-400	-165	-330	-200	5730	-180	-66	3600	-180	-270	3740	-160	-330	-250	py	M6.WD.3.3(1).13C
32.5	0.2	66.7	44.6	52.5	0.4	98.3	-400	-165	-330	-200	4170	-180	-66	3040	-180	-270	3510	-160	-330	-250	ру	M6.WD.3.3(1).13E
34.2	15.1	50.5	41.6	35.3	21.0	98.2	-400	-165	-330	-200	1230	-180	-66	1250	-180	-270	209550	380	-330	-250	cu	M6.WD.3.3(1).14A
47.4	0.1	52.2	60.3	38.1	0.2	99.0	-400	-165	-330	-200	2110	-180	-66	1480	-180	-270	1840	250	-330	-250	po	M6.WD.3.3(1).14B
47.6	0.2	52.0	60.6	38.0	0.3	99.1	-400	-165	-330	-200	810	-180	-66	1120	-180	-270	2500	350	-330	-250	po	M6.WD.3.3(1).15A

33.6	15.9	50.3	41.2	35.4	22.2	99.1	-400	-165	-330	1070	220	-180	-66	900	-180	-270	222190	420	-330	-250	cu	M6.WD.3.3(1).15B
46.6	0.1	53.0	59.3	38.7	0.1	98.6	-400	-165	-330	-200	2340	300	-66	1530	-180	-270	790	390	-330	-250	po	M6.WD.3.3(1).17A
47.4	0.1	52.2	59.2	37.5	0.1	97.4	-400	-165	340	-200	2520	510	-66	1420	-180	-270	860	410	-330	-250	po	M6.WD.3.3(1).18A
34.3	15.6	49.9	41.8	34.9	21.7	98.6	n/a	-240	n/a	610	-110	-180	-66	1440	n/a	-270	216980	-160	-330	-400	po	M6.WD.3.3(1).SG.REDO.11
46.6	0.0	53.1	59.5	38.9	0.0	98.7	n/a	-240	n/a	260	930	400	-66	1190	n/a	-270	320	-160	-330	-400	po	M6.WD.3.3(2).SG.6
34.0	15.2	50.7	42.0	36.0	21.4	99.6	n/a	-240	n/a	-200	720	-180	-66	1220	n/a	-270	213780	-160	-330	-400	cu	M6.WD.3.4(1).SG.3
47.6	0.1	52.1	60.6	38.1	0.1	99.2	n/a	-240	n/a	-200	1410	-180	-66	1700	n/a	-270	1430	-160	-330	-400	po	M6.WD.3.4(1).SG.6
46.3	0.0	53.2	58.3	38.4	0.1	97.5	-400	-165	-330	-200	4120	930	-66	1180	-180	-270	540	510	-330	-250	po	M6.WD.3.4(2).10
33.5	3.3	62.2	41.7	44.5	4.7	92.3	-400	-165	-330	290	9980	-180	-66	2340	-180	-270	47300	230	-330	-250	py	M6.WD.3.4(2).1B.FULL
46.5	0.1	52.7	59.1	38.5	0.1	98.8	-400	-165	-330	-200	8060	-180	-66	1930	-180	-270	1320	400	-330	-250	po	M6.WD.3.4(2).1C.FULL
32.7	16.7	50.3	40.0	35.4	23.2	99.0	-400	-165	-330	-200	2370	-180	-66	1020	-180	-270	231960	330	-330	-250	cu	M6.WD.3.4(2).1D
46.4	0.1	52.7	59.4	38.8	0.2	99.4	-400	-165	-330	-200	8070	-180	-66	1810	-180	-270	1710	390	-330	-250	po	M6.WD.3.4(2).1E
46.6	3.9	49.2	56.4	34.2	5.4	96.3	-400	-165	-330	-200	730	660	-66	780	-180	-270	53930	430	-330	-250	po	M6.WD.3.4(2).2
29.2	20.1	50.5	35.3	35.1	27.7	98.3	-400	-165	-330	-200	840	440	-66	800	-180	-270	276530	460	-330	-250	??	M6.WD.3.4(2).5A
46.0	0.0	53.5	58.6	39.1	0.1	98.2	-400	-165	-330	-200	2340	340	-66	1850	-180	-270	570	350	-330	-250	po	M6.WD.3.4(2).5B

Appendix 2 – Major and trace element concentrations in volcanic gas condensates from Merapi in 2004, 2005 and 2006. All data are in ppm. Symbol 'TDS' stands for 'total dissolved solids'.

Date	2006	2006	2005	2004	2004	2004	2004	2004	2004	2004	2004	2004	2004
Sample	M6W1	M6W2	G5	M4W1	M4W3	M4G1-D	M4G1-A	M4G1-I	M4G1-B	M4G1-E	M4G1-H	M4G2-1	M4G2-2
T (°C)	515	417	622	572	266	754	705	602	593	526	515	604	588
Li	0.033	0.007											
В	0.3			36.0	13.0	30.5	38.7	8.2	17.5	40.2	7.6	27.5	19.6
F	320	245	110	124	60	194	343	228	193	185	296	223	303
Na	2.31	1.21	4.57	3.43	0.60	0.74	1.14	2.71	11.50	2.11	1.20	9.00	2.00
Mg	0.25	0.47	0.38	0.89	0.37	0.07	0.12	0.32	0.60	1.24	0.14	0.81	0.46
Al	1.46	1.35	2.49	3.44	1.48	0.25	2.65	1.71	5.52	3.39	1.52	9.13	2.61
Si	31.86	23.84	1000	23.90	17.20	23.50	6.30	4.18	42.80	33.90	64.40	27.50	70.50
S	6733	10579	3438	263	520	1803	3438	2597	5307	7644	3672	3638	5207
Cl	4849	7193	957	3030	893	6620	7250	5330	3830	6710	5630	5420	6500
K	2.27	0.63	1.50	2.30	1.13	0.31	0.44	1.05	2.99	2.83	0.65	4.99	1.21
Ca	0.40	1.03		3.46		0.40	0.60	2.10	4.30	4.60	0.60	5.95	3.70
Sc	0.0087	0.0020											0.0110
Ti	0.05	0.05	0.10	0.40	0.21	0.01	0.08	0.03	0.22	1.28	0.12	0.18	0.54
V	0.00		0.26	0.01	0.01	0.20	0.13	0.18	0.24	0.19	0.12	0.04	0.09
Cr		0.01		0.06	0.02	0.10	0.11	0.08	0.07	0.10		0.12	0.11
Mn	0.04	0.02	0.05	0.10	0.07	0.03	0.03	0.05	0.11	0.39	0.03	0.15	0.12
Fe	1.43	2.02	1.70	2.58	1.48	0.12	1.06	0.91	4.69	8.00	0.65	4.30	3.06
Co	0.0078	0.0461	0.0006	0.0014	0.0009	0.0002	0.0007	0.0016	0.0020	0.0046	0.0010	0.0023	0.0019
Ni	0.0100	0.0556	0.0100	0.0290	0.0080	0.0310	0.0490	0.0460	0.0390	0.0470	0.0070	0.0140	0.0500
Cu	0.161	0.279	0.011		0.003	0.010		0.009	0.002	0.005	0.008	0.027	0.005
Zn	0.420	0.150	0.168	0.150	0.060	0.140	0.130	0.140	0.520	0.170	0.100	0.180	0.150
Ga	0.0004	0.0006	0.0005	0.0016	0.0010	0.0010	0.0020	0.0020	0.0030	0.0040	0.0020	0.0020	0.0030
Ge	0.0004	0.0005	0.0021	0.0040	0.0026	0.0030	0.0340	0.0030	0.0230	0.0090	0.0030	0.0030	0.0130
As	2.21	2.99	0.15	0.98	0.67	1.73	3.72	0.49	3.45	0.44	0.11	0.30	0.12
Se	0.044	0.046	0.024	0.034		0.043	0.012	0.066	0.031	0.021	0.137	0.068	0.110
Br	8.22	11.46	1.55	5.43	2.37	9.20	12.00	3.39	3.46	11.80	2.85	13.90	8.32
Rb			0.010										
Sr	0.020	0.019	0.008	0.075	0.015	0.006	0.007	0.011	0.048	0.026	0.003	0.082	0.030
Y	0.0004	0.0005	0.0003	0.0039	0.0007	0.0001	0.0003	0.0003	0.0017	0.0017	0.0004	0.0042	0.0014
Zr	0.0222	0.0114	0.0031	0.0121	0.0048	0.0030	0.0070	0.0050	0.0050	0.0110	0.0070	0.0160	0.0110
Mo		0.0006	0.2840	0.0200	0.0040	0.1820	0.3570	0.1480	0.2560	0.7830	0.4770	0.1610	0.3460
Pd	0.000011	0.00003		0.0003		0.0053			0.001				
Ag		0.00026											
Cď	0.086	0.0414	0.004	0.0161	0.0005	0.003	0.003	0.002	0.004	0.003	0.006	0.015	0.004

In	0.0216	0.00418	0.00091	0.00458	0.00124	0.00002	0.00014	0.0004	0.002	0.0049	0.0003	0.0017	0.0018
Sn	0.219	0.0188	0.014	0.066	0.011		0.013	0.003	0.046	0.06	0.004		0.041
Sb	0.0399	0.0213	0.0009	0.0098	0.0031	0.0012	0.007	0.0007	0.005	0.005	0.0009	0.002	0.001
Te	0.000013	0.0288	0.079	0.003	0.004	0.003	0.219	0.04	0.212	0.231	0.092	0.041	0.124
Ba	0.0342	0.0555	0.009	0.281	0.11	0.005	0.015	0.012	0.02	0.042	0.009	0.066	0.048
La	0.00023	0.000928	0.00028	0.0032	0.00078	0.0005	0.0003	0.0004	0.0012	0.0016	0.0004	0.0027	0.0017
Ce	0.001862	0.001798	0.00051	0.00718	0.0014	0.0014	0.0006	0.0006	0.003	0.0032	0.0007	0.0057	0.0031
Pr	0.000177	0.000221	0.00007	0.00084	0.00015	0.00002	0.00005	0.00007	0.0003	0.0004	0.00007	0.0008	0.0004
Nd	0.00072	0.000813	0.00027	0.00365	0.00065			0.0001	0.0012	0.0014	0.0001	0.0041	0.0011
Sm	0.000191	0.000198	0.00006	0.00089	0.00015	0.00002	0.00009	0.00007	0.0005	0.0004	0.00008	0.0008	0.0004
Eu	0.00003	0.000048	0.00002	0.00024	0.00006		0.00002	0.00002	0.0001	0.0001	0	0.0001	0.0001
Gd	0.00009	0.00014	0.00005	0.00095	0.00013	0.00001	0.0001	0.0001	0.0004	0.0004	0.00006	0.0008	0.0003
Tb	0.000013	0.000067		0.00014	0.00003				0.00005	0.0005		0.0002	0.00004
Dy	0.000094	0.000129	0.00005	0.00073	0.00011		0.00005	0.00006	0.0003	0.0003	0.00005	0.0005	0.0003
Но	0.000024	0.000023		0.00015	0.00003				0.00006	0.00006	0.00001	0.0002	0.00005
Er	0.000075	0.000086	0.00004	0.00041	0.00007		0.00002	0.00003	0.0002	0.0002	0.00003	0.0005	0.0002
Tm	0.000001	0.00002		0.00006					0.00002	0.00003			0.00002
Yb	0.000046	0.00005	0.00004	0.00041	0.00008		0.00003	0.00003	0.0001	0.0002	0.00004	0.0004	0.0001
Lu		0.00001		0.00006	0.00001				0.00003				0.00003
Hf	0.000494	0.000278	0.00008	0.00031	0.00012	0.00033	0.0002	0.0001	0.00033	0.0003	0.0002	0.0005	0.0002
Ta	0.00003	0.0000281		0.00035	0.00011	0.0001	0.0002	0.0002	0.0001	0.0002	0.0002		0.0002
W	0.0022	0.00123	0.0402	0.0047	0.0006	0.03	0.035	0.016	0.077	0.039	0.008	0.007	0.051
Re	0.000031	0.00004	0.0000455	0.0002	0.00054	0.0075	0.012	0.0027	0.0071	0.013	0.0074	0.011	0.013
Pt	0.00198	0.00121											
Au		0.00002		0.0006	0.0002							0.0005	
Hg		0.00695	0.003	0.002		0.002	0.008	0.004	0.008	0.017	0.002	0.01	0.005
Tl	0.27	0.26	0.134	0.154	0.00311	0.161	0.599	0.227	0.131	0.214	0.383	0.287	0.248
Pb	8.53	8.01	0.0851	1.41	0.07	0.26	0.08	0.42	0.07	0.03	0.36	1.31	0.44
Bi	0.257	0.256	0.034	0.023		0.478	0.178	0.499	0.128	0.064	0.567	0.091	0.282
Th	0.00011	0.00023	0.00011	0.0011	0.0003	0.00054	0.0002	0.0001	0.0002	0.0004	0.0002	0.0007	0.0005
U	0.00006	0.000079	0.00004	0.00034	0.00009		0.00003	0.00009	0.0014	0.0002	0.00006	0.0002	0.0002
TDS	61096	85120	48200	27962	11404	79000	109000		98700	205000			

Appendix 3. Concentration of major, trace and volatile elements in silicate melt inclusions from Merapi volcano. Symbol 'EMPA' stands for 'electron microprobe analysis'. EMPA results are in wt. %. Symbol 'LAICPMS' stands for 'laser ablation inductively coupled plasma mass spectrometry'. LAICPMS data are in ppm. Symbol 'SIMS' stands for 'secondary ions mass spectrometry'. SIMS data are in ppm except H2O which is in wt. %. Symbols 'ps' stands for 'polished section', 'im' for 'indium mount', 'dl' for 'dome lava', 'sc' for 'scoria', 'la' for 'lava', 'a' for 'amphibole', 'am' for 'amphibole megacryst', 'c' for 'clinopyroxene', 'cm' for 'clinopyroxene megacryst', 'p' for 'plagioclase'.

SiO ₂	MgO	Al_2O_3	FeO	Na ₂ O	CaO	K ₂ O	P_2O_5	MnO	TiO_2	Cl	S	Total	Ni	Cu	Zn	Zr	Mo	Ce	Pb	Co	CO_2	H_2O	F	S	Cl	Sample Name
						EMPA										LAI	CPMS						SIMS			
51.64	1.40	19.89	8.23	3.05	10.37	2.08	0.44	0.28	0.47	1850	645	98.15		38	149	82		43	22							M6.WD.3.4(1).4A
51.97	1.35	19.92	7.78	3.11	10.18	2.07	0.45	0.21	0.56	1820	489	97.86		38	149	82		43	22							M6.WD.3.4(1).4B
52.02	1.10	20.19	7.88	3.12	9.89	2.05	0.48	0.23	0.46	1890	469	97.69		19	116	77		39	21							M6.WD.3.3(1).1B
52.50	1.47	19.93	7.46	3.19	9.80	2.18	0.46	0.26	0.54	1620	605	98.07		23	110	88		41	19							M6.WD.3.4(1).2
53.23	1.11	20.15	7.84	2.97	9.84	2.10	0.49	0.26	0.50	2000	485	98.75		19	116	77		39	21							M6.WD.3.3(1).1A
53.51	1.57	21.34	7.20	3.64	7.71	2.39	0.48	0.20	0.62	1840	433	98.90			97	99		47	28							M6.WD.3.3(1).5A
54.11	1.60	21.56	7.08	3.61	7.54	2.46	0.44	0.21	0.63	1600	280	99.43			96	63	93	29	16							M6.WD.3.3(1).5B
54.99	1.03	20.81	5.86	3.90	6.87	2.29	0.36	0.28	0.67	1840	212	97.25			99	85	10	53	24							M6.WD.3.3(1).7A
55.31	1.25	21.51	6.46	3.95	7.18	2.20	0.36	0.18	0.75	1930	429	99.40		16	120	111		48	24							M6.WD.3.3(1).7B
56.97	0.98	19.52	6.40	4.25	6.53	3.69	0.47	0.20	0.40	2280	188	99.63			110	94		43	34							M6.WD.3.4(1).7B
57.71	1.05	19.02	6.85	4.75	6.34	2.69	0.43	0.26	0.46	2700	228	99.82			157	77		43	41							M6.WD.3.4(1).7A
60.89	1.30	19.15	5.59	4.85	3.59	4.24	0.59	0.25	0.45	1870	172	101.08	20		110	62	252	31	25							M6.WD.3.3(1).9A
62.29	0.46	16.93	3.18	4.44	2.02	4.80	0.24	0.10	0.37	2740	176	95.07														M6.NSB.1.3(2).11A
62.51	1.30	17.94	3.39	5.57	2.98	4.51	0.39	0.10	0.25	2270		99.10			61	50		25	42							WD.3.2.MGCX3.MT1.CX1.MI3
62.60	0.79	16.16	3.61	4.19	1.99	4.41	0.19	0.16	0.46	2640	284	94.81														M6.NSB.1.3(2).11B
62.82	0.55	17.59	3.92	4.51	2.09	6.40	0.18	0.18	0.50	2510	296	99.00														M6.NS.2.6(1).15C
63.29	1.25	16.62	5.52	3.76	3.04	4.71	0.33	0.18	0.54	2740	152	99.48														M6.WD.3.3(1).30
63.29	0.98	16.37	3.98	4.71	2.36	5.11	0.19	0.16	0.60	2455		97.97			68	190	3	60	43	8						M6.NS.6-10.1.13A3bis
63.37	0.60	16.45	2.80	4.45	1.90	4.46	0.20	0.12	0.46	3020	196	95.09														M6.NSB.1.3(2).8B
63.48	0.57	16.72	3.83	4.21	2.14	6.29	0.16	0.14	0.48	2490	140	98.24														M6.NS.2.6(1).7
63.67	0.45	15.46	2.68	3.80	1.85	4.65	0.13	0.03	0.29	2750	312	93.30														M6.WD.1.4(2).16A
63.95	0.80	16.71	3.69	4.75	2.38	4.57	0.16	0.15	0.53	2620	240	97.94														M6.NSB.1.3(2).4D
64.03	0.91	15.69	5.47	3.92	3.25	4.43	0.13	0.24	0.57	2680		98.87														M6.WD.3.3(2).11A
64.03	0.70	16.05	3.02	4.10	2.33	4.52	0.15	0.14	0.41	2800	204	95.71														M6.WD.1.4(2).5A1
64.09	0.40	15.38	2.59	3.65	1.80	4.79	0.10	0.15	0.31	2590	272	93.50														M6.WD.1.4(2).16B
64.12	0.68	16.12	2.92	4.00	2.24	4.54	0.16	0.14	0.38	2830	188	95.58														M6.WD.1.4(2).5A2
64.13	0.63	17.83	3.08	5.17	1.73	6.04	0.34	0.16	0.40	2590	252	99.76														M6.KALI06.1.19
64.21	0.70	15.73	2.24	4.00	2.27	5.20	0.17	0.07	0.63	3010	244	95.51														M6.KALI06.1.17A
64.21	0.72	16.93	3.75	4.93	2.67	4.50	0.17	0.17	0.55	2580	168	98.83														M6.NSB.1.3(2).4C
64.28	0.72	16.88	3.23	4.51	2.07	4.61	0.19	0.11	0.44	2740	272	97.30														M6.NSB.1.3(2).11C
64.33	0.41	16.48	3.04	4.44	1.98	4.70	0.22	0.12	0.50	2900	240	96.50														M6.NSB.1.3(2).3
64.35	0.81	16.75	3.66	4.67	2.56	4.34	0.19	0.20	0.54	2400	268	98.32														M6.NSB.1.3(2).4A
64.37	0.64	16.77	3.96	4.22	2.13	5.86	0.19	0.12	0.48	2620	244	99.00														M6.NS.2.6(1).2
64.39	0.93	16.92	3.96	4.82	2.69	4.51	0.20	0.15	0.48	2360	272	99.29	l								l					M6.NSB.1.3(2).4E

	64.52	0.70	16.31	3.77	4.12	3.33	4.70	0.17	0.20	0.35	2380		98.38													M6.WD.3.1.3A
	64.54	0.82	16.47	3.91	4.69	2.50	4.86	0.18	0.11	0.50	2690	280	98.84													M6.NSB.1.3(2).13C
	64.63	0.95	16.05	4.09	4.26	2.70	4.46	0.16	0.13	0.40	2600		98.05													M6.WD.1.4(2).8B
	64.70	0.82	14.87	4.08	4.60	1.98	4.79	0.18	0.18	0.45	3000		96.88		34	106	223	15	66	37		1.31	1335	133	3346	WD.3.2.mt1.cx2.mi3
	64.73	0.33	17.98	2.06	4.63	2.40	4.64	0.29	0.14	0.44	3020	264	97.94													M6.KALI06.1.2C
	64.74	0.93	15.88	3.08	4.86	2.61	4.90	0.10	0.14	0.38	2710	20.	97.84													M6.WD.3.4(2).17A
	64.75	1.04	15.64	4.83	4.31	2.95	4.53	0.22	0.24	0.41	2110		99.08													M6.WD.3.3(2).11B
	64.75	0.29	15.81	2.74	5.92	1.38	5.55	0.09	0.12	0.46	2500	136	97.33													M6.KALI06.1.16D2
	64.76	0.89	16.03	3.67	4.07	2.17	5.27	0.03	0.12	0.40	3180	150	97.76													M6.WD.3.1.9B
	64.83	0.73	16.51	3.63	4.96	2.31	4.75	0.11	0.13	0.47	2690	260	98.86													M6.NSB.1.3(2).13B
	64.84	0.73	16.76	3.56	4.50	2.15	5.73	0.19	0.16	0.41	2660	136	99.22													M6.NS.2.6(1).12
		0.67	16.47	3.21	4.30	2.13	4.52	0.20	0.16	0.41	2600	130	97.37													. ,
	64.85																									M6.WD.3.4(1).8B
	65.00	0.88	15.98	4.07	3.92	2.23	5.04	0.13	0.15	0.39	2450		97.98													M6.WD.3.1.9A
	65.02	0.42	15.48	2.69	5.22	1.54	5.16	0.11	0.16	0.30	3120	156	96.38													M6.WD.3.4(2).7A1
	65.03	0.69	16.35	3.62	4.09	3.44	4.85	0.14	0.18	0.36	2460		98.94													M6.WD.3.1.3B
	65.07	0.06	16.10	1.65	4.50	2.06	4.00	0.15	0.11	0.38	3000	168	94.35													M6.WD.3.3(2).13
	65.10	0.60	16.37	2.08	4.22	1.98	4.91	0.14	0.07	0.55	2800	180	96.28													M6.KALI06.1.2B
	65.12	1.09	15.32	3.31	5.10	1.81	4.25	0.15	0.13	0.29	2590		96.77		26	156	121		43	17		1.73	558	202	3319	WD.3.3.mt6.cx3.mi7
	65.14	0.98	16.09	3.53	4.10	2.87	4.80	0.13	0.19	0.45	2680		98.50													M6.WD.3.4(2).11
	65.22	0.85	15.92	3.25	4.74	2.66	4.86	0.11	0.22	0.35	2670		98.40													M6.WD.3.4(2).17B
	65.26	0.93	16.20	3.84	4.10	2.34	5.05	0.10	0.15	0.45	3260		98.67													M6.WD.3.1.9D
	65.27	0.49	16.10	2.24	4.56	1.79	5.21	0.08	0.11	0.57	2610	156	96.67													M6.KALI06.1.16F
	65.41	0.44	16.15	2.23	4.68	1.71	5.10	0.10	0.08	0.52	2810	212	96.67													M6.KALI06.1.16E
	65.43	0.84	15.80	3.61	5.18	2.67	4.69	0.11	0.12	0.53	2780	220	99.25													M6.WD.3.3(2).4C1
	65.53	0.45	15.11	2.89	3.85	1.85	4.67	0.16	0.18	0.34	3840		95.35													M6.WD.1.4(2).17
	65.61	0.92	15.62	3.40	4.90	2.26	5.31	0.12	0.22	0.50	2860		99.10													M6.WD.3.3(2).5
	65.61	0.83	15.20	3.25	4.73	2.00	4.63	0.19	0.12	0.45	2830		97.22			79	255		60	39		1.85	911	86	3207	WD.3.2.mt1.cx2.mi1(a)
	65.62	0.31	15.44	2.39	3.32	1.85	5.26	0.10	0.14	0.27	2460		94.91													M6.WD.1.4(1).8
	65.63	0.40	14.55	2.40	3.91	1.49	5.75	0.10	0.10	0.36	3040		94.92			89	210		55	45		1.98	816	193	3313	WD.3.3.mt3.cx20.mi6b
	65.68	0.98	16.00	3.52	4.02	2.26	5.14	0.13	0.17	0.36	3080		98.49													M6.WD.3.1.9C
	65.68	0.54	15.46	3.36	4.86	1.84	4.59	0.19	0.13	0.47	3490		97.38		39	94	137		42	35		1.95	841	133	3045	wd.3.2.mt1.cx18.mi1
	65.70	0.22	15.84	2.64	5.25	1.46	5.16	0.10	0.16	0.31	3110	212	97.13													M6.WD.3.4(2).7A2
	65.72	0.08	19.13	1.23	0.26	2.44	1.71	0.21	0.05	0.24	2580	496	91.39													M6.WD.3.3(2).3
	65.73	0.32	15.63	2.81	4.46	1.48	4.89	0.13	0.07	0.41	3100	180	96.21													M6.WD.3.3(2).12A
	65.85	0.76	15.82	3.40	5.15	2.66	4.56	0.11	0.21	0.54	2760	168	99.31													M6.WD.3.3(2).4C2
	65.88	0.39	15.46	2.79	5.42	1.42	4.94	0.06	0.13	0.23	3760		96.99		66	36	206		57	68		1.55	607	87	3409	WD.3.3.mt5.cx19.mi1
	65.97	1.09	16.13	3.53	4.31	2.77	4.46	0.16	0.17	0.52	2180		99.30													M6.WD.3.3(2).4A2
	65.98	0.70	15.70	3.12	4.89	1.96	4.61	0.15	0.13	0.48	2930		97.94		22	84	176		52	50						WD.3.3.MT3.CX5.MI4
	66.06	0.57	15.35	3.18	4.57	1.53	4.89	0.15	0.15	0.45	2960		97.13		46	79	238	11	59	56						WD.3.3.mt4.cx5.mi1
	66.09	1.24	16.21	3.89	2.77	3.01	4.41	0.12	0.09	0.56	2390	140	98.61													M6.WD.3.3(2).4A1
	66.11	0.76	15.84	2.20	3.99	1.99	4.95	0.13	0.11	0.45	2490	244	96.79													M6.KALI06.1.17D
	66.12	0.31	15.59	2.37	4.82	1.94	4.93	0.14	0.11	1.47	2640	136	98.04													M6.KALI06.1.16B
	66.25	0.37	15.94	3.46	4.53	0.81	6.46	0.23	0.08	0.54	4150	172	99.01													BV.1(1).12C
	66.26	0.41	16.97	2.76	4.23	1.35	6.54	0.12	0.13	0.45	2130	.,_	99.41			64	203		47	64						M6.KAL106.2.5A
	66.33	0.57	16.20	2.09	4.13	1.95	5.03	0.12	0.13	0.43	2640	152	97.46			0-1	203		77	51						M6.KALI06.1.2A
	66.34	0.44	15.74	3.05	5.13	1.52	5.06	0.08	0.11	0.33	2920	152	98.15													M6.WD.3.4(2).18
	66.52	0.54	16.17	3.52	4.31	2.26	5.42	0.08	0.21	0.33	2650	132	99.62													M6.WD.1.4(1).4
	66.55	0.54	15.17	2.69	4.75	1.41	4.94	0.12	0.17	0.37	3020		96.99			89	210		55	45		1.92	633	167	2506	wd.3.3.mt3.cx20.mi6a
	66.55	0.01	14.86	2.36	4.73	1.41	4.94	0.12	0.13	0.33	3190		96.99		57	80	200	5	51	58		1.74	033	107	2300	WD.3.3.MT2.CX17.MI2
	66.65	0.29	15.56	2.00	4.88	1.83	4.84	0.12	0.13	0.33	3450		96.09		65	66	206	J	54	58 56	1					WD.3.3.MT5.CX22.MI1A
	66.71	0.11	15.36	2.25	3.92	1.83	5.13	0.12	0.06	0.37	2650	132	96.09		0.5	00	200		J -1	50	1					M6.KALI06.1.1A
	66.72	0.84	15.48	3.23	3.92 4.89	2.05	4.54	0.16	0.10	0.47	2990	132	96.85 98.46			104	231		55	38		1.85	911	86	3207	
ı	00.72	0.64	13.21	3.23	4.89	2.03	4.34	0.13	0.22	0.39	∠990		90.40	1		104	231		33	36	1	1.65	911	00	3207	WD.3.2.mt1.cx2.mi1(b)

ı														i							ı				ı	
	66.77	0.82	15.59	3.14	5.49	2.34	4.55	0.12	0.15	0.42	2850		99.61													WD.3.3.MT5.CX23.MI1
	66.79	0.84	15.67	3.67	4.83	2.34	4.67	0.14	0.13	0.48	2960		99.78		44	144	221		58	36						WD.3.2.MT1.CX10.MI1
	66.81	0.85	15.33	3.19	3.66	1.61	6.39	0.08	0.12	0.39	2730		98.65				400		=0				400			M6.NS.2.6(1).16
	66.84	0.12	15.78	1.99	4.87	1.74	4.35	0.12	0.15	0.34	3720		96.59		26	65	193		59	66		1.29	420	167	2345	wd.3.3.MT4.CX8.MI2
	66.93	0.72	15.13	3.22	4.96	1.97	4.63	0.19	0.20	0.36	2860		98.52			82	251	13	62	45					2440	WD.3.2.MT1.CX10.MI4
	66.95	0.24	15.70	2.23	4.96	1.66	4.56	0.14	0.20	0.37	3470		97.28		61	74	169		54	66	631	1.72	575	222	3449	WD.3.3.mt4.cx8.mi4
	66.95	0.05	16.80	1.33	5.21	1.97	4.66	0.11	0.09	0.33	3160		97.74		40	80	162	14	56	70		1.45	533	248	2473	WD.3.3.mt3.cx20.mi11
	66.97	0.80	15.30	3.05	4.94	2.04	4.40	0.15	0.14	0.41	3020	120	98.42								0	0.05	115	4	47	WD.3.2.mt1.cx10.mi3
	66.98	0.51	15.33	2.08	4.08	1.39	4.90	0.11	0.06	0.45	2430	120	96.11		(2	70	102			52						M6.KALI06.1.1B
	67.13	0.14	15.49	1.96	4.82	1.88	4.36	0.14	0.10	0.34	3350	104	96.63		62	78	182		55	53						WD.3.3.MT5.CX22.MI1B
	67.18 67.23	0.14 0.35	14.76 16.42	2.06 2.91	3.84 4.65	1.90	4.13 6.37	0.13	0.14 0.13	0.27 0.42	2940 2650	184	94.82 99.89													M6.WD.1.4(2).20
	67.28	0.33	17.47		4.03	1.06 2.17		0.14		0.42		222														M6.KALI06.2.7A BV.1(1).9
	67.28	0.22	17.47	1.36 1.86	4.78	1.60	4.40 4.69	0.39	0.15	0.42	2130 2790	332 144	98.88 96.12													M6.KALI06.2.9B
	67.42	0.16	15.42	2.06	4.08	1.32	4.09	0.15	0.03	0.38	2540	216	96.12													M6.KAL106.2.9B M6.KAL106.1.1C
	67.47	0.33	15.42	2.67	4.17	1.10	6.53	0.13	0.03	0.74	2440	210	99.04			49	168		36	37						M6.KALI06.2.13C
	67.47	0.33	15.97	2.67	4.22	1.10	6.53	0.10	0.11	0.33	2440		99.04			75	224	3	54	48 0						M6.KALI06.2.13C2bis
	67.53	0.51	16.45	2.23	4.50	1.59	4.84	0.10	0.08	0.58	2600	348	98.80			13	224	,	54	40 0						M6.KAL106.1.5
	67.65	0.17	15.54	1.73	4.09	1.53	4.70	0.12	0.12	0.40	2860	124	96.28													M6.KALI06.2.9A
	67.68	0.20	16.05	2.59	5.50	0.92	6.24	0.12	0.00	0.50	2740	12-7	100.02													M6.KALI06.2.11
	67.72	0.01	16.30	1.07	5.28	2.39	3.84	0.16	0.13	0.33	2920		97.43		73	52	222		78	46						WD.3.3.MT3.CX12.MI8
	67.75	0.30	16.23	2.57	4.68	1.15	6.50	0.14	0.10	0.39	2590		100.01		, ,	51	232	5	55	57						M6.KALI06.2.13B
	67.76	0.06	15.56	1.41	5.03	1.85	4.22	0.15	0.07	0.41	3420		100.01				232		00	5,						WD.3.3.mt6.cx3.mi11x
	67.83	0.37	16.22	2.91	4.14	1.05	6.54	0.11	0.13	0.37	2640		99.90		58	49	173		57	64						M6.KALI06.2.15A
	67.85	0.43	15.54	2.70	5.84	2.00	5.17	0.10	0.18	0.39	3100		100.44			68	224		58	47						WD.3.3.mt6.cx3.mi4
	67.92	0.13	15.82	1.76	4.98	1.59	4.73	0.07	0.09	0.46	3320		97.79		29	76	232		57	48		1.79	565	163	3396	WD.3.3.mt2.cx17.mi1
	67.94	0.05	16.02	1.10	4.88	1.90	4.85	0.10	0.12	0.42	3020		97.61		71	102	178		41	46	977	1.34	521	112	2523	WD.3.3.mt6.cx3.mi5
	67.96	0.58	15.08	2.78	4.62	1.46	4.99	0.13	0.12	0.40	3470		98.40		29	81	221		49	49						WD.3.2.MT1.CX18.MI2
	67.96	0.16	16.12	1.80	4.52	1.49	4.58	0.13	0.11	0.53	2710	124	97.63													M6.KALI06.2.10A
	67.96	0.66	15.71	3.41	4.57	2.19	4.88	0.11	0.15	0.33	2750	264	100.25													M6.WD.3.3(1).28
	67.96	0.06	15.88	1.68	5.07	1.63	4.79	0.15	0.13	0.39	3420		97.99		54	80	234		64	65						WD.3.3.MT2.CX17.MI3
	67.98	0.09	15.50	1.81	4.87	1.64	4.99	0.10	0.10	0.32	3380		97.67		62	78	182		55	53						WD.3.3.MT5.CX22.MI2
	68.00	0.23	14.84	2.20	4.62	1.32	4.98	0.15	0.06	0.34	3560		97.02		38	62	240		59	57	1384	1.75	669	137	3691	WD.3.3.mt6.cx3.mi12.pt1
	68.10	0.20	15.66	1.90	4.27	1.40	4.94	0.14	0.08	0.42	2760	196	97.37													M6.KALI06.2.12A
	68.14	0.33	15.61	2.73	4.48	0.95	6.42	0.26	0.14	0.52	3050		99.83													M6.KALI06.2.17A
	68.21	0.21	14.91	1.76	3.89	1.33	4.82	0.17	0.14	0.37	2110	156	96.00													M6.KALI06.2.16A4
	68.24	0.47	15.82	2.74	6.00	1.62	4.76	0.15	0.19	0.35	3040		100.57		56	124	193		489	41	1166	1.19	937	227	3218	WD.3.3.mt4.cx8.mi3
	68.29	0.29	15.84	3.02	4.29	1.13	6.38	0.15	0.12	0.47	2750	152	100.23													M6.KALI06.2.15B
	68.45	0.15	15.18	1.71	4.15	1.20	4.82	0.16	0.07	0.41	2710	148	96.54													M6.KALI06.2.7C
	68.59	0.03	15.94	1.07	5.14	1.70	4.52	0.15	0.10	0.33	3070		97.81		54	45	211	26	58	53	212	0.99	411	95	1854	WD.3.3.mt3.cx11.mi5
	68.59	0.15	15.38	1.65	3.94	1.42	4.93	0.12	0.10	0.41	2540	176	96.92													M6.KALI06.2.16A3
	68.61	0.34	15.79	2.66	6.04	1.32	5.11	0.12	0.17	0.34	3020		100.75		51	60	173	13	50	41						WD.3.3.MT4.CX8.MI5
	68.62	0.31	15.26	2.70	3.95	1.03	6.09	0.14	0.12	0.31	2840		98.77													M6.KALI06.2.13A
	68.76	0.14	14.91	1.69	4.22	1.24	4.49	0.16	0.04	0.44	2300	224	96.32				2.52									M6.KALI06.2.16D3
	68.98	0.00	15.68	0.93	5.02	1.71	4.46	0.12	0.10	0.33	2780		97.54		41	54	263		54	41		0.00	265	1.40	1.607	WD.3.3.mt3.cx11.mi6
	69.70	0.03	16.12	1.06	1.22	2.34	3.52	0.14	0.14	0.38	2930		94.87				20.5					0.98	365	148	1607	WD.3.3.mt6.cx3.mi6
	69.81	0.28	14.68	2.77	4.05	0.80	6.55	0.20	0.08	0.54	2820		99.99			53	296		69	62						M6.KALI06.2.17B
	70.81	0.49	13.92	3.08	3.84	0.76	5.95	0.18	0.17	0.58	2130		99.94													M6.KALI06.1.4
																										M6.NS.2.6(2).1A1
																										M6.NS.2.6(2).1A2
																										M6.NS.2.6(2).1B M6.NSB.1.3(1).11A
ı														l							1					WIO.135B.1.3(1).11A

													M6.NSB.1.3(1).11B
													M6.NSB.1.3(1).12A1
													M6.NSB.1.3(1).12A2
	11	38	249		53	47		58	0.48	401	52	1766	wd.3.3.mt3.ex11.mi4
		9	119		52	33							M6.NS.11.3(1).2
25			145		57	34							M6.NS.11.3(1).6A
									0.21	199	41	401	WD.3.2.mgcx3.mt1.cx7.mi3
									0.21	• • • • • • • • • • • • • • • • • • • •		101	WD.3.3.mt6.cx2.gl1a
								6		0	1	0	WD.3.3.mt6.cx2.gl1b
	6-	4	247		72	44		330	0.43	481	142	2902	WD.3.3.mt6.cx3.mi11
4			227		51	55		330	0.15	.01		2,02	WD.3.3.mt6.cx3.mi12.pt1bis
-	, -		227		51	33		536	0.81	275	98	1694	WD.3.3.mt6.cx3.mi13
								1460	1.15	532	164	2575	WD.3.3.mt6.cx3.mi15
								88	0.45	429	150	2553	WD.3.3.mt6.cx3.mi9
	2	3	266	0	61	54	5	00	0.43	427	150	2333	M6.KALI06.2.13B2bis
	6:		234	4	75	76	4						M6.Kali06.2.17B3bis
	0.	3	234	4	13	/0	4						M6.NS.11.3(1).1
29	9 8	1	188		55	50							M6.NS.11.3(1).13A
23	, ,	1	100		33	30							
													M6.NS.11.3(1).13B
													M6.NS.11.3(1).13F
													M6.NS.11.3(1).13G
													M6.NS.18.1.1A1
													M6.NS.18.1.1A2
													M6.NS.2.6(2).11A1
													M6.NS.2.6(2).11A2
													M6.NS.2.6(2).5B
													M6.NS.2.6(2).9B
			207		43	68							M6.NS.6-10.1.11A
													M6.NS.6-10.1.11B
	_	_	100			2.5							M6.NS.6-10.1.11C
	7		198		54	37							M6.NS.6-10.1.13A1
	53	-	240		58	44							M6.NS.6-10.1.13A2
	3	4	167	0	51	41	9						M6.NS.6-10.1.13A4bis
													M6.NS.6-10.1.16A
													M6.NS.6-10.1.16B1
	13	26	175		60	37							M6.NS.6-10.1.16B2
													M6.NS.6-10.1.1A
													M6.NS.6-10.1.1B
	1	16	291		65	47							M6.NS.6-10.1.7B
													M6.NS.6-10.1.7C
													M6.NS.6-10.1.7D
													M6.NSB.1.3(1).7
													M6.NSB.1.3(1).8
	4	7	173		48	37							M6.NSB.1.4.10A1
	1-	49	187		63	26							M6.NSB.1.4.10A2
													M6.NSB.1.4.1A2
													M6.NSB.1.4.2
													M6.NSB.1.4.6A
													M6.NSB.1.4.6B1
													M6.NSB.1.4.6B2
	80	6	166		50	41							M6.NSB.1.4.7A1
	1 9:	5	152	4	47	52							M6.NSB.1.4.7A2

1	1							1					i .
								195	0.34	331	47	1272	wd.3.2.mt1.cx18.mi3
		60	23	6	57	48							WD.3.2.MT1.CX2.MI2
								1182	1.60	399	262	1697	wd.3.2.mt1.cx4.mi1
									0.19	52	36	219	WD.3.3.mt3.cx23.mi2
									0.51	170	37	687	WD.3.3.mt3.cx26.mi13
		89	47		21				0.13	58	11	190	WD.3.3.mt3.cx26.mi2
		57	21:	3	63	69							WD.3.3.MT3.CX4.MI2
			24	4	62	37							WD.3.3.MT3.CX5.MI5
													WD.3.3.MT4.CX8.MI7A
													WD.3.3.MT4.CX8.MI7b
								618	1.14	437	151	2375	WD.3.3.mt5.cx13.mi1
	5	122	112	2 0	47	20	13						M6.WD.3.3(1).7B2bis
	23	3 108	99	0	48	17	13						M6.WD.3.3(1).7B3bis
	45	5 63	102	2	42	38							M6.NS.6-10.1.3B
													M6.NS.6-10.1.5
													M6.NSB.1.3(1).10
													M6.NSB.1.3(1).1B
													M6.NSB.1.3(1).4A
													M6.NSB.1.3(1).4B
													M6.NSB.1.3(2).1
													M6.NSB.1.4.11B
													M6.NSB.1.4.4